Elucidating the molecular basis of spindle assembly checkpoint signaling

Dissertation

der Mathematisch-Naturwissenschaftlichen Fakultät

der EBERHARD KARLS UNIVERSITÄT TÜBINGEN

zur Erlangung des Grades eines

Doktors der Naturwissenschaften

(Dr. rer. nat.)

vorgelegt von

Katharina Sewart

aus München

Tübingen

2016

Gedruckt mit Genehmigung der Mathematisch-Naturwissenschaftlichen Fakultät der Eberhard Karls Universität Tübingen.

Tag der mündlichen Qualifikation:	23.12.2016
Dekan:	Prof. Dr. Wolfgang Rosenstiel
1. Berichterstatter:	Dr. Silke Hauf
2. Berichterstatter:	Prof. Dr. Ralf-Peter Jansen

For my family

ACKNOWLEDGEMENTS

This dissertation was a journey for me in many aspects and I would like to thank everyone who was in some way or another part of it and helped me reach my goal.

First and foremost, I am very grateful towards Dr. Silke Hauf for giving me the opportunity to perform my Ph.D. work in her lab and under her guidance and continuous support. She not only provided me the unique chance to work and live on two different continents, she also contributed tremendously to my personal journey towards becoming a well-trained scientist. I am deeply thankful that she never gave up believing in me and my skills, especially in times of strong self-doubts.

I would like to thank Prof. Dr. Ralf-Peter Jansen for agreeing to be my Ph.D. supervisor and, together with Dr. Silke Hauf, Prof. Dr. Boris Macek and Prof. Dr. Doron Rapaport for being my Ph.D. examiners.

I am grateful to all lab members that were part of the first phase of my journey in Tübingen for providing support, fruitful discussions, fun at work and generally a great atmosphere. Thanks to Stephanie, Julia, André, Maria, Sabine, Nadine, Eva I. and Eva S. for being such great lab mates. I am equally thankful to everyone who accompanied the second part of my journey in Blacksburg. Thanks to Julia, Tatiana, Anupreet, Jessica and Hunter for providing an equally great work atmosphere. Furthermore, I want to thank the internship students and undergrads Holda, Adef and Jacob for assisting me in my projects. I am deeply grateful to Eva I. in Tübingen and Tatiana in Blacksburg for excellent technical help and for keeping the lab in order.

I would also like to thank all my friends in and around Tübingen for making me have a great, despite relatively short, time there and furthermore all my friends in Blacksburg for helping me settle in this special American culture.

Finally, I want to express my sincere gratitude towards my parents and my brother for their continuous and unconditional support and believe in me.

TABLE OF CONTENTS

LIST OF FIGURES

ABBREVIATIONS

A	Alanine (Ala)
aa	amino acid
ABBA	Acm1 / Bub1 / BubR1 / A-type cyclin
Adh1	Alcohol dehydrogenase 1
Ala	Alanine (A)
APC/C	Anaphase-promoting complex / cyclosome
Arg	Arginine (R)
Ark1	Aurora-related kinase 1
ATP	Adenosine triphosphate
bp	Base pair
Bub	Budding uninhibited by Benzimidazole
BubR1	Bub1-related protein 1
BuGZ	Bub3 interacting GLEBS and Zinc finger domain containing protein
C	Cysteine (Cys)
CCAN	Constitutive centromere-associated network
Cdc	Cell division cycle
C. elegans	*Caenorhabditis elegans*
CENP	Centromere associated protein
CDK	Cyclin-dependent kinase
CENP-A	Centromeric protein A
cm1/2	Conserved motif 1/2
CPC	Chromosomal passenger complex
CTD	C-terminal domain
CX-MS	chemical cross-linking followed by mass spectrometry
D	Aspartate (Asp)
Da	Dalton
DAPI	4',6-diamidino-2-phenylindole
D. melanogaster	*Drosophila melanogaster*
DNA	Deoxyribonucleic acid
Dsn	Dosage Suppressor of NNF1
DTT	Dithiothreitol
E	Glutamate (Glu)
EDTA	Ethylenediaminetetraacetic acid
EGTA	Triethylene glycol diamine tetraacetic acid
EM	Electron microscopy
EMM	Edinburgh minimal medium

FRAP	Fluorescence recovery after photobleaching
GFP	Green fluorescent protein
GLEBS	Gle2-binding sequence
Gln	Glutamine (Q)
Glu	Glutamate (E)
H	Histidine (His)
h	Hours
HBD	Helix-bundle domain
HEPES	2-[4-(2-hydroxyethyl)piperazin-1-yl]ethanesulfonic acid
HORMA	protein domain named after the Hop1p, Rev7p and MAD2 proteins
I	Isoleucine (Ile)
Ile	Isoleucine (I)
IP	Immunoprecipitation
K	Lysine (Lys)
KMN	KNL1 / Mis12 complex / Ndc80 complex
Knl1	Kinetochore-null protein 1
L	Leucine (Leu)
Leu	Leucine (L)
Lys	Lysine (K)
Mad	Mitotic arrest deficient
MBC	Carbendazim, methyl-2-benizimidazole carbamate
MCC	Mitotic checkpoint complex
M	Methionine (Met)
Met	Methionine (M)
mg	Milligram
µg	Microgram
min	Minutes
MIM	Mad2-interacting motif
Mis	Missegregation
ml	Milliliter
µL	Microliter
µM	Micromolar
µm	Micrometer
Mph	Mutator phenotype
Mps	Monopolar spindle
MS	Mass spectrometry
N	Asparagine (Asn)
Ndc	Nuclear division cycle

nm	Nanometer
NMR	Nuclear magnetic resonance
nmt1	No message in thiamine
Nnf	Necessary for Nuclear Function
NPC	Nuclear pore complex
Nsl	Nnf1 Synthetic Lethal
Nuf	Nuclear filament-containing protein
Nup	Nucleoporin
P	Proline (Pro)
PAGE	Polyacrylamide gel electrophoresis
PEM	A buffer consisting of PIPES, EGTA and magnesium sulphate
PIPES	1,4-Piperazinediethanesulfonic acid
Plo1	Polo kinase 1
PMSF	phenylmethylsulfonyl fluoride
PP1	Protein phosphatase 1
PP2A	Protein phosphatase 2A
PVDF	Polyvinylidene fluoride
Q	Glutamine (Gln)
R	Arginine (Arg)
Rad	Radiation sensitive
rcf	relative centrifugal force
RNA	Ribonucleic acid
RNAi	RNA interference
Rod	Rough Deal
RZZ	Rod / Zwilch / Zw10
S	Serine (Ser)
SAC	Spindle assembly checkpoint
Scc	Sister chromatid cohesion
S. cerevisiae	*Saccharomyces cerevisiae (S.c.)*
SDS	Sodium dodecyl sulphate
Slp1	Sleepy homolog 1
SPB	Spindle pole body
Spc	*S. pombe* centromere
S. pombe	*Schizosaccharomyces pombe (S.p.)*
T	Threonine (Thr)
Thr	Threonine (T)
TPR	Tetratricopeptide repeat
Tpr	Translocated promoter region (Nup211 homolog)

Tris	Tris(hydroxymethyl)aminomethane
V	Valine (Val)
WCE	Whole cell extract
WHB	Winged-helix B
X. laevis	*Xenopus laevis*
Y	Tyrosine (Tyr)
YEA	Yeast extract supplemented with adenine
Zw10	Zeste-White 10

SUMMARY

The spindle assembly checkpoint (SAC) is a highly conserved eukaryotic surveillance mechanism that maintains genomic integrity by delaying mitotic progression until all chromosomes have become properly attached to the mitotic spindle via their kinetochores. Malfunction of this checkpoint leads to chromosome segregation errors and has been implicated in tumorigenesis. SAC protein localization to unattached kinetochores is considered to be required for checkpoint signaling.

This study employs the model organism *Schizosaccharomyces pombe* to investigate the role of different checkpoint components and their interactions with each other during the SAC signaling cascade. We examined the link between Mad1 and Bub1 to explore the connection between upstream and downstream events during checkpoint signaling. We found that conserved motifs in Bub1 and Mad1 are essential for Mad1 localization to the kinetochore and checkpoint activity. Furthermore, we revealed a hitherto unknown additional function of Mad1 in creating the checkpoint signal.

Bub1 seems to act upstream of Mad1, and certain motifs in one of the kinetochore proteins are required for kinetochore recruitment of the Bub3-Bub1 complex. Here we provide evidence that a subset of these motifs is sufficient for this recruitment and checkpoint activity.

The ultimate effector of checkpoint signaling is the mitotic checkpoint complex. It was recently found that the composition of this complex is different from previously assumed. While early work suggested the presence of one Cdc20 molecule in the complex, latest results revealed that the mitotic checkpoint complex actually contains two Cdc20 molecules when bound to the APC/C. We observed the same situation in fission yeast and describe the role of conserved motifs within the checkpoint protein Mad3 in binding to those Cdc20 molecules. We furthermore indicate a function of the APC/C subunit Apc15 in the checkpoint that was unexpected based on work in other model organisms.

Taken together, we added new facets to the picture of spindle assembly checkpoint signaling and highlight similarities and differences between organisms, which illustrate how conserved, yet versatile this signaling pathway is.

ZUSAMMENFASSUNG

Der „spindle assembly checkpoint“ (SAC) ist ein hoch konservierter, eukaryontischer Überwachungsmechanismus der die genomische Integrität aufrechterhält, indem er das Fortschreiten der Mitose so lange verhindert, bis die Mikrotubuli der mitotischen Spindel sich an alle Kinetochore angeheftet haben. Eine Fehlfunktion dieses Kontrollmechanismus führt zu Fehlern bei der Chromosomensegregation und kann zur Tumorentstehung beitragen. SAC-Proteine konzentrieren sich an unangehefteten Kinetochoren, was als Voraussetzung für die Entstehung des SAC-Signals gilt.

Diese Studie verwendet den Modellorganismus *Schizosaccharomyces pombe* um die Rolle der einzelnen SAC-Proteine und deren Interaktionen während der SAC-Signalkaskade aufzudecken. Wir haben die Verbindung zwischen Mad1 und Bub1 untersucht, um die Verknüpfung zwischen frühen und späteren Vorgängen des SAC-Signalwegs zu verstehen. Dabei haben wir herausgefunden, dass konservierte Motive in Bub1 und Mad1 essentiell sind, um Mad1 an Kinetochore zu rekrutieren und ein SAC-Signal zu generieren. Zudem haben wir gezeigt, dass Mad1 eine zusätzliche und bisher unbekannte Funktion im SAC hat.

Bub1 spielt früher als Mad1 eine Rolle in der SAC-Signalkaskade und bestimmte Motive in einem der Kinetochorproteine werden für die Rekrutierung des Bub3-Bub1 Komplexes an die Kinetochore benötigt. Wir zeigen, dass ein kleiner Teil dieser Motive bereits für die Rekrutierung und die Aktivität des Checkpoints ausreicht.

Der letztendliche Effektor des Checkpoint-Signals ist der „mitotische Checkpoint Komplex“. Es wurde kürzlich gezeigt, dass die Zusammensetzung dieses Komplexes von bisherigen Annahmen abweicht. Während frühere Arbeiten darauf hinwiesen, dass ein Molekül des Cdc20 Proteins Teil des Komplexes ist, haben neueste Ergebnisse gezeigt, dass der Komplex tatsächlich zwei Cdc20 Moleküle enthält, wenn er an den APC/C gebunden ist. Wir beobachteten eine vergleichbare Situation in Spalthefe und beschreiben wie konservierte Motive im Checkpoint Protein Mad3 zur Bindung dieser Cdc20 Moleküle beitragen. Zudem zeigen wir, dass die APC/C Untereinheit Apc15 in *S. pombe* für Checkpoint-Aktivität benötigt wird, was basierend auf Arbeiten in anderen Organismen unerwartet war.

Zusammenfassend konnten wir neue Aspekte des „spindle assembly checkpoint“ Signalwegs aufzeigen und haben sowohl Übereinstimmungen als auch Unterschiede zwischen Organismen gefunden, was verdeutlicht wie konserviert aber zugleich wandlungsfähig dieser Signalweg ist.

1 Introduction

1.1 The cell cycle

Cell division is essential for the asexual reproduction of eukaryotes, for embryonic development, for the growth of multi-cellular organisms and for tissue renewal. Hence, cell division is one of the most fundamental processes of life. The cell cycle is a highly coordinated series of events that eventually leads to the formation of new daughter cells. The cell cycle is divided into four major phases. During S phase, the DNA is replicated and subsequently distributed into the two daughter cells during mitosis and cytokinesis (M phase). Gap phases (G_1 and G_2) separate those two events of genome duplication and segregation, thereby providing time for nutrient uptake, protein synthesis and growth (Morgan, 2007). The phases between two mitoses, G_1, S and G_2, are also referred to as interphase. The time that a cell spends in each of those phases is highly variable between organisms and even the order in which the events occur is flexible to some extent. During a short time in *Drosophila melanogaster* embryonic development, nuclear division cycles occur without intervening cytokinesis and gap phases, generating a syncytium with a common cytoplasm and thousands of nuclei (Vidwans and Su, 2001). While budding yeast has a long G_1 but no distinct G_2 phase, fission yeast spends 70% of its time in G_2 and only about 10% in each other phase of the cell cycle (Forsburg, 2003). Fission yeast furthermore only completes its cell division by cytokinesis once it has passed through G_1 and S phase (Figure 1-1). Cells can exit the cell cycle after G_1 to stop proliferation and enter a resting state, so-called G_0 phase. This occurs with damaged and senescent, but also terminally differentiated or otherwise ‘quiescent’ cells (Morgan, 2007).

Key regulators that ensure a timely order of the different events during the cell cycle are cyclin-dependent kinases (CDK) and their activators (cyclins). The activity of CDKs varies throughout the cell cycle leading to a cyclical change of phosphorylation status of their substrates, which subsequently influences cell cycle progression. Driver of the CDK activity change are cyclins, which show fluctuating synthesis and degradation rates in the different cell cycle stages, while CDK abundance is constant (Morgan, 1995, 1997). Upon entry into G_1 phase, cyclin abundance and therefore

CDK activity is low but increases to allow progression through interphase and mitosis. In order to exit mitosis at the end of M phase, CDK activity needs to drop again (Morgan, 2007; Coudreuse and Nurse, 2010). To reduce CDK activity, proteasomal degradation of mitotic cyclin B is mediated by a multi-subunit E3 ubiquitin ligase called the anaphase promoting complex/cyclosome (APC/C) (Morgan, 2007; Pines, 2011)

To monitor progression through the cell cycle and ensure proper division, eukaryotes have evolved a sophisticated network of regulatory proteins that form 'checkpoints'. These are transition points where cell cycle progression can be delayed by negative signals. Checkpoints are present at all phases of the cell cycle (Hartwell and Weinert, 1989; Hoyt et al., 1991; Li and Murray, 1991).

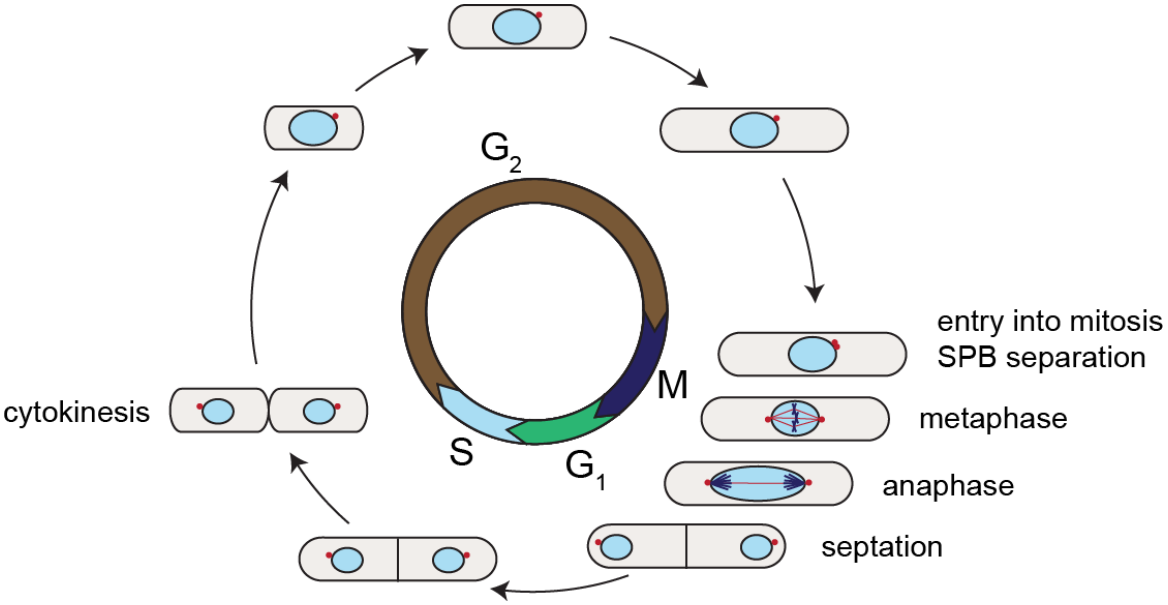

Figure 1-1 The fission yeast cell cycle
Fission yeast spends most of its time (about 70%) in G_2 phase and about 10% in each of the other three phases. In contrast to mammalian cells, fission yeast undergoes closed mitosis where the nuclear envelope stays intact. Although septation is initiated at the end of mitosis, completion of cytokinesis only happens after progression through G_1 and S phase. During interphase, the spindle pole body (SPB, red dot) resides on the cytoplasmic side of the nuclear envelope. The SPB duplicates in the cytoplasm during late G_2 phase and upon mitotic entry settles into pockets formed in the nuclear envelope. Intranuclear microtubules are formed and the two SPBs separate to form a bipolar spindle. After anaphase, the two SPBs are extruded back into the cytoplasm (Ding et al., 1997).

1.2 The model organism fission yeast

The fission yeast *Schizosaccharomyces pombe* (*S. pombe*) got its species name from the Swahili word for beer or alcohol ('pombe'), when it was first isolated in 1893 by Paul Lindner from East African millet beer. Using *S. pombe* as a research tool was pioneered in the 1940s by Swiss geneticist Urs Leupold, even though his strains were not derived from the original African beer isolate but instead from, probably rancid, French wine (Hall and Linder, 1993; Hoffman et al., 2015). The strains that are nowadays used in research labs are all descendants from Urs Leupold's yeast strains. *S. pombe* is, together with its distant cousin, the budding yeast *Saccharomyces cerevisiae*, from which it has diverged 400-1000 million years ago (Heckman et al., 2001; Wood et al., 2002), one of the most important model organisms for the study of cell and molecular biology of eukaryotes. Both yeasts are unicellular organisms and therefore provide the advantage that one can work simultaneously with a high number of individuals for the discovery of rare mutants. This is also facilitated by a generation time of only 2.5 hours at 30 °C in full medium. Since yeast is a eukaryote, like mammalian cells, it can be easily used to study processes that are conserved from yeast to humans but absent or significantly different in bacteria. The genome sequence of *S. pombe* was published in 2002 (Wood et al., 2002). The fission yeast genome consists of three relatively large chromosomes that together carry about 5000 protein-coding genes. Publication of the full genome sequence paved the way for more detailed research on the fission yeast genomic features and annotating functions to them. A big advantage for this endeavor was the active homologous recombination mechanism of yeast, with 1 centimorgan genetic distance corresponding to only 6250 base pairs (bp) in *S. pombe* (Fowler et al., 2014) and 2500 bp in *S. cerevisiae* (Olson et al., 1986) – in contrast to about 1 million bp in humans (Kong et al., 2004). Furthermore, while budding yeast underwent a whole-genome duplication, fission yeast only contains a region of about 50 kb in the sub-telomeric part of chromosomes I and II that seems to have duplicated (Wolfe and Shields, 1997; Wood et al., 2002). Another difference between fission and budding yeast is the visible chromosome condensation in fission yeast that allows easier microscopic analysis of individual chromosomes and their segregation in mitosis (Russell and Nurse, 1986). Other aspects that make fission yeast more similar to many metazoans than budding yeast, are its large modular centromeres and the presence of conserved centromere-binding proteins, like

Swi6/HP1, chromatin modifiers, telomere and centromere proteins as well as components of the RNA interference pathway, which is non-functional in *S. cerevisiae* (Forsburg, 2003).

In contrast to budding yeast, which separates the newly formed bud from the mother cell, fission yeast cells are rod-shaped and only grow at their cell ends without width change, eventually undergoing a symmetric cell division followed by formation of a medial septum (Mitchison, 1990). In addition to vegetative growth, fission yeast also has a sexual cycle where, upon nutrient starvation, two haploid cells of opposite mating types (h+ and h-) mate. This leads to formation of a diploid zygote that enters the meiotic pathway and generates four haploid nuclei. A spore wall forms around each nucleus producing an ascus with four spores within the zygote, the so-called tetrad, which eventually germinates and re-enters the vegetative cycle (Forsburg and Rhind, 2006). Fully wild-type cells can switch between h+ and h- and are called h90. This switching ability ensures that a culture or colony will always contain cells of both mating types.

S. pombe has played an important role in cell cycle research. In the 1970s, Paul Nurse identified the *cdc2* gene in fission yeast (Nurse et al., 1976). The *cdc2* gene codes for the central cyclin-dependent kinase CDK1 and turned out to be identical to the *cdc28* gene discovered in budding yeast by Leland Hartwell. Both Nurse and Hartwell showed that it is a major factor during cell cycle progression. Furthermore, Nurse cloned the corresponding human gene by complementation of the fission yeast *cdc2* mutant. This, for the first time, provided strong evidence that the cell cycle machinery is conserved across eukaryotes. The findings by Hartwell and Nurse, together with similar research performed by Tim Hunt, who discovered cyclins in sea urchin eggs, culminated in the award of the Nobel Prize in Physiology or Medicine in 2001 to the three researchers.

1.3 Mitosis

M phase is the most visually distinct phase of the cell cycle and includes both the nuclear division (mitosis) and the cellular division (cytokinesis). During mitosis, the sister chromatids of the chromosomes are separated into two identical sets and each set ends up in its own nucleus. In 1882, German anatomist Walther Flemming coined the term “mitosis” when describing his observation of a thread-like stainable scaffold within the nucleus during cellular division (Greek “mitos” means “thread”) (Paweletz,

2001). Mitosis can be divided into several individual phases that occur sequentially in a highly coordinated and timed manner: prophase, prometaphase, metaphase, anaphase and telophase. At the onset of prophase, chromatin fibers condense into discrete chromosomes, and the microtubule organizing centers (centrosomes or spindle pole bodies) separate and nucleate tubulin to form the mitotic spindle (Pereira and Schiebel, 1997). A breakdown of the nuclear envelope marks entrance into prometaphase and thereby allows microtubules to contact the condensed chromosomes. While metazoan and plant cells undergo a so-called 'open mitosis' with a complete disassembly of the nuclear envelope, many fungi, including fission yeast, perform a 'closed mitosis' where the nuclear envelope stays intact and mitosis occurs within the nucleus. During a closed mitosis, the spindle pole bodies (SPBs), which are embedded in the nuclear envelope, nucleate microtubule formation inside of the nucleus (De Souza and Osmani, 2007). In late prometaphase, microtubules originating from the centrosomes, which are functionally equivalent to SPBs, begin to search for and attach to kinetochores, large proteinaceous microtubule-binding structures that form on the chromosomal centromeres (Westhorpe and Straight, 2013; Godek et al., 2015; Pesenti et al., 2016). In metaphase, stable end-on attachments are formed between the kinetochores and microtubules (Kops et al., 2010) and the two centrosomes begin to exert force on the chromosomes towards opposite ends of the cell, resulting in alignment of the chromosomes at the metaphase or equatorial plate in the middle of the spindle. A failure to achieve bi-polar attachment or to correctly position the metaphase plate results in chromosome mis-segregation or asymmetric cell division (Gregan et al., 2011; Tan et al., 2015). Cohesin is a multi-subunit protein complex that holds sister chromatids together and thereby resists the pulling force of the microtubules Once proper bi-polar attachment is achieved for every single chromosome, cohesin complexes that initially formed a ring around the sister chromatids are rapidly opened and the chromatids are pulled towards opposite spindle poles (anaphase A). Trigger for these events is the activation of the APC/C which ubiquitinates its key substrates cyclin B and securin, thereby marking them for proteasomal degradation (Peters, 2006; Primorac and Musacchio, 2013). APC/C substrates, including cyclin B and securin, contain short sequence motifs (degrons) for interaction with APC/C coactivators. The most widespread degrons are D (destruction) and KEN (lysine-glutamate-asparagine) box (Glotzer et al., 1991; Pfleger et al., 2001; Primorac and Musacchio, 2013). While degradation of cyclin B leads to a reduction in CDK activity, loss of securin frees and

thereby activates its binding partner separase. Active separase then cleaves the Scc1 kleisin subunit of cohesion and thereby opens the cohesion ring (Oliveira and Nasmyth, 2010). In anaphase B, the sister chromatids are further pulled apart by the elongating spindle. Telophase is the reversal of pro- and prometaphase events: the spindle disassembles, a new nuclear envelope forms around the separated chromosomes and the chromosomes decondense (Sullivan and Morgan, 2007). Cytokinesis is the last step to complete cell division: the cleavage furrow develops where the metaphase plate used to be and pinches off the cytoplasm to form two daughter cells, each with its own nucleus containing the chromosomes (Burgess and Chang, 2005).

As described before, mitosis can happen with or without nuclear envelope breakdown during prophase. Another deviation from the general scheme is *Caenorhabditis elegans*, where the nuclear envelope persists until anaphase (Lee et al., 2000). The only traditional mitotic stages that are very well conserved are anaphase and cytokinesis, because disjunction and segregation of replicated sister chromatids as well as the generation of new cells are minimum requirements for cell reproduction (Pines and Rieder, 2001).

1.4 The kinetochore

The kinetochore is the proteinaceous structure that links the centromeres of the chromosomes to spindle microtubules and thereby allows forces generated by microtubule dynamics to power chromosome movement. It consists of nearly 100 proteins that are hierarchically assembled onto centromeric DNA (Foley and Kapoor, 2013; Jia et al., 2013). The kinetochore is composed of several layers: the inner kinetochore, the outer kinetochore and the ‘corona’. The centromeres are able to bind nucleosomes that contain the histone H3 variant centromeric protein A (CENP-A). This centromeric chromatin then interacts with several inner kinetochore proteins collectively known as constitutive centromere-associated network (CCAN) (Westhorpe and Straight, 2013; Pesenti et al., 2016; Weir et al., 2016). The outer kinetochore serves as microtubule-binding interface, and its core is the KMN network, a 10-subunit super-complex of KNL1 (composed of Knl1 (Spc7 in *S. pombe*) and Zwint), the MIS12 complex (MIS12-C, composed of Nnf1, Mis12, Dsn1, and Nsl1), and the NDC80 complex (NDC80-C, composed of Ndc80, Nuf2, Spc24, Spc25) (Foley and Kapoor, 2013; Pesenti et al., 2016). The CCAN subunit CENP-C has

been shown to contact CENP-A (Carroll et al., 2010; Guse et al., 2011; Kato et al., 2013) and also provides a link between the inner and outer kinetochore via direct interaction with the MIS12 complex in humans and flies (Przewloka et al., 2011; Screpanti et al., 2011). A second link between inner and outer kinetochore is formed by the CCAN subunit CENP-T, which directly connects to the NDC80 complex (Hori et al., 2008; Bock et al., 2012; Schleiffer et al., 2012; Malvezzi et al., 2013; Nishino et al., 2013). The outer kinetochore is not only the main microtubule receptor, but it also serves as a recruitment platform for numerous other proteins, including spindle assembly checkpoint (SAC) components and additional regulators of kinetochore-microtubule attachment (Musacchio and Salmon, 2007; Jia et al., 2013; Pesenti et al., 2016). The outermost kinetochore layer forms a fibrous corona consisting of a dynamic network of resident and temporary proteins stretching out 100-150 nm from the outer kinetochore. Two of the proteins in the corona are the microtubule-interacting motor protein CENP-E and the microtubule interactor CENP-F (Wan et al., 2009; Varma et al., 2013). Depletion of any of the KMN protein components *in vivo* reduces the ability of cells to establish functional kinetochore-microtubule interactions, with the most severe defects seen in cells depleted of NDC80-C components, suggesting that this complex is largely responsible for direct attachments (DeLuca and Musacchio, 2012; Kim and Yu, 2015). *In vitro* force measurements (McIntosh et al., 2008; Powers et al., 2009) as well as *in vitro* binding assays with purified NDC80-C (Cheeseman et al., 2006) are consistent with the hypothesis that this complex couples kinetochores to depolymerizing microtubules. KNL1 also showed an ability to bind microtubules *in vitro*, albeit weaker than a combination of KNL1 and MIS12-C, probably reflecting a stabilizing influence by MIS12-C (Cheeseman et al., 2006). It was furthermore shown that the MIS12 complex interacts with the C-terminus of KNL1 (Kiyomitsu et al., 2007; Petrovic et al., 2010) and with the Spc24/Spc25 subunits of the NDC80 complex while the KNL1-binding region of Nsl1 is not required for high-affinity binding of MIS12-C to NDC80-C (Petrovic et al., 2010). KNL-1 functions as the binding platform for several spindle assembly checkpoint components (Kiyomitsu et al., 2007; Krenn et al., 2014; Silio et al., 2015; Vleugel et al., 2015b).

To correct any errors that might have occurred during kinetochore-microtubule binding, cells have evolved a correction machinery involving Aurora B, a kinase subunit of the chromosomal passenger complex (CPC) (Hauf et al., 2003; Lampson et al., 2004; Cimini et al., 2006; Carmena et al., 2012). Through phosphorylation of

members of the KMN network by Aurora B, the interaction of those proteins with microtubules is weakened to resolve erroneous attachments and create free kinetochores that can then re-bind microtubules for a proper bi-orientation (Cheeseman et al., 2006; Ruchaud et al., 2007).

1.5 The spindle assembly checkpoint (SAC)

To ensure that the cells only progress into anaphase and separate their chromosomes once all of them are properly bi-oriented on the mitotic spindle, a dedicated control system delays transition from metaphase into anaphase until all errors are corrected. This control system is called the 'spindle assembly checkpoint' (SAC) or 'mitotic checkpoint'. Improperly attached kinetochores create a signal to delay the cell in prometaphase in order to gain time for error correction (Musacchio and Salmon, 2007; Lara-Gonzalez et al., 2012; Jia et al., 2013). It was shown by laser-ablation experiments that the checkpoint senses unattached kinetochores and only becomes satisfied when the last kinetochore attaches to microtubules (Rieder et al., 1995). Applying tension to a mis-attached chromosome with a micromanipulation needle, which simulates proper attachment and bi-orientation to the mitotic spindle, also strongly reduces a checkpoint-induced mitotic delay (Li and Nicklas, 1995). Recent work suggests that SAC signaling is graded and that the intensity of the SAC inhibitory signal correlates with the number of unattached kinetochores (Collin et al., 2013; Dick and Gerlich, 2013; Uchida and Hirota, 2016). The discovery of the first spindle assembly checkpoint components dates back to the early 1990's. Two independent genetic screens in budding yeast identified three MAD (mitotic arrest-deficient) and three BUB (budding uninhibited by benzimidazole) genes through discovery of mutants that fail to arrest in mitosis in response to loss of microtubule function (Hoyt et al., 1991; Li and Murray, 1991). All three encoded MAD proteins, Mad1, Mad2 and Mad3 (or BubR1, depending on the organism), and two of the three BUB proteins, Bub1 and Bub3, are indeed highly conserved core components of the SAC. The checkpoint function of the serine/threonine kinases Mps1 (Mph1 in *S. pombe*) and Aurora B (Ark1 in *S. pombe*), another two core components of the SAC, was revealed a few years later (Weiss and Winey, 1996; Biggins and Murray, 2001) (Figure 1-2). In addition to these core checkpoint proteins, it was shown that specific mutants of kinetochore proteins can impair proper kinetochore formation and SAC activation, resulting in precocious sister chromatid separation often followed by

chromosome mis-segregation (He et al., 2001). Many studies revealed that checkpoint proteins enrich at unattached kinetochores during the onset of mitosis, marking the initial step of SAC signaling (Musacchio and Salmon, 2007; Lischetti and Nilsson, 2015). In the specific kinetochore mutants with impaired SAC function, this enrichment fails and no signal is generated. To arrest the cells in prometaphase, the signal created at unattached kinetochores needs to be translated into an inhibitor of cell cycle progression. This is achieved by negative regulation of APC/C activity. Cdc20 (Slp1 in *S. pombe*) is a mitotic activator of the APC/C and the ultimate molecular target of the SAC (Hwang et al., 1998; Kim et al., 1998; Peters, 2006; Primorac and Musacchio, 2013). Cdc20 binds to the APC/C as a co-activator and recruits APC/C substrates by binding to D-boxes in the substrates (Glotzer et al., 1991; King et al., 1996; Fang et al., 1998b). The checkpoint proteins Mad2 and Mad3 can sequester Cdc20 and without free Cdc20, APC/C activity is impaired, which blocks ubiquitination and subsequent degradation of its substrates securin and cyclin B, ultimately preventing progression into anaphase. It was shown that not only unattached kinetochores but also tubulin or spindle pole body mutants, microtubule motor defects and absence or mutation of kinetochore components all activate the spindle assembly checkpoint (Hardwick et al., 1999).

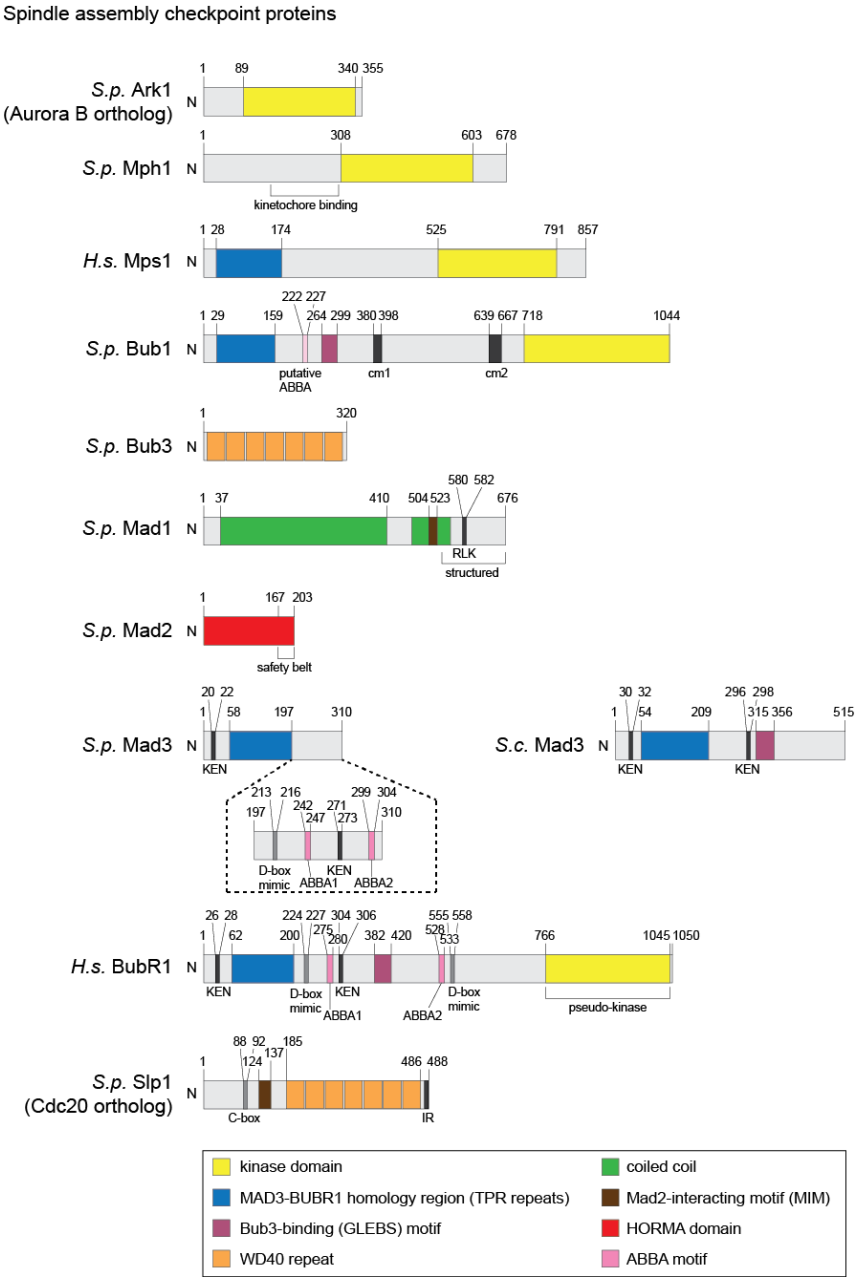

Figure 1-2 Domain organization of spindle assembly checkpoint proteins in *Schizosaccharomyces pombe*

All proteins are drawn to scale, see text for details (*S.p. = Schizosaccharomyces pombe; S.c. = Saccharomyces cerevisiae; H.s. = Homo sapiens)*.

Ark1 (Aurora B ortholog), Mph1 (Mps1 ortholog) and Bub1 contain kinase domains. The Mad3 proteins in *S. pombe* and *S. cerevisiae* lack the C-terminal pseudo-kinase domain present in the *H.s.* Mad3 ortholog BubR1. Mad3 and BubR1 contain several motifs that facilitate Slp1/Cdc20-binding but *S. pombe* Mad3 seems to lack the GLEBS motif, required for binding to Bub3. The tetratricopeptide repeats (TPR) in Bub1 and BubR1 have been shown to interact with the kinetochore component KNL1. Both Bub3 and Slp1 (Cdc20 ortholog) contain WD40 repeats folding into 7-bladed propellers. The Slp1 C-box and IR tail are both required for interaction with the APC/C. Mad2 is formed by the globular HORMA domain (for Hop1, Rev7, Mad2), a complex structure of a core, formed by beta-sheets and alpha-helices, and a C-terminal 'safety belt' that undergoes a pronounced conformational change when switching from open to closed, which in case of Mad2 is required for binding to either Mad1 or Slp1.

1.6 The SAC signaling cascade

The spindle assembly checkpoint involves many different steps to transduce the signal from the enrichment of the SAC proteins at the kinetochore to the inhibition of Cdc20 and the APC/C. The signaling cascade includes protein-protein interactions, formation of multi-subunit protein complexes, conformational changes and the post-translational modifications of proteins (Figure 1-3). The nature and order of events has been studied by genetics, biochemistry, structural biology and microscopy if living cells in various organisms. Pioneering work by Conly Rieder revealed that the SAC signal is generated by the kinetochore (Rieder et al., 1995), and consistent with this finding, it was later demonstrated that most SAC components are recruited to unattached kinetochores in a hierarchical manner and exhibit varying rates of turnover (Howell et al., 2004; Shah et al., 2004). A key unresolved question is how the SAC machinery distinguishes attached from unattached kinetochores. One hypothesis proposes that the kinetochore has different conformations depending on microtubule attachment status and thereby either allows checkpoint signaling or silences it (Aravamudhan et al., 2015). Another hypothesis suggests that a competition for kinetochore binding between SAC proteins and microtubules constitutes a direct mechanism for the detection of unattached kinetochores (Hiruma et al., 2015; Ji et al., 2015).

1.6.1 Generation of the checkpoint signal

It was shown that the KMN network of the outer kinetochore not only serves as the receptor for microtubules, but also directly or indirectly interacts with most SAC proteins, thus coupling SAC signaling to microtubule binding (Jia et al., 2013). The two most upstream components of the SAC signaling pathway are the kinases Aurora B and Mps1 (Lischetti and Nilsson, 2015). Aurora B is part of the chromosomal passenger complex (CPC) and is concentrated at the centromere, depending on interactions between other CPC components and histone H3 and H2A phosphorylations (van der Horst and Lens, 2014). Aurora B dynamically modulates kinetochore-microtubule contacts by mediating phosphorylation of Ndc80 and Knl1, which reduces their microtubule-binding affinity (Jia et al., 2013) and thereby destabilizes incorrect interactions between the kinetochore and the mitotic spindle and allows the establishment of new, corrected attachments (Cheeseman et al., 2006; DeLuca et al., 2006). The dependency between Aurora B and Mps1 differs

between organisms. While in budding yeast Aurora B (Ipl1) and Mps1 seem to localize independently (Maure et al., 2007), metazoan Mps1 localization to kinetochores has been shown to depend on Aurora B kinase activity (Vigneron et al., 2004; Santaguida et al., 2010; Saurin et al., 2011), and also in fission yeast Mps1 (Mph1) localization to the kinetochore requires Aurora B (Ark1) kinase activity (Heinrich et al., 2012). In contrast to the strong effect of Aurora B on Mps1 localization, Mps1 is only partially and largely indirectly required for localization of Aurora B (Hewitt et al., 2010; Santaguida et al., 2010; Saurin et al., 2011; Heinrich et al., 2012).

Another function of Mps1, besides its involvement in Aurora B regulation, is the phosphorylation of multiple MELT motifs (MELT standing for the amino acids Met, Glu, Leu, Thr) in the KMN network component KNL1 (Figure 1-3 A). This phosphorylation promotes recruitment and direct binding of the Bub1-Bub3 complex (London et al., 2012; Shepperd et al., 2012; Yamagishi et al., 2012; Primorac et al., 2013; Krenn et al., 2014; Zhang et al., 2014). Recent work showed that Mps1 not only phosphorylates the MELT core but also adjacent SHT motifs and both modifications are crucial for Bub1-Bub3 recruitment (Vleugel et al., 2015b). Kinetochore-localization of Bub1-Bub3 initiates enrichment of the other checkpoint components Mad1, Mad2 and Mad3/BubR1 at the kinetochore (Millband and Hardwick, 2002; Kadura et al., 2005; Essex et al., 2009; Vanoosthuyse et al., 2009; Windecker et al., 2009; Heinrich et al., 2012; London and Biggins, 2014; Moyle et al., 2014).

In metazoans, Mps1 not only modifies KNL1 but also promotes recruitment of the RZZ complex (Rod, Zwilch and Zw10) to the kinetochore, which has been shown to be required for Mad1 kinetochore localization (Karess, 2005; Kops et al., 2005a; Maciejowski et al., 2010; Santaguida et al., 2010; Silio et al., 2015). In addition, the RZZ complex also localizes a dynein/dynactin complex, a minus-end directed microtubule motor, to kinetochores through the adaptor protein spindly (Barisic and Geley, 2011). This allows dynein to strip Mad1-Mad2 from kinetochores once they have attached to microtubules and move the complex along the microtubules to the spindle poles, thereby contributing to SAC silencing (Howell et al., 2001; Sivaram et al., 2009). So far, there have been no functional homologs of the RZZ components identified in yeast. In fission yeast, dynein is not involved in stripping of Mad2 from the kinetochore (Courtheoux et al., 2007).

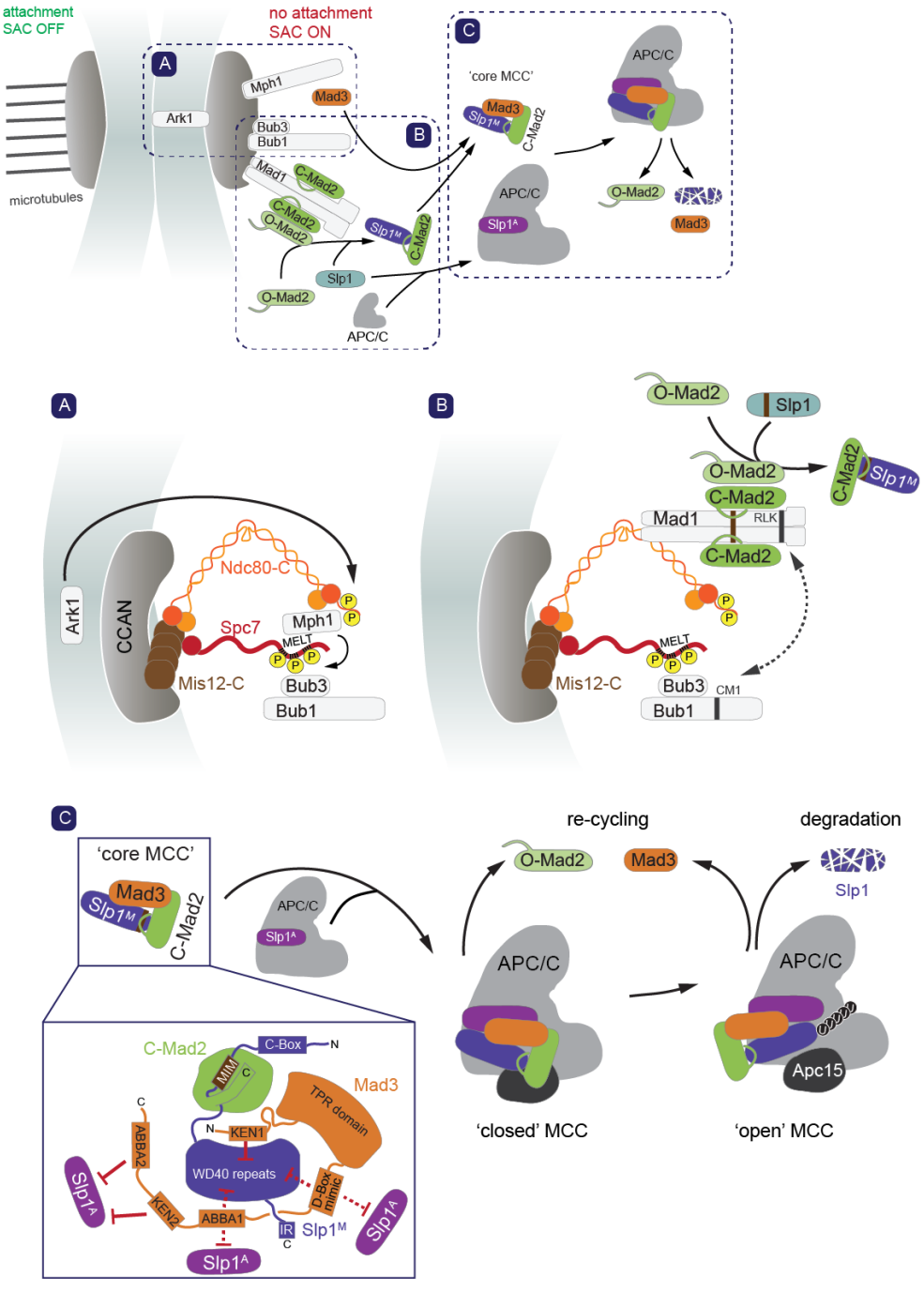

Figure 1-3 The spindle assembly checkpoint signaling cascade
Adapted from Heinrich et al. (2012); Sacristan and Kops (2015); see text for details.
The upper panel illustrates a general scheme of checkpoint signaling at the kinetochore and in the nucleoplasm triggered by unattached kinetochores. The insets show critical steps in checkpoint signaling in greater detail:
(A) Localization of kinetochore components and recruitment of upstream checkpoint proteins.
(B) Kinetochore recruitment of the Mad1-Mad2 complex and the 'Mad2 template model'.
(C) MCC formation (including details of Mad3-Slp1 interaction) and APC/C inhibition.
Solid lines indicate a direct modification or protein-protein interaction, dashed lines show a connection between proteins that is indirect or unclear. The extension at O-/C-Mad2 represents the C-terminal 'safety belt' required for Mad1- and Slp1-binding and the Mad2-binding motif (MIM) on both Mad1 and Slp1 is highlighted in brown.
'O-Mad2' = open Mad2; 'C-Mad2' = closed Mad2; '$Slp1^{M}$' = core MCC Slp1; '$Slp1^{A}$' = APC/C-bound Slp1; 'P' = phosphorylation; 'U' = ubiquitin

1.6.2 The role of Bub1 and Bub3 at the kinetochore

Bub1 is recruited to the kinetochore via its direct interaction with KNL1 and through binding to Bub3, which is also recruited to KNL1 (Kiyomitsu et al., 2007; Kiyomitsu et al., 2011; London et al., 2012; Shepperd et al., 2012; Yamagishi et al., 2012). The N-terminus of Bub1 contains two regions that are important for these interactions. An array of three divergent motifs that each adopt a tetratricopeptide repeat(TPR)-like fold occurs both in the very N-terminus of Bub1 and Mad3/BubR1 (Bolanos-Garcia et al., 2009; Bolanos-Garcia et al., 2011) and respectively binds to KI motif 1 and 2 (KI stands for Lys-Ile) within KNL1 (Krenn et al., 2012). It was shown that deletion of these TPR motifs in *S. pombe* Bub1 reduces its kinetochore localization and leads to loss of Bub3 and Mad3 recruitment, which in turn abolishes SAC function (Vanoosthuyse et al., 2004). Work with human cells, done by different groups, showed contradictory results (Taylor et al., 1998; Klebig et al., 2009; Krenn et al., 2012). While Taylor *et al.* (1998) and Krenn *et al.* (2012) demonstrated that the TPR motifs in the N-terminus of Bub1 are neither required nor sufficient for its kinetochore recruitment, Klebig *et al*. (2009) saw a complete loss of Bub1 at the kinetochore upon deletion of this domain. Introduction of point mutations into the TPR motifs perturbed interaction of Bub1 and KNL1 *in vitro* but had no effect on Bub1 kinetochore localization *in vivo* (Krenn et al., 2012). Overall, this suggests that the TPR region only plays a marginal role in kinetochore recruitment of Bub1. In addition to the TPR motifs, the Bub1 N-terminus contains a GLEBS motif (short for Gle2-binding sequence), which is alternatively referred to as Bub3-binding motif. This motif was shown to be the main contributor to kinetochore localization of Bub1 (Taylor et al., 1998; Logarinho et al., 2008; Klebig et al., 2009; Vanoosthuyse et al., 2009; Windecker et al., 2009). The GLEBS motif was initially described as an interaction site between the yeast nuclear pore component Nup116 (Nup98 in vertebrates) and the mRNA export factor and Bub3 homolog Gle2/Rae1 (Bailer et al., 1998). The Bub1 GLEBS motif mediates binding to Bub3 (Taylor et al., 1998; Wang et al., 2001; Larsen et al., 2007; Klebig et al., 2009; Vanoosthuyse et al., 2009). The Bub1-Bub3 complex is recruited to KNL1 MELT motifs (London et al., 2012; Shepperd et al., 2012; Yamagishi et al., 2012; Primorac et al., 2013; Krenn et al., 2014; Zhang et al., 2014; Vleugel et al., 2015b) (Figure 1-3 A). Recent work suggests that only a limited number of MELT repeats are “active” and that this activity correlates with the presence of an additional vertebrate-specific SHT motif adjacent to the MELT

sequence, both of which are phosphorylated by the Mps1 kinase (Vleugel et al., 2015b). The interaction between Bub1 and Bub3 via the GLEBS motif is crucial for kinetochore localization of Bub1. A deletion of the Bub1 GLEBS motif in fission yeast cells led to a loss of both Bub1 and Bub3 at the kinetochores (Windecker et al., 2009), showing that these two proteins need to be in a complex with each other for proper localization. Consistently, a reduction or deletion of either Bub1 or Bub3 results in loss of kinetochore localization of the other binding partner (Taylor et al., 1998; Kerscher et al., 2003; Vanoosthuyse et al., 2004; Logarinho et al., 2008; Windecker et al., 2009; Shepperd et al., 2012; Yamagishi et al., 2012). *In vitro* analyses showed a strong requirement of Bub1 for binding of Bub3 to KNL1 (Yamagishi et al., 2012; Primorac et al., 2013). While human cells lacking the Bub1-Bub3 interaction show a clear checkpoint defect (Klebig et al., 2009), fission yeast cells expressing *bub1-ΔGLEBS* retain a functional checkpoint (Vanoosthuyse et al., 2009; Windecker et al., 2009). Along those lines, depletion of Bub3 shows a similar outcome. While in most organisms altered levels of Bub3 led to checkpoint defects (Kalitsis et al., 2000; Campbell and Hardwick, 2003; Lopes et al., 2005; Logarinho et al., 2008), fission yeast cells lacking *bub3* fail to localize Bub1, Mad1, Mad2 and Mad3 to the kinetochore but nevertheless show active checkpoint signaling (Tange and Niwa, 2008; Vanoosthuyse et al., 2009; Windecker et al., 2009). Although we still lack a molecular explanation for this difference, it was proposed that, at least in *S. pombe*, Bub3 acts as an inhibitor of Bub1 (Yamagishi et al., 2012). If Bub1 is not associated with Bub3, as in *bub1-ΔGLEBS* or *bub3Δ*, Bub1 could retain activity, even though kinetochore localization is lost. Furthermore, problems with checkpoint inactivation could arise when Bub1 remains active due to lack of interaction with Bub3. Indeed, it was shown in fission yeast that Bub3 is necessary for efficient SAC silencing (Vanoosthuyse et al., 2009). Furthermore, the presence of an active checkpoint despite the lack of kinetochore localization of Bub1 and the Mad proteins in *bub3Δ* or *bub1-ΔGLEBS* suggests that kinetochore enrichment of the checkpoint components is not absolutely required for checkpoint signaling.

Further C-terminal of the GLEBS motif, Bub1 contains two additional highly conserved motifs, termed cm1 and cm2 (cm for conserved motif). In human cells, deletion of either of them resulted in decreased kinetochore localization of Bub1. While deletion of cm2 showed reductions in checkpoint activation, chromosome congression and kinetochore recruitment of Mad1, Mad2 and BubR1, deletion of cm1 entirely abolished SAC activity and kinetochore recruitment of Mad1, Mad2 and

BubR1, whereas chromosome congression was not influenced (Klebig et al., 2009). In agreement with these results, deletion or mutation of a region of Bub1 contain cm1 in budding yeast (Warren et al., 2002) or fission yeast (Heinrich et al., 2014) abolished SAC activity and Mad1 recruitment despite retaining Bub1 kinetochore localization. It was therefore suggested that this motif serves as an interaction site between Mad1 and Bub1, potentially together with Bub3 (Brady and Hardwick, 2000; Warren et al., 2002). The receptor for cm1 on Mad1 is supposed to be a 3-amino-acid motif (RLK) in the C-terminus downstream of the Mad2 binding site, since mutation of this motif abolishes binding of Mad1 to Bub1-Bub3 in budding yeast (Brady and Hardwick, 2000). Recent work in budding yeast showed that the Mad1-Bub1 interaction depends on Bub1 phosphorylation by Mps1 (London and Biggins, 2014). Experiments in *C. elegans* also revealed a Mad1-Bub1 interaction, but with the C-terminal kinase domain of Bub1 and the coiled-coil upstream of the Mad2 binding site of Mad1 serving as interacting regions (Moyle et al., 2014). Early work using *in vitro* translated human proteins also already reported an interaction between Mad1 and Bub1 (Seeley et al., 1999). Although it seems likely that this interaction, be it direct or indirect, is conserved across organisms, it is most likely not the sole pathway for Mad1 kinetochore recruitment. Artificial tethering of fission yeast Mph1 to kinetochores in interphase resulted in co-recruitment of Bub1-Bub3 but not Mad1, suggesting the existence of additional Mad1 recruitment mechanisms apart from Bub1 (Ito et al., 2012). While in metazoans, the RZZ complex is such an additional mechanism for Mad1 kinetochore localization (Karess, 2005; Kops et al., 2005a; Maciejowski et al., 2010; Santaguida et al., 2010; Silio et al., 2015), no functional homologs of the RZZ components have been identified in yeast so far.

At its C-terminus, Bub1 contains a kinase domain, but the kinase activity is not required for Bub1 kinetochore localization and only has a minor influence on SAC activity. Mutating the kinase domain to render it kinase-dead (Warren et al., 2002; Yamaguchi et al., 2003; Vanoosthuyse et al., 2004; Klebig et al., 2009) or deleting it entirely (Warren et al., 2002; Yamaguchi et al., 2003; Klebig et al., 2009) still allows checkpoint signaling.

Analyses of the turnover rates of Bub1 and Bub3 at the kinetochore showed that Bub1 remains stably associated (Howell et al., 2004; Shah et al., 2004) while Bub3 undergoes a more rapid turnover (Howell et al., 2004). This suggests a dynamic interaction between Bub1 and Bub3 and the existence of a Bub3-free pool of Bub1 at

the kinetochore. It is unknown how the Bub1-Bub3 complex is disassembled and which additional function(s) Bub3 might have in checkpoint signaling.

Recent work revealed another conserved motif within Bub1, termed ABBA motif because it is found and functionally relevant in A-type cyclins, Bub1, BubR1 and Acm1. This motif was also shown to have a function in SAC signaling. A peptide containing the Bub1 ABBA sequence was able to bind Cdc20 *in vitro* and cells with mutation of the motif showed reduced levels of Cdc20 at kinetochores and reduced SAC activity (Di Fiore et al., 2015). It has been suggested that Bub1 interacts via the ABBA motif with Cdc20 to localize it to kinetochores and facilitate its phosphorylation by Bub1 and Plk1 (Jia et al., 2016). In addition to the ABBA motif, Bub1 also uses KEN boxes to recruit Cdc20 for efficient phosphorylation leading to catalytic inhibition of the APC/C (Tang et al., 2004; Kang et al., 2008).

A recently described Bub3 chaperone, BuGZ, which was independently identified in human glioblastoma multiforme brain tumor stem cells and mouse embryonic stem cells, shows a KNL1-dependent kinetochore localization and can bind to Bub3 via its GLEBS motif. Knockdown of BuGZ reduces Bub3 protein levels, resulting in less Bub3 at kinetochores. Interestingly, this leads to a reduction of Bub1 levels, but the checkpoint remains active. However, the cells show chromosome alignment defects. Phylogenetic analysis indicates that BuGZ orthologs are highly conserved among eukaryotes, but are absent from yeast. These results suggest that BuGZ has evolved to facilitate Bub3 activity and chromosome congression in higher eukaryotes (Jiang et al., 2014; Toledo et al., 2014). Nevertheless, the question remains how Bub1 can be recruited to the kinetochore without competing with BuGZ for Bub3 binding. A relay model proposes that BuGZ recruits Bub3 to KNL1, subsequently dissociates from and frees Bub3, allowing it to bind free Bub1. But because Bub1-Bub3 mainly exists as a constitutive complex throughout the cell cycle, the priming model instead suggests a BuGZ-facilitated priming of KNL1 for Bub1-Bub3 binding (Ji and Yu, 2014). Future experiments are needed to test these and other possible models.

1.6.3 The role of Mad1 and Mad2 at the kinetochore

Mad1 and Mad2 form a stable heterotetramer in a 2:2 ratio (Sironi et al., 2002). This complex can assemble independently of other checkpoint proteins (Chen et al., 1999), is present throughout the cell cycle (Chen et al., 1999; Brady and Hardwick, 2000) and is recruited to unattached kinetochores and de-localizes from kinetochores

upon microtubule binding (Lara-Gonzalez et al., 2012; Foley and Kapoor, 2013). During interphase, the complex localizes to the nuclear rim through interaction with the nuclear pore complex component Tpr (Mlp1/2 in *S. cerevisiae*, Nup211 in *S. pombe*) (Lee et al., 2008; Schweizer et al., 2013). At the onset of mitosis, the Mad1-Mad2 complex is recruited to unattached kinetochores (Sironi et al., 2001; Sironi et al., 2002), most likely via Bub1 (London and Biggins, 2014; Moyle et al., 2014) and in metazoans also via RZZ (Karess, 2005; Kops et al., 2005a; Maciejowski et al., 2010; Santaguida et al., 2010; Silio et al., 2015). At the kinetochore, Mad1-Mad2 serves as a platform for downstream spindle assembly checkpoint signaling (Figure 1-3 B).

1.6.3.1 Functions of Mad1 and Mad2

Mad1 is essential for SAC signaling as cells lacking Mad1 also lack Mad2 kinetochore localization and are unable to activate the SAC (Luo et al., 2002; Martin-Lluesma et al., 2002; Gillett et al., 2004; Essex et al., 2009; Heinrich et al., 2012). In contrast, artificial kinetochore-recruitment of Mad1 showed co-recruitment of Mad2 and constitutively stimulated checkpoint signaling, regardless of microtubule attachment (Maldonado and Kapoor, 2011). Furthermore, targeting Mad1 to kinetochores during metaphase is sufficient to reestablish SAC activity after initial silencing (Ballister et al., 2014; Kuijt et al., 2014). These results led to the suggestion that the sole function of Mad1 is to serve as binding platform for Mad2 at the kinetochore (Figure 1-3 B).

The Mad1 dimer at the core of the Mad1-Mad2 complex consists of a long inter-molecular coiled-coil in its N-terminus, followed by a Mad2-interacting motif (MIM) and a structured C-terminal region (Sironi et al., 2002; Kim et al., 2012). The stretch that binds Mad2 (MIM) is <20 amino acids long and crucial for interaction with Mad2 (Luo et al., 2002). The C-terminus of Mad1 downstream of the Mad2-interacting motif consists of another coiled-coil region followed by a globular ‘head’ domain containing alpha-helices and beta-sheets (Kim et al., 2012). Both the Mad1 N-terminus and the C-terminus have been implicated in kinetochore targeting of Mad1. Yeast two-hybrid results suggest that the Mad1 N-terminus binds to the kinetochore component Ndc80/Hec1 (Martin-Lluesma et al., 2002) and findings in *X. laevis* point to a role of the N-terminus in kinetochore recruitment (Chung and Chen, 2002). On the other hand, the crystal structure of the Mad1 C-terminus adopted a fold similar to that of the kinetochore-targeting domains of the Ndc80 complex component Spc25 (Kim et

al., 2012), indicating that the Mad1 C-terminus could have a similar binding mode to kinetochores. Nevertheless, Kim et al. were unable to single out a particular domain or motif as the sole kinetochore-targeting region and instead suggest that Mad1 has an unusually extensive kinetochore-binding interface with multiple quasi-independent contacting sites, one of which involves the C-terminus (Kim et al., 2012). In contrast to the data from human cells and *X. laevis,* which suggests an involvement of the Mad1 N-terminus in kinetochore targeting, data from budding and fission yeast strongly implicates the Mad1 C-terminus (Kastenmayer et al., 2005; Scott et al., 2005; Heinrich et al., 2014). The coiled-coil region of the Mad1 C-terminus contains the conserved RLK motif (Arg-Leu-Lys), which was shown to be important for checkpoint activity by facilitating kinetochore localization of Mad1 and interaction with Bub1 (Brady and Hardwick, 2000; Kim et al., 2012; London and Biggins, 2014) (Figure 1-3 B). The molecular basis of the inter-species difference regarding the requirement of different regions of Mad1 for kinetochore binding is not understood.

Mad2 is a relatively small protein that folds as a HORMA domain (Aravind and Koonin, 1998) and is able to adopt two distinct conformations. Binding of closed Mad2 (C-Mad2) to the Mad2-interacting motif (MIM) in Mad1 recruits cytosolic open Mad2 (O-Mad2) through dimerization. This interaction in turn facilitates a conformational change from O- to C-Mad2 and subsequent binding of C-Mad2 to Cdc20. Mad1 and Cdc20 both contain a similar Mad2-interacting motif which enables them to interact with C-Mad2 in a mutually exclusive manner (Luo et al., 2002; Sironi et al., 2002). The C-terminal region of Mad2 that entraps Mad1 or Cdc20 respectively is often referred to as ‘safety belt’ or ‘seatbelt’ since it undergoes a strong conformational change and thereby wraps like a safety belt around the stretch of Mad1 or Cdc20 that contains the MIM (Luo et al., 2002; Sironi et al., 2002; Luo et al., 2004; Mapelli and Musacchio, 2007). Mps1 was shown to be essential for targeting of the Mad1-Mad2 complex to unattached kinetochores, for maintenance of that complex at kinetochores and for recruitment of O-Mad2 to the kinetochore-localized Mad1-C-Mad2 complex, all suggesting that the major role of Mps1 kinase during SAC activation is to facilitate C-Mad2 production at unattached kinetochores for subsequent binding to Cdc20 and assembly of the mitotic checkpoint complex consisting of C-Mad2, Cdc20, BubR1/Mad3 and Bub3 (Hewitt et al., 2010; Tipton et al., 2013).

1.6.3.2 The ‘Mad2 template model’

Long before structural data became available, it was already shown *in vitro* and *in vivo* that APC/C activity is inhibited by binding of Mad2 to the APC/C co-activator Cdc20 (Fang et al., 1998a; Hwang et al., 1998; Kim et al., 1998). This interaction is essential as neither Mad2 mutants that are unable to bind Cdc20 (Sironi et al., 2001; De Antoni et al., 2005a; Nezi et al., 2006) nor Cdc20 mutants lacking the Mad2-interacting motif (Hwang et al., 1998; Kim et al., 1998) are able to activate the SAC. Numerous cell biological, biochemical and structural experiments were performed to elucidate the different steps happening during the spindle assembly checkpoint signaling cascade. One focus lay on finding an explanation how Cdc20 inhibition is linked to SAC signaling.

Early work suggested an ‘exchange model’, which proposes that Mad1 recruits O-Mad2 to the kinetochore and facilitates its conformational change from open to closed Mad2. C-Mad2 subsequently dissociates from Mad1 and binds Cdc20 (Luo et al., 2004). This model depicts Mad1 as a catalyst of the conversion of O-Mad2 into C-Mad2, which, in turn, is required for Mad2 to bind Cdc20 (De Antoni et al., 2005a; Nezi et al., 2006). However, this model is weakened by structural data, indicating that Mad1 and Cdc20 bind to the same site on Mad2, which implies that Mad1 and Cdc20 compete for Mad2 binding, ruling out a role for Mad1 as direct activator of Mad2 for Cdc20 binding (De Antoni et al., 2005a). The ‘Mad2 template model’ takes this finding into account and also incorporates the discovery that the two Mad2 conformers, O- and C-Mad2, can form a conformational dimer with each other (De Antoni et al., 2005a; De Antoni et al., 2005b; Mapelli et al., 2007). In this model, kinetochore-bound Mad1 forms a stable complex with C-Mad2 (Sironi et al., 2002; Simonetta et al., 2009), which acts as a kinetochore receptor or ‘template’ for asymmetric dimerization with a free O-Mad2 molecule which is then converted into C-Mad2 and able to bind Cdc20 (De Antoni et al., 2005a; De Antoni et al., 2005b; Nasmyth, 2005; Yu, 2006; Mapelli et al., 2007) (Figure 1-3 B). In the ‘Mad2 template model’, the Mad1-bound C-Mad2 pool at the kinetochore and the free O-Mad2 pool are distinct and non-exchanging. The model therefore does not imply that Mad1 and Cdc20 compete for Mad2 binding, resolving the contradictions of the Mad2 exchange model (De Antoni et al., 2005a; Nasmyth, 2005; Nezi et al., 2006).

It has been shown that the Mad2-interacting motif of Mad1 and Cdc20 integrates into the beta-sheets of the Mad2 HORMA domain (Sironi et al., 2001; Luo et al., 2002;

Luo et al., 2004) by also adopting a beta-sheet fold (Luo et al., 2002; Luo et al., 2004). To resolve this interaction, a partial unfolding is necessary, which can explain the exceptional stability of the Mad1-Mad2 complex (Chen et al., 1999; Sironi et al., 2001). The finding that two Mad2 molecules form an asymmetric dimer rather than binding to the same conformation is strengthened by *in vitro* binding experiments (De Antoni et al., 2005b) and sterical clashes in the crystal structure (Mapelli et al., 2007). Although Yang et al. (2008) report the crystal structure of a symmetric C–C Mad2 dimer and that it is able to inhibit Cdc20 from activating the APC/C *in vitro*, it is questionable if this unusual complex exists *in vivo.* The cells that were used to analyze SAC activity were supposed to produce solely C-Mad2 by expressing a mutant that renders Mad2 to be constitutively closed (Mad2-L13A) without the ability to adopt the open conformation. But it seems that also a wild type copy of Mad2 was expressed in the same cells, which can adopt both open and closed conformation and interact with the constitutively closed Mad2. This could potentially allow the formation of the asymmetric O-C Mad2 complex, which can inhibit Cdc20.

It was shown that Mad2 requires two highly conserved residues, Arg133 and Gln134 (Arg126, Gln127 in *S. cerevisiae*) for dimerization (Sironi et al., 2001; De Antoni et al., 2005a; De Antoni et al., 2005b; Mapelli et al., 2007). Mutation of either one or both amino acids interferes with Mad2 dimerization (Sironi et al., 2001; Sironi et al., 2002; De Antoni et al., 2005a; De Antoni et al., 2005b; Nezi et al., 2006; Mapelli et al., 2007) and SAC activity (De Antoni et al., 2005a; Nezi et al., 2006). Nevertheless, these mutations still allow Mad2 to undergo its conformational change and therefore do not interfere with Mad1 binding (Sironi et al., 2001; Nezi et al., 2006). While the mutants also retained the ability to bind to Cdc20 *in vitro* (Sironi et al., 2001; Nezi et al., 2006), although with slower kinetics (Sironi et al., 2001; Simonetta et al., 2009), this interaction was not detectable *in vivo* (Nezi et al., 2006). This explains the SAC defect that was observed and underlines the importance of the Mad2 dimerization and conformational change for binding of Cdc20 and effective downstream checkpoint signaling. The ‘template model’ furthermore suggested that the Cdc20-bound C-Mad2 can recruit another O-Mad2 through O-C Mad2 heterodimerization. Hence, the Mad2-Cdc20 complex would serve as a ‘template’ for formation of new Mad2-Cdc20 complexes and thereby amplify itself by self-propagation away from the kinetochores, potentially explaining the sensitivity of the spindle checkpoint (Yu, 2006). However, it was recently shown that the dimerization surface of Mad2 in the Mad2-Cdc20 complex is, when not bound to kinetochores, blocked by Mad3 (Chao et

al., 2012; Mariani et al., 2012). It seems the dimerization interface of Mad2 is required for Cdc20-Mad2 binding at the kinetochores and for stabilization of this complex away from kinetochores (Mariani et al., 2012).

Since O-Mad2 is interacting with a kinetochore-bound stable Mad1-C-Mad2 complex, Mad2 needs to be present in excess over Mad1. Furthermore, all Mad1 is associated with Mad2, at least in human cells (Shah et al., 2004). Experiments performed in budding yeast (Chen et al., 1999; Ghaemmaghami et al., 2003), *X. laevis* (Chen et al., 1998; Chung and Chen, 2002) and human cells (Fava et al., 2011) all support the assumption that the levels of Mad2 exceed those of Mad1, resulting in a Mad1-free pool of Mad2. In addition to measuring the levels of Mad1 and Mad2, FRAP experiments performed in mitotic cells revealed the dynamics of these proteins at kinetochores and gave information about the different Mad2 pools (Howell et al., 2000; Howell et al., 2004; Shah et al., 2004; Vink et al., 2006). Mad1 at kinetochores, presumably bound to Mad2, is mostly nonexchangeable (Howell et al., 2004; Shah et al., 2004). In contrast, two equally sized pools of kinetochore-associated Mad2 either cycle on and off rapidly or are more stably bound (Shah et al., 2004). While the dynamic pool that only transiently localizes to kinetochores most likely corresponds to O-Mad2 being recruited to the Mad1-C-Mad2 complex, the latter presumably represents the stably bound pool (Howell et al., 2004; Shah et al., 2004; Vink et al., 2006). It was furthermore shown that the O-Mad2 conformation is the physiological state of cytosolic Mad2 in the absence of Mad1 or Cdc20 (Luo et al., 2004; De Antoni et al., 2005a). All these findings are in agreement with the Mad2 ‘template model’ and support the critical role of Mad2 dimerization and conformational change during the spindle assembly checkpoint signaling.

1.6.4 The mitotic checkpoint complex (MCC)

1.6.4.1 Proteins that form the MCC

The mitotic checkpoint complex (MCC) is the ultimate effector of the spindle assembly checkpoint and associates with the APC/C, thereby inhibiting its E3 ubiquitin ligase activity and preventing mitotic exit (Musacchio, 2015b). It was shown that Mad2-Cdc20 alone is not sufficient for SAC signaling, as cells lacking Mad3/BubR1 are still able to form the Mad2-Cdc20 complex but nevertheless fail to arrest in mitosis (Hardwick et al., 2000; Chen, 2002; Nilsson et al., 2008; Li et al.,

2010). These findings place Mad3/BubR1 downstream of Mad1 and Mad2 in the SAC signaling cascade and show that it is another essential component for a functional checkpoint. It was originally proposed that MCC isolated from mitotic HeLa cells contains a single copy of Mad2, BubR1, Bub3, and Cdc20 (Sudakin et al., 2001), but newer results expand this view. A 'core' MCC containing a single copy of each subunit seems to bind a second molecule of Cdc20 (Primorac and Musacchio, 2013; Izawa and Pines, 2015; Musacchio, 2015b) (Figure 1-3 C). Recent structures of APC/C-bound MCC obtained by electron microscopy also showed simultaneous binding of two Cdc20 molecules (Alfieri et al., 2016; Yamaguchi et al., 2016).

Mad3, BubR1 and Bub1 share a common ancestor called Madbub, which contains conserved motifs for checkpoint signaling (as seen in Mad3 and BubR1) as well as a functional kinase domain (as seen in Bub1) (Suijkerbuijk et al., 2012a). While the kinase domain in Bub1 is active, the same domain in BubR1 has been shown to be a non-functional 'pseudokinase' due to several inactivating mutations (Suijkerbuijk et al., 2012a). Although the BubR1 kinase domain is inactive and does not contribute to SAC signaling, the kinase domain has been shown to enhance protein stability (Lara-Gonzalez et al., 2011; Suijkerbuijk et al., 2012a; Suijkerbuijk et al., 2012b). The BubR1 and Mad3 orthologs differ in the presence or absence of the C-terminal kinase domain. Organisms like budding or fission yeast express Mad3-like proteins that have lost the kinase domain, whereas organisms such as *D. melanogaster*, *X. laevis* or *H. sapiens* express BubR1-like proteins that still contain the kinase domain (Suijkerbuijk et al., 2012a; Vleugel et al., 2012).

Both BubR1 and Mad3 contain a variety of different domains and motifs that are important for kinetochore localization, MCC formation, Bub3 binding and SAC activity. Both proteins contain two KEN boxes (KEN1 and KEN2, KEN standing for the amino acids Lys, Glu, Asn), which are crucial for checkpoint activity (Burton and Solomon, 2007; King et al., 2007; Sczaniecka et al., 2008; Malureanu et al., 2009; Elowe et al., 2010). KEN1, which is embedded in a helix-loop-helix motif in the very N-terminus of Mad3/BubR1, is required for MCC formation (Davenport et al., 2006; King et al., 2007; Sczaniecka et al., 2008; Elowe et al., 2010; Lara-Gonzalez et al., 2011). Once the core MCC is formed, it can interact with a second, most likely APC/C-associated Cdc20 molecule. KEN2 is located further downstream and is not required for core MCC assembly (Burton and Solomon, 2007; King et al., 2007; Chao et al., 2012). Instead, it blocks substrate recruitment to the APC/C, potentially by occupying the substrate-binding pocket between Cdc20 and the APC/C subunit

Apc10 (Lara-Gonzalez et al., 2011; Chao et al., 2012). Recent work furthermore assigns KEN2 a function in binding the second Cdc20 molecule (Izawa and Pines, 2015; Alfieri et al., 2016; Yamaguchi et al., 2016). The region between the two KEN boxes folds into a TPR domain similar to Bub1 (D'Arcy et al., 2010), which has been shown to interact with KNL1 (Kiyomitsu et al., 2011; Krenn et al., 2012), suggesting a direct interaction with the kinetochore. A region between the TPR domain and KEN2 contains another motif termed the 'D-box mimic', which directly interacts with the WD40-repeats of Cdc20 (Burton and Solomon, 2007; Chao et al., 2012; Izawa and Pines, 2015). It was suggested that the D-box mimic blocks the D-box binding site in Cdc20, which is required for substrate binding. This mode of action was called 'pseudosubstrate inhibition' as BubR1 blocks access of the APC/C to its substrates by competing with these substrates for Cdc20 binding (Burton and Solomon, 2007). While only one D-box mimic can be found in Mad3, BubR1 contains a second such motif in its middle region and the latest MCC-APC/C structures show that both motifs interact with Cdc20 (Alfieri et al., 2016; Yamaguchi et al., 2016). Mad3 and BubR1 contain two more motifs that mediate interaction with Cdc20. These motifs were named A-motif, Phe-box or ABBA motif, depending on the publication, but all describe the same motifs required for interaction with Cdc20 or Cdh1, another co-activator of the APC/C (Burton et al., 2011; Di Fiore et al., 2015; Diaz-Martinez et al., 2015). ABBA motif might be the most descriptive name, as it can be found in cyclin A, BubR1, Bub1, and Acm1 (Di Fiore et al., 2015). The motif is embedded in an 'internal Cdc20-binding site', which was shown to be involved in interaction of BubR1 with Cdc20 and facilitates kinetochore recruitment of Cdc20 (Lischetti et al., 2014; Di Fiore et al., 2015). However, it should be noted that others did not observe any influence of BubR1 on Cdc20 kinetochore localization (Diaz-Martinez et al., 2015). Interestingly, also Bub1 contains an ABBA motif, which is crucial for kinetochore recruitment of Cdc20 (Di Fiore et al., 2015; Vleugel et al., 2015a). Furthermore, both Mad3 and BubR1 contain a GLEBS motif for interaction with Bub3 (Larsen et al., 2007). This motif is truncated in *S. pombe* Mad3, which supposedly lacks the capability to interact with Bub3 (Sczaniecka et al., 2008). BubR1, but not Mad3, additionally contains a kinetochore attachment regulatory domain (KARD) motif preceding the C-terminal kinase, mediating a phosphorylation-dependent interaction with the PP2A phosphatase (Suijkerbuijk et al., 2012b; Kruse et al., 2013; Xu et al., 2013).

Cdc20, another component of the MCC and co-activator of the APC/C is similarly rich in motifs for interaction with other proteins. The initial activation of Cdc20 requires binding of the chaperonin CCT to the WD40 repeats of Cdc20 (Camasses et al., 2003). In its N-terminus, Cdc20 contains a C-box motif important for its co-activator function by mediating interaction with the APC/C (Schwab et al., 2001; da Fonseca et al., 2011; Primorac and Musacchio, 2013; Hein and Nilsson, 2014). Another motif in the Cdc20 N-terminus is the Mad2-interacting motif (MIM), also referred to as the KILR motif (for the amino acids Lys, Ile, Leu, Arg), which was shown to have a double function: mediate binding to the APC/C or interaction with Mad2. Mutation of all four amino acids resulted in loss of ability to bind and activate the APC/C and abolished formation of the MCC (Izawa and Pines, 2012). Interestingly, mutation of only the Arg residue retained APC/C interaction and activation but eliminated binding of Cdc20 to Mad2 (Kim et al., 1998; Zhang and Lees, 2001; Nilsson et al., 2008; Izawa and Pines, 2012). The Cdc20 β-propeller, formed by WD40 repeats, contains several degron binding sites for interaction with BubR1/Mad3 and other Cdc20 substrates that contain D-boxes, KEN-boxes or ABBA motifs (Musacchio, 2015b). The last two amino acids in the C-terminus of Cdc20 are highly conserved forming the IR tail (IR standing for the amino acids Ile, Arg), which was shown to be important for binding the APC/C subunit Apc3 and an active checkpoint (Vodermaier et al., 2003; Izawa and Pines, 2012; Hein and Nilsson, 2014; Zhang et al., 2016).

All these findings together showed that the MCC consists of C-Mad2, Cdc20, BubR1/Mad3 and Bub3 and binds to the APC/C, which can already be associated with a second Cdc20 molecule. Recent studies indicate that Mad2 is present in sub-stoichiometric amounts in the MCC-APC/C complex and may play a catalytic role (Nilsson et al., 2008; Kulukian et al., 2009; Han et al., 2013). Thus, the BubR1-Cdc20 complex has been proposed to be the final inhibitor of the APC/C (Han et al., 2013).

Although in many species Bub3 is part of the MCC, its role in MCC function is unclear. Bub3 forms a complex with BubR1/Mad3 (Hardwick et al., 2000; Fraschini et al., 2001; Larsen et al., 2007), but neither *in vitro* nor *in vivo* studies could find a synergistic effect of Bub3 with Mad2 and Mad3/BubR1 in MCC formation and APC/C inhibition (Fang, 2002; Kulukian et al., 2009; Izawa and Pines, 2015; Alfieri et al., 2016; Yamaguchi et al., 2016). Furthermore, fission yeast MCC lacks Bub3 entirely in the complex and only consist of Mad2, Mad3 and Slp1 (Sczaniecka et al., 2008; Chao et al., 2012).

1.6.4.2 Formation of the MCC

Formation of the mitotic checkpoint complex happens in a stepwise manner and involves interactions between many different motifs in the proteins that make up the MCC (Figure 1-3 B,C). It was shown that the MCC can form away from kinetochores (Kulukian et al., 2009) and directly binds cytosolic APC/C (Herzog et al., 2009), thereby blocking its activity. The first step is the formation of the Mad2-Cdc20 complex, which involves entrapping of the Mad2-interacting motif (MIM/KILR) of Cdc20 with the Mad2 'safety belt' (Nilsson et al., 2008; Sczaniecka et al., 2008; Kulukian et al., 2009). In a second step, Mad3/BubR1 and Bub3 bind to this pre-formed complex and lastly associate with the APC/C (Sudakin et al., 2001). It was shown that the full MCC is a more effective inhibitor of the APC/C than Mad2 alone (Sudakin et al., 2001; Fang, 2002; Kulukian et al., 2009). While the interaction of Mad2 with Cdc20 only involves one region in each of the proteins for their binding, the interaction of Mad3/BubR1 with the Mad2-Cdc20 complex is more complex and involves several different motifs and receptors throughout the proteins (Figure 1-3 C). The N-terminal KEN1 box of Mad3 is embedded in a helix-loop-helix motif which simultaneously interacts with Mad2 and Cdc20. Interaction with Mad2 positions KEN1 towards the KEN receptor on top of the WD40 propeller of Cdc20 (Figure 1-4), underlining the necessity of Mad2 for Mad3-Cdc20 interaction and MCC formation (Tipton et al., 2011; Chao et al., 2012). The Mad2-Mad3 interaction shields the Mad2 dimerization site. This blocks O-Mad2 from accessing Cdc20-bound C-Mad2, so that the complex cannot serve as a 'template' for further C-Mad2-Cdc20 sequestration (Mariani et al., 2012). The crystal structure of the fission yeast MCC only contained one Cdc20 molecule and indicated an interaction of a D-box mimic of Mad3 with the D-box recognition site in the WD40 repeats of Cdc20 (Chao et al., 2012). The new structures of APC/C-bound MCC with two Cdc20 molecules revealed that BubR1 contains two D-box mimics. The D-box in the middle segment of BubR1 (D2) binds to the 'core' Cdc20 ($Cdc20^{MCC}$), while the N-terminal D-box (D1), located between the TPRs and the second KEN box, interacts with the second Cdc20 ($Cdc20^{APC/C}$) and forms the interface between $Cdc20^{APC/C}$ and $Cdc20^{MCC}$ (Alfieri et al., 2016; Yamaguchi et al., 2016) (Figure 1-4, Figure 1-5). This explains how mutating D1 disrupts MCC binding to a second Cdc20 molecule without affecting 'core' MCC integrity (Izawa and Pines, 2015) while mutation of D2 leads to a decrease of MCC formation (Diaz-Martinez et al., 2015). The D-box receptor in Cdc20 is a channel

between blades 1 and 7 of the WD40 propeller (Chao et al., 2012; Alfieri et al., 2016; Yamaguchi et al., 2016) (Figure 1-4, Figure 1-5). Cdc20 with a mutated D-box receptor showed reduced binding to a pre-formed recombinant core MCC *in vitro* but could still be incorporated into the core MCC *in vivo*, indicating that the D-box receptor is required for binding of a second Cdc20 molecule to the core MCC (Izawa and Pines, 2015). BubR1 contains an ABBA motif (A1) in close proximity to D1 and the second KEN2 box. While these motifs were not part of the fission yeast MCC crystal structure, the new EM structures show that all three are binding to $Cdc20^{APC/C}$ (Alfieri et al., 2016; Yamaguchi et al., 2016) (Figure 1-4, Figure 1-5), again confirming the results from previous studies, which indicated that the second KEN box is not involved in 'core' MCC formation but rather mediates binding to the second Cdc20 molecule (Burton and Solomon, 2007; Lara-Gonzalez et al., 2011; Izawa and Pines, 2015). The second ABBA motif (A2), located in the middle region of BubR1, contacts $Cdc20^{MCC}$ (Alfieri et al., 2016) and mutation of this motif was shown to cause a reduction in MCC formation (Di Fiore et al., 2015; Diaz-Martinez et al., 2015). $Cdc20^{MCC}$ and $Cdc20^{APC/C}$ bind to the respective ABBA motifs of BubR1 through an ABBA receptor located between blades 2 and 3 of the WD40 repeats of Cdc20 (Di Fiore et al., 2015; Alfieri et al., 2016) (Figure 1-4, Figure 1-5). Mutation of two residues within the receptor retained the ability of Cdc20 to activate the APC/C but weakened binding of BubR1 *in vitro* and *in vivo* (Di Fiore et al., 2015). Lastly, a CRY degron in Cdc20 mediates interaction between the two Cdc20 molecules (Alfieri et al., 2016; Yamaguchi et al., 2016) (Figure 1-4, Figure 1-5).

It is unclear in how far all these interactions are conserved between BubR1 and Mad3, especially since Mad3 is shorter than BubR1 and does not seem to contain as many Cdc20 binding sites as BubR1. In addition to the two KEN boxes, *S. pombe* Mad3 contains one D-box and two ABBA motifs, first suggested by the MCC crystal structure (Chao et al., 2012) and motif searches with the ABBA consensus sequence Fx[ILV][FHY]x[DE] (Di Fiore et al., 2015). *S. cerevisiae* Mad3 does not contain any amino acid sequence matching the ABBA consensus but does contain a D-box in its C-terminus, mutation of which reduces Cdc20 binding (Burton and Solomon, 2007). It remains to be seen with which of the two Cdc20 molecules the ABBA and D-box motifs that are present in Mad3 are interacting.

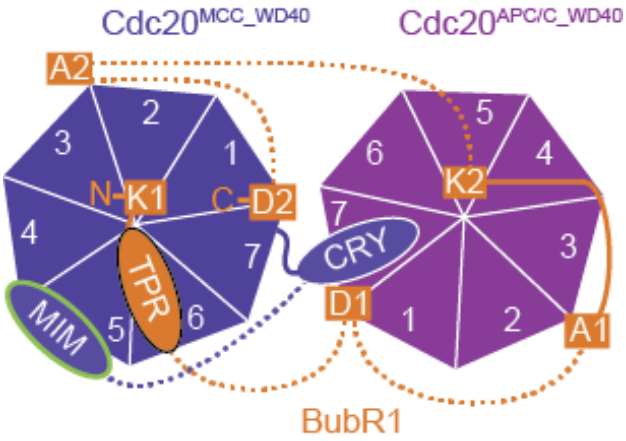

Figure 1-4 Interactions of BubR1 with two Cdc20 molecules
Adapted from Alfieri et al. (2016)
The schematic representation of the top view of the $Cdc20^{MCC}$ and $Cdc20^{APC/C}$ WD40 domains (blades are numbered) shows the positions where BubR1 KEN-boxes (K1, K2), D-boxes (D1, D2) and ABBA motifs (A1, A2) interact with the two Cdc20 molecules. The CRY degron mediates $Cdc20^{MCC}$ interaction with $Cdc20^{APC/C}$ and the MIM sequence of $Cdc20^{MCC}$ provides a Mad2 binding surface. 'N' and 'C' mark the N-terminal and C-terminal ends of BubR1. The solid line depicts a segment of BubR1 that is fully visible in the cryo-EM structure (Alfieri et al., 2016) while dashed lines indicate more flexible and therefore invisible segments (for cryo-EM structure of MCC-APC/C see Figure 1-5).

1.6.4.3 Inhibition of the APC/C

In order to prevent the APC/C from ubiquitinating Cyclin B and Securin, which would promote mitotic exit, Cdc20 needs to be inhibited from activating the APC/C. When the MCC binds the APC/C, $Cdc20^{MCC}$ takes a different position than in the APC/C-Cdc20 complex. As an activator, Cdc20 is positioned opposite of Apc10 and together they form a D-box receptor. Within the core MCC, Cdc20 is shifted away from Apc10 (Herzog et al., 2009; Alfieri et al., 2016; Yamaguchi et al., 2016). This displacement of Cdc20 brings it closer to the catalytic core of the APC/C, which might allow the ubiquitination and subsequent proteolysis of Cdc20, thus turning the APC/C co-activator into an APC/C substrate. As mentioned earlier, it was proposed (Primorac and Musacchio, 2013), and shown (Izawa and Pines, 2015), that the core MCC inhibits APC/C already in complex with the regulatory subunit Cdc20 (APC/C-Cdc20). $Cdc20^{APC/C}$ faces Apc10 and both together form the D-box receptor for binding of APC/C substrates. Newest electron microscopy structures of the MCC-APC/C complex showed strong conformational variability. The whole complex can adopt either an open or a closed conformation, which differ in the rotation of the MCC-$Cdc20^{APC/C}$ assembly relative to the APC/C (Figure 1-3 C). Furthermore, the catalytic core of the APC/C formed by the subunits Apc2 and Apc11 can be found in an up or down position, which determines if the APC/C is catalytically active towards

$Cdc20^{MCC}$ (Alfieri et al., 2016; Yamaguchi et al., 2016). It was shown that Cdc20 abundance fluctuates during the cell cycle and that Cdc20 is ubiquitinated by the APC/C and subsequently degraded both at mitotic exit (Sullivan and Morgan, 2007) and in an MCC-dependent manner during active checkpoint signaling (Reddy et al., 2007; Mansfeld et al., 2011; Foster and Morgan, 2012; Uzunova et al., 2012). Cdc20 degradation can counteract its synthesis in mitosis and reduces the amount of Cdc20 that needs to be inactivated by the checkpoint. Cdc20 may release Mad2 and Mad3 from the APC/C, which could help checkpoint inactivation once the upstream signaling has stopped (Reddy et al., 2007). Upon MCC disassembly, Mad2 has to be re-converted from C-Mad2 to O-Mad2 (Luo et al., 2004; Fava et al., 2011). This ensures the presence of free O-Mad2 available for Cdc20 binding. The molecular mechanisms underlying the disassembly of the MCC and the 'recycling' of Mad2 have just started to be revealed (Musacchio, 2015a).

'Empty' apo-APC/C without Cdc20 has its catalytic core in the 'down' position, which masks the binding site for the E2 ubiquitin-conjugating enzyme, leading to autoinhibition of the APC/C (Chang et al., 2014). If the APC/C is in complex with Cdc20, the catalytic core shifts into the 'up' position and is freed from autoinhibition, allowing the complex to be active and bind and ubiquitinate its substrates (Yamaguchi et al., 2016; Zhang et al., 2016). The MCC docks into the APC/C in a cavity directly below $Cdc20^{APC/C}$, and interacts with $Cdc20^{APC/C}$ such that the two Cdc20 WD40 domains of $Cdc20^{APC/C}$ and $Cdc20^{MCC}$ are arranged in an almost perpendicular fashion (Alfieri et al., 2016). In response to MCC binding, the WD40 domain of $Cdc20^{APC/C}$ is tilted by roughly 40° and rotated 90° about its central axis (Alfieri et al., 2016; Zhang et al., 2016), which disrupts the D-box-binding site formed by the interface of $Cdc20^{APC/C}$ and Apc10 (Chang et al., 2014, 2015). While the IR tail of $Cdc20^{APC/C}$ becomes disengaged from Apc3, the N-terminal domain of $Cdc20^{APC/C}$ maintains the same interactions with Apc8 and Apc1 as seen in APC/C^{Cdc20} (Alfieri et al., 2016; Zhang et al., 2016). BubR1 mediates contacts between the two Cdc20 molecules and furthermore interacts through its TPRs with the winged-helix B (WHB) domain of Apc2, which is part of the catalytic core of the APC/C (Alfieri et al., 2016; Yamaguchi et al., 2016). During active checkpoint signaling when the MCC is bound to the APC/C, the catalytic core is in the 'up' position but the MCC-APC/C complex is closed, which blocks E2 access (Alfieri et al., 2016; Yamaguchi et al., 2016). The C-terminal IR tail of $Cdc20^{MCC}$ binds to a site on Apc8A that is structurally equivalent to the $Cdc20^{APC/C}$ C-box binding site on Apc8B (Chang et al., 2015; Alfieri et al., 2016;

Yamaguchi et al., 2016). Furthermore, the lower surface of the Cdc20^{MCC} WD40 domain interacts with the Apc4 helix-bundle domain (HBD), close to the binding site for the ubiquitin-conjugating enzyme (Brown et al., 2015; Chang et al., 2015; Alfieri et al., 2016). During checkpoint silencing, the MCC presumably rotates into the open position, with the catalytic core still facing up, which allows access for ubiquitin-conjugating enzymes that mediate ubiquitination of Cdc20^{MCC} (Yamaguchi et al., 2016).

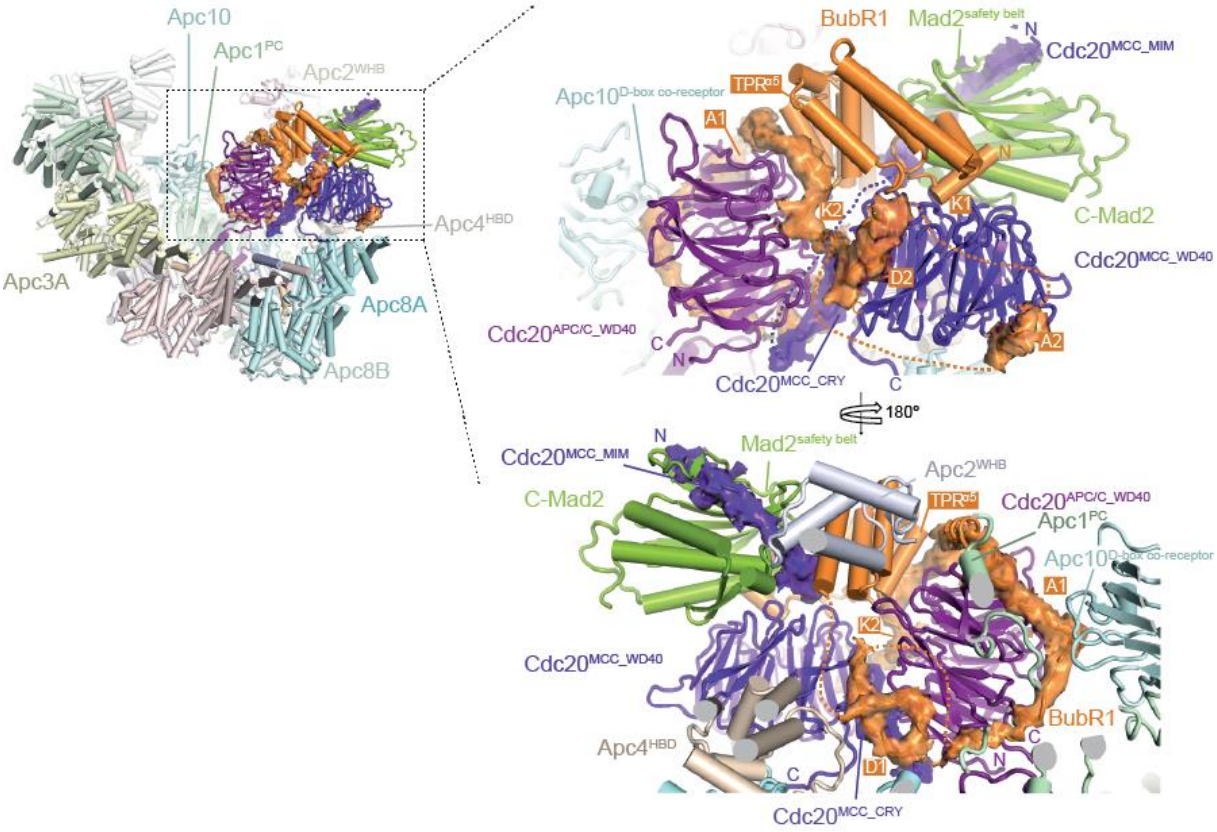

Figure 1-5 Cryo-EM structure of the MCC-APC/C complex
Adapted from Alfieri et al. (2016)
Overall and close-up views show details of the MCC-APC/C complex. Cryo-EM densities of Cdc20-binding KEN-boxes (K1, K2), D-boxes (D1, D2) and ABBA motifs (A1, A2) in BubR1 are shown, as well as Cdc20^{MCC} CRY box and MIM. Interactions of the BubR1 A1 motif with the Apc10$^{D\text{-box co-receptor}}$ and Apc1; BubR1^{TPR} with Apc2^{WHB}; and Cdc20^{MCC} with Apc4^{HBD} are indicated.

The structures of closed MCC-APC/C and APC/C bound to coactivators are similar except for a region containing the platform subunits Apc4, Apc5 and Apc15, which displayed major conformational differences (Alfieri et al., 2016). It was shown that the N-terminal helix of Apc15 influences the transition between open and closed conformations of the MCC-APC/C complex and is necessary to stabilize the complex in the open position (Alfieri et al., 2016). Depletion of Apc15 selectively impairs

Cdc20 ubiquitination during checkpoint signaling without affecting MCC binding to the APC/C or APC/C ubiquitination activity towards other substrates (Mansfeld et al., 2011; Foster and Morgan, 2012; Uzunova et al., 2012). In agreement with these findings, new results showed that APC/C-Cdc20 lacking Apc15 retained substrate ubiquitination activity and could be inhibited by the MCC, but ubiquitination of specifically $Cdc20^{MCC}$ was impaired (Yamaguchi et al., 2016). EM structures of the complex lacking Apc15 showed an increase in the population with the MCC rotated into the closed configuration, accompanied by relative rotation in Apc4 and Apc5 regions (Alfieri et al., 2016; Yamaguchi et al., 2016). Only few complexes adopted the open position but those were still catalytically inactive since Apc2-Apc11 was in the 'down' position, which is typically observed in apo-APC/C and prohibits binding of ubiquitin-conjugating enzymes (Alfieri et al., 2016; Yamaguchi et al., 2016). The shift towards a majority of the MCC-APC/C complexes in the closed position when lacking Apc15 underlines the importance of Apc15 for stabilization of the MCC in the open position to allow Cdc20 ubiquitination.

1.6.5 Influence of protein levels on SAC signaling

For the spindle assembly checkpoint to work reliably and robustly, all aforementioned protein modifications, protein-protein interactions and various complex formations need to take place in a controlled and ordered fashion to sense unattached kinetochores and propagate the checkpoint signal. In addition, the checkpoint needs to tolerate fluctuating protein abundances. A single unattached kinetochore is sufficient to delay anaphase onset (Rieder et al., 1994) and the cells quickly exit mitosis upon removal of the last unattached kinetochore by laser ablation (Rieder et al., 1995). Early work by Rieder et al. (1994) observed no difference in the delay of mitotic exit evoked from a single or several unattached kinetochores and therefore suggested that the checkpoint generates a switch-like 'all-or-none' response. More recent reports instead argue that the checkpoint is rather a quantitative signal (Kops et al., 2005b) and that the extent of APC/C inhibition correlates with the number of unattached chromosomes and the strength of the SAC signal, consistent with a graded SAC response (Collin et al., 2013; Dick and Gerlich, 2013).

The checkpoint does not only need to work reliably, it also needs to be robust towards natural fluctuations in protein abundance. While concentrations of some checkpoint proteins were determined in cell extracts from mammalian cells and

budding yeast and showed a low abundance (Howell et al., 2000; Ghaemmaghami et al., 2003; Poddar et al., 2005; Nilsson et al., 2008), it was unknown if this would also go along with a strong fluctuation that is often seen for low abundant proteins (Bar-Even et al., 2006; Newman et al., 2006). Such variations could potentially cause problems in checkpoint signaling. New data from *S. pombe* show that although the checkpoint proteins are low abundant, their noise level is kept low as well, thus ensuring robust checkpoint signaling (Heinrich et al., 2013).

Normal cells have a robust mitotic checkpoint in which one or more unattached kinetochores can produce a signal that is strong enough to inhibit all cellular APC/C activity and thereby block progression into anaphase. This is not necessarily true when checkpoint components are mutated or their concentrations are altered. Striking examples for this are Mad1 and Mad2. Overexpression of Mad1 sequesters the complete pool of free Mad2 and thereby leads to a checkpoint defect which could be reversed by increasing the amount of Mad2 in *X. laevis* egg extract (Chung and Chen, 2002). In fission yeast, Mad1 overexpression also caused a checkpoint defect but only showed a reduction, not a full sequestration, of the pool of free Mad2 (Heinrich et al., 2013). In contrast, Mad2 overexpression causes a mitotic arrest (He et al., 1997; Chen et al., 1998; Fang et al., 1998a; Kim et al., 1998; Howell et al., 2000; De Antoni et al., 2005a; Sotillo et al., 2007; Essex et al., 2009; Rossio et al., 2010; Rowald et al., 2016) and can overcome the requirement for Mad1 to induce a checkpoint arrest in fission yeast and *X. laevis*, indicating a formation of the inhibitory Mad2-Cdc20 complex independently of Mad1 (Chen et al., 1998; Millband and Hardwick, 2002). In contrast, human cells, budding yeast and *C. elegans* require the presence of Mad1 for a SAC arrest induced by Mad2 overexpression (Sironi et al., 2001; Essex et al., 2009; Rossio et al., 2010). However, one report showed that artificial tethering of Mad2 to Cdc20 can render Mad1 dispensable for a checkpoint arrest in budding yeast (Lau and Murray, 2012). One can speculate that the relative abundance of Mad1 to Mad2 and the strength of the Mad2-Cdc20 interaction are critical for checkpoint signaling. But not only overexpression of checkpoint proteins can cause problems, also lowering the abundance can have negative effects on SAC activity. Reduced levels of Mad2 and BubR1 in human cells and mice by expression from only one intact gene copy instead of two lead to loss of checkpoint activity, resulting in higher chromosome mis-segregation rates and enhanced tumor development (Michel et al., 2001; Dai et al., 2004). Fission yeast also reacted to expression of lower Mad2 or Mad3 levels by reducing or completely losing its ability

to arrest in mitosis, depending on the expression level (Heinrich et al., 2013). This is in agreement with data from budding yeast, where a reduction of Mad2 expression resulted in an increased rate of chromosome loss, which could be rescued by simultaneous reduction of Mad1 levels (Barnhart et al., 2011). At least in fission yeast, a key to checkpoint activity seems to be the relative levels between Mad2, Mad3 and Slp1, the proteins that form the MCC. Reducing the level of Slp1 in cells that were checkpoint defective due to lower Mad2 or Mad3 levels rescued checkpoint activity (Heinrich et al., 2013). In turn, overexpression of Slp1 to about twice the endogenous level enhanced the effect of lowering Mad2 or Mad3, and the checkpoint was impaired even when Mad2 and Mad3 were unchanged (Heinrich et al., 2013). This is in agreement with data from budding yeast showing that overexpression of Cdc20 by about threefold impaired the SAC (Pan and Chen, 2004), suggesting that Mad2 and Mad3 become limiting under this condition.

1.7 Checkpoint silencing

Once kinetochores have been properly attached to the mitotic spindle, the spindle assembly checkpoint signal needs to be quickly and robustly silenced. How the signal is turned off once the checkpoint has been satisfied is only partially understood but recent findings start to shed light onto this process. The checkpoint silencing mechanism involves protein delocalization from kinetochores, disruption of inhibitory protein-protein interactions, MCC disassembly and reversal of mitosis-specific phosphorylations (Etemad and Kops, 2016). Mps1 is the initiator of MCC production and, in human cells and fission yeast, is one of the SAC proteins that needs to be delocalized from kinetochores upon microtubule attachment, as preventing its removal by artificial kinetochore tethering of Mps1 retains SAC proteins at kinetochores and delays SAC silencing (Jelluma et al., 2010; Heinrich et al., 2012; Ito et al., 2012). If Mps1 kinase activates the SAC by phosphorylating some proteins at the kinetochore, the reversal of these phosphorylation events is likely required to silence the checkpoint. Mitotic phosphorylations are counteracted by phosphatases such as PP1 (protein phosphatase 1). PP1 inhibition delays mitotic exit (Pinsky et al., 2009; Vanoosthuyse and Hardwick, 2009) and PP1 recruitment to the N-terminus of KNL1 has been shown to be required for counteracting Aurora B function and support checkpoint inactivation (Meadows et al., 2011; Rosenberg et al., 2011). Therefore, the balance of kinase and phosphatase activity at the kinetochore is likely

central for SAC silencing and KNL1 seems to be placed as a bridge between checkpoint activation (via Bub1) and checkpoint silencing (via PP1). Like seen for Mps1, artificial tethering of Mad1 to bi-oriented chromosomes also prolonged a checkpoint-dependent mitotic arrest after chromosomes have become attached (Maldonado and Kapoor, 2011; Ballister et al., 2014; Kuijt et al., 2014). Removal of Mad1 and Mad2 from kinetochores and transport to the minus-ends of the microtubules is a dynein-dependent process (Howell et al., 2001) but additional dynein-independent de-localization of Mad1 and Mad2 has also been observed (Courtheoux et al., 2007; Gassmann et al., 2010).

Another important part of SAC silencing is the prevention of additional MCC formation and disassembly of the MCC that is already present. The $p31^{comet}$ protein was identified as a Mad2 interactor and can block Mad2 dimerization and MCC formation. $p31^{comet}$ adopts a very similar fold as Mad2, blocks the Mad2-Mad2 dimerization interface and thereby prevents binding of an O-Mad2 molecule to C-Mad2 (Xia et al., 2004; Mapelli et al., 2006; Yang et al., 2007; Teichner et al., 2011; Westhorpe et al., 2011). $p31^{comet}$ seems to act predominantly on the C-Mad2 that is part of the MCC, as O-Mad2 recruitment to Mad1-C-Mad2 complexes at kinetochores is unaffected in cells with altered $p31^{comet}$ levels (Westhorpe et al., 2011). It is unclear how $p31^{comet}$ can distinguish between these two C-Mad2 pools. The $p31^{comet}$-dependent removal of C-Mad2 from the MCC has been suggested to support Mad2 recycling in an active checkpoint, potentially by facilitating the transition from C-Mad2 to O-Mad2 (Westhorpe et al., 2011). Both MCC disassembly and MCC extraction from the APC/C are ATP-dependent processes that depend on energy from ATP hydrolysis (Miniowitz-Shemtov et al., 2010; Teichner et al., 2011). The requirements for $p31^{comet}$ activity and ATP hydrolysis were connected by the recent discovery of the AAA+ ATPase TRIP13/PCH2. TRIP13/PCH2 binds to C-Mad2 which is then converted to O-Mad2 in a manner that depends on ATP hydrolysis and on the activity of $p31^{comet}$ (Eytan et al., 2014; Wang et al., 2014; Ye et al., 2015).

Upon inactivation of the upstream SAC signal, not only APC/C-MCC complexes are disassembled but also free MCCs not bound to the APC/C (Ma and Poon, 2011). MCC disassembly is additionally facilitated by MCC-dependent Cdc20 ubiquitination by the APC/C during SAC silencing and helps to recycle the MCC components (Reddy et al., 2007; Mansfeld et al., 2011; Foster and Morgan, 2012; Uzunova et al., 2012). The APC/C subunit Apc15 is important for the turnover of the MCC on the APC/C (Mansfeld et al., 2011; Uzunova et al., 2012). Human and budding yeast cells

lacking Apc15 exhibit a delayed exit from mitosis without having problems to activate the SAC, indicative for a malfunction in checkpoint silencing (Mansfeld et al., 2011; Foster and Morgan, 2012; Uzunova et al., 2012). In human cells depleted of Apc15, MCC components and ubiquitinated Cdc20 are not released from the APC/C, which prevents crucial substrate ubiquitination by the APC/C at the metaphase-to-anaphase transition once the SAC has been satisfied (Mansfeld et al., 2011; Uzunova et al., 2012). Both $p31^{comet}$-dependent inhibition of Mad2 and ubiquitination of Cdc20 are critical mechanisms of checkpoint inactivation. They act in parallel to promote Mad2 dissociation from Cdc20 (Jia et al., 2011).

If Mps1 kinase activates the SAC by phosphorylating some proteins at the kinetochore, the reversal of these phosphorylation events is likely required to silence the checkpoint. Mitotic phosphorylations are counteracted by phosphatases such as PP1 (protein phosphatase 1). PP1 inhibition delays mitotic exit (Pinsky et al., 2009; Vanoosthuyse and Hardwick, 2009) and PP1 recruitment to the N-terminus of KNL1 has been shown to be required for counteracting Aurora B function and support checkpoint inactivation (Meadows et al., 2011; Rosenberg et al., 2011). Therefore, the balance of kinase and phosphatase activity at the kinetochore is likely central for SAC silencing and KNL1 seems to be placed as a bridge between checkpoint activation (via Bub1) and checkpoint silencing (via PP1).

Neither the dynein-mediated stripping of Mad1 and Mad2 from kinetochores nor the Mad2-interactor $p31^{comet}$ are conserved in yeast. Instead, disassembly of the MCC on the APC/C seems to be the more evolutionarily ancient mechanism as Apc15-dependent checkpoint inactivation through MCC disassembly and Cdc20 ubiquitination as well as kinase-counteracting phosphatases have also been found in yeast (reviewed in Lara-Gonzalez et al., 2012).

Although cells can arrest in mitosis for a long time, satisfaction and silencing of the SAC is not necessarily required to exiting mitosis. This alternative mode of exit, which requires ubiquitination and proteolysis of cyclin B, is termed ‘mitotic slippage’ (Hunt et al., 1992; Andreassen and Margolis, 1994; Brito and Rieder, 2006) and can occur in cancer cells escaping treatment with spindle poisons (Rieder and Maiato, 2004; Gascoigne and Taylor, 2008; Orth et al., 2008; Gascoigne and Taylor, 2009; Chan et al., 2012). If the slow decline in cyclin B levels and thereby CDK activity is indeed the cause for slipping out of mitosis is currently debated. Recent results in *S. cerevisiae* showed an increase in cyclin B levels (Clb2 in *S. cerevisiae*) shortly before mitotic slippage and only then an abrupt degradation (Vernieri et al., 2013). Until now, the

APC/C was the only known ubiquitin ligase to mediate the degradation of cyclin B in mitosis and it was suggested that either a possible failure of the SAC mechanism after a prolonged arrest could lead to APC/C activity (Lee et al., 2010), or, at least in budding yeast, the sudden activation of the APC/C rather than a 'residual' activity in arrested cells causes the mitotic exit (Vernieri et al., 2013). These views both got challenged now by Balachandran et al. (2016) who show that slippage also happens when the APC/C is inactive and identify another ubiquitin ligase ($CRL2^{ZYG11}$) as the one targeting cyclin B in the cells that slip out of a SAC arrest when the APC/C is inhibited. Mitotic slippage was in part viewed as a breakdown of the checkpoint mechanism in response to artificial and prolonged spindle drug treatment. The discovery of the $CRL2^{ZYG11}$ pathway of cyclin B degradation suggests for the first time that slippage is a genuine cellular safety mechanism (Brandeis, 2016).

1.8 Aim of this study

The spindle assembly checkpoint is a highly conserved and essential cellular safeguard that prevents eukaryotic cells from missegregating chromosomes. Despite extensive knowledge about the individual proteins that make up the checkpoint signal, which was obtained by cell biological, biochemical and structural studies, the complex interplay between checkpoint proteins *in vivo* still remains only partially understood.

One salient question is the connection between the Bub1-Bub3 complex and Mad1. While *in vivo* studies indicated an interaction between Mad1 and Bub1, an understanding of the detailed mechanism was largely missing. Therefore, I wanted to address if this functional connection is conserved across species by analysis of point mutants of fission yeast Mad1 and Bub1 that were shown to abolish the interaction between these two proteins in budding yeast. Since a crystal structure of the Mad1 C-terminus revealed a highly organized globular fold and furthermore contained the putative Bub1-binding motif, I wanted to determine if and how the Mad1 C-terminus is involved in checkpoint signaling.

Moreover, I also wanted to investigate how the kinetochore-recruitment of Bub1-Bub3 to phosphorylated MELT motifs of Spc7/KNL1 influences checkpoint activity and how this is linked to recruitment of Mad1 to promote checkpoint signaling.

Another aspect of the checkpoint that was explored for a long time without being fully understood is the nature of the mitotic checkpoint complex and how it manages to

prevent Cdc20 from activating the APC/C prematurely in mitosis. Following reports about several motifs in human BubR1 that mediate interaction with Cdc20 and the finding that the human MCC can simultaneously bind two Cdc20 molecules, I tested if this property is conserved in *S. pombe*. In addition to immunoprecipitation experiments to reveal a possible binding of a second Slp1/Cdc20 molecule to the MCC, I also mutated motifs in Mad3 that were shown to mediate Cdc20 binding in BubR1 of other organisms to dissect their role in MCC formation and checkpoint signaling. In the context of these experiments, we found that *S. pombe* differed from other organisms in that deletion of the APC/C subunit Apc15 resulted in a defect in checkpoint activity rather than checkpoint silencing. The phenotype is similar to some Mad3 mutants, which raises interesting further questions about the biochemistry of the APC/C inhibition by the MCC.

2 Results

2.1 Mad1 contribution to spindle assembly checkpoint signaling goes beyond presenting Mad2 at kinetochores

Stephanie Heinrich[1], Katharina Sewart[1], Hanna Windecker[1,2], Maria Langegger[1], Nadine Schmidt[1], Nicole Hustedt[1,3], Silke Hauf[1]

[1]Friedrich Miescher Laboratory of the Max Planck Society, Tübingen, Germany
[2]Present address: IMB (Institute of Molecular Biology), Mainz, Germany
[3]Present address: Friedrich Miescher Institute, Basel, Switzerland

Correspondence: silke.hauf@vt.edu

Published in **EMBO Reports**, Volume 15, p.291-298 (2014)
DOI: 10.1002/embr.201338114

Author contributions:
I performed the experiments and analyzed the data shown in Fig. 1G, H; Fig. 2D,E,F(right); Fig. 3E,F,H; Fig. S1C; Fig. S2B; Fig. S3A (*cdc25-22* arrest),C and Fig. S4C,D,H. Furthermore, I performed the experiments shown in Fig. 3G (analysis was performed by **Stephanie Heinrich**) and Supplementary Information (Mad1 IP for re-annotation of start codon). In addition, together with Maria Langegger and Nadine Schmidt, I gave input to the writing of the manuscript.

Stephanie Heinrich performed the experiments and analyzed the data shown in Fig. 1C,D,F; Fig. 2A-C,F(left); Fig. 3B-D; Fig. S1A,B,D,F; Fig. S2C-E and Fig. S4B,G and contributed to writing the manuscript together with Silke Hauf.

Hanna Windecker constructed the Mad1-RLK/AAA mutant, and performed the experiments in Fig. 1E and Fig. S1B.

Maria Langegger performed the experiments and analyzed the data shown in Fig. 1F (Mad1-RLK/ALA mutant), Fig. S2F and Fig. S4A.

Nadine Schmidt performed the experiments and analyzed the data shown in Fig. 1 J-L; Fig. S1G-I and Fig. S3B.

Nicole Hustedt performed the experiments and analyzed the data shown in Fig. S3A (*nda3-KM311* arrest).

Silke Hauf supervised the study and wrote the manuscript together with Stephanie Heinrich and with input by the other authors.

Published online: January 29, 2014

Scientific Report

SOURCE DATA | TRANSPARENT PROCESS | OPEN ACCESS

EMBO reports

Mad1 contribution to spindle assembly checkpoint signalling goes beyond presenting Mad2 at kinetochores

Stephanie Heinrich, Katharina Sewart[†], Hanna Windecker[‡], Maria Langegger, Nadine Schmidt, Nicole Hustedt[§] & Silke Hauf[*,†]

Abstract

The spindle assembly checkpoint inhibits anaphase until all chromosomes have become attached to the mitotic spindle. A complex between the checkpoint proteins Mad1 and Mad2 provides a platform for Mad2:Mad2 dimerization at unattached kinetochores, which enables Mad2 to delay anaphase. Here, we show that mutations in Bub1 and within the Mad1 C-terminal domain impair the kinetochore localization of Mad1:Mad2 and abrogate checkpoint activity. Artificial kinetochore recruitment of Mad1 in these mutants co-recruits Mad2; however, the checkpoint remains non-functional. We identify specific mutations within the C-terminal head of Mad1 that impair checkpoint activity without affecting the kinetochore localization of Bub1, Mad1 or Mad2. Hence, Mad1 potentially in conjunction with Bub1 has a crucial role in checkpoint signalling in addition to presenting Mad2.

Keywords fission yeast; kinetochore; Mad1; mitosis; spindle assembly checkpoint

Subject Categories Cell Cycle; Chromatin, Epigenetics, Genomics & Functional Genomics

DOI 10.1002/embr.201338114 | Received 16 October 2013 | Revised 8 January 2014 | Accepted 9 January 2014 | Published online 28 January 2014

EMBO Reports (2014) 15, 291–298

See also: **T Kruse *et al*** (March 2014)

Introduction

Mad1 is part of the spindle assembly checkpoint, a conserved mitotic signalling pathway that protects genome integrity by monitoring chromosome attachment to the mitotic spindle and delaying anaphase until all chromosomes have achieved proper attachment [1]. Mad1 forms a tetrameric complex with the checkpoint protein Mad2 [2]. At unattached kinetochores, Mad1-bound Mad2 dimerizes with soluble Mad2 to induce binding of the latter to Cdc20 [1,3], an essential co-activator of the anaphase-promoting complex/cyclosome (APC/C) [4]. This enables binding of Mad3 (BubR1 in many organisms) to Cdc20 to form the mitotic checkpoint complex (MCC), which is a potent inhibitor of the APC/C [4–6]. In *S. pombe*, the kinases Ark1 and Mph1, as well as Bub1 and Bub3, are required to bring Mad1:Mad2 to unattached kinetochores [7]. Similar dependencies exist in other organisms [1]. Consistent with the important role of the Mad1:Mad2 complex in initiating Cdc20 inhibition, preventing the Mad1:Mad2 interaction abolishes checkpoint activity [8–11]. Hence, Mad1 is important to present Mad2 at unattached kinetochores.

Mad1 has approximately 80 kDa; yet, the stretch that binds Mad2 is <20 amino acids long. This raises the question whether the remaining parts only have a structural role. The Mad1 part N-terminal to the Mad2-binding site is predicted to form a long coiled-coil. The structure of the C-terminal end of this coiled-coil (α1) together with the Mad2-binding site bound to Mad2 as well as a C-terminal helix (α2) indicated that α1 mediates Mad1 dimerization [2]. Another structure of the C-terminal part following α2 showed another intermolecular coiled-coil (α3) and a globular head [12] (see Figs 1A and 4A). The Mad1 C-terminus has repeatedly been implicated in kinetochore binding [12–14]; some studies have suggested a role for the N-terminus [15,16]. Budding yeast Mad1 interacts with Bub1, which requires a conserved motif (RLK, Arg-Leu-Lys) in the Mad1 α3 helix [17] and a conserved stretch in Bub1 [18]. This interaction is important for checkpoint activity [17], and in human cells, the RLK motif is required for kinetochore localization of Mad1 [12]. Overall, these observations indicate that the structured parts of Mad1 are required to bring the Mad1:Mad2 complex to kinetochores to allow checkpoint signalling, potentially through an interaction between Mad1 and Bub1.

Here, we show using fission yeast that the Mad1 C-terminus promotes checkpoint activity in a way that is independent of its role in bringing the Mad1:Mad2 complex to kinetochores.

Friedrich Miescher Laboratory of the Max Planck Society, Tübingen, Germany
*Corresponding author. Tel: +1 540 231 7318; Fax: +1 540 231 2606; E-mail: silke.hauf@vt.edu
[†]Current address: Department of Biological Sciences and Virginia Bioinformatics Institute, Virginia Polytechnic Institute and State University, Blacksburg, VA, USA
[‡]Current address: Institute of Molecular Biology (IMB), Mainz, Germany
[§]Current address: Friedrich Miescher Institute, Basel, Switzerland

© 2014 The Authors. This is an open access article under the terms of the Creative Commons Attribution-NonCommercial-NoDerivs License, which permits use and distribution in any medium, provided the original work is properly cited, the use is non-commercial and no modifications or adaptations are made.

Published online: January 29, 2014
EMBO reports

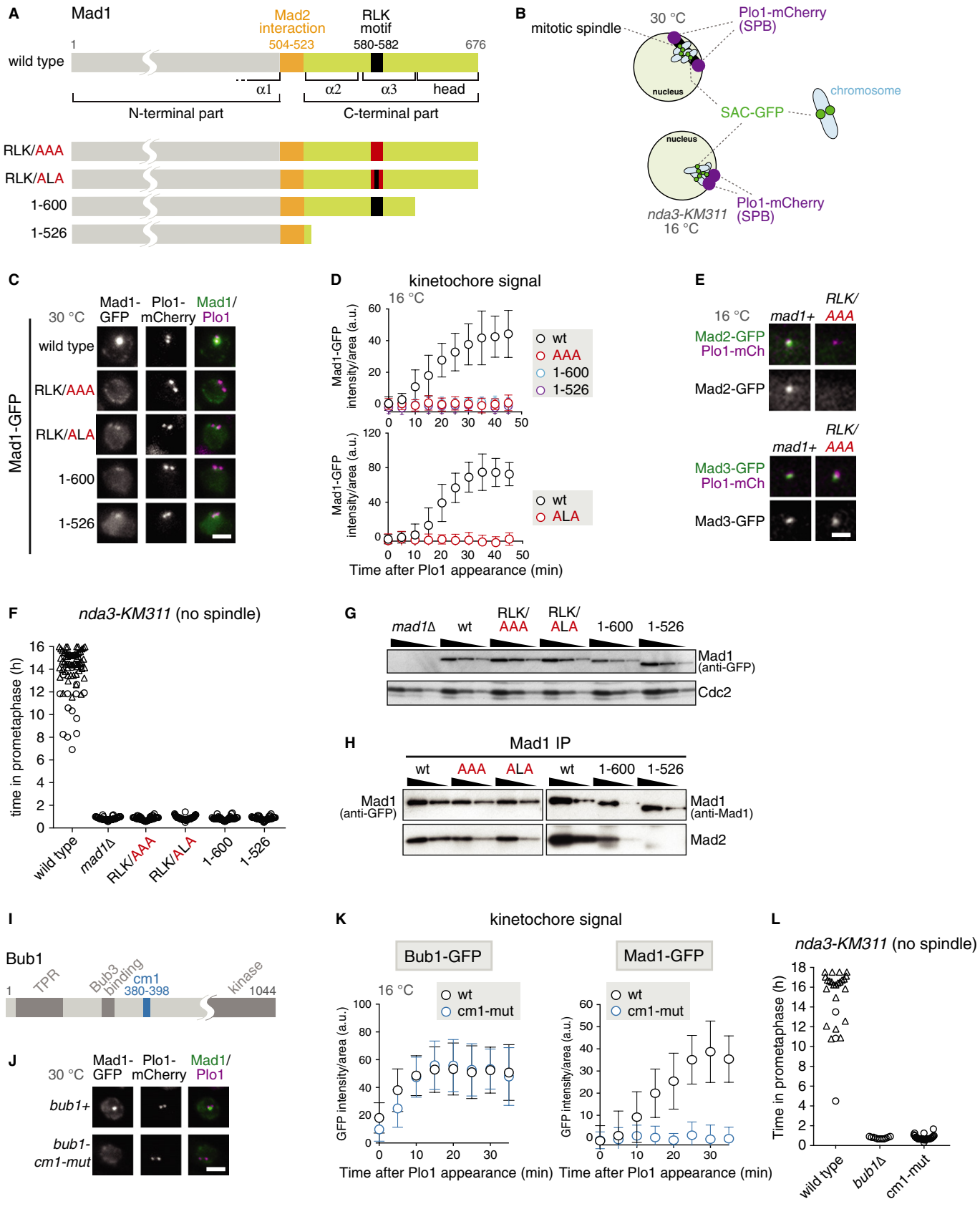

© 2014 The Authors

Figure 1. The Mad1 RLK motif and Bub1-cm1 are required for Mad1 kinetochore localization and checkpoint activity.

A Domain structure of Mad1; point mutations and truncations employed in this study.

B Schematic of fission yeast nuclei in prometaphase. Shown are the three chromosomes (light blue), the mitotic spindle (black) and kinetochores decorated with GFP-tagged SAC components (green). Plo1-mCherry (purple) is specifically recruited to spindle pole bodies (SPBs) in mitosis [37]. In interphase and early mitosis, kinetochores cluster at SPBs. In the conditional *nda3-KM311* tubulin mutant, microtubule formation is impaired at restrictive temperature (16°C) and spindle pole bodies are unable to separate. Signals from the three chromosomes can typically not be microscopically resolved at early mitosis.

C Cells expressing *plo1+-mCherry*, *nda3-KM311* and the indicated Mad1-GFP fusion proteins were grown at the permissive temperature for *nda3-KM311* (30°C). Representative nuclei of mitotic cells are shown; Plo1 was used as marker for mitosis (scale bar: 2 μm; see Supplementary Fig S1A for a larger field of view).

D The same strains as in (C) were analysed at the restrictive temperature for *nda3-KM311* (16°C), which prevents microtubule formation. Cells were followed by live-cell microscopy and the Mad1-GFP signals were quantified at the kinetochore as cells entered mitosis (a.u. = arbitrary units; error bars = s.d.; $n \geq 20$ cells).

E Cells expressing *plo1+-mCherry*, *nda3-KM311*, the indicated GFP fusion proteins and either wild-type Mad1 (*mad1+*) or *mad1-RLK/AAA* were imaged at 16°C. Representative nuclei of mitotic cells are shown. Scale bar: 2 μm.

F Cells expressing *plo1+-mCherry* and *nda3-KM311* and the indicated mutations or truncations in *mad1* were analysed by live-cell imaging at 16°C. The time that each cell spent in prometaphase was determined by the localized Plo1-mCherry signal at SPBs (circle). Cells that had not yet exited mitosis when filming stopped are indicated by triangles.

G Immunoblotting of cell extracts using anti-GFP (to detect the Mad1-GFP fusion proteins) and anti-Cdc2 (loading control) antibodies. A dilution series was loaded for each strain to compare intensities.

H Anti-Mad1 immunoprecipitations of the indicated strains were analysed for the presence of Mad1 and Mad2 using anti-GFP (left), anti-Mad1 (right) and anti-Mad2 antibodies. Input and flow through are shown in Supplementary Fig S1C.

I Domain structure of Bub1 (TPR: tetratricopeptide repeats; Bub3 binding: Bub3-binding motif, also called GLEBS; cm1: conserved motif 1; kinase: kinase domain).

J Cells expressing *mad1+-GFP*, *plo1+-mCherry*, *nda3-KM311* and either wild-type Bub1 (*bub1+*) or the Bub1-cm1-mutant (*bub1-cm1-mut*) were imaged at 30°C as in (C). Representative nuclei of mitotic cells are shown (scale bar: 2 μm; see Supplementary Fig S1H for a larger field of view). The Bub1-cm1 mutant contains aa changes S381A, T383A and T386A (alignment in Supplementary Fig S1E). The cellular abundance of wild-type and mutant Bub1-GFP was similar (Supplementary Fig S1F).

K Bub1-GFP or Mad1-GFP signals were quantified at the kinetochore as in (D) (a.u. = arbitrary units; error bars = s.d.; $n \geq 24$ cells for Bub1-GFP, $n \geq 18$ cells for Mad1-GFP).

L Checkpoint function of the indicated strains was analysed as in (F).

Source data are available online for this figure.

Results and Discussion

Mad1-RLK motif and Bub1-conserved motif 1 are required for kinetochore localization of Mad1 and checkpoint activity

To assess potential roles of Mad1 apart from Mad2-binding, we focused on the RLK motif (amino acid (aa) 580–582) within α3 [17]. When we mutated all motif residues to alanine in *S. pombe*, kinetochore localization of Mad1 and Mad2 was impaired (Fig 1A, C–E), whereas localization to the nuclear envelope stayed intact (Supplementary Fig S1A and D). Checkpoint activity was lost in the Mad1-RLK/AAA mutant (Fig 1F), although kinetochore localization of Ark1, Bub1, Bub3 and Mad3 was preserved (Fig 1E, Supplementary Fig S1B) and although Mad1-RLK/AAA was present at normal levels (Fig 1G) and the Mad1:Mad2 interaction was intact (Fig 1H). This suggests that the failure to bring Mad1:Mad2 to kinetochores causes the checkpoint defect. A similar loss of Mad1 localization and checkpoint activity occurred when only the outward-facing amino acids R and K of the RLK motif were mutated or when the C-terminus was truncated (Fig 1). The latter supports results from budding yeast [19]. Like RLK/AAA, the RLK/ALA mutation preserved Mad2 interaction, whereas truncation of the C-terminus led to a gradual loss of this interaction (Fig 1H). Although the Mad1 C-terminus was necessary for kinetochore binding (Fig 1C and D), it did not seem sufficient (Supplementary Fig S2). In contrast to the C-terminus, the Mad1 N-terminus was required for nuclear envelope localization, but was at least partly dispensable for kinetochore localization (Supplementary Fig S2).

The RLK motif has been implicated in binding to Bub1 in budding yeast [17,18], which involves a region of Bub1 that contains the "conserved motif 1" (cm1; [20]). Indeed, mutation of Bub1-cm1 phenocopied Mad1-RLK mutants (Fig 1I–L). Bub1 itself (Fig 1K) as well as Bub3 and Mad3 (Supplementary Fig S1I) still localized to kinetochores, but Mad1 and Mad2 were strongly reduced (Fig 1J and K, Supplementary Fig S1I) and cells lacked checkpoint activity (Fig 1L). We conclude that the C-terminus of Mad1 (with the RLK motif) and Bub1-cm1 are involved in recruiting Mad1 to kinetochores and both regions are important for checkpoint function.

The Mad1 RLK motif and Bub1-cm1 promote checkpoint activity independently of their role in Mad1 kinetochore localization

Since Bub1 and Mad1 have been observed to interact in budding yeast [17], it is conceivable that Bub1 and Mad1 interact through cm1 and RLK motif and that this interaction is required for Mad1 kinetochore localization and checkpoint activity. Surprisingly, we were unable to detect an interaction between these two proteins when immunoprecipitating either of them from cells with an active checkpoint (Supplementary Fig S3A and B), similar to the situation in human cells [12]. To test whether the loss of checkpoint activity in the Mad1-RLK/AAA or Bub1-cm1 mutant (Fig 1F and L) is at all related to the loss of Mad1 from kinetochores, we tested checkpoint activity after artificially recruiting Mad1 to kinetochores through fusion to the kinetochore protein Mis12 (Fig 2). Although the levels of tethered Mad1 at unattached kinetochores were slightly lower than for wild-type Mad1 (Fig 2E and F), the checkpoint was functional at least in a large fraction of the cells (Fig 2B and D). Tethering of Mad1-RLK/AAA, however, did not provide checkpoint activity (Fig 2B), even though Mad2 was co-recruited to the kinetochore at similar levels as in tethered wild-type Mad1 (Fig 2F). Similarly, artificially recruiting Mad1 in either *bub1Δ* or *bub1-cm1* cells did not restore the checkpoint (Fig 2D and E). This suggests that Bub1-cm1 and the Mad1 C-terminus have an additional role within the spindle assembly checkpoint, apart from recruiting Mad1 and Mad2 to kinetochores.

© 2014 The Authors

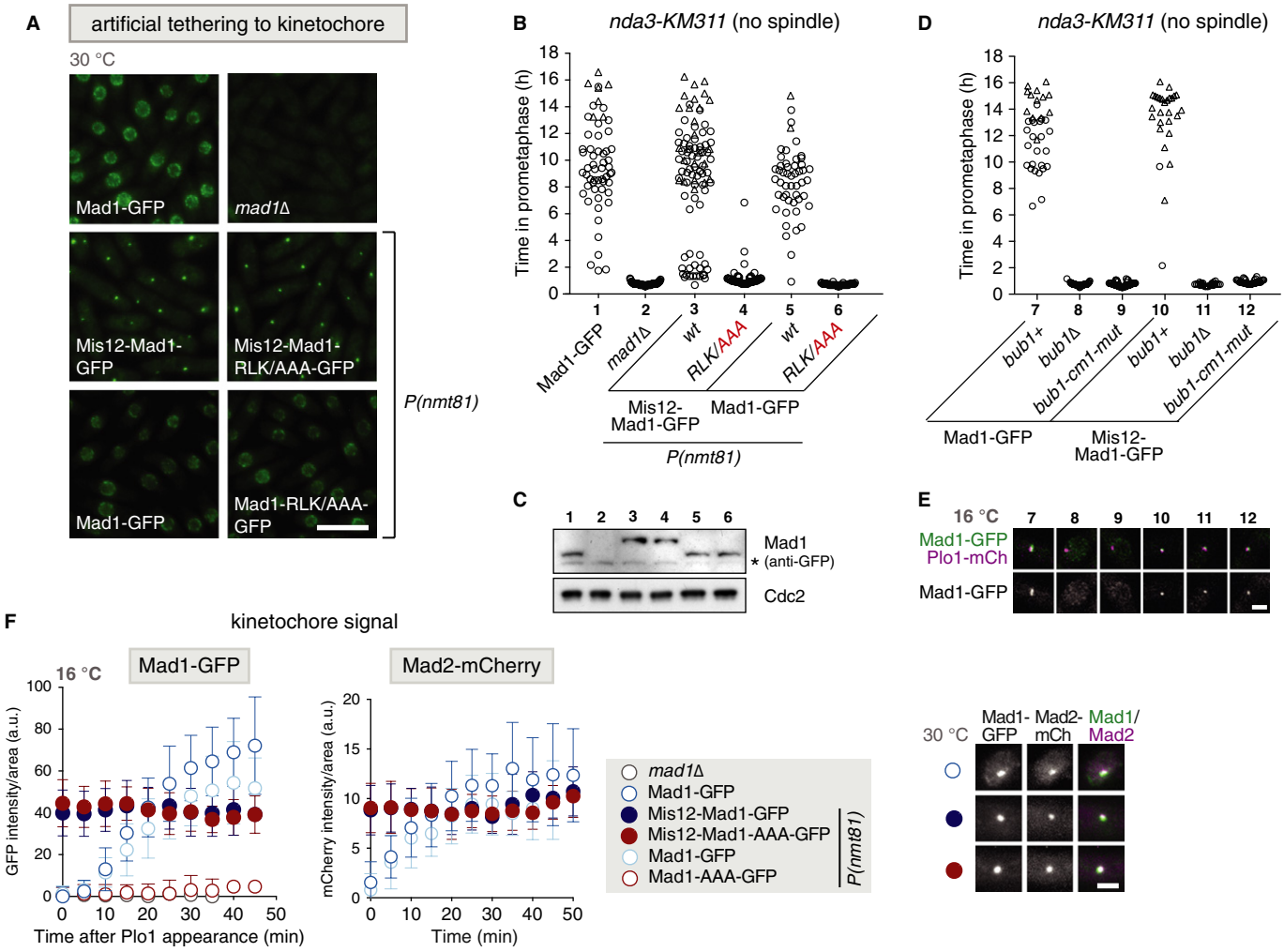

Figure 2. The Mad1 RLK motif and Bub1-cm1 have a role in signalling beyond their role in Mad1 kinetochore localization.

A Representative images of cells expressing *nda3-KM311* and the indicated GFP fusion proteins. Cells were imaged at the permissive temperature for *nda3-KM311* (30°C). Fusion to the kinetochore protein Mis12 artificially tethers Mad1 to the kinetochore. Some constructs were expressed from the inducible *nmt81* promoter, *P(nmt81)*; the endogenous *mad1* gene was deleted in these strains. Scale bar: 10 μm.

B Checkpoint function of cells expressing *plo1+-mCherry*, *nda3-KM311* and the indicated Mad1-GFP fusion proteins [same strains as in (A)] was analysed at 16°C as in Fig 1F.

C Immunoblotting of cell extracts using anti-GFP and anti-Cdc2 (loading control) antibodies. Strains are the same as in (A) and (B). The asterisk indicates a cross-reaction of the antibody.

D Checkpoint function of cells expressing *plo1+-mCherry*, *nda3-KM311* and the indicated *bub1* variants and Mad1-GFP fusion proteins was analysed as in Fig 1F.

E Representative nuclei of mitotic cells of the strains analysed in (D). Scale bar: 2 μm.

F Mad1-GFP (from cells in (B)) or Mad2-mCherry signals were quantified at the kinetochore as cells entered mitosis (a.u. = arbitrary units; error bars = s.d.; $n \geq 20$ cells). Representative nuclei are shown on the right. (Scale bar: 2 μm; see Supplementary Fig S3C for a larger field of view).

Source data are available online for this figure.

Mutations in the C-terminus of Mad1 abolish checkpoint signalling although kinetochore localization of Bub1, Mad1 and Mad2 is intact

If Bub1 and Mad1 have an additional role in the checkpoint, unrelated to Mad1 kinetochore localization, it should be possible to identify separation-of-function mutants that preserve kinetochore localization but are deficient in checkpoint signalling. We screened for such mutations in the structured and conserved C-terminus of Mad1. An initial screen narrowed down the region of interest to the very C-terminus (Supplementary Fig S4A). We noticed a conserved, negatively charged surface patch on "top" of the Mad1 "head," which we either mutated (EDD/QNN) or which we removed by truncating the protein before the last α helix (Δhelix) (Fig 3A). Both mutants maintained Mad1 kinetochore localization (Fig 3B and C), but strongly or entirely lost checkpoint activity (Fig 3D), despite being present at similar levels as wild-type Mad1 (Fig 3E). Both immunoprecipitation (Fig 3F) and co-recruitment to the kinetochore (Fig 3G, Supplementary Fig S4C) demonstrated that the interaction of Mad1 with Mad2 was largely preserved. In addition, Bub1 still

 © 2014 The Authors

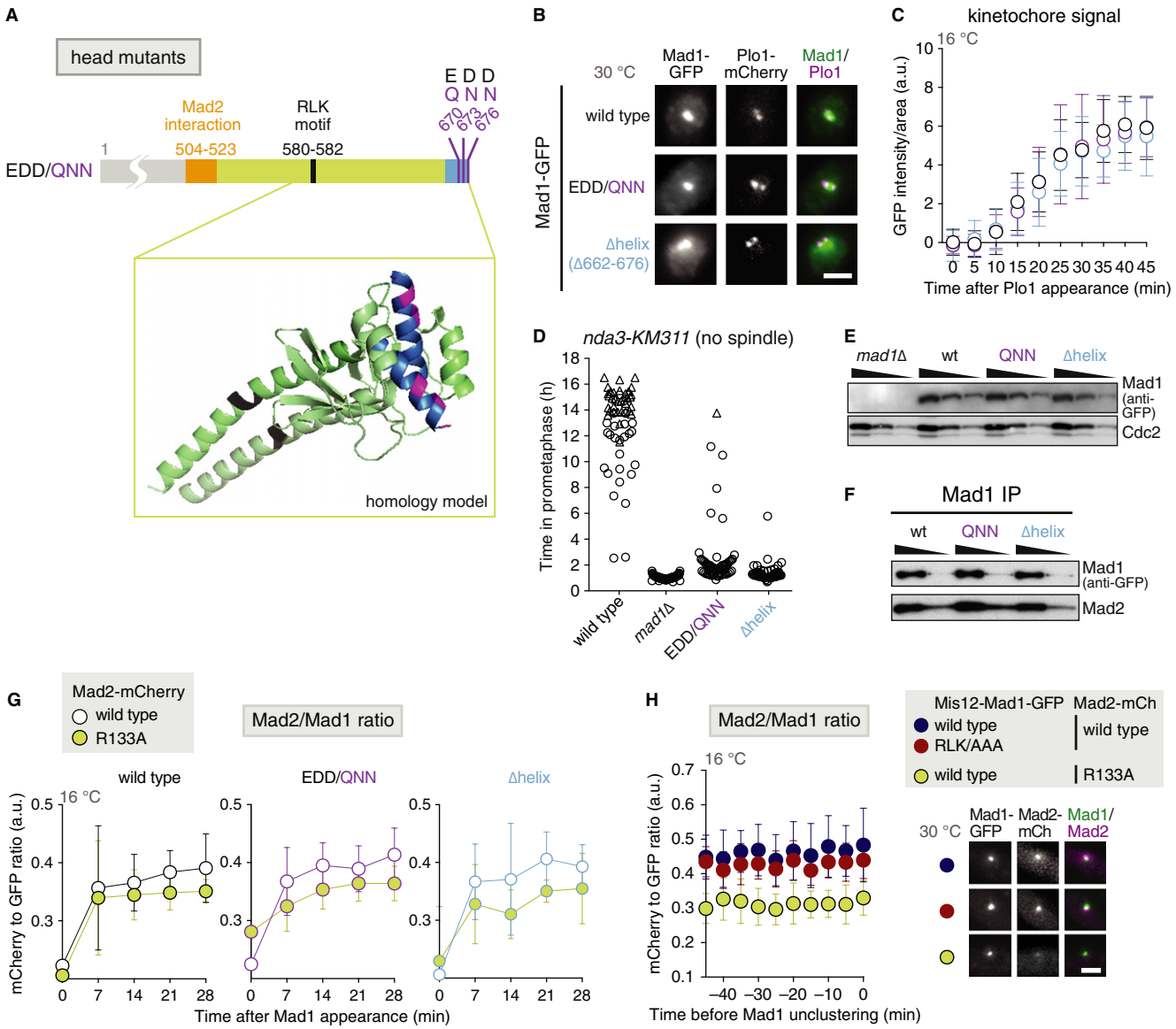

Figure 3. The top of the globular C-terminal head of Mad1 is required for checkpoint signalling, but not for kinetochore localization of Mad1:Mad2.

A Position of the head mutations in Mad1. The inset shows a homology model of the C-terminus of *Schizosaccharomyces pombe* Mad1 (aa 562-676) based on the crystal structure of the dimeric *H. sapiens* Mad1 C-terminal domain (PDB code: 4ZDO, [12]). (black: RLK motif (aa 580-582); blue: last helix of the C-terminal head (aa 662-676); purple: aa E670/D673/D676).

B Cells expressing *plo1+-mCherry*, *nda3-KM311* and the indicated Mad1-GFP fusion proteins were imaged as in Fig 1C. Representative nuclei of mitotic cells are shown (scale bar: 2 μm; see Supplementary Fig S4B for a larger field of view).

C The same strains as in (B) were analysed at the restrictive temperature for *nda3-KM311* (16°C) as in Fig 1D. Mad1-GFP signals were quantified at the kinetochore as cells entered mitosis (a.u. = arbitrary units; error bars = s.d.; $n \geq 22$ cells).

D Checkpoint function of the indicated strains was analysed at 16°C as in Fig 1F.

E Immunoblotting of cell extracts using anti-GFP and anti-Cdc2 (loading control) antibodies. A dilution series was loaded for each strain to compare intensities. Strains are the same as in (D).

F Anti-Mad1 immunoprecipitations of the indicated strains were analysed for the presence of Mad1 and Mad2 using anti-GFP and anti-Mad2 antibodies. Input and flow through of the immunoprecipitation are shown in Supplementary Fig S4D.

G Cells expressing *nda3-KM311*, the indicated *mad1-GFP* constructs and either *mad2+-mCherry* or *mad2-R133A-mCherry* were followed by live-cell imaging at 16°C. The Mad2-mCherry/Mad1-GFP ratio at kinetochores was determined as cells entered mitosis (a.u. = arbitrary units; error bars = s.d.). Mad1-wt + Mad2-wt: $n = 13$; Mad1-wt + Mad2-R133A: $n = 21$; Mad1-QNN + Mad2-wt: $n = 16$; Mad1-QNN + Mad2-R133A: $n = 14$; Mad1-Δhelix + Mad2-wt: $n = 10$; Mad1-Δhelix + Mad2-R133A: $n = 8$; statistical analysis in Supplementary Fig S4E. Representative images for Mad1-GFP and Mad2-mCherry localization in Supplementary Fig S4C.

H Strains were followed by live-cell imaging as in (G) and Fig 2F. The Mad2-mCherry/Mad1-GFP ratio at kinetochores was determined as cells entered mitosis (a.u. = arbitrary units; error bars = s.d.; $n \geq 14$ cells; statistical analysis in Supplementary Fig S4F). Representative nuclei are shown on the right (scale bar: 2 μm).

Source data are available online for this figure.

© 2014 The Authors

localized to kinetochores (Supplementary Fig S4G). Hence, in these Mad1 mutants Bub1, Mad1 and Mad2 are at kinetochores; yet, checkpoint signalling is strongly impaired.

The C-terminal part of Mad1 (α3 and head) has been proposed to fold back onto Mad1-α2 [2], which would bring the Mad1 head in close vicinity to Mad2. Because Mad1-bound Mad2 needs to dimerize with additional Mad2 to support checkpoint function [3,21], we suspected that the Mad1 C-terminal head promotes this dimerization. As in human cells [22], the Mad2/Mad1 ratio at kinetochores is reduced in a dimerization-deficient Mad2 mutant (Mad2-R133A [23]; Fig 3G), presumably because Mad2 cannot be recruited to the kinetochore through Mad2:Mad2 dimerization, but only through binding to Mad1. In both the Mad1-EDD/QNN and -Δhelix mutant, the Mad2/Mad1 ratio at kinetochores was similar to Mad1 wild-type cells, and in both mutants, there was less Mad2 relative to Mad1 at kinetochores when the Mad2-R133A mutant was expressed instead of wild-type Mad2 (Fig 3G). This strongly indicates that Mad2 dimerization is intact. Similarly, the Mad2/Mad1 ratio after artificially tethering Mad1-RLK/AAA was more similar to wild-type than to Mad2-R133A-expressing cells (Fig 3H). Hence, the Mad1 C-terminal head and the RLK motif promote checkpoint function, but seemingly not through facilitating Mad2 dimerization.

Our data indicate that the C-terminal head of Mad1 has a previously unrecognized role in checkpoint signalling, which is neither related to the requirement for the C-terminus to bring Mad1 to kinetochores (Fig 1) nor related to the role of Mad1 in recruiting Mad2, either directly or through Mad2:Mad2 dimerization (Figs 2 and 3). Since very similar findings have been made in human cells [11], this function of Mad1 is probably conserved across eukaryotes. Current models for the spindle assembly checkpoint mainly see Mad1 as a passive platform for presenting Mad2 at kinetochores. Our findings revise this picture and make Mad1 an active player in checkpoint signalling. How the Mad1 C-terminus promotes checkpoint activity and how Bub1 fits into the picture remains unclear (Fig 4). Our finding that the very C-terminal Mad1 head is required for checkpoint activity without being required for any of the known Mad1 functions provides a basis to elucidate the molecular mechanism. How the head is arranged with respect to the remainder of the molecule is still unclear (Fig 4). In any case, we suspect that the head, like similar folds in other kinetochore proteins [24–27], mediates a protein–protein interaction (Fig 4B). The interacting partner could be Mad2 or another (checkpoint) protein. Although we find Mad2 dimerization apparently intact in the Mad1-EDD/QNN, Mad1-Δhelix or Mad1-RLK/AAA mutant (Fig 3), it remains possible that these regions are involved in promoting the conformational change of Mad2 that is required for binding of free Mad2 to Cdc20 [28,29] (Fig 4B). It would be interesting to perform cross-linking experiments to determine which arrangement the Mad1 C-terminus takes *in vivo* and which proteins the different regions interact with (Fig 4B).

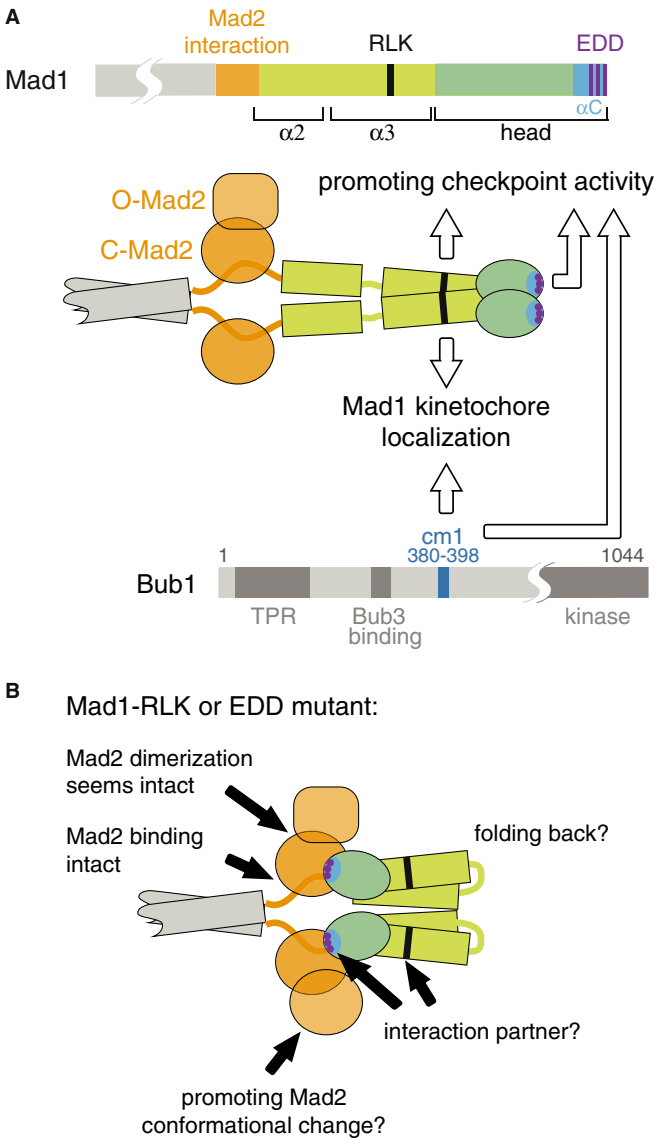

Figure 4. Mad1 C-terminus and Bub1-cm1 promote checkpoint signalling independently of their role in Mad1:Mad2 kinetochore recruitment.

A Schematic of the Mad1 and Bub1 proteins with suggested functions for the Mad1-RLK motif, the Mad1 C-terminal head and Bub1-cm1.

B It is unknown how Mad1 α3 and head arrange with respect to α2. A straight conformation is shown in (A), folding back [2] is shown in (B). How the Mad1 C-terminus promotes checkpoint signalling remains unclear. Findings and ideas are indicated by black arrows and discussed in the text.

Materials and Methods

Schizosaccharomyces pombe strains

Strains are listed in Supplementary Table 1. For the amino acid (aa) numbering of Mad1, note that we corrected the annotation of the start codon, which shifted by 13 aa (Supplementary Information).

In general, mutants were integrated into the endogenous locus using PCR-based gene targeting [30] and replaced the wild-type allele. *P(nmt81)-(mis12-)mad1-(AAA)-GFP* constructs were integrated into the *leu1* locus using the pDUAL system [31], and the endogenous *mad1+* gene was deleted. *Schizosaccharomyces pombe* strains with the following mutations or modifications have been described: *nda3-KM311* [32], *mad1+-GFP≪kanR*, *mad2+-GFP≪kanR*, *mad3+-GFP≪kanR*, *plo1+-mCherry*, *ark1+*-GFP [7], *bub1+-GFP≪kanR* [33], *bub3+-GFP≪kanR* [10], *mad1Δ::ura4+* [34], *bub1Δ::ura4+* [35].

 © 2014 The Authors

Culture conditions

For live-cell imaging, cells were grown at 30°C in either rich medium (YEA) or Edinburgh minimal medium (EMM) containing the necessary supplements. Mad1 constructs expressed from *P(nmt81)* at the *leu1* locus were cultured for 19 h in EMM without thiamine to induce expression, then washed three times with EMM containing 16 μM thiamine and resuspended in EMM containing 16 μM thiamine before shifting to 16°C for imaging.

Live-cell imaging to assess checkpoint functionality

Live-cell imaging was performed on a DeltaVision microscope (Applied Precision/GE Healthcare) as previously described [7].

Quantification of GFP and mCherry signals in the nucleus and at the kinetochore

To determine the intensity of checkpoint protein-GFP or -mCherry signals at the kinetochores, mitotic cells were identified by the appearance of localized Plo1-mCherry signal at SPBs, or by localized Mad1-GFP or Mad2-mCherry signal at kinetochores. In cells expressing constitutive kinetochore-tethered Mad1 (Mis12-Mad1) and lacking a fluorescent tag on Plo1 (so that entry into mitosis could not be judged), signals were measured for 50 min before the kinetochores unclustered. The unclustering (Supplementary Fig S2D) indicates that the cell is in mitosis. An area was placed around kinetochores (for checkpoint protein-GFP or -mCherry strains) or SPBs (for Plo1-mCherry strains; because kinetochores cluster at the SPB in early mitosis, this captures the signal at kinetochores). The GFP or mCherry signal in this area was traced over time. To determine signal intensity at the kinetochore, the total signal intensity per area of a similarly sized region in the nucleoplasm was subtracted from the total signal intensity per area around the kinetochore.

Fluorescence microscopy of asynchronous cell cultures

Images of living cells were acquired with a CoolSnap EZ (Roper) camera using a 63 × /1.4 Plan Apochromat oil objective on a Zeiss AxioImager microscope and were processed with MetaMorph software (Molecular Devices Corporation). Typically, a Z-stack of about 3 μm thickness, with single planes spaced by 0.3 μm, was acquired and subsequently projected. Shown are sum intensity projections of the Z-stack for checkpoint proteins and maximum intensity projections of the Z-stack for Plo1.

Immunoprecipitation

Immunoprecipitation was performed as previously described [10] using rabbit anti-Mad1 [10] or mouse anti-GFP (Roche, 11814460001) antibodies and protein A-coated magnetic beads (Dynabeads, Invitrogen 10002D).

Cell extracts, SDS–PAGE and immunoblotting

Protein extraction was performed as previously described [7]. Mouse anti-GFP (Roche, 11814460001), rabbit anti-Mad1 [10], rabbit anti-Mad2 [36], mouse anti-HA (Roche, 12CA5) or rabbit anti-Cdc2 (Santa Cruz, SC-53) were used as primary antibodies. Secondary antibodies were anti-mouse or anti-rabbit HRP conjugates (Dianova, 115-035-003, 111-035-003) and were read out using chemiluminescence.

Supplementary information for this article is available online: http://embor.embopress.org

Acknowledgements
We thank Jan Hasenauer for statistical analysis, Julia Kamenz for valuable suggestions, Katrin Bertram, Holda Anagho, Eva Illgen, Julia Binder, Julia Sauerwald, Alexandra Dudek and Philipp Spät for excellent technical help, Andrei Lupas for advice on coiled-coil truncations, the Proteome Center of the University of Tübingen for mass spectrometric analysis and Jakob Nilsson and his group for communicating unpublished results. We are grateful for funding by the Max Planck Society; St.H. was additionally supported by the Ernst Schering Foundation.

Author contributions
SHe (Figs 1–3, Supplementary Figs S1–4), KS (Figs 1–3, Supplementary Figs S1–4), HW (Fig 1), ML (Figs 1 and 2, Supplementary Fig S4), NS (Fig 1, Supplementary Figs S1 and 3) and NH (Supplementary Fig S3) designed and performed experiments; SHa devised the project and wrote the manuscript together with SHe and input from all other authors.

Conflict of interest
The authors declare that they have no conflict of interest.

References

1. Lara-Gonzalez P, Westhorpe FG, Taylor SS (2012) The spindle assembly checkpoint. *Curr Biol* 22: R966 – R980
2. Sironi L, Mapelli M, Knapp S, De Antoni A, Jeang KT, Musacchio A (2002) Crystal structure of the tetrameric Mad1-Mad2 core complex: implications of a safety belt binding mechanism for the spindle checkpoint. *EMBO J* 21: 2496 – 2506
3. De Antoni A, Pearson CG, Cimini D, Canman JC, Sala V, Nezi L, Mapelli M, Sironi L, Faretta M, Salmon ED, Musacchio A (2005) The Mad1/Mad2 complex as a template for Mad2 activation in the spindle assembly checkpoint. *Curr Biol* 15: 214 – 225
4. Primorac I, Musacchio A (2013) Panta rhei: the APC/C at steady state. *J Cell Biol* 201: 177 – 189
5. Chao WC, Kulkarni K, Zhang Z, Kong EH, Barford D (2012) Structure of the mitotic checkpoint complex. *Nature* 484: 208 – 213
6. Jia L, Kim S, Yu H (2013) Tracking spindle checkpoint signals from kinetochores to APC/C. *Trends Biochem Sci* 38: 302 – 311
7. Heinrich S, Windecker H, Hustedt N, Hauf S (2012) Mph1 kinetochore localization is crucial and upstream in the hierarchy of spindle assembly checkpoint protein recruitment to kinetochores. *J Cell Sci* 125: 4720 – 4727
8. Emre D, Terracol R, Poncet A, Rahmani Z, Karess RE (2011) A mitotic role for Mad1 beyond the spindle checkpoint. *J Cell Sci* 124: 1664 – 1671
9. Mariani L, Chiroli E, Nezi L, Muller H, Piatti S, Musacchio A, Ciliberto A (2012) Role of the Mad2 dimerization interface in the spindle assembly checkpoint independent of kinetochores. *Curr Biol* 22: 1900 – 1908

© 2014 The Authors

10. Heinrich S, Geissen EM, Kamenz J, Trautmann S, Widmer C, Drewe P, Knop M, Radde N, Hasenauer J, Hauf S (2013) Determinants of robustness in spindle assembly checkpoint signalling. *Nat Cell Biol* 15: 1328 – 1339
11. Kruse T, Larsen MSY, Sedgwick GG, Sigurdsson JO, Streicher W, Olsen JV, Nilsson J (2014) A direct role of Mad1 in the spindle assembly checkpoint beyond Mad2 kinetochore recruitment. *EMBO Rep* DOI 10.1002/embr.201338101
12. Kim S, Sun H, Tomchick DR, Yu H, Luo X (2012) Structure of human Mad1 C-terminal domain reveals its involvement in kinetochore targeting. *Proc Natl Acad Sci USA* 109: 6549 – 6554
13. Kastenmayer JP, Lee MS, Hong AL, Spencer FA, Basrai MA (2005) The C-terminal half of *Saccharomyces cerevisiae* Mad1p mediates spindle checkpoint function, chromosome transmission fidelity and CEN association. *Genetics* 170: 509 – 517
14. Scott RJ, Lusk CP, Dilworth DJ, Aitchison JD, Wozniak RW (2005) Interactions between Mad1p and the nuclear transport machinery in the yeast *Saccharomyces cerevisiae*. *Mol Biol Cell* 16: 4362 – 4374
15. Chung E, Chen RH (2002) Spindle checkpoint requires Mad1-bound and Mad1-free Mad2. *Mol Biol Cell* 13: 1501 – 1511
16. Martin-Lluesma S, Stucke VM, Nigg EA (2002) Role of Hec1 in spindle checkpoint signaling and kinetochore recruitment of Mad1/Mad2. *Science* 297: 2267 – 2270
17. Brady DM, Hardwick KG (2000) Complex formation between Mad1p, Bub1p and Bub3p is crucial for spindle checkpoint function. *Curr Biol* 10: 675 – 678
18. Warren CD, Brady DM, Johnston RC, Hanna JS, Hardwick KG, Spencer FA (2002) Distinct chromosome segregation roles for spindle checkpoint proteins. *Mol Biol Cell* 13: 3029 – 3041
19. Chen RH, Brady DM, Smith D, Murray AW, Hardwick KG (1999) The spindle checkpoint of budding yeast depends on a tight complex between the Mad1 and Mad2 proteins. *Mol Biol Cell* 10: 2607 – 2618
20. Klebig C, Korinth D, Meraldi P (2009) Bub1 regulates chromosome segregation in a kinetochore-independent manner. *J Cell Biol* 185: 841 – 858
21. Nezi L, Rancati G, De Antoni A, Pasqualato S, Piatti S, Musacchio A (2006) Accumulation of Mad2-Cdc20 complex during spindle checkpoint activation requires binding of open and closed conformers of Mad2 in *Saccharomyces cerevisiae*. *J Cell Biol* 174: 39 – 51
22. Hewitt L, Tighe A, Santaguida S, White AM, Jones CD, Musacchio A, Green S, Taylor SS (2010) Sustained Mps1 activity is required in mitosis to recruit O-Mad2 to the Mad1-C-Mad2 core complex. *J Cell Biol* 190: 25 – 34
23. Sironi L, Melixetian M, Faretta M, Prosperini E, Helin K, Musacchio A (2001) Mad2 binding to Mad1 and Cdc20, rather than oligomerization, is required for the spindle checkpoint. *EMBO J* 20: 6371 – 6382
24. Wei RR, Schnell JR, Larsen NA, Sorger PK, Chou JJ, Harrison SC (2006) Structure of a central component of the yeast kinetochore: the Spc24p/Spc25p globular domain. *Structure* 14: 1003 – 1009
25. Ciferri C, Pasqualato S, Screpanti E, Varetti G, Santaguida S, Dos Reis G, Maiolica A, Polka J, De Luca JG, De Wulf P, Salek M, Rappsilber J, Moores CA, Salmon ED, Musacchio A (2008) Implications for kinetochore-microtubule attachment from the structure of an engineered Ndc80 complex. *Cell* 133: 427 – 439
26. Corbett KD, Yip CK, Ee LS, Walz T, Amon A, Harrison SC (2010) The monopolin complex crosslinks kinetochore components to regulate chromosome-microtubule attachments. *Cell* 142: 556 – 567
27. Schmitzberger F, Harrison SC (2012) RWD domain: a recurring module in kinetochore architecture shown by a Ctf19-Mcm21 complex structure. *EMBO Rep* 13: 216 – 222
28. Luo X, Yu H (2008) Protein metamorphosis: the two-state behavior of Mad2. *Structure* 16: 1616 – 1625
29. Mapelli M, Musacchio A (2007) MAD contortions: conformational dimerization boosts spindle checkpoint signaling. *Curr Opin Struct Biol* 17: 716 – 725
30. Bahler J, Wu JQ, Longtine MS, Shah NG, McKenzie A III, Steever AB, Wach A, Philippsen P, Pringle JR (1998) Heterologous modules for efficient and versatile PCR-based gene targeting in *Schizosaccharomyces pombe*. *Yeast* 14: 943 – 951
31. Matsuyama A, Shirai A, Yashiroda Y, Kamata A, Horinouchi S, Yoshida M (2004) pDUAL, a multipurpose, multicopy vector capable of chromosomal integration in fission yeast. *Yeast* 21: 1289 – 1305
32. Hiraoka Y, Toda T, Yanagida M (1984) The NDA3 gene of fission yeast encodes beta-tubulin: a cold-sensitive nda3 mutation reversibly blocks spindle formation and chromosome movement in mitosis. *Cell* 39: 349 – 358
33. Yamaguchi S, Decottignies A, Nurse P (2003) Function of Cdc2p-dependent Bub1p phosphorylation and Bub1p kinase activity in the mitotic and meiotic spindle checkpoint. *EMBO J* 22: 1075 – 1087
34. Vanoosthuyse V, Valsdottir R, Javerzat JP, Hardwick KG (2004) Kinetochore targeting of fission yeast Mad and Bub proteins is essential for spindle checkpoint function but not for all chromosome segregation roles of Bub1p. *Mol Cell Biol* 24: 9786 – 9801
35. Bernard P, Hardwick K, Javerzat JP (1998) Fission yeast bub1 is a mitotic centromere protein essential for the spindle checkpoint and the preservation of correct ploidy through mitosis. *J Cell Biol* 143: 1775 – 1787
36. Yamada HY, Matsumoto S, Matsumoto T (2000) High dosage expression of a zinc finger protein, Grt1, suppresses a mutant of fission yeast slp1(+), a homolog of CDC20/p55CDC/Fizzy. *J Cell Sci* 113(Pt 22): 3989 – 3999
37. Mulvihill DP, Petersen J, Ohkura H, Glover DM, Hagan IM (1999) Plo1 kinase recruitment to the spindle pole body and its role in cell division in *Schizosaccharomyces pombe*. *Mol Biol Cell* 10: 2771 – 2785

 © 2014 The Authors

Figure S1

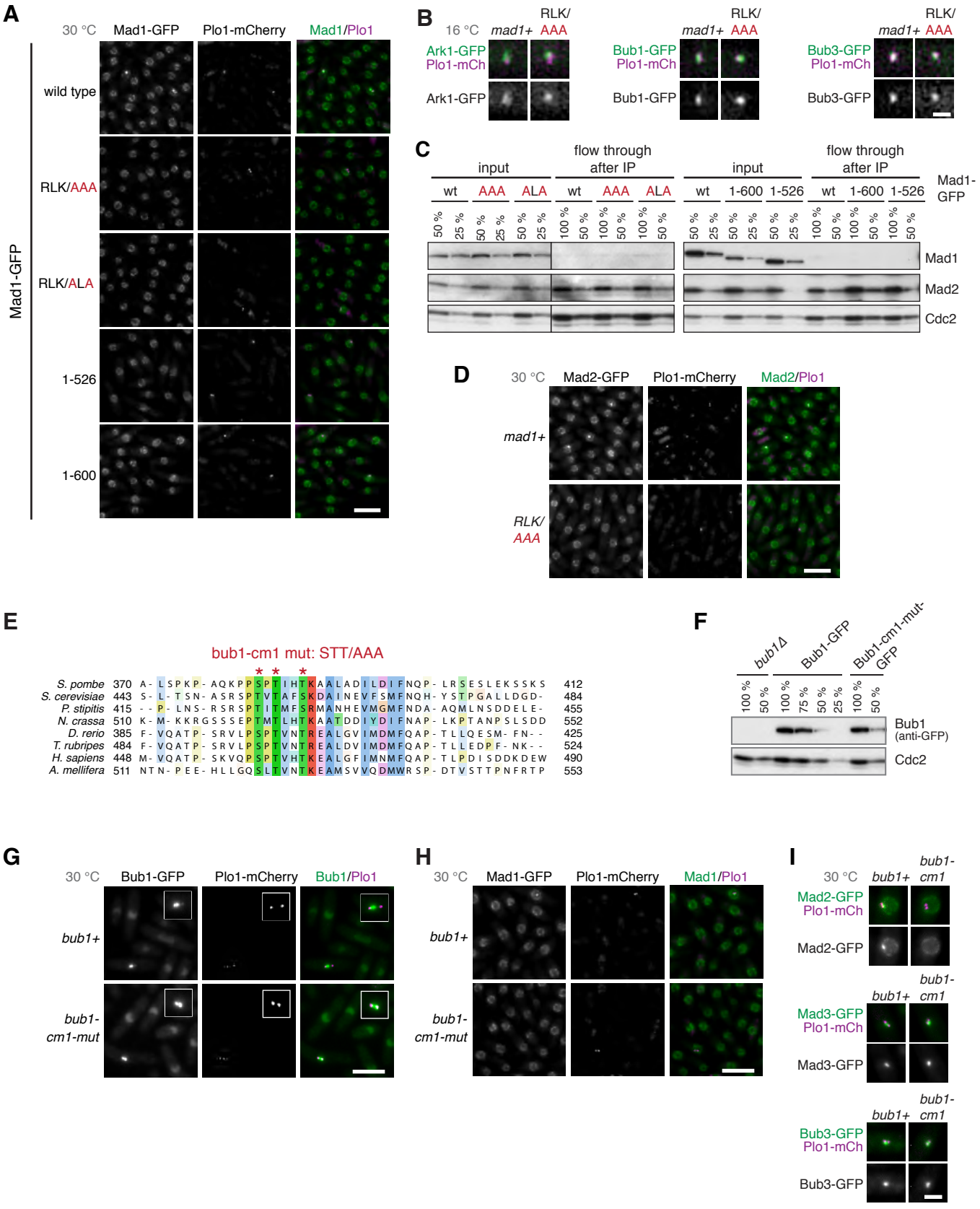
A
30 °C
Mad1-GFP
Plo1-mCherry
Mad1/Plo1
Mad1-GFP
wild type
RLK/AAA
RLK/ALA
1-526
1-600
B
16 °C
mad1+
RLK/AAA
Ark1-GFP Plo1-mCh
Ark1-GFP
Bub1-GFP Plo1-mCh
Bub1-GFP
Bub3-GFP Plo1-mCh
Bub3-GFP
C
input
flow through after IP
wt
AAA
ALA
1-600
1-526
Mad1-GFP
Mad1
Mad2
Cdc2
D
30 °C
Mad2-GFP
Plo1-mCherry
Mad2/Plo1
mad1+
RLK/AAA
E
bub1-cm1 mut: STT/AAA
S. pombe 370 A-LSPKP-AQKPPSPTIHTKAALADILDIFNQP-LRSESLEKSSKS 412
S. cerevisiae 443 S-L-TSN-ASRSPTVTAFSKDAINEVFSMFNQH-YSTPGALLDGD- 484
P. stipitis 415 --P-LNS-RSRSPTITMFSRMANHEVMGMFNDA-AQMLNSDDELE- 455
N. crassa 510 K-M-KKRGSSSEPTMTLHTKAATDDIYDIFNAP-LKPTANPSLSDD 552
D. rerio 385 F-VQATP-SRVLPSPTVNTREALGVIMDMFQAP-TLLQESM-FN-- 425
T. rubripes 484 F-VQATP-SRVLPSPTVNTREALDVIMDMFQAP-TLLEDPF-NK-- 524
H. sapiens 448 M-VQATP-SKVQPSPTVHTKEALGFIMNMFQAP-TLPDISDDKDEW 490
A. mellifera 511 NTN-PEE-HLLGQSLTVNTKEAMSVVQDMWRSP-DTVSTTPNFRTP 553
F
bub1Δ
Bub1-GFP
Bub1-cm1-mut-GFP
Bub1 (anti-GFP)
Cdc2
G
30 °C
Bub1-GFP
Plo1-mCherry
Bub1/Plo1
bub1+
bub1-cm1-mut
H
30 °C
Mad1-GFP
Plo1-mCherry
Mad1/Plo1
bub1+
bub1-cm1-mut
I
30 °C
bub1+
bub1-cm1
Mad2-GFP Plo1-mCh
Mad2-GFP
Mad3-GFP Plo1-mCh
Mad3-GFP
Bub3-GFP Plo1-mCh
Bub3-GFP

Figure S1 Additional analysis of Mad1-RLK and Bub1-cm1 mutants

A Mad1-RLK mutants and C-terminal truncations localize to the nuclear rim

Representative images of cells expressing *plo1+-mCherry*, *nda3-KM311* and the indicated *mad1-GFP* fusions. Cells were grown at permissive temperature for *nda3-KM311* (30 °C). A localized Plo1-mCherry signal indicates that cells are in mitosis (scale bar: 10 *μ*m).

B Ark1, Bub1 and Bub3 localize to kinetochores in the *mad1-RLK/AAA* mutant

Cells expressing *plo1+-mCherry*, *nda3-KM311* and the indicated GFP fusion proteins were analysed at the restrictive temperature for *nda3-KM311* (16 °C) as in Fig 1E. Representative nuclei of mitotic cells are shown (scale bar: 2 *μ*m).

C Mad1 is efficiently depleted by immunoprecipitation

Input and flow through of the anti-Mad1 immunoprecipitation shown in Fig 1H. To detect the Mad1-RLK mutants, anti-GFP antibody was used; to detect the Mad1 truncations, anti-Mad1 antibody was used. Cdc2 serves as loading control. The C-terminal truncations Mad1-1-600 and Mad1-1-526 contain more Mad2 in the flow through, in agreement with inefficient binding of Mad2 to Mad1 (Fig 1H).

D Mad2 localisation to kinetochores is strongly reduced in the *mad1-RLK/AAA* mutant

Representative images of cells expressing *mad1+* or *mad1-RLK/AAA*, as well as *mad2+-GFP*, *plo1+-mCherry* and *nda3-KM311*. Cells were grown at permissive temperature for *nda3-KM311* (30 °C). Mad2-GFP localisation to the nuclear rim in interphase is similar between wild type and *mad1-RLK/AAA* cells, but localisation to the kinetochore in mitosis is impaired in the *mad1-RLK/AAA* mutant (scale bar: 10 *μ*m).

E Alignment of the Bub1 region containing the conserved motif 1 (cm1).

Sequences from OrthoMCL group OG5_130700 were aligned using M-Coffee. Selected sequences are shown with Clustal X colouring scheme. Red asterisks indicate the amino acids mutated in the *bub1-cm1* mutant (S381A, T383A and T386A).

F Bub1-cm1 mutant is present at similar levels as wild type Bub1

Extracts were analysed by immunoblotting using anti-GFP (to detect Bub1-GFP or Bub1-cm1-mut-GFP) and anti-Cdc2 (loading control) antibodies. Percentages on top indicate how much of the extract was loaded.

G Bub1-cm1 mutant localisation resembles Bub1 wt localisation

Representative images of cells expressing *bub1-GFP* (wild type or cm1 mutant), *plo1+-mCherry* and *nda3-KM311*. Cells were grown at permissive temperature for *nda3-KM311* (30 °C). Both wild type Bub1 and Bub1-cm1 enrich in the nucleus in interphase. Inset: Plo1-mCherry marks mitotic spindle pole bodies, and both Bub1 and Bub1-cm1 localize to the region of the mitotic spindle (most likely by localizing to unattached kinetochores). Scale bar: 10 *μ*m. Insets are additionally magnified 1.87-fold.

H Mad1-GFP localisation to the nuclear rim is not impaired by the *bub1-cm1* mutation

Representative images of cells expressing *bub1* (wild type or cm1 mutant), *mad1+-GFP, plo1+-mCherry* and *nda3-KM311*. Cells were grown at permissive temperature for *nda3-KM311* (30 °C). Nuclei of mitotic cells with Mad1-GFP signal from these panels are shown in Fig 1J. Scale bar: 10 *μ*m.

I Bub1-cm1 mutation affects kinetochore localisation of Mad2 but not Mad3 and Bub3

Representative nuclei of mitotic cells expressing *bub1* (wild type or cm1 mutant), the indicated GFP fusions, *plo1+-mCherry* and *nda3-KM311*. Cells were grown at permissive temperature for *nda3-KM311* (30 °C). Scale bar: 2 *μ*m

Figure S2

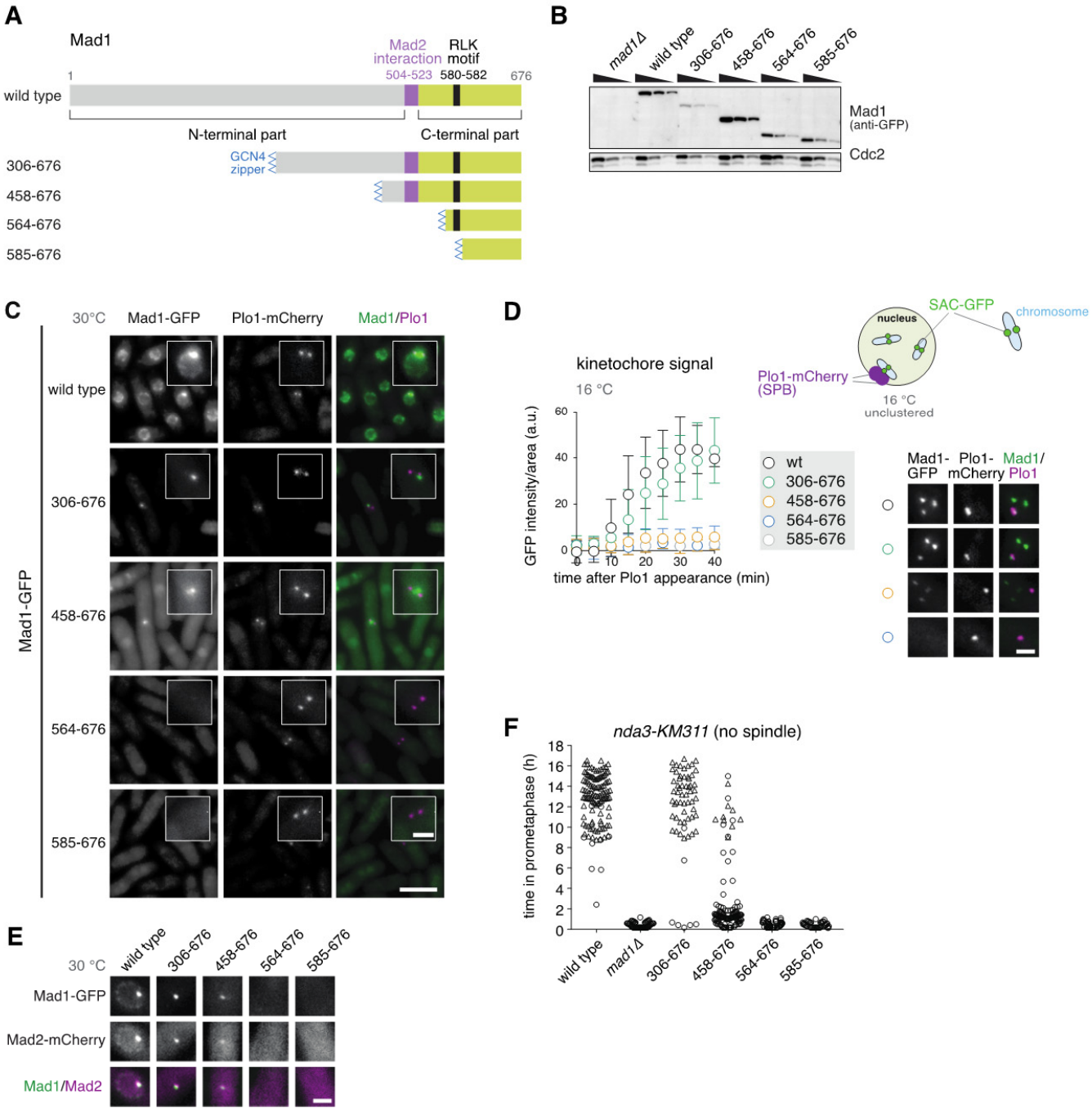
A
Mad1
Mad2 interaction
RLK motif
1
504-523
580-582
676
wild type
N-terminal part
C-terminal part
306-676
GCN4 zipper
458-676
564-676
585-676
B
mad1Δ
wild type
306-676
458-676
564-676
585-676
Mad1 (anti-GFP)
Cdc2
C
30°C
Mad1-GFP
Plo1-mCherry
Mad1/Plo1
wild type
306-676
458-676
564-676
585-676
Mad1-GFP
D
kinetochore signal
16 °C
GFP intensity/area (a.u.)
time after Plo1 appearance (min)
wt
306-676
458-676
564-676
585-676
nucleus
SAC-GFP
chromosome
Plo1-mCherry (SPB)
16 °C unclustered
Mad1-GFP
Plo1-mCherry
Mad1/Plo1
E
30 °C
wild type
306-676
458-676
564-676
585-676
Mad1-GFP
Mad2-mCherry
Mad1/Mad2
F
nda3-KM311 (no spindle)
time in prometaphase (h)
wild type
mad1Δ
306-676
458-676
564-676
585-676

Figure S2 The Mad1 N-terminal part is not required for kinetochore localisation, the C-terminal part is not sufficient

A Domain structure of the Mad1 protein and N-terminal truncations

A fragment of *S. cerevisiae* Gcn4p (aa250-277; GCN4 zipper) was used to aid coiled-coil formation of the remaining alpha-helical parts and dimerization [1, 2].

B N-terminal truncation mutants of Mad1 are expressed, but to different levels

Immunoblotting of cell extracts using anti-GFP and anti-Cdc2 (loading control) antibodies. A dilution series was loaded for each strain to compare intensities. The N-terminal Mad1 truncations were expressed, but not all to the same level as wild type Mad1-GFP (also see (C)).

C Truncation of the Mad1 N-terminus abolishes nuclear rim localisation

Representative images of cells expressing *plo1+-mCherry*, *nda3-KM311* and the indicated *mad1-GFP* fusions. Cells were grown at permissive temperature for *nda3-KM311* (30 °C). Scale bar: 10 µm; scale bar in inset: 2 µm. Nuclear rim localisation was lost in all N-terminal truncations, whereas kinetochore localisation was at least partly preserved in mutants that retained parts of the N-terminal coiled-coil. The C-terminal part of Mad1 was not sufficient for kinetochore localisation.

D Only the shortest N-terminal Mad1 truncation (Mad1-306-676) preserves kinetochore localisation of Mad1-GFP at the restrictive temperature for *nda3-KM311*

The same strains as in (C) were shifted to the restrictive temperature for *nda3-KM311* (16 °C) and imaged as in Fig 1C. Mad1-GFP signals were quantified at the kinetochore as cells entered mitosis (a.u. = arbitrary units; error bars = s.d.; n ≥ 20 cells). The kinetochore localisation of Mad1-458-676 was almost undetectable in live cell imaging (left panel), but was visible at 16 °C when the same image acquisition settings as in (C) were used (right panel; representative nuclei of mitotic cells). Mad1-458-676 localisation seems weaker at 16 °C than at 30 °C. The schematic depicts the situation in the example pictures and shows a nucleus with unclustered chromosomes (light blue). Unclustering occurs in the absence of microtubules when cells delay in mitosis.

E Mad2-mCherry shows the same localisation pattern as Mad1-GFP in the truncation mutants

Cells expressing *mad2+-mCherry*, *nda3-KM311* and the indicated *mad1-GFP* fusions were imaged at 30 °C. Representative nuclei of cells in mitosis are shown. Scale bar: 2 µm. Mad1-306-676 and Mad1-458-676 co-recruit Mad2 to the kinetochore, indicating that the interaction with Mad2 is preserved.

F The shorter N-terminal Mad1 truncation (Mad1-306-676) largely preserves checkpoint activity.

Checkpoint function in the indicated strains was analysed as in Fig 1F. Checkpoint activity in Mad1-306-676 was largely preserved (although the abundance seemed lower than wild type Mad1 (B,C)). Checkpoint activity in Mad1-458-676 was impaired, which coincided with an

impairment of localisation to the kinetochore that was more pronounced at 16 °C (C,D,E). The two shortest Mad1 fragments (Mad1-564-676 and 585-676) were checkpoint-deficient, which was expected from the lack of the Mad2-interaction motif.

Supplementary References

1. Kammerer RA, Schulthess T, Landwehr R, Lustig A, Engel J, Aebi U, Steinmetz MO (1998) An autonomous folding unit mediates the assembly of two-stranded coiled coils. *Proc Natl Acad Sci U S A* **95:** 13419-13424

2. O'Shea EK, Klemm JD, Kim PS, Alber T (1991) X-ray structure of the GCN4 leucine zipper, a two-stranded, parallel coiled coil. *Science* **254:** 539-544

Figure S3

A

	Mad1-GFP IP *cdc25-22* release		Mad1-GFP IP *nda3-KM311* arrest		Bub1-GFP IP *nda3-KM311* arrest	
	pep.	seq.cov.	pep.	seq.cov.	pep.	seq.cov.
Mad1	111	81 %	94	82 %	0	0 %
Mad2	16	62 %	15	55 %	2	8 %
Bub1	0	0 %	0	0 %	75	62 %
Bub3	0	0 %	0	0 %	20	58 %
Spc7	0	0 %	0	0 %	15	15 %
Mis12	0	0 %	0	0 %	3	13 %
Mis13	0	0 %	0	0 %	6	20 %
Mis14	0	0 %	0	0 %	5	32 %
Nnf1	0	0 %	0	0 %	3	15 %
Ndc80	0	0 %	0	0 %	16	29 %
Nuf2	0	0 %	0	0 %	3	7 %
Spc24	0	0 %	0	0 %	3	21 %
Spc25	0	0 %	0	0 %	5	19 %
Nup211	45	28 %	2	1.1 %	0	0 %

B

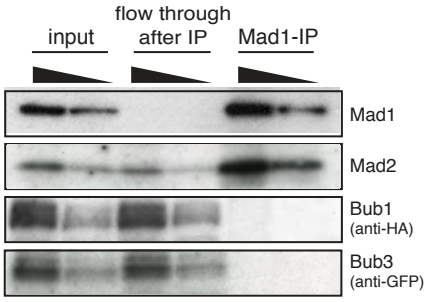

C

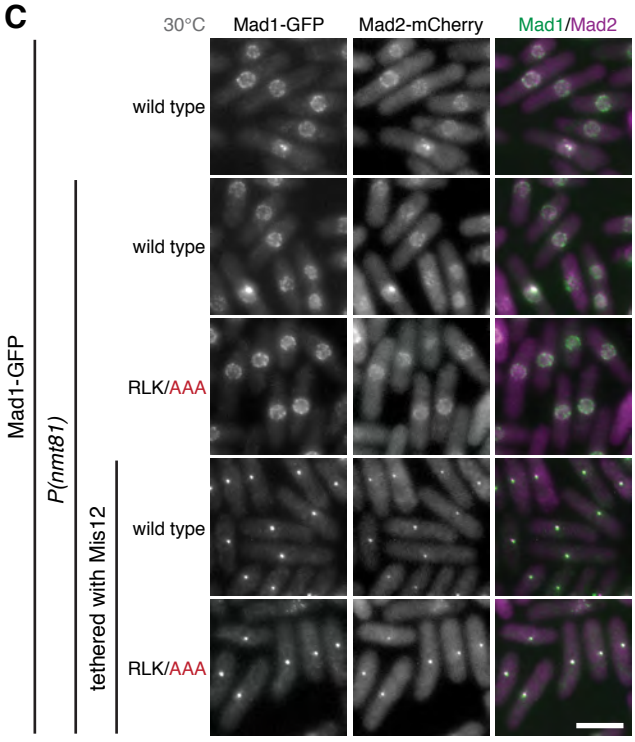

Figure S3 Absence of evidence for Bub1-Mad1 interaction and supplementary data for Mad1 kinetochore-tethering

A Mass spectrometry of immunoprecipitations of Mad1 and Bub1. Mad1-GFP was either immunoprecipitated from cells that were released from a *cdc25-22* arrest (at G2/M), were treated with the microtubule drug MBC and were harvested in mitosis (86 % mitotic cells) or from cells that were delayed in mitosis by the spindle assembly checkpoint due to the *nda3-KM311* tubulin mutant. Bub1-GFP was immunoprecipitated from cells that were delayed in mitosis by the spindle assembly checkpoint due to the *nda3-KM311* mutant. Samples were analysed by mass spectrometry. The table shows the number of identified peptides (pep.) and the amino acid sequence coverage (seq.cov.) reached for each protein, which are semi-quantitative measures for the abundance of the protein in the immunoprecipitate. Mad2 and Nup211 were recovered as interaction partners in the Mad1 immunoprecipitates, Bub3 and outer kinetochore proteins were recovered as interaction partners in the Bub1 immunoprecipitate.

B Anti-Mad1 immunoprecipitations from cells that were delayed in mitosis by the spindle assembly checkpoint due to the *nda3-KM311* tubulin mutant were analysed for the presence of Mad1, Mad2, Bub1 and Bub3 using anti-Mad1, anti-Mad2, anti-HA (Bub1) and anti-GFP (Bub3) antibodies. Input and flow through are shown on the left. A 1:2 dilution is additionally loaded for each sample.

C Mad2 colocalizes with Mad1-RLK/AAA

Representative images of cells expressing *mad2+-mCherry*, *nda3-KM311* and the indicated *mad1 wild type* or *RLK/AAA-GFP* fusions. Cells were grown at permissive temperature for the nda3-KM311 mutant (30 °C). *P(nmt81)* indicates expression of the construct from the *nmt81* promoter rather than from the endogenous *mad1* promoter. Scale bar: 10 μm.

Figure S4

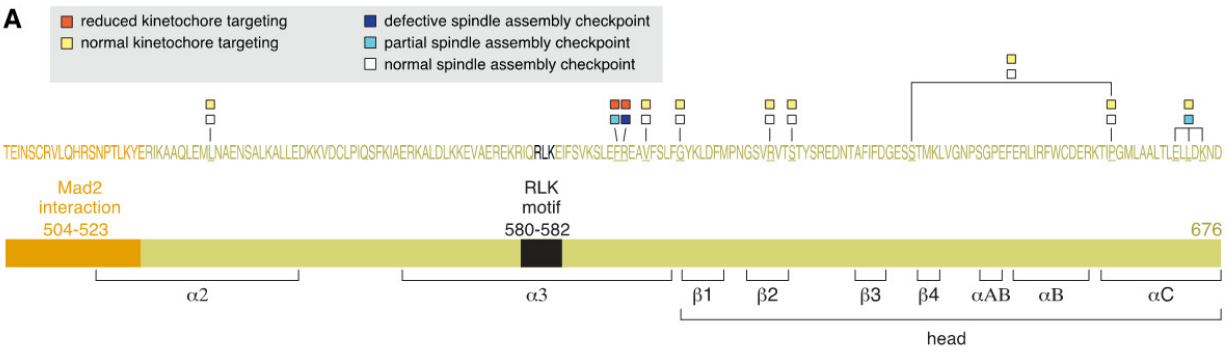
A
reduced kinetochore targeting
normal kinetochore targeting
defective spindle assembly checkpoint
partial spindle assembly checkpoint
normal spindle assembly checkpoint
Mad2 interaction 504-523
RLK motif 580-582
676
α2
α3
β1
β2
β3
β4
αAB
αB
αC
head

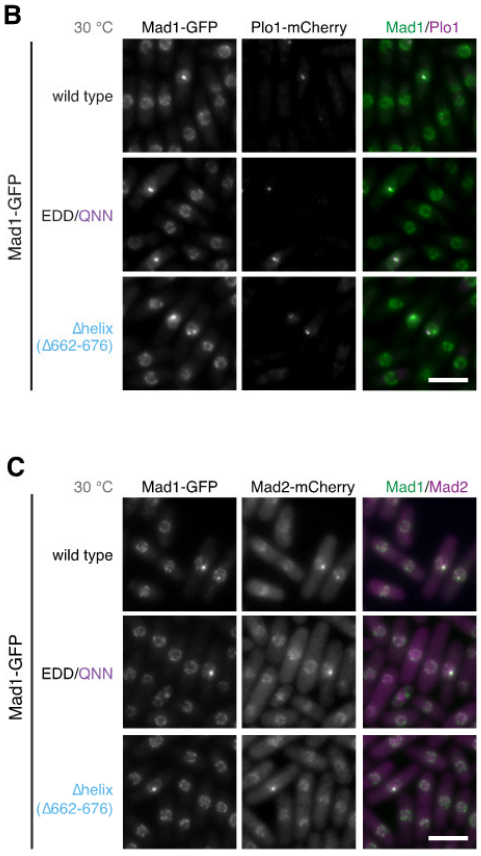
B
30 °C
Mad1-GFP
Plo1-mCherry
Mad1/Plo1
wild type
EDD/QNN
Δhelix (Δ662-676)
Mad1-GFP

C
30 °C
Mad1-GFP
Mad2-mCherry
Mad1/Mad2
wild type
EDD/QNN
Δhelix (Δ662-676)
Mad1-GFP

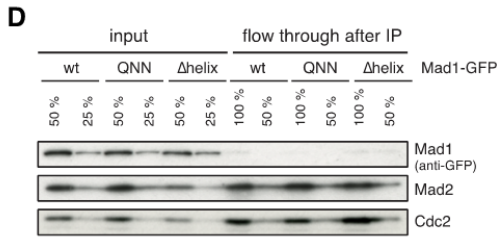
D
input
flow through after IP
wt
QNN
Δhelix
Mad1-GFP
Mad1 (anti-GFP)
Mad2
Cdc2

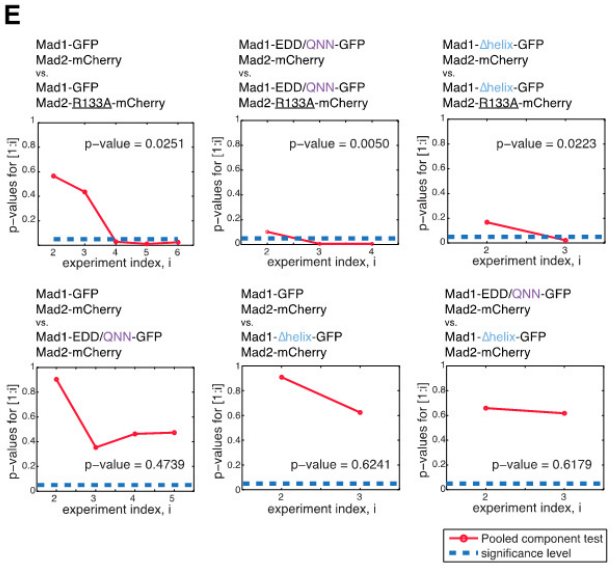
E
Mad1-GFP
Mad2-mCherry
vs.
Mad1-GFP
Mad2-R133A-mCherry
p-value = 0.0251
Mad1-EDD/QNN-GFP
Mad2-mCherry
vs.
Mad1-EDD/QNN-GFP
Mad2-R133A-mCherry
p-value = 0.0050
Mad1-Δhelix-GFP
Mad2-mCherry
vs.
Mad1-Δhelix-GFP
Mad2-R133A-mCherry
p-value = 0.0223
Mad1-GFP
Mad2-mCherry
vs.
Mad1-EDD/QNN-GFP
Mad2-mCherry
p-value = 0.4739
Mad1-GFP
Mad2-mCherry
vs.
Mad1-Δhelix-GFP
Mad2-mCherry
p-value = 0.6241
Mad1-EDD/QNN-GFP
Mad2-mCherry
vs.
Mad1-Δhelix-GFP
Mad2-mCherry
p-value = 0.6179
p-values for [1:i]
experiment index, i
Pooled component test
significance level

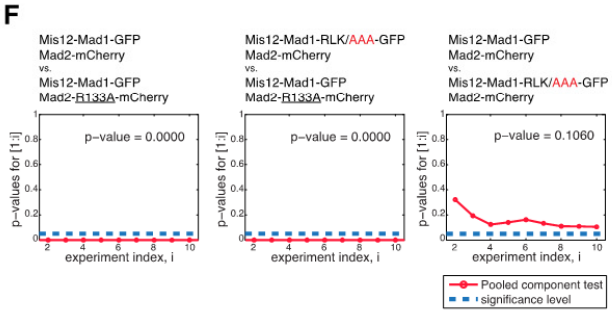
F
Mis12-Mad1-GFP
Mad2-mCherry
vs.
Mis12-Mad1-GFP
Mad2-R133A-mCherry
p-value = 0.0000
Mis12-Mad1-RLK/AAA-GFP
Mad2-mCherry
vs.
Mis12-Mad1-GFP
Mad2-R133A-mCherry
p-value = 0.0000
Mis12-Mad1-GFP
Mad2-mCherry
vs.
Mis12-Mad1-RLK/AAA-GFP
Mad2-mCherry
p-value = 0.1060
p-values for [1:i]
experiment index, i
Pooled component test
significance level

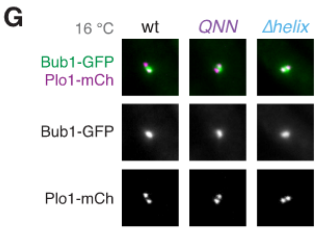
G
16 °C
wt
QNN
Δhelix
Bub1-GFP
Plo1-mCh
Bub1-GFP
Plo1-mCh

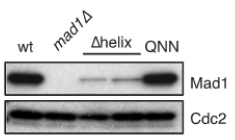
H
wt
mad1Δ
Δhelix
QNN
Mad1
Cdc2

Figure S4 Supplementary data for C-terminal Mad1 mutants

A Additional Mad1 mutants screened for kinetochore targeting ability and spindle assembly checkpoint activity

Individual residues in Mad1 were mutated to alanine, with the exception of S633, which was mutated to glycine. Checkpoint activity was assayed in cells expressing *plo1+-mCherry* and *nda3-KM311* as in Fig 1F. Mad1 localisation to kinetochores was scored as cells entered mitosis.

B Mad1-EDD/QNN and Mad1-∆helix show similar localisation to wild type Mad1

Representative images of cells expressing *plo1+-mCherry*, *nda3-KM311* and the indicated *mad1-GFP* fusions. Cells were grown at permissive temperature for the *nda3-KM311* mutant (30 °C). Scale bar: 10 µm

C Mad2-mCherry localisation is not perturbed by *mad1-EDD/QNN* or *mad1-∆helix*

Representative images of cells expressing *mad2+-mCherry*, *nda3-KM311* and the indicated *mad1-GFP* fusions. Cells were grown at permissive temperature for the *nda3-KM311* mutant (30 °C). Scale bar: 10 µm

D Input and flow through of the anti-Mad1 immunoprecipitation shown in Fig 3F. Cdc2 was used as loading control.

E Statistical analysis of Mad2/Mad1 ratios shown in Fig 3G. Intensity curves of the indicated strains were compared by a pooled component test [3]. The cumulative p-value is plotted in red. A p-value of 0.05 is shown as dashed blue line. Only time points with at least 7 cells of all strains were considered. The experiment index (i) increases with each time point. There is a statistically significant difference between the Mad1-GFP wild type or mutants strains expressing *mad2+-mCherry* and the same strains expressing the Mad2 dimerization mutant *mad2-R133A-mCherry* (upper row), indicating that in both Mad1 mutants Mad2 dimerization is not impaired. Differences between Mad1 wt and Mad1 mutant strains expressing wild type *mad2+-mCherry* were not statistically significant (lower row).

F Statistical analysis of Mad2/Mad1 ratios shown in Fig 3H. Intensity curves of the indicated strains were compared by a pooled component test [3] as in (E). There is a statistically significant difference between the Mis12-Mad1-GFP wild type or RLK/AAA strains expressing *mad2+-mCherry* and the Mis12-Mad1-GFP wild type strain expressing the Mad2 dimerization mutant *mad2-R133A-mCherry*. This indicates that Mad2 dimerization in Mis12-Mad1-RLK/AAA-GFP is not impaired.

G Bub1-GFP localisation is not perturbed in untagged *mad1-EDD/QNN* or *mad1-∆helix* cells

Representative nuclei of cells expressing *bub1+-GFP, plo1+-mCherry*, *nda3-KM311* and the indicated *mad1* variants (wild type, EDD/QNN or ∆helix). Cells were grown at permissive temperature for the *nda3-KM311* mutant (30 °C). Scale bar: 2 µm

H Expression level of untagged *mad1-Δhelix* is reduced compared to *mad1+* and *mad1-EDD/QNN*

Immunoblotting of cell extracts using anti-Mad1 and anti-Cdc2 (loading control) antibodies. The Mad1 antibody targets an N-terminal peptide [4]. Cell extracts of two different clones expressing *mad1-Δhelix* were loaded. Both Mad1 mutants were detectable but Mad1-Δhelix abundance was lower than wild type Mad1 or Mad1-EDD/QNN abundance. Note that C-terminal GFP-tagging of Mad1-Δhelix seems to rescue protein stability (Fig 3E). Bub1 localisation in all strains was preserved (G).

Supplementary References

3. Wu Y, Genton MG, Stefanski LA (2006) A multivariate two-sample mean test for small sample size and missing data. *Biometrics* **62:** 877-885

4. Heinrich S *et al* (2013) Determinants of robustness in spindle assembly checkpoint signalling. *Nat Cell Biol* **15:** 1328-1339

Supplementary Table 1 | S. pombe strains

Figure 1C,D		
SK891	*h+*	*leu1 mad1+-GFP<<kanR plo1+-mCherry<<natR nda3-KM311*
SM001	*h-*	*leu1 mad1-RLK/AAA(R580A/L581A/K582A)-GFP<<kanR plo1+-mCherry<<natR nda3-KM311*
ST146	*h+*	*leu1 mad1-RLK/ALA(R580A/K582A)-GFP<<kanR plo1+-mCherry<<natR nda3-KM311*
SM090	*h+*	*mad1-1-600-GFP<<kanNT3 plo1+-mCherry<<natR nda3-KM311*
SM091	*h+*	*mad1-1-526-GFP<<kanNT3 plo1+-mCherry<<natR nda3-KM311*
Figure 1E		
SK842	*h+*	*leu1 mad2+-GFP<<kanR plo1+-mCherry<<natR nda3-KM311*
SL905	*h-*	*leu1 mad2+-GFP<<kanR plo1+-mCherry<<natR nda3-KM311 mad1-RLK/AAA*
SL759	*h-*	*leu1 mad3+-GFP<<kanR plo1+-mCherry<<natR nda3-KM311*
SL907	*h-*	*leu1 mad3+-GFP<<kanR plo1+-mCherry<<natR nda3-KM311 mad1-RLK/AAA*
Figure 1F,G		
SK891	*h+*	*leu1 mad1+-GFP<<kanR plo1+-mCherry<<natR nda3-KM311*
SK893	*h+*	*leu1 ade6-M216 mad1Δ::ura4+ plo1+-mCherry<<natR nda3-KM311*
SM001	*h-*	*leu1 mad1-RLK/AAA-GFP<<kanR plo1+-mCherry<<natR nda3-KM311*
ST146	*h+*	*leu1 mad1-RLK/ALA-GFP<<kanR plo1+-mCherry<<natR nda3-KM311*
SM090	*h+*	*mad1-1-600-GFP<<kanNT3 plo1+-mCherry<<natR nda3-KM311*
SM091	*h+*	*mad1-1-526-GFP<<kanNT3 plo1+-mCherry<<natR nda3-KM311*
Figure 1H		
SK891	*h+*	*leu1 mad1+-GFP<<kanR plo1+-mCherry<<natR nda3-KM311*
SM001	*h-*	*leu1 mad1-RLK/AAA-GFP<<kanR plo1+-mCherry<<natR nda3-KM311*
ST146	*h+*	*leu1 mad1-RLK/ALA-GFP<<kanR plo1+-mCherry<<natR nda3-KM311*
SM090	*h+*	*mad1-1-600-GFP<<kanNT3 plo1+-mCherry<<natR nda3-KM311*
SM091	*h+*	*mad1-1-526-GFP<<kanNT3 plo1+-mCherry<<natR nda3-KM311*
Figure 1J		
SK892	*h+*	*leu1 mad1+-GFP<<kanR plo1+-mCherry<<natR nda3-KM311*
ST045	*h-*	*bub1-STT/AAA mad1+-GFP<<kanR plo1+-mCherry<<natR nda3-KM311*
Figure 1K		
SL901	*h+*	*leu1 bub1+-GFP<<kanR plo1+-mCherry<<natR nda3-KM311*
SP705	*h-*	*leu1 bub1-STT/AAA-GFP<<kanR plo1+-mCherry<<natR nda3-KM311*
SK892	*h+*	*leu1 mad1+-GFP<<kanR plo1+-mCherry<<natR nda3-KM311*
ST045	*h-*	*bub1-STT/AAA mad1+-GFP<<kanR plo1+-mCherry<<natR nda3-KM311*
Figure 1L		
SL901	*h+*	*leu1 bub1+-GFP<<kanR plo1+-mCherry<<natR nda3-KM311*
SI437	*h+*	*leu1 ade6-M216 (ura4DS/E?) bub1::ura4+ plo1+-GFP<<kanR nda3-KM311*
SP705	*h-*	*leu1 bub1-STT/AAA-GFP<<kanR plo1+-mCherry<<natR nda3-KM311*
Figure 2A,B,C		
SK891	*h+*	*leu1 mad1+-GFP<<kanR plo1+-mCherry<<natR nda3-KM311*
SK893	*h+*	*leu1 ade6-M216 mad1Δ::ura4+ plo1+-mCherry<<natR nda3-KM311*
SM814	*h+*	*ade6-M216 mad1Δ::ura4+ pDUAL-Pnmt81-mis12-mad1+-GFP<<leu1+ plo1+-mCherry<<natR nda3-KM311*
SM815	*h+*	*ade6-M216 mad1Δ::ura4+ pDUAL-Pnmt81-mis12-mad1-RLK/AAA-GFP<<leu1+ plo1+-mCherry<<natR nda3-KM311*
SM827	*h+*	*(ade6-M216?) mad1Δ::ura4+ pDUAL-Pnmt81-mad1+-GFP<<leu1+ plo1+-mCherry<<natR nda3-KM311*
SM828	*h+*	*(ade6-M216?) mad1Δ::ura4+ pDUAL-Pnmt81-mad1-RLK/AAA-GFP<<leu1+ plo1+-mCherry<<natR nda3-KM311*
Figure 2D,E		
SK891	*h+*	*leu1 mad1+-GFP<<kanR plo1+-mCherry<<natR nda3-KM311*
SL777	*h+*	*leu1 ura4? his2? ade6-M216 plo1+-mCherry<<natR mad1+-GFP<<kanR bub1Δ::ura4+ nda3-KM311*
ST045	*h-*	*bub1-STT/AAA mad1+-GFP<<kanR plo1+-mCherry<<natR nda3-KM311*
SM814	*h+*	*ade6-M216 mad1Δ::ura4+ pDUAL-Pnmt81-mis12-mad1+-GFP<<leu1+ plo1+-mCherry<<natR nda3-KM311*
ST150	*h+*	*ade6-M216 mad1Δ::ura4+ bub1Δ::ura4+ Pnmt81-mis12-mad1-GFP<<leu1+ plo1+-mCherry<<natR nda3-KM311*
ST490	*h+*	*mad1Δ::ura4+ bub1-STT/AAA Pnmt81-mis12-mad1-GFP<<leu1+ plo1+-mCherry<<natR nda3-KM311*
Figure 2F		
SK891	*h+*	*leu1 mad1+-GFP<<kanR plo1+-mCherry<<natR nda3-KM311*
SK893	*h+*	*leu1 ade6-M216 mad1Δ::ura4+ plo1+-mCherry<<natR nda3-KM311*
SM814	*h+*	*ade6-M216 mad1Δ::ura4+ pDUAL-Pnmt81-mis12-mad1+-GFP<<leu1+ plo1+-mCherry<<natR nda3-KM311*
SM815	*h+*	*ade6-M216 mad1Δ::ura4+ pDUAL-Pnmt81-mis12-mad1-RLK/AAA-GFP<<leu1+ plo1+-mCherry<<natR nda3-KM311*
SM827	*h+*	*(ade6-M216?) mad1Δ::ura4+ pDUAL-Pnmt81-mad1+-GFP<<leu1+ plo1+-mCherry<<natR nda3-KM311*
SM828	*h+*	*(ade6-M216?) mad1Δ::ura4+ pDUAL-Pnmt81-mad1-RLK/AAA-GFP<<leu1+ plo1+-mCherry<<natR nda3-KM311*
ST162	*h-*	*mad1+-GFP<<kanR mad2+-mCherry<<natR nda3-KM311*
ST167	*h-*	*(ura4-D18?) mad2+-mCherry<<natR mad1Δ::ura4+ pDUAL-Pnmt81-mis12-mad1+-GFP<<leu1+ nda3-KM311*
ST168	*h-*	*(ura4-D18?) mad2+-mCherry<<natR mad1Δ::ura4+ pDUAL-Pnmt81-mis12-mad1-RLK/AAA-GFP<<leu1+ nda3-KM311*
ST170	*h-*	*(ura4-D18?) mad2+-mCherry<<natR mad1Δ::ura4+ pDUAL-Pnmt81-mad1+-GFP<<leu1+ nda3-KM311*
Figure 3B,C,F		
SK891	*h+*	*leu1 mad1+-GFP<<kanR plo1+-mCherry<<natR nda3-KM311*
ST174	*h-*	*leu1 mad1-EDD/QNN(E670Q/D673N/D676N)-GFP<<kanR plo1+-mCherry<<natR nda3-KM311*
ST190''	*h-*	*leu1 mad1-1-661-GFP<<kanR plo1+-mCherry<<natR nda3-KM311*
Figure 3D,E		
SK891	*h+*	*leu1 mad1+-GFP<<kanR plo1+-mCherry<<natR nda3-KM311*
SK893	*h+*	*leu1 ade6-M216 mad1Δ::ura4+ plo1+-mCherry<<natR nda3-KM311*
ST174	*h-*	*leu1 mad1-EDD/QNN-GFP<<kanR plo1+-mCherry<<natR nda3-KM311*
ST190''	*h-*	*leu1 mad1-1-661-GFP<<kanR plo1+-mCherry<<natR nda3-KM311*
Figure 3G		
ST162	*h-*	*mad1+-GFP<<kanR mad2+-mCherry<<natR nda3-KM311*
ST443	*h+*	*leu1 mad1-EDD/QNN-GFP<<kanR mad2+-mCherry<<natR nda3-KM311*
ST448	*h-*	*leu1 mad1+-GFP<<kanR mad2-R133A-mCherry<<natR nda3-KM311*
ST460	*h+*	*ade6-M216 leu1 mad1-1-661-GFP<<kanR mad2+-mCherry<<natR nda3-KM311*
ST486	*h+*	*leu1 mad1-EDD/QNN-GFP<<kanR mad2-R133A-mCherry<<natR nda3-KM311*
ST488	*h+*	*leu1 mad1-aa1-661-GFP<<kanR mad2-R133A-mCherry<<natR nda3-KM311*
Figure 3H		
ST167	*h-*	*(ura4-D18?) mad2+-mCherry<<natR mad1Δ::ura4+ pDUAL-Pnmt81-mis12-mad1+-GFP<<leu1+ nda3-KM311*
ST168	*h-*	*(ura4-D18?) mad2+-mCherry<<natR mad1Δ::ura4+ pDUAL-Pnmt81-mis12-mad1-RLK/AAA-GFP<<leu1+ nda3-KM311*
ST447	*h+*	*ade6-M216 mad1Δ::ura4+ pDUAL-Pnmt81-mis12-mad1+-GFP<<leu1+ mad2-R133A-mCherry<<natR nda3-KM311*
Figure S1A,C		
SK891	*h+*	*leu1 mad1+-GFP<<kanR plo1+-mCherry<<natR nda3-KM311*
SM001	*h-*	*leu1 mad1-RLK/AAA-GFP<<kanR plo1+-mCherry<<natR nda3-KM311*
ST146	*h+*	*leu1 mad1-RLK/ALA-GFP<<kanR plo1+-mCherry<<natR nda3-KM311*

SM090	*h+*	*mad1-1-600-GFP<<kanNT3 plo1+-mCherry<<natR nda3-KM311*
SM091	*h+*	*mad1-1-526-GFP<<kanNT3 plo1+-mCherry<<natR nda3-KM311*

Figure S1B

SL894	*h+*	*leu1 ade6-M210 ark1+-GFP<<kanR plo1+-mCherry<<natR nda3-KM311*
SL891	*h+*	*leu1 ark1+-GFP<<kanR plo1+-mCherry<<natR nda3-KM311 mad1-RLK/AAA*
SL900	*h-*	*leu1 bub1+-GFP<<kanR plo1+-mCherry<<natR nda3-KM311*
SL898	*h-*	*leu1 bub1+-GFP<<kanR plo1+-mCherry<<natR nda3-KM311 mad1-RLK/AAA*
SM092	*h-*	*leu1 ade6-M216 bub3+-S(GGGGS)3-GFP<<kanR plo1+-mCherry<<natR nda3-KM311*
SL358	*h-*	*leu1 bub3+-S(GGGGS)3-GFP<<kanR plo1+-mCherry<<natR nda3-KM311 mad1-RLK/AAA*

Figure S1D

SK842	*h+*	*leu1 mad2+-GFP<<kanR plo1+-mCherry<<natR nda3-KM311*
SL905	*h-*	*leu1 mad1Δ::mad1-RLK/AAA mad2+-GFP<<kanR plo1+-mCherry<<natR nda3-KM311*

Figure S1F

SP784	*h+*	*leu1 rpl42::cyhR(sP56Q) bub1Δ::rpl42+hphNT1*
PX938	*h-*	*leu1 bub1+-GFP<<kanR*
SP297	*h-*	*leu1 bub1-STT/AAA-GFP<<kanR*

Figure S1G

SK442	*h+*	*leu1 bub1+-GFP<<kanR plo1+-mCherry<<natR*
SP705	*h-*	*leu1 bub1-STT/AAA-GFP<<kanR plo1+-mCherry<<natR nda3-KM311*

Figure S1H

SK892	*h+*	*leu1 mad1+-GFP<<kanR plo1+-mCherry<<natR nda3-KM311*
ST045	*h-*	*bub1-STT/AAA mad1+-GFP<<kanR plo1+-mCherry<<natR nda3-KM311*

Figure S1I

SK713	*h-*	*leu1 plo1+-mCherry<<natR mad2+-GFP<<kanR nda3-KM311*
ST053	*h+*	*leu1 bub1-STT/AAA mad2+-GFP<<kanR plo1+-mCherry<<natR nda3-KM311*
SL759	*h-*	*leu1 mad3+-GFP<<kanR plo1+-mCherry<<natR nda3-KM311*
ST051	*h+*	*leu1 bub1-STT/AAA mad3+-GFP<<kanR plo1+-mCherry<<natR nda3-KM311*
SM092	*h-*	*leu1 ade6-M216 bub3+-S(GGGGS)3-GFP<<kanR plo1+-mCherry<<natR nda3-KM311*
ST050	*h-*	*leu1 bub1-STT/AAA bub3+-S(GGGGS)3-GFP<<kanR plo1+-mCherry<<natR nda3-KM311*

Figure S2B

SK891	*h+*	*leu1 mad1+-GFP<<kanR plo1+-mCherry<<natR nda3-KM311*
SK893	*h+*	*leu1 ade6-M216 mad1Δ::ura4+ plo1+-mCherry<<natR nda3-KM311*
ST141	*h+*	*leu1 ade6-M216 GCN4(250-277)-mad1-306-676-GFP<<kanR plo1+-mCherry<<natR nda3-KM311*
ST441	*h+*	*leu1 GCN4(250-277)-mad1-458-676-GFP<<kanR plo1+-mCherry<<natR nda3-KM311*
ST408	*h-*	*leu1 GCN4(250-277)-mad1-564-676-GFP<<kanR plo1+-mCherry<<natR nda3-KM311*
ST417	*h+*	*leu1 ade6-M216 GCN4(250-277)-mad1-585-676-GFP<<kanR plo1+-mCherry<<natR nda3-KM311*

Figure S2C,D

SK891	*h+*	*leu1 mad1+-GFP<<kanR plo1+-mCherry<<natR nda3-KM311*
ST141	*h+*	*leu1 ade6-M216 GCN4(250-277)-mad1-306-676-GFP<<kanR plo1+-mCherry<<natR nda3-KM311*
ST442	*h+*	*leu1 GCN4(250-277)-mad1-458-676-GFP<<kanR plo1+-mCherry<<natR nda3-KM311*
ST408	*h-*	*leu1 GCN4(250-277)-mad1-564-676-GFP<<kanR plo1+-mCherry<<natR nda3-KM311*
ST417	*h+*	*leu1 ade6-M216 GCN4(250-277)-mad1-585-676-GFP<<kanR plo1+-mCherry<<natR nda3-KM311*

Figure S2E

ST162	*h-*	*mad1+-GFP<<kanR mad2+-mCherry<<natR nda3-KM311*
ST748	*h-*	*leu1 (ade6-M216?) GCN4(250-277)-mad1-306-676-GFP<<kanR mad2+-mCherry<<natR nda3-KM311*
ST750	*h+*	*leu1 (ade6-M216?) GCN4(250-277)-mad1-458-676-GFP<<kanR mad2+-mCherry<<natR nda3-KM311*
ST752	*h-*	*leu1 (ade6-M216?) GCN4(250-277)-mad1-564-676-GFP<<kanR mad2+-mCherry<<natR nda3-KM311*
ST754	*h+*	*leu1 (ade6-M216?) GCN4(250-277)-mad1-585-676-GFP<<kanR mad2+-mCherry<<natR nda3-KM311*

Figure S2F

SK891	*h+*	*leu1 mad1+-GFP<<kanR plo1+-mCherry<<natR nda3-KM311*
SK893	*h+*	*leu1 ade6-M216 mad1Δ::ura4+ plo1+-mCherry<<natR nda3-KM311*
ST141	*h+*	*leu1 ade6-M216 GCN4(250-277)-mad1-306-676-GFP<<kanR plo1+-mCherry<<natR nda3-KM311*
ST142	*h+*	*leu1 ade6-M216 GCN4(250-277)-mad1-306-676-GFP<<kanR plo1+-mCherry<<natR nda3-KM311*
ST441	*h+*	*leu1 GCN4(250-277)-mad1-458-676-GFP<<kanR plo1+-mCherry<<natR nda3-KM311*
ST442	*h+*	*leu1 GCN4(250-277)-mad1-458-676-GFP<<kanR plo1+-mCherry<<natR nda3-KM311*
ST408	*h-*	*leu1 GCN4(250-277)-mad1-564-676-GFP<<kanR plo1+-mCherry<<natR nda3-KM311*
ST409	*h-*	*leu1 ade6-M216 GCN4(250-277)-mad1-564-676-GFP<<kanR plo1+-mCherry<<natR nda3-KM311*
ST417	*h+*	*leu1 ade6-M216 GCN4(250-277)-mad1-585-676-GFP<<kanR plo1+-mCherry<<natR nda3-KM311*
ST419	*h-*	*leu1 ade6-M216 GCN4(250-277)-mad1-585-676-GFP<<kanR plo1+-mCherry<<natR nda3-KM311*

Figure S3A

SM822	*h+*	*plo1+-mCherry<<natR mad1+-GFP<<kanR cdc25-22*
SK671	*h-*	*lys1 hph<<ark1-as3 (L166A, S229A) plo1+-mCherry<<natR mad1+-GFP<<kanR nda3-KM311*
SK676	*h-*	*lys1 hph<<ark1-as3 (L166A, S229A) plo1+-mCherry<<natR bub1+-GFP<<kanR nda3-KM311*

Figure S3B

SL355	*h+*	*leu1 (ade6-M216?) nda3-KM311 bub1+-HA<<hph bub3+S(GGGGS)3-GFP<<kanR plo1+-mCherry<<natR*

Figure S3C

ST162	*h-*	*mad2+-mCherry<<natR mad1+-GFP<<kanR nda3-KM311*
ST167	*h-*	*(ura4-D18?) mad2+-mCherry<<natR mad1Δ::ura4+ pDUAL-Pnmt81-mis12-mad1+-GFP<<leu1+ nda3-KM311*
ST168	*h-*	*(ura4-D18?) mad2+-mCherry<<natR mad1Δ::ura4+ pDUAL-Pnmt81-mis12-mad1-RLK/AAA-GFP<<leu1+ nda3-KM311*
ST170	*h-*	*(ura4-D18?) mad2+-mCherry<<natR mad1Δ::ura4+ pDUAL-Pnmt81-mad1+-GFP<<leu1+ nda3-KM311*
ST171	*h-*	*(ura4-D18?) mad2+-mCherry<<natR mad1Δ::ura4+ pDUAL-Pnmt81-mad1-RLK/AAA-GFP<<leu1+ nda3-KM311*

Figure S4A

SP903	*h-*	*leu1 mad1-L533A-GFP<<kanR plo1+-mCherry<<natR nda3-KM311*
SP965	*h?*	*leu1 ade6-M216 mad1-F592A-GFP<<kanR plo1+-mCherry<<natR nda3-KM311*
SP986	*h+*	*leu1 mad1-R593A-GFP<<kanR plo1+-mCherry<<natR nda3-KM311*
SP983	*h+*	*leu1 mad1-V596A-GFP<<kanR plo1+-mCherry<<natR nda3-KM311*
SP967	*h+*	*leu1 mad1-G601A-GFP<<kanR plo1+-mCherry<<natR nda3-KM311*
ST115	*h+*	*leu1 ade6-M216 mad1-R613A-GFP<<kanR plo1+-mCherry<<natR nda3-KM311*
SP476	*h+*	*leu1 ade6-M216 mad1-S616A-GFP<<kanR plo1+-mCherry<<natR nda3-KM311*
SP511	*h+*	*leu1 mad1-P661A-GFP<<kanR plo1+-mCherry<<natR nda3-KM311*
SP513	*h+*	*leu1 mad1-P661A/S633G-GFP<<kanR plo1+-mCherry<<natR nda3-KM311*
SP597	*h-*	*leu1 mad1-ELK/AAA(E670A/L672A/K674A)-GFP<<kanR plo1+-mCherry<<natR nda3-KM311*
ST148	*h-*	*leu1 mad1-ELK/AAA plo1+-mCherry<<natR nda3-KM311*

Figure S4B,D

SK891	*h+*	*leu1 mad1+-GFP<<kanR plo1+-mCherry<<natR nda3-KM311*
ST174	*h-*	*leu1 mad1-EDD/QNN-GFP<<kanR plo1+-mCherry<<natR nda3-KM311*
ST190"	*h-*	*leu1 mad1-1-661-GFP<<kanR plo1+-mCherry<<natR nda3-KM311*

Figure S4C

ST162	*h-*	*mad1-GFP<<kanR mad2+-mCherry<<natR nda3-KM311*
ST443	*h+*	*leu1 mad1-EDD/QNN-GFP<<kanR mad2+-mCherry<<natR nda3-KM311*
ST460	*h+*	*ade6-M216 leu1 mad1-1-661-GFP<<kanR mad2+-mCherry<<natR nda3-KM311*

Figure S4G

SK443	*h-*	*leu1 plo1+-mCherry<<natR bub1+-GFP<<kanR*
ST764'	*h-*	*(leu1?) mad1-aa1-661 bub1+-GFP<<kanR plo1+-mCherry<<natR nda3-KM311*
ST766	*h-*	*leu1 (ura4-D18?) mad1-EDD/QNN bub1+-GFP<<kanR plo1+-mCherry<<natR nda3-KM311*

Figure S4H

JY265	*h-*	*leu1*
SP010	*h-*	*leu1 mad1Δ::ura4+*
ST812	*h+*	*leu1 rpl42::cyhR(sP56Q) mad1-aa1-661*
ST812'	*h+*	*leu1 rpl42::cyhR(sP56Q) mad1-aa1-661*
ST481	*h+*	*leu1 mad1-EDD/QNN*

Supplementary Information

Re-annotation of the Mad1 start codon

In the *Schizosaccharomyces pombe* genome database (www.pombase.org; Jan 8th, 2014), the *mad1+* coding sequence is annotated to start at position 1,277,098 on chromosome II. Alignment with the sequence of other *Schizosaccharomyces* species [5] indicates that the first 13 amino acids (MSSKLTVYQATTS) are not conserved and that it is likely that the start codon is amino acid 14, another Methionine. To corroborate this notion, we performed mass spectrometric analysis of immunopurified Mad1, digested with either Asp-N, Lys-C or Trypsin. We identified peptides supporting both the first as well as the second Methionine as start codon. In one experiment, where peptides for both termini were found (see below; LTVYQATTSM(ox)ADSPR (amino acid 5-19) supporting the first Methionine, and (ac)ADS(ph)PRDPFQSR (amino acid 15-25) supporting the second Methionine), the intensity of the second peptide was 170-times higher than of the first. Together with the phylogenetic evidence, this suggests that the second Methionine is the more prominent start codon, although the first one can be used. The annotation in the *Schizosaccharomyces pombe* genome database will be revised accordingly (Val Wood, personal communication).

Peptide 1 supporting translation from first Methionine:

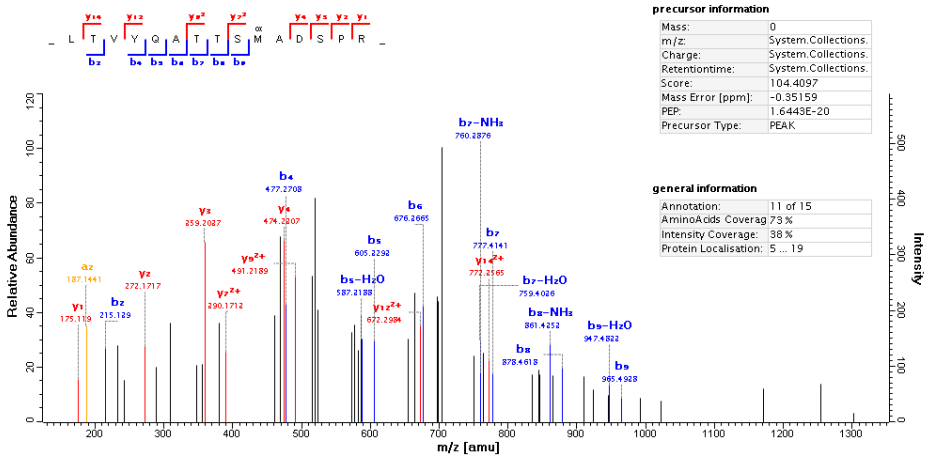

a ion		b ion					y ion		y^{2+} ion	
Δ dalton	mass	Δ dalton	mass		seq		Δ dalton	mass	Δ dalton	mass
	86.09643		114.0913	1	L	14				
+0.107437	187.1441	-0.017483	215.139	2	T	13	1543.706		772.3565	+0.451557
	286.2125		314.2074	3	V	12	1442.658		1442.658	
	449.2758	+0.147757	477.2708	4	Y	11	1343.59		672.2984	+0.07247
	577.3344	+0.094794	605.3293	5	Q	10	1180.526		1180.526	
	648.3715	+0.061282	676.3665	6	A	9	1052.468		1052.468	
	749.4192	+0.023064	777.4141	7	T	8	981.4306		491.2189	-0.054625
	850.4669	+0.046796	878.4618	8	T	7	880.3829		880.3829	
	937.4989	+0.083127	965.4938	9	S	6	779.3352		390.1713	+0.078564
	1084.534		1112.529	10	M	5	692.3032		692.3032	
	1155.571		1183.566	11	A	4	545.2678		545.2678	
	1270.598		1298.593	12	D	3	474.2307	-0.055517	474.2307	
	1357.63		1385.625	13	S	2	359.2037	+0.13201	359.2037	
	1454.683		1482.678	14	P	1	272.1717	-0.107019	272.1717	
				15	R	0	175.119	-0.006541	175.119	

Peptide 2 supporting translation from second Methionine:

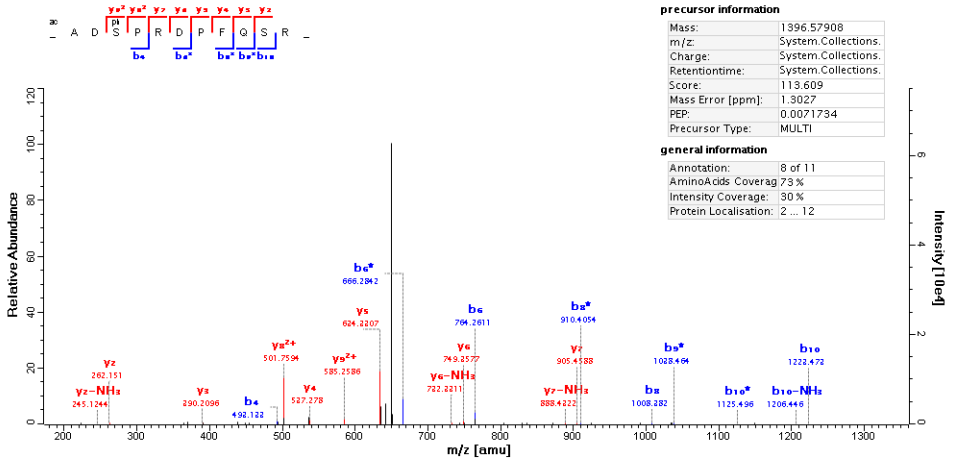

b ion					y ion		y^{2+} ion	
Δ dalton	mass		seq		Δ dalton	mass	Δ dalton	mass
	114.05495494	1	A	10				
	229.08189797	2	D	9	1284.5368556		1284.5368556	
	396.08025679	3	S	8	1169.5099126		585.25859453	+0.0152092
-0.1849616	493.13302064	4	P	7	1002.5115538		501.75941512	+0.0294032
	649.23413167	5	R	6	905.45878993	+0.0629996	905.45878993	
+0.0287813	764.2610747	6	D	5	749.3576789	+0.1810174	749.3576789	
	861.31383856	7	P	4	634.33073587	+0.0019668	634.33073587	
+0.0844223	1008.3822525	8	F	3	537.27797202	-0.1872127	537.27797202	
	1136.44083	9	Q	2	390.2095581	+0.1191772	390.2095581	
+0.1417656	1223.4728584	10	S	1	262.15098059	+0.0349935	262.15098059	
		11	R	0	175.11895218		175.11895218	

Supplementary References

5. Rhind N *et al* (2011) Comparative functional genomics of the fission yeasts. *Science* **332:** 930-936

2.2 Bub3-Bub1 binding to Spc7/KNL1 toggles the spindle checkpoint switch by licensing the interaction of Bub1 with Mad1-Mad2

Maria del Mar Mora-Santos[1], America Hervas-Aguilar[1], Katharina Sewart[2], Theresa C. Lancaster[1], John C. Meadows[1,3], Jonathan B.A. Millar[1]

[1]Division of Biomedical Sciences, Warwick Medical School, University of Warwick, Coventry, UK
[2]Department of Biological Sciences and Biocomplexity Institute, Virginia Tech, Blacksburg, VA, USA
[3]Institute of Advanced Study, University of Warwick, Coventry, UK

Correspondence: j.millar@warwick.ac.uk

Published in **Current Biology**, Volume 26, p.2642-2650 (2016)
DOI: 10.1016/j.cub.2016.07.040

Author contributions:
I performed experiments and analyzed the data shown in Fig. 1B and Fig. S1D. Furthermore, I gave input to the writing of the manuscript.

Maria del Mar Mora-Santos carried out all other experiments with the exception of single-cell analysis of Bub1 and Bub3 binding to the kinetochore (performed by **John C. Meadows**).

America Hervas-Aguilar and Theresa C. Lancaster aided with molecular biology and strain construction.

Jonathan B.A. Millar conceived the project and wrote the manuscript with input from **Maria del Mar Mora-Santos**, **John C. Meadows** and me**.**

Report

Current Biology

Bub3-Bub1 Binding to Spc7/KNL1 Toggles the Spindle Checkpoint Switch by Licensing the Interaction of Bub1 with Mad1-Mad2

Highlights

- Spc7 (KNL1) MELT array acts a phospho-dependent spindle checkpoint toggle switch
- The threshold of the Spc7 MELT toggle switch is set by Bub3 and Bub1 protein levels
- Interaction of Mad1-Mad2 with Bub1 is controlled by Mph1 kinase and PP1 phosphatase
- Binding of Bub3-Bub1 to Spc7 (KNL1) permits interaction of Mad1-Mad2 with Bub1

Authors

Maria del Mar Mora-Santos, America Hervas-Aguilar, Katharina Sewart, Theresa C. Lancaster, John C. Meadows, Jonathan B.A. Millar

Correspondence

j.millar@warwick.ac.uk

In Brief

Mora-Santos et al. show that phospho-dependent binding of Bub3-Bub1 to the Spc7 (KNL1) MELT array acts as a toggle switch for the spindle checkpoint by converting Bub3 from a concentration-dependent inhibitor to an activator of Bub1 through licensing Mph1 (Mps1) kinase-dependent interaction of Bub1 with the Mad1-Mad2 complex.

Mora-Santos et al., 2016, Current Biology *26*, 2642–2650
October 10, 2016 © 2016 Elsevier Ltd.
http://dx.doi.org/10.1016/j.cub.2016.07.040

CellPress

Current Biology
Report

Bub3-Bub1 Binding to Spc7/KNL1 Toggles the Spindle Checkpoint Switch by Licensing the Interaction of Bub1 with Mad1-Mad2

Maria del Mar Mora-Santos,[1] America Hervas-Aguilar,[1] Katharina Sewart,[2] Theresa C. Lancaster,[1] John C. Meadows,[1,3] and Jonathan B.A. Millar[1,4,*]

[1]Division of Biomedical Sciences, Warwick Medical School, University of Warwick, Gibbet Hill, Coventry CV4 7AL, UK
[2]Department of Biological Sciences and Biocomplexity Institute, Virginia Tech, Blacksburg, VA 24061, USA
[3]Institute of Advanced Study, University of Warwick, Gibbet Hill, Coventry CV4 7AL, UK
[4]Lead Contact
*Correspondence: j.millar@warwick.ac.uk
http://dx.doi.org/10.1016/j.cub.2016.07.040

SUMMARY

The spindle assembly checkpoint (SAC) ensures that sister chromatids do not separate until all chromosomes are attached to spindle microtubules and bi-oriented. Spindle checkpoint proteins, including Mad1, Mad2, Mad3 (BubR1), Bub1, Bub3, and Mph1 (Mps1), are recruited to unattached and/or tensionless kinetochores. SAC activation catalyzes the conversion of soluble Mad2 (O-Mad2) into a form (C-Mad2) that binds Cdc20, BubR1, and Bub3 to form the mitotic checkpoint complex (MCC), a potent inhibitor of the anaphase-promoting complex (APC/C). SAC silencing de-represses Cdc20-APC/C activity allowing poly-ubiquitination of Securin and Cyclin B, leading to the dissolution of sister chromatids and anaphase onset [1]. Understanding how microtubule interaction at kinetochores influences the timing of anaphase requires an understanding of how spindle checkpoint protein interaction with the kinetochore influences spindle checkpoint signaling. We, and others, recently showed that Mph1 (Mps1) phosphorylates multiple conserved MELT motifs in the Spc7 (Spc105/KNL1) protein to recruit Bub1, Bub3, and Mad3 (BubR1) to kinetochores [2–4]. In budding yeast, Mps1 phosphorylation of a central non-catalytic region of Bub1 promotes its association with the Mad1-Mad2 complex, although this association has not yet been detected in other organisms [5]. Here we report that multisite binding of Bub3 to the Spc7 MELT array toggles the spindle checkpoint switch by permitting Mph1 (Mps1)-dependent interaction of Bub1 with Mad1-Mad2.

RESULTS AND DISCUSSION

Bub3-Bub1 Binding to Spc7 MELT Motifs Toggles the Spindle Checkpoint Switch

The N terminus of the fission yeast KNL1 homolog, Spc7, contains 12 MELT motifs that can be phosphorylated by Mph1 (Mps1) kinase in vitro [3, 4]. To examine the role of MELT motifs in controlling Bub1 binding and checkpoint signaling, we created a sequence of mutants, *spc7-12TA*, *spc7-9TA*, *spc7-7TA*, *spc7-5TA*, *spc7-3TA*, or *spc7-1TA*, in which some or all of the threonine and serine residues in these motifs were mutated to non-phosphorylatable alanine (Figure S1A). Binding of Bub1 to kinetochores was assayed in these mutants by quantitative fluorescence microscopy in cells that were arrested in mitosis by overexpression of Mad2. This revealed a wide dynamic range of Bub1 binding to kinetochores in individual cells and, as the number of phosphorylatable MELT sites was reduced, progressively lower average binding to kinetochores and inversely higher levels of nucleoplasmic Bub1 (Figures 1A, S1B, and S1C), while the total Bub1 abundance stayed constant (Figure S1E).

In parallel, we measured the ability of individual *spc7* mutant cells, bearing a cold-sensitive allele of β-tubulin (*nda3-KM311*) and a marker for high Cdk1 activity (Plo1-GFP), to mount a spindle checkpoint arrest. While most *spc7-1TA*, *spc7-3TA*, *spc7-5TA*, and *spc7-7TA* cells fully arrested, *spc7-9TA* and *spc7-12TA* cells mounted only a partial checkpoint response compared to wild-type cells (Figures 1B, S1C, and S1D). Similar results were observed in population studies of synchronized *nda3-KM311 spc7* mutant cells, which express a marker that only appears in anaphase (Nsk1-GFP). While a partial checkpoint response was still mounted in *spc7-7TA* cells, *spc7-9TA* and *spc7-12TA* cells were largely defective (Figures 1C and S1G). We note that the checkpoint in *spc7-12TA* cells is not as defective as in cells lacking *mad3*, suggesting that the spindle assembly checkpoint (SAC) can be partially activated in this mutant (Figures 1B and 1C).

Spindle checkpoint protein homeostasis is crucial for the robustness of the checkpoint response in that even minor changes in the protein concentration of Mad1, Mad2, Mad3, and Cdc20 alter the threshold at which cells are able to delay anaphase onset in response to unattached kinetochores [6]. To examine whether the switch-like spindle checkpoint response from the Spc7-MELT array is sensitive to changes in Bub1 and Bub3 levels, we altered the expression of these proteins in a mutant defective in their kinetochore binding. Deletion of Bub3 strongly suppressed the checkpoint deficiency in *spc7-12TA* cells, as previously observed (Figures 1D and S1H) [4]. This effect is not due to the upregulation of Bub1 protein levels

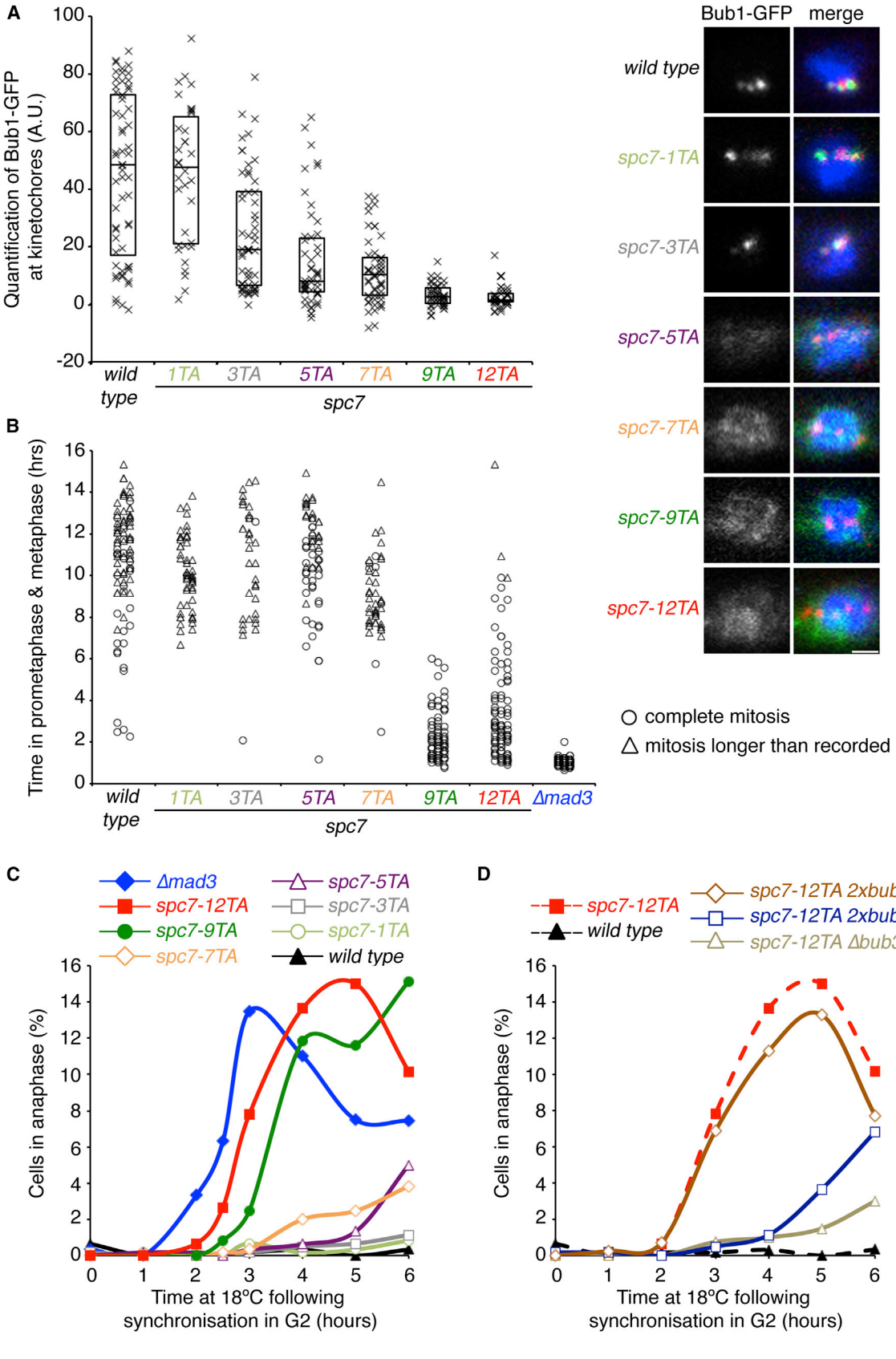

(legend on next page)

(Figure S1F). Conversely, expression of an extra copy of Bub1 also strongly suppressed the checkpoint deficiency of *spc7-12TA* cells, whereas expression of an extra copy of Bub3 had no effect (Figure 1D). We conjecture that the inability of cells to mount a checkpoint response, when Bub3-Bub1 is not recruited to kinetochores, can be overcome by an excess of non-kinetochore-bound Bub1 over Bub3. Together, these results suggest that the toggle switch for the spindle checkpoint at kinetochores is not only dependent on the availability of phosphorylatable MELT motifs but also on the relative abundance of Bub1 and Bub3.

Bub3 Inhibits Bub1-Dependent SAC Signaling When Not Bound to Spc7/KNL1

This prompted us to examine whether Bub3 acts as an inhibitor of Bub1 when not bound to kinetochores. Importantly, crystallographic data have revealed that the phosphorylated threonines in MELT motifs from the budding yeast KNL1 homolog, Spc105, form ionic bonds with the Bub3 β-propeller toroid and that mutation of Arg^{217} and Arg^{239} in Bub3 abolishes localization of Bub3 and Bub1 to kinetochores and prevents budding yeast cells from mounting a spindle checkpoint response [7]. However, since Bub3 is also a component of the mitotic checkpoint complex (MCC) in budding yeast, it is unclear whether checkpoint failure in this mutant is due to an inability of Bub3 to interact with Spc105 or because these mutations disrupt the structural integrity of the MCC complex, or both. Importantly, Bub3 is not essential for checkpoint activation and Bub3 is not a component of the MCC in fission yeast [8].

For this reason, we created a *bub3-R201A,K221A* mutant at the endogenous locus, which, based on crystallography and homology, should be defective in binding phospho-MELT repeats of Spc7 but which would not influence MCC stability (Figure S2A; hereafter referred to as *bub3-RA,KA* mutant). In *bub3-RA,KA* cells, Bub1 remained in the nucleus but failed to accumulate at the kinetochore (Figure 2A), even though interaction of Bub1 with the Bub3-RA,KA mutant protein remained intact (Figure 2B). Consistently, the Bub3-RA,KA-GFP protein failed to localize to the kinetochore (Figure 2A). This was probably due to the inability of Bub3-Bub1 to interact with phosphorylated Spc7 MELT repeats, since GST-Spc7-T9E proteins were unable to precipitate the Bub3-Bub1 complex from extracts of *bub3-RA,KA* cells (Figure 2C). Indeed, no GFP foci were observed in interphase or mitotic *bub1-GFP bub3-RA,KA spc7-9TE* or *bub3-RA,KA-GFP spc7-9TE* cells, indicating that interaction of the Bub3-Bub1 complex with phosphorylated Spc7 is disrupted in the *bub3-RA,KA* mutant (Figure 2A).

To our surprise, expression of *bub3-RA,KA* from its endogenous locus displayed little defect in checkpoint signaling (Figure 2D). We noted, however, that the steady-state level of the Bub3-RA,KA-GFP protein was ~40% lower than the corresponding Bub3-GFP wild-type protein, as judged by western analysis (Figure 2E). To examine whether this accounted for the lack of effect of the *bub3-RA,KA* allele on checkpoint signaling, we integrated a second copy of the mutant *bub3-RA,KA* gene at the *lys1* locus. By itself (i.e., in a *Δbub3* background), the *lys1::bub3-RA,KA* allele also had only a minor effect on checkpoint signaling (Figure S2B). However, when both copies were expressed in the same cell (2x*bub3-RA,KA*), the total amount of the Bub3-RA,KA-GFP protein was 10% greater than that seen in wild-type cells (Figure 2E) and the defect in checkpoint signaling was comparable to that observed in *spc7-9TA* cells (Figures 2D and 1C). Importantly, the checkpoint-signaling defect in the 2x*bub3-RA,KA* mutant was suppressed in *bub1(ΔGLEBS)* cells, which lack the GLEBS domain in Bub1 that is required for Bub3 binding [9], or when a second copy of Bub1 (2Xbub1) was introduced, indicating that, when not bound to phosphorylated MELT motifs, Bub3 exerts its dose-dependent inhibitory effect on checkpoint signaling through interaction with Bub1 (Figure 2D). The fact that checkpoint signaling is not completely abrogated in *spc7-12TA* or bub3-*RA,KA* mutants suggests that a fraction of Bub1 can escape the inhibitory effect of Bub3.

Mph1/Mps1 Kinase and Dis2/PP1 Phosphatase Antagonistically Regulate the Interaction of Mad1-Mad2 with Bub1

We reasoned that kinetochore association of Bub3-Bub1 may relieve the inhibitory effect of Bub3 by altering the interaction of Bub1 with other components of the spindle checkpoint. To test this, we prepared extracts from *nda3-KM311 bub1-6HA* cells expressing *mad1-GFP*, *mad2-GFP*, or *mad3-GFP* and tested them for co-immunoprecipitation. We found that Mad1, Mad2, and Mad3 all interacted with Bub1 in checkpoint-arrested cells; however, the interaction between Mad1 and Bub1 was weak, possibly because the *mad1-GFP* allele was not fully functional (Figures 3A and S3A). Notably, the interaction of Mad2 with Bub1 was observed in checkpoint-arrested, but not log-phase, cells, whereas the formation of Mad1-Mad2 and Mad3-Bub1 complexes was observed in both conditions, although this was increased in checkpoint-arrested cells (Figure 3B).

In budding yeast, Mps1-mediated phosphorylation of Bub1 recruits the Mad1-Mad2 complex to kinetochores and this is required for checkpoint signaling [5]. This prompted us to assess the phosphorylation requirements for the interaction of Bub1 with Mad1, Mad2, and Mad3 in fission yeast. We found that, in the absence of Dis2, the major form of type 1 phosphatase (PP1), the interaction of both Mad1 and Mad2 with Bub1 was

Figure 1. Levels of Bub1-Bub3 at Kinetochores Threshold the Activity of the SAC

(A) Bub1 bound to kinetochores decreases as MELT motifs are abolished. Levels of Bub1-GFP, normalized against inner kinetochore Fta3-RFP, were calculated in individual *spc7* mutant cells arrested in mitosis by overexpression of Mad2. Representative images are shown on the right. Scale bar, 1 μm.

(B) Switch-like checkpoint response of the Spc7 MELT array. The duration of mitosis prior to anaphase was determined by live-cell imaging of Plo1-GFP in individual *nda3-KM311 spc7* mutant cells at the restrictive temperature.

(C) Anaphase onset was determined by measuring the appearance of Nsk1-GFP at the times indicated in *nda3-KM11 nsk1-gfp spc7* mutant cells.

(D) An extra copy of Bub1 rescues the checkpoint defect in *spc7-12TA* cells. Log-phase cultures of the illustrated strains were treated as in (C). Dashed line indicates the same control culture data as in (C).

See also Figure S1.

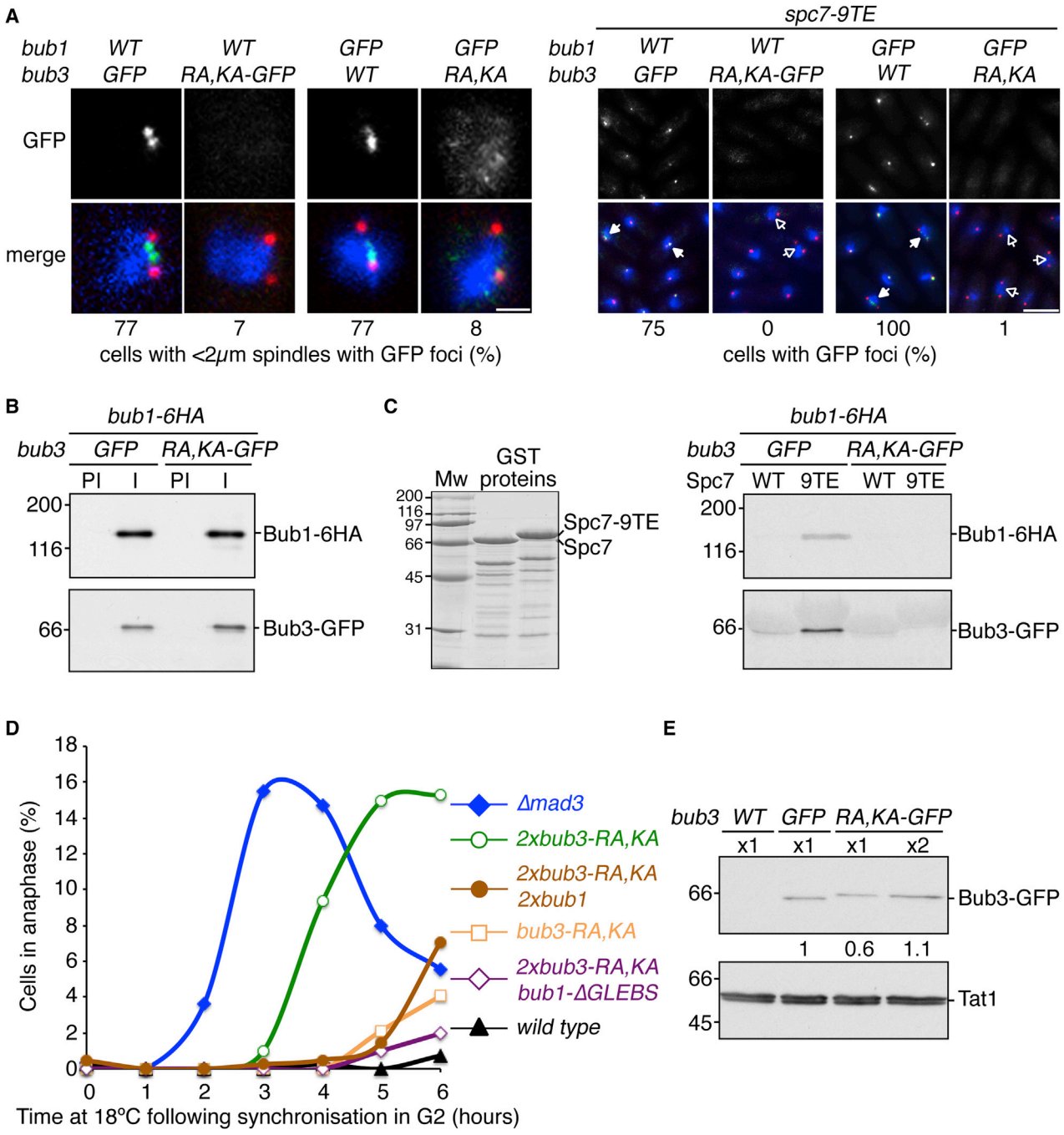

Figure 2. Bub3 Inhibits the Spindle Checkpoint When It Is Not Bound at Kinetochores

(A) Bub1 and Bub3 do not bind the kinetochore in *bub3-R201A,K221A* mutant cells. Log-phase cultures of wild-type (left) or *spc7-T9E* cells (right) expressing *sid4-TdTomato* were fixed, and the percentage of cells with a <2 μm mitotic spindle (left; scale bar, 1 μm) or the percentage of all *spc7-9TE* cells (right; scale bar, 5 μm) that were positive for GFP foci was determined. Filled arrowheads indicate mitotic cells with GFP foci and open arrowheads indicate those without.

(B) Bub1 interacts with Bub3-RA,KA in vivo. Log-phase NP-40 extracts from the indicated strains were immunoprecipitated with rabbit anti-GFP (I) or normal rabbit serum (PI). Complexes were analyzed by immunoblot using anti-HA or sheep anti-GFP antibodies.

(C) Bub3-RA,KA does not interact with Spc7-9TE in vitro. Fusion proteins, purified by Sepharose beads (left), were incubated with the indicated extracts and analyzed by immunoblot using anti-HA or anti-sheep GFP antibodies (right). Mw, molecular weight marker.

(D) Maintenance of the spindle checkpoint is defective in *2xbub3*(*RA,KA*) cells. The indicated *nda3-KM11* strains were fixed at the times shown, and the percentage of anaphase cells (Nsk1-GFP positive) was determined.

(E) Bub3-RA,KA is less stable than Bub3. Extracts from the indicated cells were analyzed by immunoblotting using sheep anti-GFP and anti-Tat1 (tubulin) antibodies. Quantification of normalized GFP levels is shown (Bub3 RA,KA-GFP ± 0.185; 2XBub3 RA,KA-GFP ± 0.23 [±SD]).

See also Figure S2.

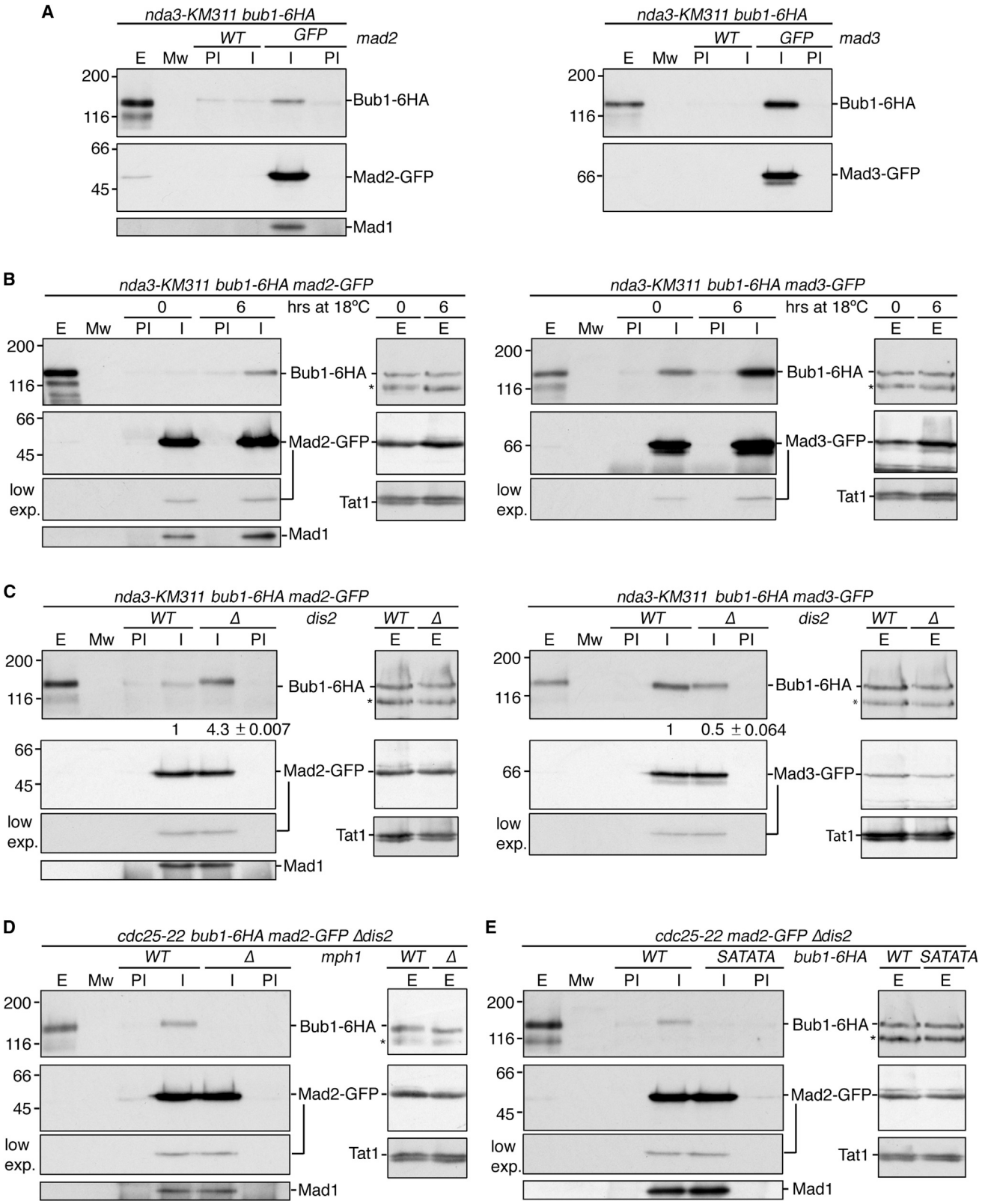

(legend on next page)

enhanced, whereas, to our surprise, the interaction of Mad3 with Bub1 was diminished (Figures 3C and S3B). Since cells lacking Mph1 kinase are checkpoint defective, we arrested *cdc25-22* allele cells in late G2 before releasing them synchronously into mitosis in the presence of carbendazim (CBZ), an inhibitor of microtubule polymerization. The addition of CBZ completely blocked the onset of anaphase in control cells, but not in *Δmad3* cells, and it only delayed anaphase onset in *spc7-12TA* cells by 5 min (Figure S3C). Importantly, we found that, as in budding yeast, the interaction of Mad2 with Bub1 in CBZ-treated prometaphase cells was dependent on Mph1 (Mps1) kinase (Figures 3D and S3D).

We and others previously showed that localization of Mad1 and Mad2 to kinetochores is dependent on a conserved RLK motif of Mad1 and a conserved central motif of Bub1 (cm1) [10–12]. The motif cm1 contains three conserved residues, Ser381, Thr383, and Thr386, which are phosphorylated in checkpoint-arrested fission yeast cells (A.H.-A. and J.B.A.M., unpublished data). Mutation of these residues (Bub1(SATATA)) abolishes recruitment of Mad1 and Mad2 to kinetochores and disables checkpoint signaling [10]. We found that the association of both Mad1 and Mad2 to Bub1 also depends on these residues (Figure 3E and S3E), but the interaction of Mad3 with Bub1 does not (Figure S3E). Together, these data indicate that Mph1 (Mps1) kinase and Dis2 (PP1) phosphatase antagonistically regulate the interaction of Mad1 and Mad2 with Bub1 in fission yeast, most likely through phosphorylation of the conserved central motif of Bub1.

Bub3 Licenses Phospho-Dependent Interaction of Bub1 with the Mad1-Mad2 Complex

We next sought to understand how kinetochore association of Bub3-Bub1 protein influences checkpoint signaling. In fission yeast, Bub3 is not required for spindle checkpoint arrest as Bub3 is not a component of the MCC, but, instead, it is necessary for efficient checkpoint activation and silencing [8, 13, 14]. Indeed, Bub1 interacts with both Mad2 and Mad3 in checkpoint-arrested cells lacking Bub3 (Figure 4A). This suggests that Bub3 is not strictly required for the interaction of the Mad1-Mad2 complex with Bub1. Notably, however, we found that the interaction of Mad2 with Bub1 was drastically reduced in *spc7-12TA* cells compared to wild-type cells, while the interaction of Mad3 with Bub1 increased (Figures 4B and S4A). Importantly, the interaction of Mad1 and Mad2 with Bub1 in *spc7-12TA* was restored by the deletion of Bub3, indicating that Bub3 acts as a negative regulator of Bub1:Mad2 interaction when it is not bound at kinetochores (Figures 4C and S4B). Conversely, the deletion of Bub3 decreases the interaction of Mad3 with Bub1 in *spc7-12TA* cells (Figure S4C). This antagonistic relationship suggests that Mad3 may participate in Bub3-dependent regulation of Mad1-Mad2 binding to Bub1. Identification of Mad3 mutants that specifically fail to associate to Bub1, but retain the ability to form the MCC, would help clarify this issue.

Taken together, our data indicate that the Spc7 (KNL1) MELT array acts as a multisite phospho-dependent toggle switch for the spindle checkpoint at kinetochores, which relies on the conversion of Bub3 from an inhibitor to a facilitator of spindle checkpoint signaling by controlling the interaction of Mad1-Mad2 with Bub1. Once occupancy of Spc7 (KNL1) by Bub3-Bub1 drops below a critical threshold, the rate of MCC generation drops below the rate of MCC turnover, permitting APC/C activation and anaphase onset. This would explain why kinetochore binding of Bub3-Bub1 reduces as cells enter metaphase but does not completely disappear until late anaphase. We postulate that, just like Mad2, Bub3-Bub1 undergoes a conformational change that is dependent on its interaction with phosphorylated MELT motifs of Spc7 (KNL1), which permits the interaction of Mad1-Mad2 with Bub1 (Figure 4D). Reconstitution and structural studies will be needed to test this hypothesis.

Importantly, in human cells, the spindle checkpoint behaves like a rheostat rather than a toggle switch in response to increasing levels of microtubule-kinetochore detachment [15, 16]. This is seemingly at odds with the finding that only a small number of MELT motifs in KNL1 are needed to mount a checkpoint response [17–19]. However, these latter experiments were performed in the presence of reversine, an inhibitor of Mps1 kinase. More recent analysis indicates that human cells possess two distinct means to recruit the Mad1-Mad2 complex to kinetochores: the KNL1-Bub3-Bub1 (KBB) pathway and a second KNL1-independent mechanism mediated by the RZZ-spindly complex, which is absent in yeast [20]. One possibility that merits further analysis is that the RZZ-spindly complex obscures the switch-like behavior of the KBB pathway, which is only revealed in the presence of reversine. We contend that modulation of Bub3 levels by BuGZ [21, 22], phosphorylation of Bub3 by PKM2 kinase [23], or simply alteration of kinetochore number (and therefore number of MELT motifs) influences either the threshold or amplitude of the KBB toggle switch and, in doing so, contributes to chromosome instability in aneuploid cancer cells.

Figure 3. The Mitotic Interaction between Mad2 and Bub1 Is Antagonistically Regulated by Mph1 Kinase and Dis2/PP1 Phosphatase

(A) Bub1 interacts with both Mad2 and Mad3 in vivo. Following incubation at 18°C for 6 hr, extracts were prepared from the illustrated strains and then immunoprecipitated with rabbit anti-GFP (I) or normal rabbit serum (PI), and complexes were analyzed by immunoblot using anti-HA, rabbit anti-Mad1, and sheep anti-GFP antibodies.

(B) Bub1 and Mad2 interact specifically in mitosis. The indicated cells were incubated at either 30°C or 18°C for 6 hr and then immunoprecipited as in (A).

(C) Bub1 interactions with Mad2 and Mad3 are differentially regulated by PP1. The indicated strains were treated and analyzed as in (A). Quantification of normalized Bub1-6HA levels is shown (±SD).

(D) Mph1 kinase is required for Bub1 to interact with Mad2. The strains shown were shifted to 35.5°C for 4 hr and released at 25°C. After 10 min, CBZ was added at 200 μg/ml and cells were collected 15 min later. Extracts were immunoprecipitated and analyzed as in (A).

(E) Bub1-conserved motif 1 (cm1) is required for its interaction with Mad2. The indicated strains were treated and analyzed as in (D). Mw, molecular weight marker. Migration of molecular markers (in kilodaltons) is shown to the left of each blot. 5% input of NP-40 yeast extracts (E) is shown. Asterisks indicate unspecific binding.

See also Figure S3.

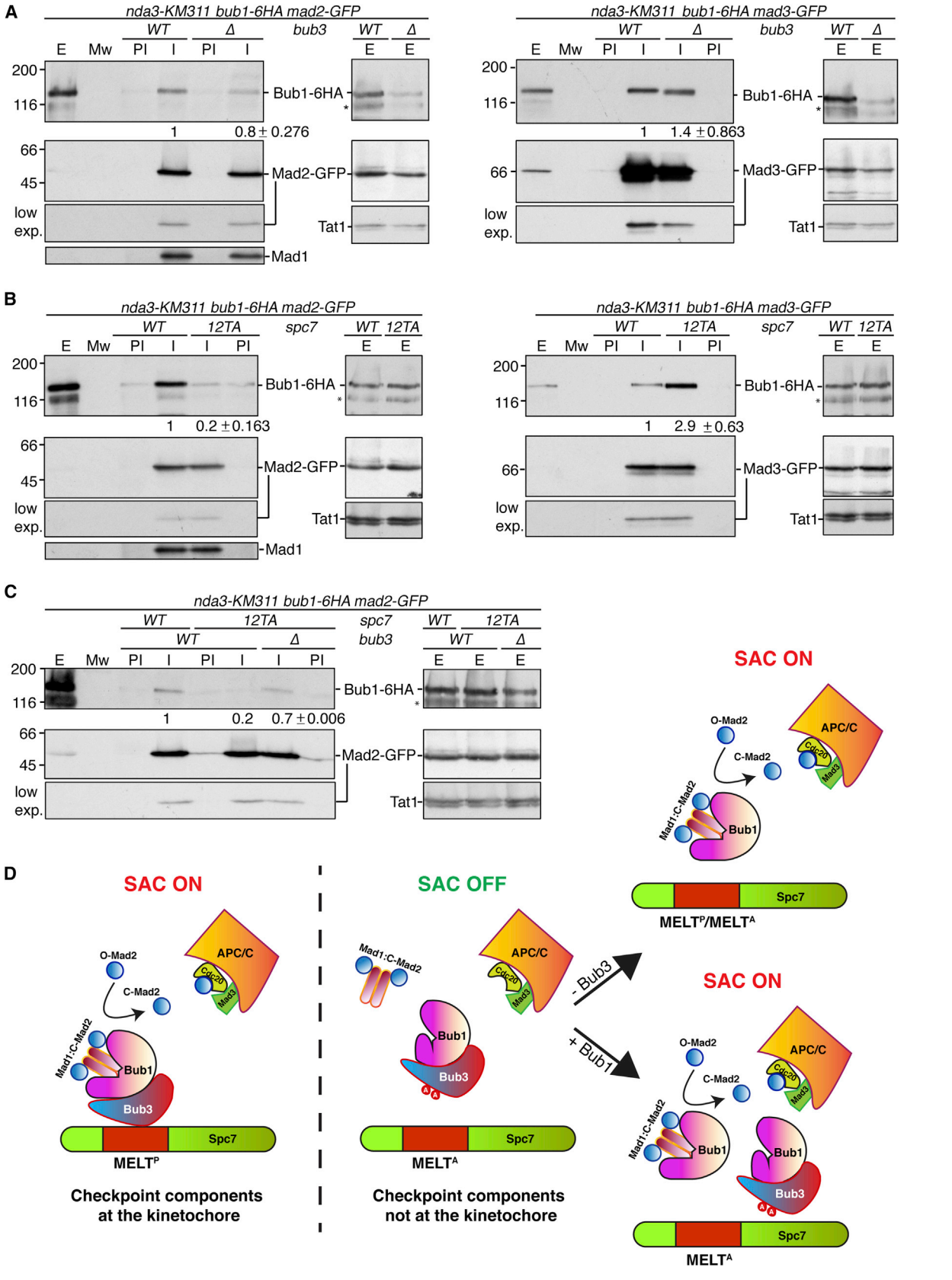

(legend on next page)

EXPERIMENTAL PROCEDURES

See the Supplemental Experimental Procedures.

SUPPLEMENTAL INFORMATION

Supplemental Information includes Supplemental Experimental Procedures and four figures and can be found with this article online at http://dx.doi.org/10.1016/j.cub.2016.07.040.

AUTHOR CONTRIBUTIONS

The project was conceived by J.B.A.M. All experiments were carried out by M.M.-S. with the exception of single-cell analysis of Bub1 and Bub3 binding to the kinetochore (J.C.M.) and single-cell checkpoint response (K.S.). A.H.-A. and T.C.L. aided with molecular biology and strain construction. The manuscript was written by J.B.A.M. with help from M.M.-S., K.S., and J.C.M.

ACKNOWLEDGMENTS

We thank Andrew McAinsh for critical reading of the manuscript. This work was supported by a program grant (MR/K001000/1) from the Medical Research Council UK (J.B.A.M.), a Global Research Fellowship from the Warwick Institute of Advanced Study (J.C.M.), and funds from Virginia Tech (K.S.).

Received: April 13, 2016
Revised: June 22, 2016
Accepted: July 15, 2016
Published: September 8, 2016

REFERENCES

1. Musacchio, A. (2015). The molecular biology of spindle assembly checkpoint signaling dynamics. Curr. Biol. *25*, R1002–R1018.
2. London, N., Ceto, S., Ranish, J.A., and Biggins, S. (2012). Phosphoregulation of Spc105 by Mps1 and PP1 regulates Bub1 localization to kinetochores. Curr. Biol. *22*, 900–906.
3. Shepperd, L.A., Meadows, J.C., Sochaj, A.M., Lancaster, T.C., Zou, J., Buttrick, G.J., Rappsilber, J., Hardwick, K.G., and Millar, J.B. (2012). Phosphodependent recruitment of Bub1 and Bub3 to Spc7/KNL1 by Mph1 kinase maintains the spindle checkpoint. Curr. Biol. *22*, 891–899.
4. Yamagishi, Y., Yang, C.H., Tanno, Y., and Watanabe, Y. (2012). MPS1/Mph1 phosphorylates the kinetochore protein KNL1/Spc7 to recruit SAC components. Nat. Cell Biol. *14*, 746–752.
5. London, N., and Biggins, S. (2014). Mad1 kinetochore recruitment by Mps1-mediated phosphorylation of Bub1 signals the spindle checkpoint. Genes Dev. *28*, 140–152.
6. Heinrich, S., Geissen, E.M., Kamenz, J., Trautmann, S., Widmer, C., Drewe, P., Knop, M., Radde, N., Hasenauer, J., and Hauf, S. (2013). Determinants of robustness in spindle assembly checkpoint signalling. Nat. Cell Biol. *15*, 1328–1339.
7. Primorac, I., Weir, J.R., Chiroli, E., Gross, F., Hoffmann, I., van Gerwen, S., Ciliberto, A., and Musacchio, A. (2013). Bub3 reads phosphorylated MELT repeats to promote spindle assembly checkpoint signaling. eLife *2*, e01030.
8. Vanoosthuyse, V., Meadows, J.C., van der Sar, S.J., Millar, J.B., and Hardwick, K.G. (2009). Bub3p facilitates spindle checkpoint silencing in fission yeast. Mol. Biol. Cell *20*, 5096–5105.
9. Wang, X., Babu, J.R., Harden, J.M., Jablonski, S.A., Gazi, M.H., Lingle, W.L., de Groen, P.C., Yen, T.J., and van Deursen, J.M. (2001). The mitotic checkpoint protein hBUB3 and the mRNA export factor hRAE1 interact with GLE2p-binding sequence (GLEBS)-containing proteins. J. Biol. Chem. *276*, 26559–26567.
10. Heinrich, S., Sewart, K., Windecker, H., Langegger, M., Schmidt, N., Hustedt, N., and Hauf, S. (2014). Mad1 contribution to spindle assembly checkpoint signalling goes beyond presenting Mad2 at kinetochores. EMBO Rep. *15*, 291–298.
11. Klebig, C., Korinth, D., and Meraldi, P. (2009). Bub1 regulates chromosome segregation in a kinetochore-independent manner. J. Cell Biol. *185*, 841–858.
12. Kim, S., Sun, H., Tomchick, D.R., Yu, H., and Luo, X. (2012). Structure of human Mad1 C-terminal domain reveals its involvement in kinetochore targeting. Proc. Natl. Acad. Sci. USA *109*, 6549–6554.
13. Tange, Y., and Niwa, O. (2008). Schizosaccharomyces pombe Bub3 is dispensable for mitotic arrest following perturbed spindle formation. Genetics *179*, 785–792.
14. Windecker, H., Langegger, M., Heinrich, S., and Hauf, S. (2009). Bub1 and Bub3 promote the conversion from monopolar to bipolar chromosome attachment independently of shugoshin. EMBO Rep. *10*, 1022–1028.
15. Collin, P., Nashchekina, O., Walker, R., and Pines, J. (2013). The spindle assembly checkpoint works like a rheostat rather than a toggle switch. Nat. Cell Biol. *15*, 1378–1385.
16. Dick, A.E., and Gerlich, D.W. (2013). Kinetic framework of spindle assembly checkpoint signalling. Nat. Cell Biol. *15*, 1370–1377.
17. Vleugel, M., Tromer, E., Omerzu, M., Groenewold, V., Nijenhuis, W., Snel, B., and Kops, G.J. (2013). Arrayed BUB recruitment modules in the kinetochore scaffold KNL1 promote accurate chromosome segregation. J. Cell Biol. *203*, 943–955.
18. Zhang, G., Lischetti, T., and Nilsson, J. (2014). A minimal number of MELT repeats supports all the functions of KNL1 in chromosome segregation. J. Cell Sci. *127*, 871–884.
19. Krenn, V., Overlack, K., Primorac, I., van Gerwen, S., and Musacchio, A. (2014). KI motifs of human Knl1 enhance assembly of comprehensive spindle checkpoint complexes around MELT repeats. Curr. Biol. *24*, 29–39.
20. Silió, V., McAinsh, A.D., and Millar, J.B. (2015). KNL1-Bubs and RZZ provide two separable pathways for checkpoint activation at human kinetochores. Dev. Cell *35*, 600–613.

Figure 4. Bub3 Regulates the Interaction between Mad2 and Bub1 Differentially at the Kinetochore or in the Nucleoplasm

(A) Bub1 interacts with Mad2 and Mad3 in the absence of Bub3. The indicated strains were incubated for 4 hr at 18°C. Extracts were prepared and immunoprecipitated with rabbit anti-GFP (I) or normal rabbit serum (PI) and analyzed by immunoblot using anti-HA, rabbit anti-Mad1, and sheep anti-GFP antibodies.
(B) Altering kinetochore binding of Bub1 affects its interaction with Mad2 and Mad3 differentially. Indicated strains were treated and analyzed as in (A).
(C) Bub3 inhibits the interaction between Bub1 and Mad2 in the nucleoplasm. Indicated strains were treated and analyzed as in (A).
(D) Model to illustrate how spindle checkpoint regulation is altered by kinetochore-bound or non-kinetochore-bound interactions. Bub3 at the kinetochore (left) allows the formation of a Bub1-Mad1-Mad2 complex that can efficiently catalyze C-Mad2 formation and arrest anaphase. When kinetochore recruitment is disrupted (middle) by MELT motif or Bub3 mutation, Bub1 interaction with Mad1-Mad2 is abolished, resulting in the failure to generate an inhibitory signal and anaphase onset. Checkpoint functionality can be restored, however, by either deleting Bub3, allowing interaction between Bub1 and Mad1-Mad2 in the nucleoplasm, or by increasing the amount of Bub1 to effectively titrate out Bub3 (right). Mw, molecular weight marker. Migration of molecular markers (in kilodaltons) is shown to the left of each blot. 5% input of NP-40 yeast extracts (E) is shown. Quantification of normalized Bub1-6HA levels is shown (±SD). Asterisks indicate unspecific binding.
See also Figure S4.

21. Jiang, H., He, X., Wang, S., Jia, J., Wan, Y., Wang, Y., Zeng, R., Yates, J., 3rd, Zhu, X., and Zheng, Y. (2014). A microtubule-associated zinc finger protein, BuGZ, regulates mitotic chromosome alignment by ensuring Bub3 stability and kinetochore targeting. Dev. Cell *28*, 268–281.

22. Toledo, C.M., Herman, J.A., Olsen, J.B., Ding, Y., Corrin, P., Girard, E.J., Olson, J.M., Emili, A., DeLuca, J.G., and Paddison, P.J. (2014). BuGZ is required for Bub3 stability, Bub1 kinetochore function, and chromosome alignment. Dev. Cell *28*, 282–294.

23. Jiang, Y., Li, X., Yang, W., Hawke, D.H., Zheng, Y., Xia, Y., Aldape, K., Wei, C., Guo, F., Chen, Y., and Lu, Z. (2014). PKM2 regulates chromosome segregation and mitosis progression of tumor cells. Mol. Cell *53*, 75–87.

Current Biology, Volume *26*

Supplemental Information

Bub3-Bub1 Binding to Spc7/KNL1 Toggles the Spindle Checkpoint Switch by Licensing the Interaction of Bub1 with Mad1-Mad2

Maria del Mar Mora-Santos, America Hervas-Aguilar, Katharina Sewart, Theresa C. Lancaster, John C. Meadows, and Jonathan B.A. Millar

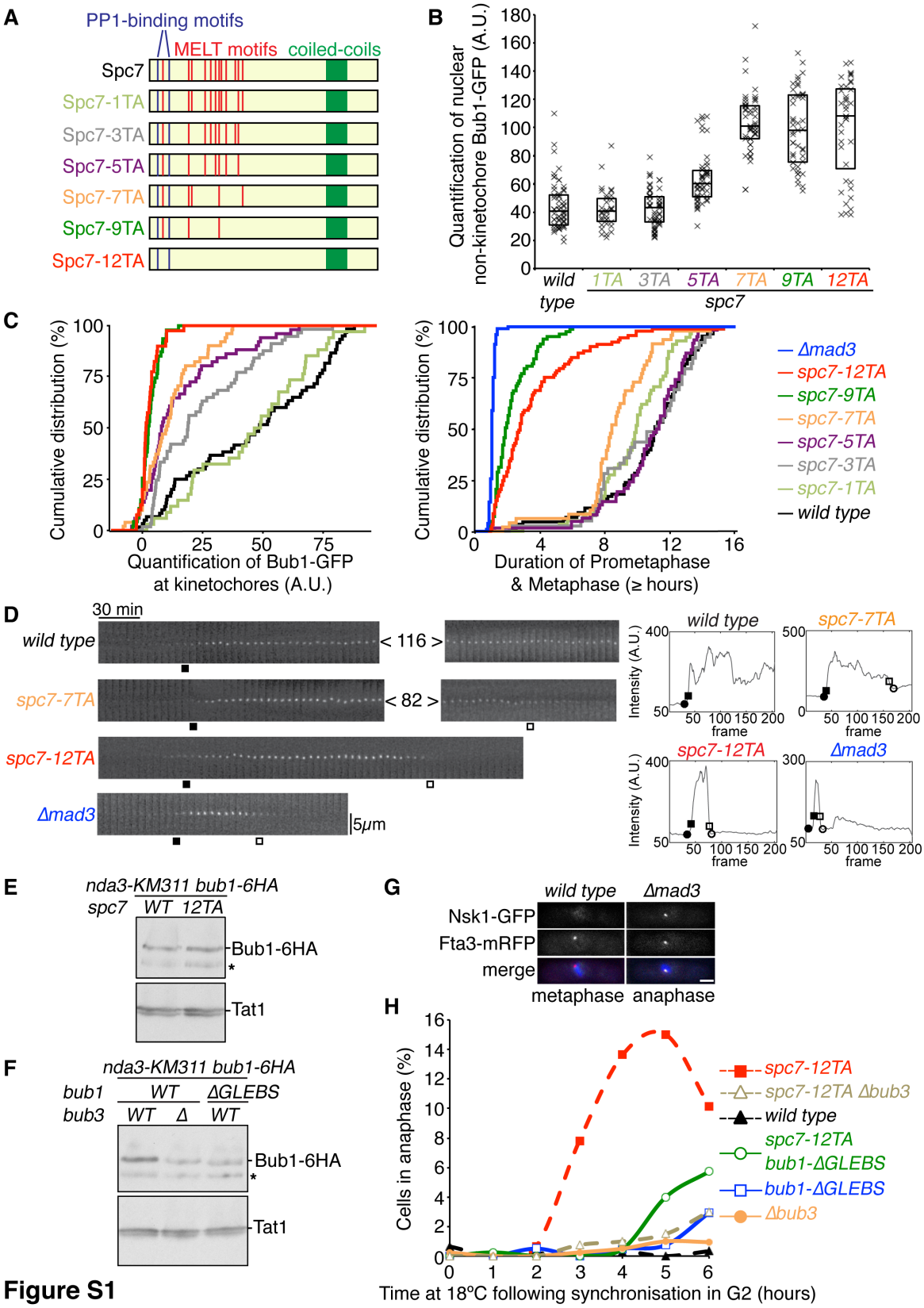
A
PP1-binding motifs
MELT motifs
coiled-coils
Spc7
Spc7-1TA
Spc7-3TA
Spc7-5TA
Spc7-7TA
Spc7-9TA
Spc7-12TA
B
Quantification of nuclear non-kinetochore Bub1-GFP (A.U.)
wild type
1TA
3TA
5TA
7TA
9TA
12TA
spc7
C
Cumulative distribution (%)
Quantification of Bub1-GFP at kinetochores (A.U.)
Duration of Prometaphase & Metaphase (≥ hours)
Δmad3
spc7-12TA
spc7-9TA
spc7-7TA
spc7-5TA
spc7-3TA
spc7-1TA
wild type
D
30 min
wild type
spc7-7TA
spc7-12TA
Δmad3
5μm
Intensity (A.U.)
frame
E
nda3-KM311 bub1-6HA
spc7 WT 12TA
Bub1-6HA
Tat1
F
nda3-KM311 bub1-6HA
bub1 WT ΔGLEBS
bub3 WT Δ WT
Bub1-6HA
Tat1
G
wild type
Δmad3
Nsk1-GFP
Fta3-mRFP
merge
metaphase
anaphase
H
Cells in anaphase (%)
Time at 18ºC following synchronisation in G2 (hours)
spc7-12TA
spc7-12TA Δbub3
wild type
spc7-12TA bub1-ΔGLEBS
bub1-ΔGLEBS
Δbub3

Figure S1

A

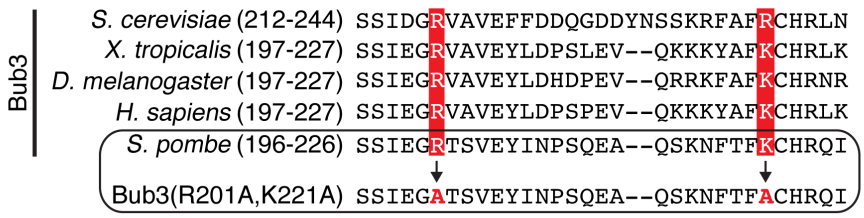
Bub3
S. cerevisiae (212-244) SSIDGRVAVEFFDDQGDDYNSSKRFAFRCHRLN
X. tropicalis (197-227) SSIEGRVAVEYLDPSLEV--QKKKYAFKCHRLK
D. melanogaster (197-227) SSIEGRVAVEYLDHDPEV--QRRKFAFKCHRNR
H. sapiens (197-227) SSIEGRVAVEYLDPSPEV--QKKKYAFKCHRLK
S. pombe (196-226) SSIEGRTSVEYINPSQEA--QSKNFTFKCHRQI
Bub3(R201A,K221A) SSIEGATSVEYINPSQEA--QSKNFTFACHRQI

B

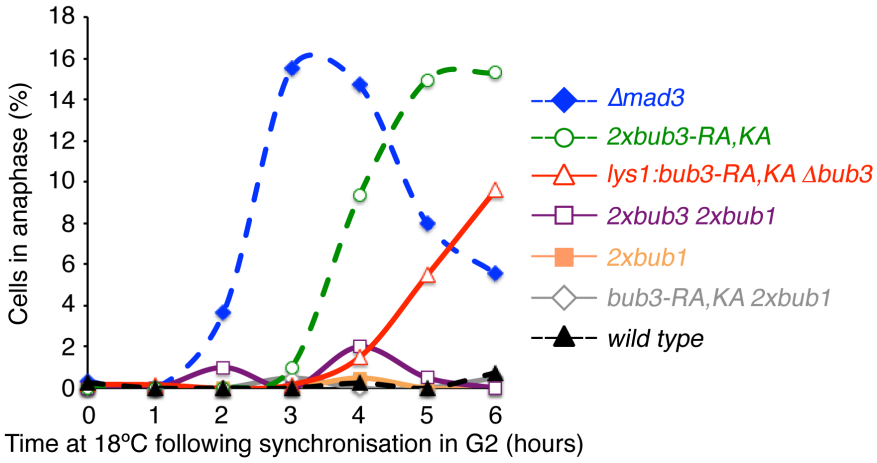
Cells in anaphase (%)
18
16
14
12
10
8
6
4
2
0
0 1 2 3 4 5 6
Time at 18ºC following synchronisation in G2 (hours)
Δmad3
2xbub3-RA,KA
lys1:bub3-RA,KA Δbub3
2xbub3 2xbub1
2xbub1
bub3-RA,KA 2xbub1
wild type

Figure S2

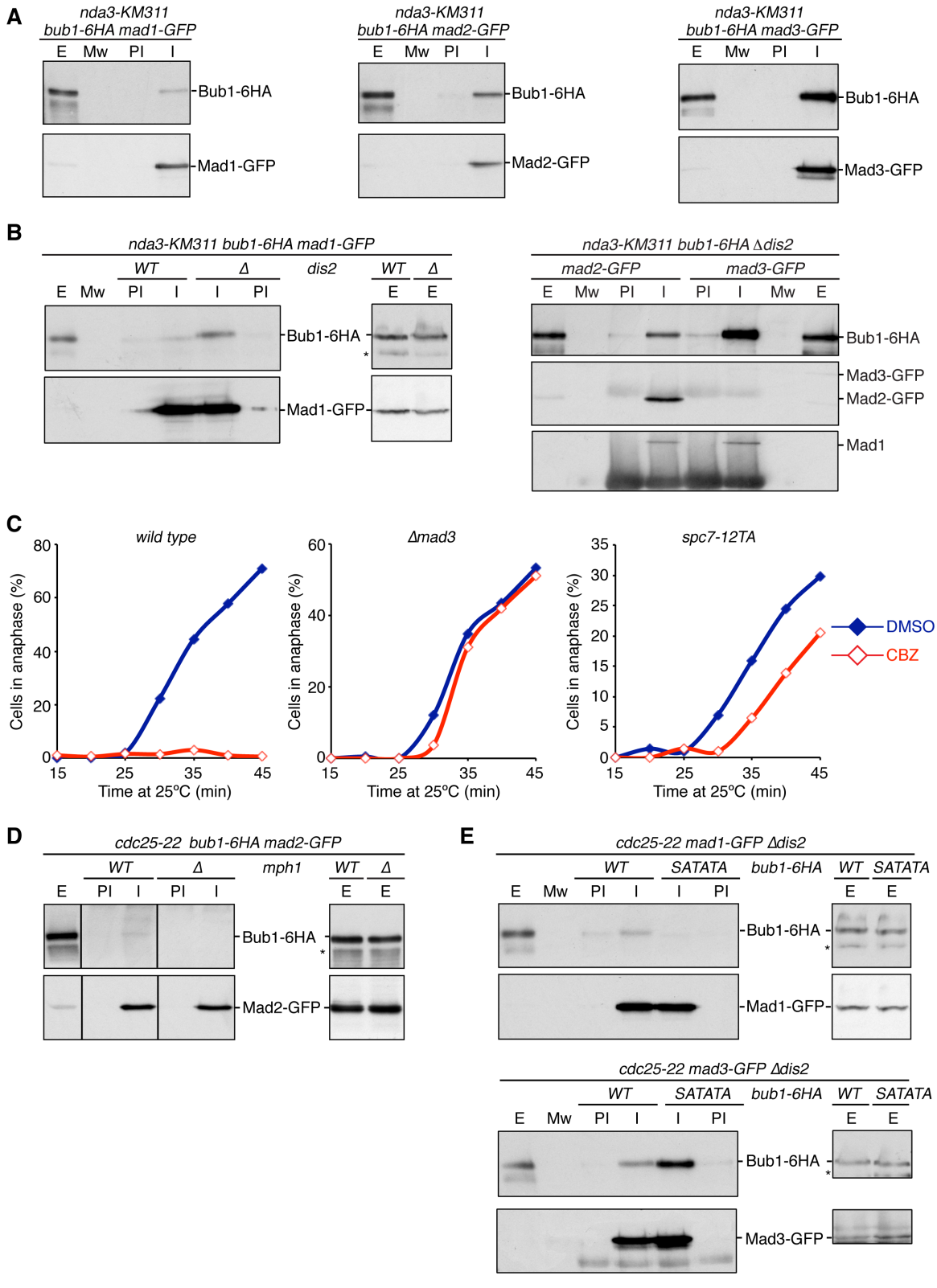
A
nda3-KM311 bub1-6HA mad1-GFP
E Mw PI I
Bub1-6HA
Mad1-GFP
nda3-KM311 bub1-6HA mad2-GFP
E Mw PI I
Bub1-6HA
Mad2-GFP
nda3-KM311 bub1-6HA mad3-GFP
E Mw PI I
Bub1-6HA
Mad3-GFP
B
nda3-KM311 bub1-6HA mad1-GFP
WT Δ dis2 WT Δ
E Mw PI I I PI E E
Bub1-6HA
Mad1-GFP
nda3-KM311 bub1-6HA Δdis2
mad2-GFP mad3-GFP
E Mw PI I PI I Mw E
Bub1-6HA
Mad3-GFP
Mad2-GFP
Mad1
C
wild type
Δmad3
spc7-12TA
Cells in anaphase (%)
Time at 25°C (min)
DMSO
CBZ
D
cdc25-22 bub1-6HA mad2-GFP
WT Δ mph1 WT Δ
E PI I PI I E E
Bub1-6HA
Mad2-GFP
E
cdc25-22 mad1-GFP Δdis2
WT SATATA bub1-6HA WT SATATA
E Mw PI I I PI E E
Bub1-6HA
Mad1-GFP
cdc25-22 mad3-GFP Δdis2
WT SATATA bub1-6HA WT SATATA
E Mw PI I I PI E E
Bub1-6HA
Mad3-GFP

Figure S3

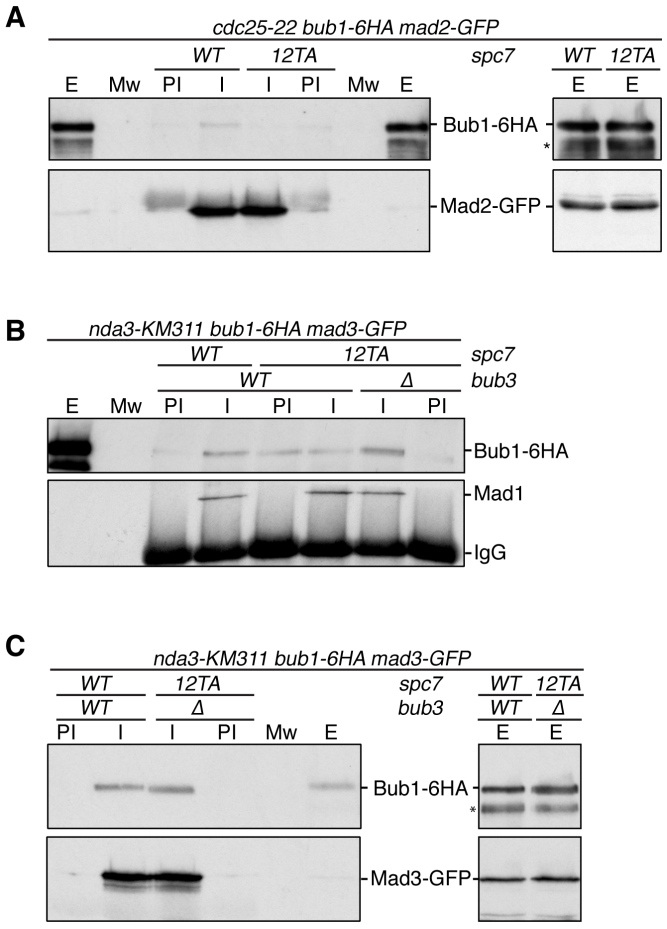
A
cdc25-22 bub1-6HA mad2-GFP
WT
12TA
spc7
WT
12TA
E
Mw
PI
I
I
PI
Mw
E
E
E
Bub1-6HA
*
Mad2-GFP
B
nda3-KM311 bub1-6HA mad3-GFP
WT
12TA
spc7
WT
Δ
bub3
E
Mw
PI
I
PI
I
I
PI
Bub1-6HA
Mad1
IgG
C
nda3-KM311 bub1-6HA mad3-GFP
WT
12TA
spc7
WT
12TA
WT
Δ
bub3
WT
Δ
PI
I
I
PI
Mw
E
E
E
Bub1-6HA
*
Mad3-GFP

Figure S4

Supplemental Figure Legends

Figure S1, related to Figure 1
(A) Diagram showing wild type Spc7 and the mutant alleles used in this study. Red lines indicate unmutated MELT motifs. **(B)** *bub1-GFP fta3-RFP pREP3x-mad2* cells expressing the *spc7* mutant alleles illustrated or wild type *spc7* were grown to mid-log phase in the presence of thiamine and then arrested in metaphase by growing in the absence of thiamine for 18 hours. Following fixation, the level of Bub1-GFP in the nucleus but not at kinetochores was calculated in individual cells. **(C)** Graphs to show the cumulative distributions of the data from Figures 1A (left panel) and 1B (right panel). (**D**) (Left panel) Kymographs of the spindle region of representative mitotic cells expressing the tubulin mutant *nda3-KM311* and *plo1-GFP* from Figure 1B. Cells were followed by live-cell microscopy at 16°C and Plo1-GFP appearance highlighted by closed squares and its disappearance by open squares. The *wild type* cell still showed a localized Plo1-GFP signal when recording was stopped. Frames removed for space constraints are represented as <n>. Time between frames: 5 minutes. (Right panel) Graphs show Plo1-GFP maximum intensity over time for the representative cells shown. Points indicated by circles and squares were determined by a custom MATLAB script. Closed circles mark the time-point before the first strong increase in Plo1-GFP signal and open circles the one after the last strong decrease. Time points where Plo1-GFP intensity increases above (closed squares) or decreases below (open squares) 1.3x the baseline and are used to determine the time spent in mitosis. **(E)** *nda3-KM311 bub1-6HA mad2-GFP* cells in the presence and absence of Spc7-12TA were grown to mid log phase before shifting to 18 ºC for 4 hours to arrest in mitosis and then harvested. NP-40 extracts were separated by SDS-PAGE and analysed by immunoblotting using anti-HA and anti-Tat1 antibodies. **(F)** Log phase cultures of *bub1-6HA*, *bub1-6HA Δbub3* and *bub1(ΔGLEBS)-6HA* cells expressing *nda3-KM311 mad2-GFP* were arrested in mitosis for 6 hours at 18 ºC and then harvested. NP-40 extracts were separated by SDS-PAGE and analysed by immunoblotting using anti-HA and anti-Tat1 antibodies. **(G)** Representative cells expressing the tubulin mutant *nda3-KM311* and the anaphase marker *nsk1-GFP* in the presence and absence of Mad3 from Figure 1C were grown to mid log phase before being synchronised in G2 by lactose gradient and incubated at 18 ºC for 3 hours. Bar, 2µm. **(H)** Log phase cultures of the illustrated strains expressing *nda3-KM311 nsk1-GFP* were synchronised in G2 by lactose gradient and incubated at 18 ºC for the times indicated. Cells were fixed and the percentage of anaphase cells (Nsk1-GFP positive) determined. Dashed lines indicate control data reproduced from Figure 1D. Asterisks indicate unspecific binding.

Figure S2, related to Figure 2
(A) Alignment of Bub3 from the indicated organisms. **(B)** Log phase cultures of the illustrated strains expressing *nda3-KM311 nsk1-GFP* were synchronised in G2 by lactose gradient and incubated at 18 ºC for the times indicated. Cells were fixed and the percentage of anaphase cells (Nsk1-GFP positive) determined. Dashed lines indicate control data reproduced from Figure 2D.

Figure S3, related to Figure 3
(A) Following incubation for 6 hours at 18 ºC to arrest in mitosis, NP-40 extracts were prepared from *mad1-GFP*, *mad2-GFP* and *mad3-GFP* strains expressing *nda3-KM311 bub1-6HA*. These were then immunoprecipitated with rabbit anti-GFP (I) or rabbit serum (PI) and complexes analysed by immunoblot using anti-HA and sheep anti-GFP. **(B)** Log phase cultures of *mad1-GFP, mad2-GFP* or *mad3-GFP* cells expressing *nda3-KM311 bub1-6HA* and either $dis2^+$ or Δ*dis2* were treated as in (A). Extracts of *mad2-GFP* or *mad3-GFP* cells expressing *nda3-KM311 bub1-6HA* and either $dis2^+$ or Δ*dis2* were inmunoprecipitated with rabbit anti-Mad1(I) or rabbit serum (PI) and complexes analysed by immonoblot using anti-HA, sheep anti-GFP and rabbit anti-Mad1 antibody. **(C)** *sid4-tdTomato cdc25-22* cells in the presence or absence of Mad3 and Spc7-12TA were grown to mid log phase before shifting to 35.5 ºC for 4 hours to arrest at the G2/M boundary. This was followed by release at 25 ºC. After 10 min, either CBZ at 200 µg/ml or an equal volume of DMSO was added and cells fixed at the times indicated. The percentage of anaphase cells (Nsk1-GFP positive) was determined. **(D)** Mid log phase *bub1-6HA mad2-GFP cdc25-22* strains expressing either *mph1* or *Δmph1* were shifted to 35.5 ºC for 4 hours and released at 25 ºC. After 10 min, CBZ was added at 200 µg/ml and cells collected 15 min later. Extracts were immunoprecipitated and analysed as in (A). **(E)** *mad1-GFP* or *mad3-GFP* Δ*dis2 cdc25-22* strains expressing either bub1-6HA or bub1-SATATA-6HA were treated as in (D) and analysed as in (A). (Mw) Molecular weight marker. 5% input of NP-40 yeast extracts (E). Asterisk shows non-specific binding.

Figure S4, related to Figure 4

(A) Log phase cultures of *cdc25-22 bub1-6HA mad2-GFP* cells expressing either *spc7* or *spc7-T12A* were shifted to 35.5 ºC for 4 hours to arrest at G2/M and then released at 25 ºC. After 10 min, CBZ was added at 200 μg/ml and cells were collected 15 min later. NP-40 extracts were immunoprecipitated with rabbit anti-GFP (I) or rabbit serum (PI). Immunoprecipitated material was subsequently analysed by immunoblot using anti-HA and sheep anti-GFP. **(B)** Following incubation for 4 hours at 18 ºC to arrest in mitosis, NP-40 extracts were prepared from *mad3-GFP* strains expressing *nda3-KM311 bub1-6HA*. Extracts were immunoprecipitated with rabbit anti-Mad1 (I) or rabbit serum (PI) and complexes were analysed by immunoblot using anti-HA and rabbit anti-Mad1. (**C)** Log phase *nda3-KM311 bub1-6HA mad3-GFP* strains expressing either *spc7 bub3*$^{+}$ or *spc7-12TA* Δ*bub3* were incubated at 18 ºC for 4 hours. Extracts were immunoprecipitated and analysed as in (A). (Mw) Molecular weight marker. 5% input of NP-40 yeast extracts (E). Asterisk shows non-specific binding.

Supplemental Experimental Procedures

Cell culture and synchronisation

Media, growth and maintenance of strains were as described previously [S1]. Strains used in this study are listed below. YES 10-40% lactose gradients were prepared in a Fisherbrand gradient mixer. Cells in mid log phase were placed on the top and after centrifugation, synchronised early G2 cells were taken from the top of the broad band of cells concentrated at the centre of the gradient. For *cdc25-22* arrest, cells were grown in YES medium overnight at 25 ºC to mid log phase and then shifted to 35.5 ºC for 4 hours. To release, the culture was rapidly cooled to 25 ºC. For mitotic arrests, mid log phase *nda3-KM311* cells growing in YES were arrested at 18 ºC for different durations. Mad2 overexpression assays were made by growing *pREP3x-mad2* strains in minimal glutamate medium supplemented with 5 µg/ml thiamine overnight at 30 ºC. Mid log phase cells were washed twice with the same medium lacking thiamine, and inoculated into fresh media. Cells were then incubated for either 16 or 18 hours at 30 ºC.

Plasmid and strain construction

DNA containing full length *spc7* and ~500 bp 5' promoter and ~200 bp of 3' UTR was cloned into the *SphI* and *BamHI* sites of *pLYS1U* [S2]. Integration at the *lys1* locus was confirmed by PCR. To create mutants of *spc7*, fragments of 1.4 Kb flanked by unique restriction sites *MscI* and *AgeI* were synthesised by GeneArt (Life TechnologiesTM) with the following threonines or serine mutated to alanine T77, S221, T257, T338, T366, T395, T413, T422, T453, T507, T529, T552 (*spc7-12TA*) or T257, T338, T366, T395, T422, T453, T507, T529, T552 (*spc7-9TA*) or T338, T366, T395, T422, T453, T507, T529 (*spc7-7TA*) or T257, T366, T422, T507, T552 (*spc7-5TA*) or T257, T422, T552 (*spc7-3TA*) or T507 (*spc7-1TA*) or with the following threonines mutated to glutamic acid T257, T338, T366, T395, T422, T453, T507, T529, T552 (*spc7-9TE*). These fragments were excised from the GeneArt vector pMA-RQ using *MscI* and *AgeI* and cloned into *pLYS1U-Spc7*. Wild type and mutants were transformed into *spc7::natMX6/spc7*$^{+}$ heterozygous diploid [S3] after digestion with *NotI*. Carboxy-terminal tagging with GFP was performed by two-step PCR-based gene targeting as described previously [S4, S5] using oligos listed below. *bub1-6HA* or *bub1-ΔGLEBS-6HA* expressed at the endogenous locus were created by cutting the plasmid *pBub1-6HA* [S6] with the single *ClaI* site lying within *bub1* sequence. To express an additional copy of *bub1*, the genomic sequence of *bub1* was cloned as a 4 Kb fragment using restriction sites *BamHI* and *KpnI* into *pJK148* [S7]. Plasmids were linearised with *NruI* and integrated into strains with the *leu1.32* auxotrophic marker. Stable integrations at the *leu1* locus were confirmed by PCR. A fragment containing full length *bub3* or *bub3-R201A,K221A* and ~500bp 5' promoter and ~300bp of 3' UTR and a *bub1* fragment containing the specific mutations in S381A, T383A and T386A (called *bub1-SATATA*) was synthesised by GeneArt (Life TechnologiesTM) and excising from the GeneArt vector *pMA-RQ* using *SfiI*. Bub3 fragments were transformed into a *bub3::ura4* strain [S8] or *SalI* or *BssHII* used to clone it into *pLYS1U* or *pLYS1K*. The *bub1* mutant was first cloned as a 2.3 Kb fragment using restriction sites *XhoI* and *SpeI* into *pBSK-bub1*$^{+}$. This Plasmid was then linearised with *BamHI* and *SphI* and transformed into a *bub1::ura4* strain [S6]. Integration of *bub1-SATATA* and *bub3-R201,K221A* at their endogenous loci was selected for on agar plates containing 0.5 mg/ml 5-FOA (Fermentas) and verified by PCR-sequencing. To generate *6HisGST-spc7* and *6HisGST-Spc7-9TE*, a gene fragment encoding Spc7 residues 241-561 was amplified by PCR from *pLYS1U-spc7* or *pLYS1U-Spc7-9TE* plasmids respectively using Gateway Technology (ThermoFisher Scientific).

List of the strains used in this study annotated by initial appearance

Figure 1A
JM8876: *h? bub1-GFP:kanR fta3-mRFP:hygR spc7::natR lys1::spc7:ura4+pREP3x-mad2*
JM8878: *h? bub1-GFP:kanR fta3-mRFP:hygR spc7::natR lys1::spc7-1TA:ura4+pREP3x-mad2*
JM8880: *h? bub1-GFP:kanR fta3-mRFP:hygR spc7::natR lys1::spc7-3TA:ura4+pREP3x-mad2*
JM8882: *h? bub1-GFP:kanR fta3-mRFP:hygR spc7::natR lys1::spc7-5TA:ura4+pREP3x-mad2*
JM8884: *h? bub1-GFP:kanR fta3-mRFP:hygR spc7::natR lys1::spc7-7TA:ura4+pREP3x-mad2*
JM7080: *h? bub1-GFP:kanR fta3-mRFP:hygR spc7::natR lys1::spc7-9TA:ura4+pREP3x-mad2*
JM8888: *h? bub1-GFP:kanR fta3-mRFP:hygR spc7::natR lys1::spc7-12TA:ura4+pREP3x-mad2*

Figure 1B

JM9533: *h? nda3-KM311 plo1-GFP:kanR mad3::ura4*
JM9519: *h? nda3-KM311 plo1-GFP:kanR spc7::natMX6 lys1::spc7:ura4*
JM9522: *h? nda3-KM311 plo1-GFP:kanR spc7::natMX6 lys1::spc7-1TA:ura4*
JM9523: *h? nda3-KM311 plo1-GFP:kanR spc7::natMX6 lys1::spc7-3TA:ura4*
JM9525: *h? nda3-KM311 plo1-GFP:kanR spc7::natMX6 lys1::spc7-5TA:ura4*
JM9527: *h? nda3-KM311 plo1-GFP:kanR spc7::natMX6 lys1::spc7-7TA:ura4*
JM9529: *h? nda3-KM311 plo1-GFP:kanR spc7::natMX6 lys1::spc7-9TA:ura4*
JM9531: *h? nda3-KM311 plo1-GFP:kanR spc7::natMX6 lys1::spc7-12TA:ura4*

Figure 1C

JM7964: *h- nda3-KM311 fta3-mRFP:hygR nsk1-GFP:kanR spc7::natMX6 lys1::spc7:ura4*
JM7969: *h+ nda3-KM311 fta3-mRFP:hygR nsk1-GFP:kanR mad3::ura4*
JM8530: *h? nda3-KM311 fta3-mRFP:hygR nsk1-GFP:kanR spc7::natMX6 lys1::spc7-1TA:ura4*
JM8531: *h? nda3-KM311 fta3-mRFP:hygR nsk1-GFP:kanR spc7::natMX6 lys1::spc7-3TA:ura4*
JM8533: *h? nda3-KM311 fta3-mRFP:hygR nsk1-GFP:kanR spc7::natMX6 lys1::spc7-5TA:ura4*
JM8535: *h? nda3-KM311 fta3-mRFP:hygR nsk1-GFP:kanR spc7::natMX6 lys1::spc7-7TA:ura4*
JM7965: *h+ nda3-KM311 fta3-mRFP:hygR nsk1-GFP:kanR spc7::natMX6 lys1::spc7-9TA:ura4*
JM7967: *h- nda3-KM311 fta3-mRFP:hygR nsk1-GFP:kanR spc7::natMX6 lys1::spc7-12TA:ura4*

Figure 1D

JM7964: *h- nda3-KM311 fta3-mRFP:hygR nsk1-GFP:kanR spc7::natMX6 lys1::spc7:ura4*
JM7967: *h- nda3-KM311 fta3-mRFP:hygR nsk1-GFP:kanR spc7::natMX6 lys1::spc7-12TA:ura4*
JM9293: *h+nda3-KM311 fta3-mRFP:hygR nsk1-GFP:kanR spc7::natMX6 lys1::spc7-12TA:ura4 leu1::bub1*
JM8706: *h- nda3-KM311 fta3-mRFP:hygR nsk1-GFP:kanR spc7::natMX6 lys1::spc7-12TA:ura4 bub3::ura4*
JM9311: *h? nda3-KM311 fta3-mRFP:hygR nsk1-GFP:kanR spc7::natMX6 lys1::spc7-12TA:ura4 his::bub3:kanR*

Figure 2A

JM8891: *h+ sid4-TdTomato:natMX6 bub3-L-GFP:kanR*
JM8893: *h+ sid4-TdTomato:natMX6 bub3-RA,KA-L-GFP:kanR*
JM7375: *h+ nda3-KM311 sid4-TdTomato:natMX6 bub1-GFP:kanR bub3::hygR lys::bub3:ura4*
JM7378: *h- nda3-KM311 sid4-TdTomato:natMX6 bub1-GFP:kanR bub3::hygR lys::bub3-RA, KA:ura4*
JM9134: *h- sid4-TdTomato:hygR bub3-L-GFP:kanR spc7::natMX6 lys1::spc7-9TE:ura4*
JM9136: *h+sid4-TdTomato:hygR bub3-RA,KA-L-GFP:kanR spc7::natMX6 lys1::spc7-9TE:ura4*
JM9166: *h? sid4-TdTomato:hygR bub1-GFP:kanR bub3:hygR spc7::natMX6 lys1::spc7-9TE:ura4*
JM9168: *h? sid4-TdTomato:hygR bub1-GFP:kanR bub3-RA,KA:hygR spc7::natMX6 lys1::spc7-9TE:ura4*

Figure 2B

JM7546: *h- bub1-6HA:ura4 bub3::hygR lys1::bub3-GFP:kanR*
JM7548: *h- bub1-6HA:ura4 bub3::hygR lys1::bub3-RA,KA-GFP:kanR*

Figure 2C

JM7546: *h- bub1-6HA:ura4 bub3::hygR lys1::bub3-GFP:kanR*
JM7548: *h- bub1-6HA:ura4 bub3::hygR lys1::bub3-RA,KA-GFP:kanR*

Figure 2D

JM8097: *h? nda3-KM311 fta3-TdTomato:natMX6 nsk1-GFP:kanR mad3::hygR*
JM8933: *h? nda3-KM311 fta3-TdTomato:natMX6 nsk1-GFP:kanR bub3:hygR*
JM8889: *h? nda3-KM311 fta3-TdTomato:natMX6 nsk1-GFP:kanR bub3-RA,KA:hygR*
JM8935: *h? nda3-KM311 fta3-TdTomato:natMX6 nsk1-GFP:kanR bub3-RA,KA:hygR lys::bub3-RA,KA:ura4*
JM9003: *h? nda3-KM311 fta3-TdTomato:natMX6 nsk1-GFP:kanR bub3-RA,KA:hygR lys::bub3-RA,KA:ura4 bub1(ΔGLEBS) ade6-M210*
JM9662: *h? nda3-KM311 fta3-TdTomato:natMX6 nsk1-GFP:kanR bub3-RA,KA:hygR lys::bub3-RA,KA:ura4 leu1::bub1*

Figure 2E
JM4300: *h+ nda3-KM311*
JM8990: *h- bub3-L-GFP:hygR*
JM9068: *h- bub3-RA,KA-L-GFP:hygR*
JM9104: *h- bub3-RA,KA-L-GFP:hygR lys1::bub3-RA,KA-L-GFP:kanR*

Figure 3A
JM8826: *h+ nda3-KM311 bub1-6HA:ura4*
JM8729: *h? nda3-KM311 mad2-GFP:kanR bub1-6HA:ura4*
JM8733: *h? nda3-KM311 mad3-GFP:kanR bub1-6HA:ura4*

Figure 3B
JM8729: *h? nda3-KM311 mad2-GFP:kanR bub1-6HA:ura4*
JM8733: *h? nda3-KM311 mad3-GFP:kanR bub1-6HA:ura4*

Figure 3C
JM8729: *h? nda3-KM311 mad2-GFP:kanR bub1-6HA:ura4*
JM9399: *h? nda3-KM311 mad2-GFP:kanR bub1-6HA:ura4 dis2::natR*
JM8733: *h? nda3-KM311 mad3-GFP:kanR bub1-6HA:ura4*
JM9374: *h? nda3-KM311 mad3-GFP:kanR bub1-6HA:ura4 dis2::natR*

Figure 3D
JM9392: *h? cdc25-22 bub1-6HA:ura4 mad2-GFP:kanR dis2::natR*
JM9403: *h? cdc25-22 bub1-6HA:ura4 mad2-GFP:kanR dis2::natR mph1::hygR*

Figure 3E
JM9392: *h? cdc25-22 bub1-6HA:ura4 mad2-GFP:kanR dis2::natR*
JM9488: *h? cdc25-22 bub1(SATATA)-6HA:ura4 mad2-GFP:kanR dis2::natR*

Figure 4A
JM8729: *h? nda3-KM311 mad2-GFP:kanR bub1-6HA:ura4*
JM8901: *h+ nda3-KM311 mad2-GFP:kanR bub1-6HA:ura4 bub3::hygR*
JM8733: *h? nda3-KM311 mad3-GFP:kanR bub1-6HA:ura4*
JM8903: *h+ nda3-KM311 mad3-GFP:kanR bub1-6HA:ura4 bub3::hygR*

Figure 4B
JM8729: *h? nda3-KM311 mad2-GFP:kanR bub1-6HA:ura4*
JM8970: *h- nda3-KM311 mad2-GFP:kanR bub1-6HA:ura4 spc7::natMX6 lys1::spc7-12TA:ura4*
JM8733: *h? nda3-KM311 mad3-GFP:kanR bub1-6HA:ura4*
JM8972: *h- nda3-KM311 mad3-GFP:kanR bub1-6HA:ura4 spc7::natMX6 lys1::spc7-12TA:ura4*

Figure 4C
JM8729: *h? nda3-KM311 mad2-GFP:kanR bub1-6HA:ura4*
JM8970: *h- nda3-KM311 mad2-GFP:kanR bub1-6HA:ura4 spc7::natMX6 lys1::spc7-12TA:ura4*
JM9229: *h? nda3-KM311 mad2-GFP:kanR bub1-6HA:ura4 spc7::natMX6 lys1::spc7-12TA:ura4 bub3::hygR*

Supplemental Figure 1B
JM8876: *bub1-GFP:kanR fta3-mRFP:hygR spc7::natR lys1::spc7:ura4+pREP3x-mad2*
JM8878: *bub1-GFP:kanR fta3-mRFP:hygR spc7::natR lys1::spc7-1TA:ura4+pREP3x-mad2*
JM8880: *bub1-GFP:kanR fta3-mRFP:hygR spc7::natR lys1::spc7-3TA:ura4+pREP3x-mad2*
JM8882: *bub1-GFP:kanR fta3-mRFP:hygR spc7::natR lys1::spc7-5TA:ura4+pREP3x-mad2*
JM8884: *bub1-GFP:kanR fta3-mRFP:hygR spc7::natR lys1::spc7-7TA:ura4+pREP3x-mad2*
JM7080: *bub1-GFP:kanR fta3-mRFP:hygR spc7::natR lys1::spc7-9TA:ura4+pREP3x-mad2*
JM8888: *bub1-GFP:kanR fta3-mRFP:hygR spc7::natR lys1::spc7-12TA:ura4+pREP3x-mad2*

Supplemental Figure 1C
JM8876: *bub1-GFP:kanR fta3-mRFP:hygR spc7::natR lys1::spc7:ura4+pREP3x-mad2*
JM8878: *bub1-GFP:kanR fta3-mRFP:hygR spc7::natR lys1::spc7-1TA:ura4+pREP3x-mad2*
JM8880: *bub1-GFP:kanR fta3-mRFP:hygR spc7::natR lys1::spc7-3TA:ura4+pREP3x-mad2*
JM8882: *bub1-GFP:kanR fta3-mRFP:hygR spc7::natR lys1::spc7-5TA:ura4+pREP3x-mad2*
JM8884: *bub1-GFP:kanR fta3-mRFP:hygR spc7::natR lys1::spc7-7TA:ura4+pREP3x-mad2*
JM7080: *bub1-GFP:kanR fta3-mRFP:hygR spc7::natR lys1::spc7-9TA:ura4+pREP3x-mad2*
JM8888: *bub1-GFP:kanR fta3-mRFP:hygR spc7::natR lys1::spc7-12TA:ura4+pREP3x-mad2*
JM9533: *h$^{?}$ nda3-KM311 plo1-GFP:kanR mad3::ura4*
JM9519: *h$^{?}$ nda3-KM311 plo1-GFP:kanR spc7::natMX6 lys1::spc7:ura4*
JM9522: *h$^{?}$ nda3-KM311 plo1-GFP:kanR spc7::natMX6 lys1::spc7-1TA:ura4*
JM9523: *h$^{?}$ nda3-KM311 plo1-GFP:kanR spc7::natMX6 lys1::spc7-3TA:ura4*
JM9525: *h$^{?}$ nda3-KM311 plo1-GFP:kanR spc7::natMX6 lys1::spc7-5TA:ura4*
JM9527: *h$^{?}$ nda3-KM311 plo1-GFP:kanR spc7::natMX6 lys1::spc7-7TA:ura4*
JM9529: *h$^{?}$ nda3-KM311 plo1-GFP:kanR spc7::natMX6 lys1::spc7-9TA:ura4*
JM9531: *h$^{?}$ nda3-KM311 plo1-GFP:kanR spc7::natMX6 lys1::spc7-12TA:ura4*

Supplemental Figure 1D
JM9533: *h$^{?}$ nda3-KM311 plo1-GFP:kanR mad3::ura4*
JM9519: *h$^{?}$ nda3-KM311 plo1-GFP:kanR spc7::natMX6 lys1::spc7:ura4*
JM9527: *h$^{?}$ nda3-KM311 plo1-GFP:kanR spc7::natMX6 lys1::spc7-7TA:ura4*
JM9531: *h$^{?}$ nda3-KM311 plo1-GFP:kanR spc7::natMX6 lys1::spc7-12TA:ura4*

Supplemental Figure 1E
JM8729: *h$^{?}$ nda3-KM311 mad2-GFP:kanR bub1-6HA:ura4*
JM8970: *h^{-} nda3-KM311 mad2-GFP:kanR bub1-6HA:ura4 spc7::natMX6 lys1::spc7-12TA:ura4*

Supplemental Figure 1F
JM8729: *h$^{?}$ nda3-KM311 mad2-GFP:kanR bub1-6HA:ura4*
JM8901: *h^{+}nda3-KM311 mad2-GFP:kanR bub1-6HA:ura4 bub3::hygR*
JM8741: *h$^{?}$ nda3-KM311 mad2-GFP:kanR bub1(ΔGLEBS)-6HA:ura4*

Supplemental Figure 1G
JM7969: *h^{+} nda3-KM311 fta3-mRFP:hygR nsk1-GFP:kanR mad3::ura4*
JM7964: *h^{-} nda3-KM311 fta3-mRFP:hygR nsk1-GFP:kanR spc7::natMX6 lys1::spc7:ura4*

Supplemental Figure 1H
JM7964: *h^{-} nda3-KM311 fta3-mRFP:hygR nsk1-GFP:kanR spc7::natMX6 lys1::spc7:ura4*
JM7967: *h^{-} nda3-KM311 fta3-mRFP:hygR nsk1-GFP:kanR spc7::natMX6 lys1::spc7-12TA:ura4*
JM8690: *h^{-} nda3-KM311 fta3-mRFP:hygR nsk1-GFP:kanR spc7::natMX6 lys1::spc7:ura4 bub1(ΔGLEBS) ade6-210*
JM8698: *h^{-} nda3-KM311 fta3-mRFP:hygR nsk1-GFP:kanR spc7::natMX6 lys1::spc7-12TA:ura4 bub1(ΔGLEBS) ade6-210*
JM8700: *h^{-} nda3-KM311 fta3-mRFP:hygR nsk1-GFP:kanR spc7::natMX6 lys1::spc7:ura4 bub3::ura4*
JM8706: *h^{-} nda3-KM311 fta3-mRFP:hygR nsk1-GFP:kanR spc7::natMX6 lys1::spc7-12TA:ura4 bub3::ura4*

Supplemental Figure 2B
JM8097: *h$^{?}$ nda3-KM311 fta3-TdTomato:natMX6 nsk1-GFP:kanR mad3::hygR*
JM8935: *h$^{?}$ nda3-KM311 fta3-TdTomato:natMX6 nsk1-GFP:kanR bub3-RA,KA:hygR lys::bub3-RA,KA:ura4*
JM8107: *h$^{?}$ nda3-KM311 fta3-TdTomato:natMX6 nsk1-GFP:kanR bub3::hygR lys1::bub3-RA, KA:ura4*
JM9660: *h$^{?}$ nda3-KM311 fta3-TdTomato:natMX6 nsk1-GFP:kanR bub3-RA,KA:hygR leu1::bub1*
JM9667: *h$^{?}$ nda3-KM311 fta3-TdTomato:natMX6 nsk1-GFP:kanR bub3:hygR leu1::bub1*
JM9668: *h$^{?}$ nda3-KM311 fta3-TdTomato:natMX6 nsk1-GFP:kanR bub3:hygR lys::bub3:ura4 leu1::bub1*

Supplemental Figure 3A
JM8725: *h$^{?}$ nda3-KM311 mad1-GFP:kanR bub1-6HA:ura4*

JM8729: *h? nda3-KM311 mad2-GFP:kanR bub1-6HA:ura4*
JM8733: *h? nda3-KM311 mad3-GFP:kanR bub1-6HA:ura4*

Supplemental Figure 3B
JM8725: *h? nda3-KM311 mad1-GFP:kanR bub1-6HA:ura4*
JM9452: *h+ nda3-KM311 mad1-GFP:kanR bub1-6HA:ura4 dis2::natR*
JM9399: *h? nda3-KM311 mad2-GFP:kanR bub1-6HA:ura4 dis2::natR*
JM9374: *h? nda3-KM311 mad3-GFP:kanR bub1-6HA:ura4 dis2::natR*

Supplemental Figure 3C
JM4267: *h+ cdc25-22 sid4-tdtomato:natMX6 nsk1-gfp:KanR*
JM9231: *h+ cdc25-22 sid4-tdtomato:natMX6 nsk1-gfp:KanR mad3::hygR*
JM9116: *h? cdc25-22 nsk1-gfp:KanR spc7::natMX6 lys1::spc7(T12A):ura4*

Supplemental Figure 3D
JM8978: *h? cdc25-22 bub1-6HA:ura4 mad2-GFP:kanR*
JM9319: *h+ cdc25-22 bub1-6HA:ura4 mad2-GFP:kanR mph1::hygR*

Supplemental Figure 3E
JM9455: *h- cdc25-22 mad1-GFP:kanR bub1-6HA:ura4 dis2::natR*
JM9465: *h? cdc25-22 mad1-GFP:kanR bub1(SATATA)-6HA:ura4 dis2::natR*
JM9376: *h? cdc25-22 mad3-GFP:kanR bub1-6HA:ura4 dis2::natR*
JM9479: *h? cdc25-22 mad3-GFP:kanR bub1(SATATA)-6HA:ura4 dis2::natR*

Supplemental Figure 4A
JM8978: *h? cdc25-22 mad2-GFP:kanR bub1-6HA:ura4*
JM9083: *h- cdc25-22 mad2-GFP:kanR bub1-6HA:ura4 spc7::natMX6 lys1::spc7-12TA:ura4*

Supplemental Figure 4B
JM8733: *h? nda3-KM311 mad3-GFP:kanR bub1-6HA:ura4*
JM8972: *h- nda3-KM311 mad3-GFP:kanR bub1-6HA:ura4 spc7::natMX6 lys1::spc7-12TA:ura4*
JM9219: *h? nda3-KM311 mad3-GFP:kanR bub1-6HA:ura4 spc7::natMX6 lys1::spc7-12TA:ura4 bub3::hygR*

Supplemental Figure 4C
JM8733: *h? nda3-KM311 mad3-GFP:kanR bub1-6HA:ura4*
JM9219: *h? nda3-KM311 mad3-GFP:kanR bub1-6HA:ura4 spc7::natMX6 lys1::spc7-12TA:ura4 bub3::hygR*

List of oligonucleotides used in this study

Construction of pLYSU-Spc7
SphI FW
5'TTTATA*GCATGC*TTCTTACAACCGCACATT 3'
BamHI
5'TTTATA*GGATCC*GCGCATTACGGGTTTAACA 3'

Construction of pJK148-bub1
BamHI FW
5'CGCGGATCCCTACAACCTGTTTTTCGCTCATATTCG 3'
KpnI RV
5'CGCGGTACCGTTGTTTAGGAAAGAAAAACTAACCCCAATAAA 3'

C-terminal GFP-tagging of *mad3* and *bub3* alleles
mad3w
5'GATGGCCAACCTGGGACCTGGC3'

mad3x
5’TCCAGTGAAAAGTTCTTCTCCTTTACTCATGAATTCGATATCAAGCTTATCGATACCGTCGACTTC
TTTCGATACTTCCTCATC3’
mad3y
5’GTTTAAACGAGCTCGAATTCATCGATATTAGATTAACAACTATTGT3’
mad3z
5’TATAGAGGTGTAATTACTTATC3’

bub3w
5’CGACCTAAAATTTCATCCGATTCATCA3’
bub3x
5’GGGGATCCGTCGACCTGCAGCGTACGACATGAATTCGATATCAAGCTTATCGATACCGTCGACTG
ACTTTAACTTTGGAGCTGCAAAGTTGGATTC3’
bub3y
5’GTTTAAACGAGCTCGAATTCATCGATAATCGCTCATCAAAAAGCTTCATCCATGTA3’
bub3z
5’CCAAATAGTGTCACATTGTTTTTATATTAAGTA3’

Gateway cloning for expression of Spc7 fusion proteins
attB FW
5’GGGGACAAGTTTGTACAAAAAAGCAGGCTTCGCCACGAGAGAGCAGGTTAATGAT3’
attB RV
5’GGGGACCACTTTGTACAAGAAAGCTGGGTCTTAGTTTCCACGGATTTGAAAAGCCAC3’

Fixed cell fluorescence microscopy

Cells were fixed in 3.7 % formaldehyde for 10 min and mounted in Vectashield mounting medium containing DAPI. Fluorescence imaging of cells expressing GFP, RFP or TdTomato tagged proteins was performed on a Nikon TE-2000 inverted microscope with a 100x 1.49 N.A. objective lens equipped with a Photometrics Coolsnap-HQ2 liquid cooled CCD camera (Photometrics, Tucson, AZ). Images were collected and analysed using Metamorph (version 7.5.9.0 MAG Biosystems Software). Exposure times of 1 second were used for GFP, RFP and TdTomato and 0.25 seconds for DAPI (shown in blue in all images). Stacks of 18 z-sections (0.2µm apart) were taken and projected images were made followed by intensity adjustments. Experiments were conducted at least three times and the mean value presented, more than 250 cells were counted in each repeat.

Protein quantification

bub1-GFP fta3-RFP pREP3x-mad2 cells expressing various *spc7* mutant alleles or wild type *spc7* were grown to mid-log phase in the presence of thiamine and then arrested in metaphase by growing in the absence of thiamine for 18 hours. Following fixation, Bub1-GFP levels were measured in individual cells both at kinetochores *via* colocalisation with Fta3-RFP and in the nucleoplasm. In each case background levels of cellular fluorescence were first removed and for kinetochore-bound Bub1-GFP signal was normalised against background-subtracted Fta3-RFP levels. Average signal intensity measurements in a 10 pixel diameter circle ($0.32\mu m^2$) localised at the maximal intensity of the RFP signal were calculated using MetaMorph (version 7.5.9.0 MAG Biosystems Software). Measurements were taken over three experiments and the individual profiles plotted. Cumulative distributions were generated using R [S9, S10]. Quantification of protein levels across multiple immunoblots was conducted with ImageJ (Gel Analyzer) and distribution of signal between experiments represented with standard deviation throughout. Quantification was performed in the linear range as determined *via* serial exposure intensity analysis. Tat1 (anti-Tubulin) was used to normalise signal intensities were possible.

Single cell analysis of checkpoint maintenance

Cells were grown in YEA medium at 30°C and mounted in # 1.5 glass-bottom culture dishes (Ibidi) that had been coated with 100 µg/ml lectin (Sigma, L1395). Imaging was performed on a DeltaVision Core system (Applied Precision/GE Healthcare) equipped with a climate chamber (set to 16°C). Cells were incubated on the microscope stage at 16°C for 1.5 hours before recording. Pictures were taken with a CoolSnap HQ camera using

a 60x/1.4 Plan Apo oil objective (Olympus) and the 'optical axis integration' algorithm of the SoftWorx software (Applied Precision/GE Healthcare). All images were deconvolved using SoftWorx software. The time of appearance and disappearance of Plo1-GFP at spindle pole bodies was determined by a custom MATLAB (MathWorks) script. The custom MATLAB (MathWorks) script is applied to images of single cells and first determines the maximum intensity within a region of interest, smoothed over five time points. The first and second derivative are used to detect the first strong increase in signal as well as the last strong decrease in signal. The Plo1-GFP maximum intensity before and after these time points is considered the 'baseline'. Additional parameters are used to ensure that the baseline intensities at the start of the increase and at the end of the decrease are in the same range - unless in cells where Plo1-GFP has not delocalised by the end of image acquisition. The time point where Plo1-GFP intensity increases above or decreases below 1.3x the baseline are taken as start and stop to determine the time in mitosis. The automatically detected values are displayed to the user and can be corrected manually, if necessary. Kymographs were assembled using a custom MATLAB (MathWorks) script. Cells that died during mitosis were removed from the analysis.

***in vitro* binding assay**

Expression of fusion proteins was induced in *Escherichia coli BL21 DE3 plysS* cells by incubation with 1mM isopropyl-β-D-thiogalactoside (IPTG) for 3.5 hours at 37ºC. Cells were lysed in ice cold lysis buffer containing 150 mM NaCl, 1 % NP40, 10 mM TrisCl pH 8, 10 % glycerol, 1 mM DTT, 1 mM PMSF and Complete mini EDTA-free Protease Inhibitor Cocktail Tablets (Roche Applied Science) followed by sonication with 20 sec pulse for six cycles (Sonics, Vibra-Cell). Fusion proteins were purified from bacterial lysates *via* their affinity to glutathione-Sepharose beads for 30 min (GE Healthcare). For the *in vitro* assay, yeast lysates (5 mg) were incubated with 6HisGST-Spc7 or 6HisGST-Spc7-9TE bound to Sepharose beads for 2 hours. Beads were washed six times with lysis buffer and proteins were eluted by the addition of SDS-sample buffer heated at 95 ºC for 5 min.

Immunoblot analysis

Cell lysates were prepared by lysing cells in NP40 buffer (1 % NP40, 10 mM TrisCl pH 7.5, 150 mM NaCl, 10 % glycerol) containing 1 mM PMSF, Complete mini EDTA-free Protease Inhibitor Cocktail and Phosphatase Inhibitor Tablets (Roche Applied Science). Concentration was determined using a Bradford assay. Proteins were separated by SDS-polyacrylamide gel electrophoresis (SDS-PAGE), transferred to nitrocellulose membranes and probed with the following antibodies: anti-HA peroxidase rat antibody (Roche Applied Science), mouse anti-Tat1 antibody (a gift from Keith Gull), sheep anti-GFP antibody (a gift from Kevin Hardwick), rabbit anti-Mad1 antibody [S11]. Proteins were visualized using the enhanced chemiluminescence (ECL) detection system according to the manufacturer's instructions (GE Healthcare). In all cases statistics are derived from at least three independent experiments.

Co-immunoprecipitation

Yeast extracts (2 mg) were incubated with normal rabbit serum for 30 min and subsequently with protein A-Sepharose beads (GE Healthcare) for 45 min at 4 ºC. After centrifugation, beads were kept as pre-immune (*PI*) and the same extract was incubated with polyclonal anti-GFP (Immune systems) or rabbit anti-Mad1 antibody [S11] for 2 hours followed by an incubation with protein A-Sepharose beads for another 45 min and the beads were kept as immune (*I*). Beads were washed six times with NP40 buffer and bound proteins were solubilised by the addition of SDS-sample buffer heated at 95 ºC for 5 min.

Supplemental References

S1. Moreno, S., Klar, A., and Nurse, P. (1991). Molecular genetic analysis of fission yeast Schizosaccharomyces pombe. Methods Enzymol *194*, 795-823.

S2. Matsuyama, A., Shirai, A., and Yoshida, M. (2008). A novel series of vectors for chromosomal integration in fission yeast. Biochem Biophys Res Commun *374*, 315-319.

S3. Meadows, J.C., Shepperd, L.A., Vanoosthuyse, V., Lancaster, T.C., Sochaj, A.M., Buttrick, G.J., Hardwick, K.G., and Millar, J.B. (2011). Spindle checkpoint silencing requires association of PP1 to both Spc7 and kinesin-8 motors. Dev Cell *20*, 739-750.

S4. Bahler, J., Wu, J.Q., Longtine, M.S., Shah, N.G., McKenzie, A., 3rd, Steever, A.B., Wach, A., Philippsen, P., and Pringle, J.R. (1998). Heterologous modules for efficient and versatile PCR-based gene targeting in Schizosaccharomyces pombe. Yeast *14*, 943-951.

S5. Krawchuk, M.D., and Wahls, W.P. (1999). High-efficiency gene targeting in Schizosaccharomyces pombe using a modular, PCR-based approach with long tracts of flanking homology. Yeast *15*, 1419-1427.

S6. Bernard, P., Hardwick, K., and Javerzat, J.P. (1998). Fission yeast bub1 is a mitotic centromere protein essential for the spindle checkpoint and the preservation of correct ploidy through mitosis. J Cell Biol *143*, 1775-1787.

S7. Keeney, J.B., and Boeke, J.D. (1994). Efficient targeted integration at leu1-32 and ura4-294 in Schizosaccharomyces pombe. Genetics *136*, 849-856.

S8. Vanoosthuyse, V., Meadows, J.C., van der Sar, S.J., Millar, J.B., and Hardwick, K.G. (2009). Bub3p facilitates spindle checkpoint silencing in fission yeast. Mol Biol Cell *20*, 5096-5105.

S9. R Core Team (2016). R: A language and environment for statistical computing.

S10. Wickham, H. (2009). ggplot2: Elegant Graphics for Data Analysis, (Springer-Verlag New York).

S11. Heinrich, S., Sewart, K., Windecker, H., Langegger, M., Schmidt, N., Hustedt, N., and Hauf, S. (2014). Mad1 contribution to spindle assembly checkpoint signalling goes beyond presenting Mad2 at kinetochores. EMBO Rep *15*, 291-298.

2.3 Different modes of Cdc20 inhibition by the mitotic checkpoint

Katharina Sewart[1], Silke Hauf[1]

[1]Department of Biological Sciences and Biocomplexity Institute, Virginia Tech, Blacksburg, VA, USA

Correspondence: silke.hauf@vt.edu

To be submitted as manuscript to **EMBO Reports**

Author contributions:
I performed all experiments and analyzed all data (except Fig. 4A,E). Furthermore, I contributed to the writing of the manuscript.

Silke Hauf supervised the study, performed the experiments in Fig. 4A,E, and wrote the manuscript.

Different modes of Cdc20 inhibition by the mitotic checkpoint

Katharina Sewart and Silke Hauf

Department of Biological Sciences and Biocomplexity Institute, Virginia Tech, Blacksburg, VA 24061, USA

*Correspondence:
Silke Hauf
Virginia Tech, Department of Biological Sciences
Biocomplexity Institute, 1015 Life Science Circle
Blacksburg, VA 24061, USA
ph: +1-540-231-7318
silke@vt.edu

Running head: Modes of Cdc20 inhibition

Abstract

The mitotic checkpoint is a cellular safeguard that prevents eukaryotic cells from missegregating chromosomes. The effector of this conserved signalling pathway is the 'mitotic checkpoint complex' (MCC). In the classical model for checkpoint signalling, the MCC prevents anaphase by sequestering Cdc20, the activator of the anaphase-promoting complex/cyclosome (APC/C). More recently, work in human cells showed that the MCC binds two Cdc20 molecules, one in the classical mode, and the other one through additional binding sequences in the MCC component Mad3/BubR1. Here, we show in fission yeast that the 'one Cdc20 mode' is sufficient for checkpoint activity at low Cdc20 concentrations, but that the 'two Cdc20 mode' is required at physiologic Cdc20 concentrations. Our analysis of several Mad3 point mutants strongly corroborates recent structural data on the Cdc20-MCC interaction. We find a strong similarity between mutants in the Mad3 C-terminus deletion of the APC/C subunit Apc15. This contrasts with results in other organisms and indicates an interesting divergence in phenotype, although the underlying molecular mechanisms are likely conserved.

Introduction

The spindle assembly checkpoint (SAC, or 'mitotic checkpoint') is a signalling pathway that secures correct chromosome segregation in dividing, eukaryotic cells. Proteins of this pathway bind to kinetochores that are not properly attached to the mitotic spindle. Concentration of these checkpoint proteins at the kinetochore starts a signalling cascade of protein-protein interactions and post-translational modifications that ultimately prevent the anaphase-promoting complex (APC/C) from initiating anaphase [1-3]. Suboptimal functioning of the SAC has been implicated in the chromosome missegregation observed in cancer cells [4-6]. SAC dysfunction may therefore contribute to the genetic malleability of cancer cells that hampers treatment.

The key downstream effector of the SAC is the mitotic checkpoint complex (MCC), which consists of the proteins Mad2 and Mad3/BubR1, as well as the APC/C-activator Cdc20 [1, 2]. MCC formation is initiated when Mad2 binds Cdc20 through a 'seatbelt mechanism' that involves a structural change within Mad2 from its 'open' to its 'closed' form [7, 8]. Mad3/BubR1 binds to this Mad2-Cdc20 complex and contacts both Mad2 and Cdc20 [9-11]. We refer to this assembly as the 'core MCC' [1, 12]. In many eukaryotes, Bub3 is an additional subunit of the MCC that binds to Mad3/BubR1, but evidence for an essential role of Bub3 as part of the MCC is lacking [13-16]. The *mad3+* gene of several fission yeast species, including *S. pombe*, is truncated before the interaction site with Bub3 (**Supplementary Figure** 1A), but the checkpoint remains intact.

The APC/C is an E3 ubiquitin-ligase that initiates anaphase and mitotic exit by targeting several proteins, including the CDK1-activating subunit cyclin B, for proteasomal degradation [17]. Cdc20 (*S. pombe* Slp1) plays a dual role in APC/C activation, serving as substrate adaptor and as bona fide APC/C activator that promotes E2 efficiency [18]. Just like Cdc20, the entire MCC can bind to the APC/C. An initial cryo-electron microscopy structure of this complex suggested that Cdc20 within MCC is displaced with respect to the position where it normally binds when activating the APC/C [19]. Recent work demonstrated that the core MCC binds a second Cdc20 molecule [12, 16, 20]. In the entire APC/C-MCC assembly, this second Cdc20 molecule ($Cdc20^{A}$) is closer to its activating position on the APC/C, albeit rotated and tilted compared to APC/C-Cdc20 in the absence of the MCC [20]. The notion that the MCC may bind two Cdc20 molecules emerged from the analysis of conserved regions within Mad3/BubR1 [17]. In the core MCC, Mad3/BubR1 binds Cdc20 through a KEN (Lysine-Glutamate-Asparagine) motif in its N-terminus (Mad3-KEN1) [9, 14, 21-25]. A second, conserved KEN motif further C-terminal in Mad3/BubR1 (KEN2) was known to be important for checkpoint activity, but not for core MCC formation [14, 21-24, 26]. The recent high resolution structures, along with biochemical experiments, now revealed that KEN2 contacts a second molecule of Cdc20 [12, 16, 20].

Additional motifs adjacent to Mad3/BubR1-KEN2 also contact this second Cdc20 molecule (**Figure** 1A): a D-box-mimicking motif N-terminal of KEN2 binds $Cdc20^{A}$ and is required for full checkpoint activity [12, 16, 20]; and an ABBA motif [27] close to KEN2 also binds $Cdc20^{A}$, although its role for checkpoint activity *in vivo* has not been addressed [16, 20]. All these motifs resemble APC/C degradation signals that allow substrates to be recognized by the APC/C and its coactivators, Cdc20 or Cdh1 [28]. Overall, this suggests that Mad3 is a pseudosubstrate inhibitor [15, 21], where the Mad3 stretch surrounding KEN2 occupies substrate-recognition sites on $Cdc20^{A}$, thereby preventing substrate recruitment to the APC/C [14].

Despite the existing high resolution views of the MCC and APC/C-MCC interaction [16, 20], the functional analysis of different Mad3 motifs *in vivo* is currently lacking behind. Here, we dissect the role of these motifs in the fission yeast *S. pombe*, which is an ideal organism to study this problem, because Mad3 has over evolutionary timescales been trimmed down to a minimal Cdc20-inhibitory fragment [3, 15] (**Figure** 1). While our results substantiate the structural and biochemical analyses in human cells, we also identify interesting differences that will yield deeper insight into checkpoint signalling.

Results and Discussion

Several conserved motifs in the Mad3 C-terminus are required for checkpoint activity

To address the relative importance of sequence motifs within Mad3 for checkpoint functionality, we mutated the KEN boxes and several conserved motifs in the C-terminus (**Figure** 1A) and replaced the endogenous *S. pombe mad3*$^{+}$ gene with the respective mutated gene. Both the wild type gene as well as the mutants were C-terminally tagged with GFP and showed similar protein abundance (**Figure** S1F). We tested checkpoint activity by using a conditional cold-sensitive tubulin mutation to abolish microtubule formation (*nda3-KM311* [29]) and measured the time that single cells delayed in mitosis by following localization of Plo1-mCherry to spindle pole bodies [30]. Formation of the MCC was analyzed by immunoprecipitation of Mad3-GFP from mitotic cells (see Methods). As expected [24], mutation of Mad3-KEN1 abolished checkpoint activity (**Figure** 1B) as well as formation of the core MCC (**Figure** 1C). In contrast, but also in agreement with previous results [24], mutation of KEN2 strongly diminished checkpoint activity, but without impairing core MCC formation (**Figure** 1B,C). Mutation of the D-box-mimicking motif [9] lead to a partial checkpoint defect (**Figure** 1B, **Supplementary Figure** S1G). We identified two potential ABBA motifs within the C-terminal part of Mad3 (**Figure** 1A). Mutation of ABBA1 strongly diminished checkpoint activity; mutation of the ABBA2 lead to a weaker checkpoint defect (**Figure** 1B). Truncating the Mad3 C-terminus containing ABBA2 as well as adjacent conserved sequences (*mad3-ΔCterm*) abrogated checkpoint activity (**Figure** 1B). Similar to the KEN2 mutant, this truncation did not abolish core MCC formation (**Figure** 1C).

We wanted to exclude that any of the effects caused by C-terminal truncation of Mad3 were influenced by a potential loss of Bub3 interaction. In many eukaryotes, the GLEBS (or B3BD) motif that mediates interaction of Mad3 with Bub3 is downstream of Mad3-KEN2 [31-33] (**Figure** 1A). In several fission yeast species, including *S. pombe*, Mad3 ends after the KEN2, but before the GLEBS motif (**Supplementary Figure** S1A), making it unlikely that *S. pombe* Bub3 directly binds to Mad3. Nevertheless, immunoprecipitation of *S. pombe* Mad3 co-precipitates Bub3 and vice versa [34] (**Supplementary Figure** S1C-E). We find that this interaction is likely indirect, since it is abolished by deletion of *bub1*$^{+}$ (**Supplementary Figure** S1D,E) and largely unaffected by truncation of the Mad3 C-terminus (**Supplementary Figure** S1D). Bub1 is a plausible mediator of the Bub3-Mad3 interaction, because it forms a complex with Bub3 [32, 35, 36], and the human Bub1 ortholog interacts directly with Mad3/BubR1 [37]. We conclude that our functional analysis of Mad3 as part of the MCC is unaffected by Bub3.

In conclusion, several motifs within Mad3, surrounding KEN2, are required for checkpoint activity

without being required for core MCC formation, and are non-redundant in their function. Recent analysis of the human APC/C-MCC assembly suggests that these motifs contact a second Cdc20 molecule, other than the one that is part of the core MCC (**Figure** 1D) [12, 16, 20].

Conserved motifs in the Mad3 C-terminus allow binding of a second Cdc20^{Slp1} molecule to the MCC

To directly test binding of additional Cdc20 to the core MCC, we expressed N-terminally superfolder GFP (sfGFP)-tagged Slp1^{Cdc20} from the endogenous promoter at the endogenous locus and expressed an additional copy of untagged Slp1^{Cdc20} under the endogenous regulatory sequences from an exogenous locus. Immunoprecipitation of sfGFP-Slp1^{Cdc20} from mitotic cells co-purified untagged Slp1^{Cdc20} (**Figure** 1E, lane 2). When we prevented core MCC formation through deletion of *mad2* or the Mad3-KEN1AAA mutation, co-purification of untagged Slp1^{Cdc20} with sfGFP-Slp1^{Cdc20} was abolished (**Figure** 1E, lane 4, 5), indicating that tagged and untagged Slp1^{Cdc20} do not directly bind to each other, nor does untagged Slp1^{Cdc20} directly bind to the GFP antibody. Consistent with results from human cells [12], binding of this additional, untagged Slp1^{Cdc20} did not require the MIM/KILR motif in the Slp1^{Cdc20} N-terminus that mediates binding to Mad2 (*slp1-mr63* mutant*;* **Figure** 1E, lane 3*)*. In contrast, mutation of Mad3-KEN2 or truncation of Mad3 (Mad3-ΔCterm) abolished the interaction (**Figure** 1E, lane 6, 7). Hence, additional Cdc20 (Cdc20^{A}) interacts with the core MCC through the Mad3 C-terminal sequence motifs, but not by canonical Mad2-binding. Although the interaction of the Mad3 C-terminal part with Cdc20 is likely to be direct, the interaction needs the presence of the core MCC: when *mad3-KEN1* is mutated, the interaction between Mad3 and Slp1^{Cdc20} is abolished, even if the C-terminal Mad3 sequences that are required for binding of additional Slp1^{Cdc20} remain intact (**Figure** 1E, lane 5). Hence, the C-terminal Mad3 motifs are required for Cdc20 interaction, but not sufficient.

A Cdc20^{Slp1} mutant that is unable to bind Mad2 can be prevented from initiating anaphase

The expression of Cdc20 that is unable to bind to Mad2 (like Slp1^{Cdc20}-mr63) leads to a checkpoint defect in several species [38-40]. We reasoned that Cdc20 that is unable to bind to Mad2 should still be subject to checkpoint control through the Mad3 C-terminus, as long as core MCC can be formed. We therefore co-expressed tagged, wild type sfGFP-Slp1^{Cdc20} and untagged, mutant Slp1^{Cdc20}-mr63. Expression of Slp1^{Cdc20}-mr63 alone leads to checkpoint failure, as expected (**Supplementary Figure** S1H) [39]. The checkpoint was also non-functional when equal levels of wild type and mutant Slp1^{Cdc20}-mr63 were expressed (**Figure** 1F). However, when expression of Slp1^{Cdc20}-mr63 was reduced, the checkpoint could be partially restored, as long as wild type Slp1^{Cdc20} was present (**Figure** 1F, **Supplementary Figure** S1H). As expected,

Slp1^{Cdc20}-mr63 bound to the MCC (**Figure** 1G). To make APC/C activation entirely dependent on Slp1^{Cdc20}-mr63, we mutated the C-box in the Slp1^{Cdc20} copy that was Mad2-binding proficient. The C-box is essential for Cdc20's ability to bind and activate the APC/C [41-43], but is not required for the core MCC to bind the APC/C [44]. The checkpoint rescue was enhanced when the tagged, Mad2-binding competent Slp1^{Cdc20} carried a mutation in the Cdc20 C-box (**Figure** 1F). In this situation, APC/C activation solely relies on Slp1^{Cdc20}-mr63, which remained efficiently inhibited by checkpoint activity despite lacking the Mad2-binding sequences (**Figure** 1F). Mutation of Mad3-KEN2 abolished binding of Slp1^{Cdc20}-mr63 to the core MCC and lead to a checkpoint defect (**Figure** 1F,G). Similarly, truncation of the Mad3 C-terminus lead to a checkpoint defect (**Figure** 1F). Hence, Slp1^{Cdc20}-mr63, which is unable to bind Mad2, can be inhibited by the mitotic checkpoint through the Mad3 C-terminus as long as core MCC formation is initiated by Mad2-binding-competent Slp1^{Cdc20}.

The 'core MCC' inhibition mode is sufficient at high checkpoint protein to Cdc20^{Slp1} ratio

Although each of the Mad3-KEN boxes is required for the SAC, mutation of KEN1 tends to abolish checkpoint activity more than mutation of KEN2, both in our assays (**Figure** 2A, inset) and in human cells [14, 26]. This hints to a more crucial role of KEN1. Indeed, Mad3-KEN1 is needed for interaction of both Cdc20^{M} and Cdc20^{A} with the MCC, whereas Mad3-KEN2 is only needed for interaction of Cdc20^{A} (**Figure** 1E) [12]. Because Cdc20^{M} can be tightly captured in the core MCC, we reasoned that core MCC formation alone could theoretically be sufficient for checkpoint activity, as long as the amount of Cdc20 is low enough. We therefore lowered Slp1^{Cdc20} abundance by expressing the gene from the promoter of *rad21* (cohesin) [45]. This considerably reduced the Slp1^{Cdc20} level (**Supplementary Figure** S2A) and partially rescued checkpoint activity in the *mad3-KEN2AAA* and *mad3-ΔCterm* mutants, but not in *mad3-KEN1AAA* cells (**Figure** 2A). Increasing the abundance of Mad2 and Mad3 slightly enhanced the effect (**Figure** 2B). The mitotic delay was dependent on core MCC formation, since using the Mad2-binding deficient Slp1^{Cdc20}-mr63 mutant instead of wild type Slp1^{Cdc20} abolished the delay (**Figure** 2B). We obtained similar results when expressing *slp1^{cdc20}* from the *adh1* promoter, which increases Slp1^{Cdc20} abundance in interphase but lowers the level in mitosis (**Supplementary Figure** 2A,C). To have yet better control over Slp1^{Cdc20} abundance, we expressed the gene from the regulatable *nmt41* promoter [46]. When titrating down Slp1^{Cdc20} abundance, the mitotic arrest in response to microtubule depolymerization progressively improved in *mad3-KEN2AAA* and *mad3-ΔCterm* cells (**Figure** 2C, D). This confirmed the effect we had seen by expression from the *rad21* or *adh1* promoter. We conclude that the mitotic checkpoint can rely solely on core MCC formation at low Slp1^{Cdc20} concentrations.

Since KEN2 became at least partially dispensable at low Slp1^{Cdc20} concentrations, we asked whether some organisms may dispense with a second KEN box. In several Drosophila species, the KEN2 motif seems to have become QEN (Glutamine instead of Lysine) (**Supplementary Figure** S1A,B). Introducing this change into the *S. pombe mad3* gene, however, did not impair checkpoint activity (**Supplementary Figure** S1F,I). In contrast, the same change was not tolerated at KEN1 (**Supplementary Figure** S1I). Although the interpretation is complicated by instability of the Mad3-KEN1QEN protein (**Supplementary Figure** S1F), this supports the different functionality of KEN1 and KEN2, as is also illustrated by a pre-KEN2 sequence in human BubR1 that is important for inhibitory activity and not shared with KEN1 [16].

An intact Mad3 C-terminus and Apc15 are required for MCC disassembly

We noticed that the amount of MCC was increased when binding of Cdc20^{A} was prevented by Mad3-KEN2AAA or Mad3-ΔCterm (e.g. **Figure** 1E,G). Since it is difficult to rationalize how these mutations would enhance assembly, we hypothesized that MCC disassembly is impaired. Indeed, in Mad3-KEN2AAA and Mad3-ΔCterm cells, the MCC (including Slp1^{Cdc20}) was present in interphase cells, where it is normally absent in *S. pombe* (**Figure** 3A-D, **Supplementary Figure** S3A). Since the Slp1^{Cdc20} protein normally accumulates exclusively in mitosis [47] (**Supplementary Figure** S2A), this suggests that Slp1^{Cdc20} is stabilized by incorporation into the partially defective MCC. Deletion of *bub1*$^{+}$ largely abolished the presence of MCC in interphase (**Figure** 3A). Minor amounts of the MCC could still be detected in interphase Mad3-KEN2AAA or Mad3-ΔCterm cells after *bub1*$^{+}$ deletion (**Figure** 3A) – presumably because Mad2 dimerization can initiate some MCC formation even in the absence of Bub1 [9, 48]. The causative events and sequence of steps in MCC disassembly are not entirely clear [17, 49, 50]. However, the APC/C subunit Apc15 plays a key role in MCC disassembly in human cells and budding yeast [51-53]. Consistently, we also detected MCC in *S. pombe apc15Δ* interphase cells (**Figure** 3A-C). Hence, Apc15 and the Mad3 C-terminus, which is required for integration of a second Cdc20 into the MCC, are required for MCC disassembly in *S. pombe.* Disassembly of the core MCC seems to require Cdc20 ubiquitination [54, 55]. It is conceivable that interaction of Cdc20^{A} with the core MCC is required to promote the ubiquitination and disassembly.

An intact Mad3 C-terminus and Apc15 are required for MCC binding to *S. pombe* APC/C

In human cells and budding yeast, deletion of *APC15* (budding yeast *MND1*) impairs checkpoint silencing, and therefore prolongs mitosis [51-53]. Surprisingly, deletion of *apc15*$^{+}$ in *S. pombe* considerably impairs activation of the spindle assembly checkpoint (**Figure** 4A) (K. Hardwick personal communication). Overall, deletion of *apc15*$^{+}$ and mutations of the Mad3 C-terminus

therefore have a similar phenotype: an inability to properly activate the SAC and a defect in MCC disassembly. Unlike in *mad3-KEN2AAA* cells, we find both sfGFP-Slp1 and untagged Slp1 in an sfGFP-Slp1 immunoprecipitation from *apc15Δ* cells (**Figure** 4B). Hence, in *apc15Δ* cells, the entire MCC assembles – yet, cells show a checkpoint defect. We reasoned that competition between the MCC and $Slp1^{Cdc20}$ for binding to the APC/C may be deficient in these cells. Indeed, the MCC-APC/C interaction is strongly diminished in both *apc15Δ* and in *mad3-KEN2AAA* or *mad3-ΔCterm* cells. When we immunoprecipitated Mad3-GFP from mitotic cells, we found considerably less of the APC/C subunit Lid1/Apc4 associated compared to wild type cells (**Figure** 4C), and immunoprecipitation of the APC/C subunit Cut9/Apc6-GFP brought down considerably less Mad2 and Mad3 (**Figure** 4D). $Slp1^{Cdc20}$ was still found associated with the APC/C in *apc15Δ*, *mad3-KEN2AAA* and *mad3-ΔCterm* cells, explaining how these cells exit mitosis. Given the strong similarities in phenotype between deletion of *apc15*$^{+}$ and mutations in the Mad3 C-terminus, we tested whether Apc15 also becomes dispensable for the SAC at lower Cdc20 concentrations. Indeed, lowering the abundance of Cdc20 efficiently rescued checkpoint activity in *apc15Δ* cells (**Figure** 4E). This was even more efficient than in *mad3-ΔCterm* cells – possibly because the MCC in *mad3-ΔCterm* only captures one $Slp1^{Cdc20}$, whereas it likely captures two $Slp1^{Cdc20}$ molecules in *apc15Δ* cells. Hence, sequestration of $Slp1^{Cdc20}$ should be very efficient in *apc15Δ* cells (**Figure** 5). Indeed, immunoprecipitation of Mad3-GFP left hardly any $Slp1^{Cdc20}$ in the supernatant of *apc15Δ* cells when lower levels of $Slp1^{Cdc20}$ were expressed from the *rad21* promoter (**Figure** 4F). We therefore argue that inhibition of the APC/C by the MCC encompasses (i) sequestration of one $Slp1^{Cdc20}$ in the core MCC, (ii) inhibition of a second $Slp1^{Cdc20}$ molecule through the Mad3 C-terminus, and (iii) competition between the MCC and other free $Slp1^{Cdc20}$ for APC/C binding. Only (iii) is defective in *apc15Δ* cells, whereas (ii) and (iii) are defective in *mad3Δ-Cterm* cells (**Figure** 5). All, (i), (ii) and (iii) are defective in the *mad3-KEN1AAA* mutant – explaining the different extents of checkpoint impairment.

Which subcomplexes are present and how are they disassembled?

We want to point out that an apparently complete depletion of Mad3 by immunoprecipitation does not deplete the APC/C subunit Lid1/Apc4 from checkpoint-active wild type cells, nor does it deplete $Slp1^{Cdc20}$ (data not shown). Because this indicates that not all APC/C is in complex with the MCC, this is an apparent contradiction to the competition model (**Figure** 5). However, co-depletion of both Mad2 and Mad3 depletes the majority of $Slp1^{Cdc20}$ (data not shown). This indicates that a fraction of $Slp1^{Cdc20}$ is bound to Mad2, without being simultaneously bound to Mad3. For this fraction to act as a competitor on the APC/C, it would be able to bind the APC/C. This would be in contrast to findings in budding yeast that Mad2-Cdc20 does not efficiently

associate with the APC/C [51]. We currently do not have the right combination of antibodies and tags to perform sequential immunoprecipitates to further resolve the existing subcomplexes, and the resolution of gel filtration may not be high enough. Another puzzling aspect are the dynamics of these complexes. Both *mad3-ΔCterm* and *apc15Δ* cells can considerably delay anaphase when $Slp1^{Cdc20}$ levels are lowered (**Figure** 2, 4E). These mutants also show impaired MCC disassembly (**Figure** 3). Yet, when we release these mutants from a checkpoint-mediated arrest, they exit mitosis efficiently (data not shown). It would be interesting to know whether this release relies on new $Slp1^{Cdc20}$ synthesis, or whether any of the existing complexes must be disassembled for this release from the checkpoint-mediated arrest. Differences between the disassembly of free MCC and APC/C-bound MCC have been observed previously [56]. It is unclear whether different free MCC complex or subcomplexes could have different requirements for disassembly.

Why does lack of Apc15 have different functional consequences in different eukaryotes?

Whereas fission yeast cells lacking Apc15 have a checkpoint defect (**Figure** 4A), both human and budding yeast cells lacking the Apc15 ortholog have a functional checkpoint [51-53]. This discrepancy can be explained because fission yeast cells without Apc15 seem to lack MCC-APC/C interaction (**Figure** 4C,D). In contrast, absence of the human and budding yeast Apc15 does not seem to impair MCC-APC/C interaction [16, 20, 51]. Because these organisms also differ in the presence or absence of Bub3 within the MCC, one could speculate that Bub3 in the human and budding yeast MCC can compensate for the absence of Apc15 and possibly mediate binding to the APC/C. However, Bub3 was not visible in electron microscopy structures of the human APC/C-MCC [16, 20], which suggests that it is not tightly bound to the APC/C. It is possible that structural changes in the remaining APC/C that are caused by the absence of Apc15 have different consequences on MCC binding in these organisms. A direct structural comparison of the APC/C could shed light on this question.

Materials and Methods

S. pombe strains

Strains are listed in Supplementary Table S1. In general, mutants or tags were integrated into the endogenous locus using PCR-based gene targeting [57] and replaced the wild type allele. The *apc15Δ::kanR* and *mad2Δ::hygR* deletions were created by replacement of the endogenous locus with a resistance cassette using PCR-based gene targeting. To create strains with expression of a second *slp1*$^{+}$ gene, the *slp1*$^{+}$ genomic region from 1,504 base pairs (bp) 5′ to 549 bp 3′ of the open reading frame was integrated into the *leu1* locus using the pDUAL system [58]. The *hygroR<<Pnmt41-slp1*$^{+}$ promoter change at the endogenous locus was created as described [46]. *Schizosaccharomyces pombe* strains with the following mutations or modifications have been described: *cdc25-22* [59], *nda3-KM311* [29], *mad2+-GFP≪kanR*, *mad3+-GFP≪kanR*, *plo1+-mCherry* [60], *kanR<<Prad21-slp1+* [61], *hph<<Pmad2(259bp)-mad2+-GFP<<kanR, hph<<Pmad3(150bp)-mad3+-GFP<<kanR* [45], *bub1Δ::ura4+* [62], *mad3Δ::ura4+* [36].

Mutations within Mad3 were:

name	original aa sequence	mutation	reference
KEN1AAA	18-QS**KEN**IE-24	18-QS**AAA**IE-24	[24]
Dbox-mimic L/K	210-TNSVNP**L**QT-218	210-TNSVNP**K**QT-218	this study
Dbox-mimic VNPL/ANPA	210-TNS**V**NP**L**QT-218	210-TNS**A**NP**A**QT-218	this study
ABBA1 mut	240-FK**F**S**VY**S**D**ADG-250	240-FK**A**S**AA**S**A**ADG-250	this study
KEN2AAA	269-RR**KEN**NI-275	269-RR**AAA**NI-275	[24]
ABBA2 mut	297-GK**F**Q**VH**C**D**EEV-307	297-GK**A**Q**AA**C**A**EEV-307	this study
ΔCterm	Mad3-aa1-310	Mad3-aa1-281	this study

Mutations within Slp1^{Cdc20} were:

name	original aa sequence	mutation	reference
mr63	126-NTRVL**AF**KLD-135	126-NTRVL**PY**KLD-135	[39]
Cbox-mut	86-RS**DRFIP**SR-94	86- RS**AAAAA**SR-94	[41]

Culture conditions

For live-cell imaging and protein extraction, cells were grown at 30°C in rich medium (YEA), unless indicated otherwise. Strains with *slp1*$^{+}$ expressed from *Pnmt41* were grown in Edinburgh

minimal medium (EMM) containing the necessary supplements. For immunoprecipitation from synchronized cultures, strains expressing *cdc25-22* were grown at 25°C in EMM containing the necessary supplements until they reached a concentration of 6-8 x 10^6 cells/mL. Cells were arrested at the G2/M transition by shifting to 36°C for 5 hours, and released by reducing the temperature. For mitotic cells, the cultures were released by shifting to 16°C with addition of 50 μg/mL Carbendazim (MBC, Sigma, 378674) and were harvested after 65 minutes. For synchronous interphase cells, the arrested cultures were shifted to 25°C and harvested after 50 minutes. For harvest of asynchronously growing cells, cultures were grown at 30°C in rich medium (YEA) until they reached a concentration of 6-8 x 10^6 cells/mL.

Live cell imaging

Imaging on a DeltaVision Core system (Applied Precision/GE Healthcare) was performed as previously described [63], with the exception of using 40-100 μg/ml lectin (Sigma, L1395) to coat # 1.5 glass-bottom culture dishes (Ibidi). For imaging strains with *Pnmt41-slp1*$^+$, YAM2 [64] was added at final concentrations between 0 nM (only the solvent, DMSO) and 350 nM. YAM2 was added to cells before shifting to 16°C. The time of appearance and disappearance of Plo1-mCherry at spindle pole bodies was analyzed as described previously [65].

Fluorescence microscopy

Methanol-fixed cells were washed once with PEM/50 %methanol (PEM = 100 mM PIPES, 1 mM EGTA, 1 mM MgSO4; pH 6.8 with KOH) and once with PEM. For DNA staining, cells were resuspended in 500 µL PEM containing 1 µg/mL DAPI (Sigma) and incubated at RT for 10 min. Cells were pelleted, washed once with 500 µL PEM and resuspended in 500 µL PEM. For microscopy, 2.7 µL of the pellet was mounted. Images were acquired with a CoolSnap EZ (Roper) camera using a 63x/1.4 Plan Apochromat oil objective on a Zeiss Axio Imager.M1 microscope and were processed with MetaMorph software (Molecular Devices Corporation). 14 individual planes spaced by 0.3 µm were acquired. To create color-combined pictures, out-of-focus planes were removed; 11 sections of the GFP channel (sum intensity projection), 11 sections of the mCherry channel (maximum intensity projection) and 4 sections of the DAPI channel (maximum intensity projection) were projected to a single image and signal intensity was adjusted for all pictures in a similar way.

Immunoprecipitation

Asynchronously growing or synchronized cells were harvested, washed with EMM and frozen as droplets in liquid N_2. Cell extracts were prepared using a ball mill (RETSCH MM400), followed by

resuspension in extraction buffer (50 mM HEPES pH 7.5, 150 mM NaCl, 2 mM EDTA, 0.5 % NP-40, 1 mM PMSF) or low-salt extraction buffer (25 mM Tris-HCl pH 7.5, 50 mM NaCl, 0.1% NP-40, 1 mM PMSF, 1mM DTT, 10μM Bortezomib (Velcade, LC laboratories, B-1408)) supplemented with protease inhibitors (Complete EDTA-free, Roche, 1187358001) and phosphatase inhibitors (PhosSTOP, Roche, 4906837001) to a protein concentration of 10 mg/mL. The extract was spun down for 10 min at 16,600 rcf at 4 °C and the supernatant was collected. Protein G-coated magnetic beads (Dynabeads, Invitrogen 10003D) were coupled to mouse anti-GFP antibodies (Roche, 11814460001, 8 μg per 100 μL beads) and incubated with the supernatant for 15 min at 4 °C. Samples were taken before ('input') and after ('supernatant') incubation with the beads. The beads were washed 5 times with extraction buffer or no-salt extraction buffer (50 mM Tris-HCl pH 7.5, 20% glycerol, 1 mM PMSF, 1mM DTT, 10μM Bortezomib) including protease and phosphatase inhibitors, and elution from the beads was performed by adding 100 mM citric acid. The pH of the eluate was raised with 1M Tris pH 9.2, and 2x SDS sample buffer (125 mM Tris pH 6.8, 4 % SDS, 0.02 % bromophenol blue, 20 % glycerol, 200 mM DTT) was added.

Cell extracts, SDS-PAGE, immunoblotting

Protein extraction was performed as previously described [66], with the exception of resuspension of the cell pellet in 100 μl 2x SDS sample buffer (125 mM Tris pH 6.8, 4% (w/v) SDS, 20% (v/v) glycerol, 200 mM DTT, 0.02% (w/v) bromophenol blue) and using a ball mill (RETSCH MM400) for cell disruption. Proteins were separated by SDS-PAGE and transferred onto PVDF membranes (Immobilon-P, Millipore) using a semi-dry transfer system (Amersham Biosciences). Mouse anti-GFP (Roche, 11814460001), rabbit anti-Mad2 (this study and [47]), rabbit anti-Mad3 (this study), mouse anti-tubulin (Sigma, T5168), rabbit anti-Cdc2 (Santa Cruz, SC-53), rabbit anti-Slp1 (this study and [39]) and rabbit anti-c-myc (Cell Signaling Technology, 2278) were used as primary antibodies. Secondary antibodies were anti-mouse or anti-rabbit HRP conjugates (Dianova, 115-035-003, 111-035-003) and were read out using chemiluminescense.

Acknowledgments

We thank Julia Kamenz for valuable suggestions, Jacob W. Alder and Nadine Schmidt for generating yeast strains, Tatiana Boluarte for excellent technical help, Nicole Hustedt, Boris Macek and the Proteome Centre of the University of Tübingen for mass spectrometric analysis, and Andrea Ciliberto for discussions.

References

1. Musacchio A (2015) The Molecular Biology of Spindle Assembly Checkpoint Signaling Dynamics. *Curr Biol* **25:** R1002-1018

2. London N, Biggins S (2014) Signalling dynamics in the spindle checkpoint response. *Nat Rev Mol Cell Biol* **15:** 736-747

3. Vleugel M, Hoogendoorn E, Snel B, Kops GJ (2012) Evolution and function of the mitotic checkpoint. *Dev Cell* **23:** 239-250

4. Gordon DJ, Resio B, Pellman D (2012) Causes and consequences of aneuploidy in cancer. *Nat Rev Genet* **13:** 189-203

5. Kops GJ, Weaver BA, Cleveland DW (2005) On the road to cancer: aneuploidy and the mitotic checkpoint. *Nat Rev Cancer* **5:** 773-785

6. Schvartzman JM, Sotillo R, Benezra R (2010) Mitotic chromosomal instability and cancer: mouse modelling of the human disease. *Nat Rev Cancer* **10:** 102-115

7. Mapelli M, Musacchio A (2007) MAD contortions: conformational dimerization boosts spindle checkpoint signaling. *Curr Opin Struct Biol* **17:** 716-725

8. Luo X, Yu H (2008) Protein metamorphosis: the two-state behavior of Mad2. *Structure* **16:** 1616-1625

9. Chao WC, Kulkarni K, Zhang Z, Kong EH, Barford D (2012) Structure of the mitotic checkpoint complex. *Nature* **484:** 208-213

10. Mariani L, Chiroli E, Nezi L, Muller H, Piatti S, Musacchio A, Ciliberto A (2012) Role of the Mad2 dimerization interface in the spindle assembly checkpoint independent of kinetochores. *Curr Biol* **22:** 1900-1908

11. Tipton AR, Wang K, Link L, Bellizzi JJ, Huang H, Yen T, Liu ST (2011) BUBR1 and closed MAD2 (C-MAD2) interact directly to assemble a functional mitotic checkpoint complex. *J Biol Chem* **286:** 21173-21179

12. Izawa D, Pines J (2015) The mitotic checkpoint complex binds a second CDC20 to inhibit active APC/C. *Nature* **517:** 631-634

13. Kulukian A, Han JS, Cleveland DW (2009) Unattached kinetochores catalyze production of an anaphase inhibitor that requires a Mad2 template to prime Cdc20 for BubR1 binding. *Dev Cell* **16:** 105-117

14. Lara-Gonzalez P, Scott MI, Diez M, Sen O, Taylor SS (2011) BubR1 blocks substrate recruitment to the APC/C in a KEN-box-dependent manner. *J Cell Sci* **124:** 4332-4345

15. Malureanu LA, Jeganathan KB, Hamada M, Wasilewski L, Davenport J, van Deursen JM (2009) BubR1 N terminus acts as a soluble inhibitor of cyclin B degradation by APC/C(Cdc20) in interphase. *Dev Cell* **16:** 118-131

16. Yamaguchi M *et al* (2016) Cryo-EM of Mitotic Checkpoint Complex-Bound APC/C Reveals Reciprocal and Conformational Regulation of Ubiquitin Ligation. *Mol Cell* **63:** 593-607

17. Primorac I, Musacchio A (2013) Panta rhei: the APC/C at steady state. *J Cell Biol* **201:** 177-189

18. Chang L, Barford D (2014) Insights into the anaphase-promoting complex: a molecular machine that regulates mitosis. *Curr Opin Struct Biol* **29:** 1-9

19. Herzog F, Primorac I, Dube P, Lenart P, Sander B, Mechtler K, Stark H, Peters JM (2009) Structure of the anaphase-promoting complex/cyclosome interacting with a mitotic checkpoint complex. *Science* **323:** 1477-1481

20. Alfieri C, Chang L, Zhang Z, Yang J, Maslen S, Skehel M, Barford D (2016) Molecular basis of APC/C regulation by the spindle assembly checkpoint. *Nature* **536:** 431-436

21. Burton JL, Solomon MJ (2007) Mad3p, a pseudosubstrate inhibitor of APCCdc20 in the spindle assembly checkpoint. *Genes Dev* **21:** 655-667

22. Elowe S, Dulla K, Uldschmid A, Li X, Dou Z, Nigg EA (2010) Uncoupling of the spindle-checkpoint and chromosome-congression functions of BubR1. *J Cell Sci* **123:** 84-94

23. King EM, van der Sar SJ, Hardwick KG (2007) Mad3 KEN boxes mediate both Cdc20 and Mad3 turnover, and are critical for the spindle checkpoint. *PLoS One* **2:** e342

24. Sczaniecka M, Feoktistova A, May KM, Chen JS, Blyth J, Gould KL, Hardwick KG (2008) The spindle checkpoint functions of Mad3 and Mad2 depend on a Mad3 KEN box-mediated interaction with Cdc20-anaphase-promoting complex (APC/C). *J Biol Chem* **283:** 23039-23047

25. Tian W, Li B, Warrington R, Tomchick DR, Yu H, Luo X (2012) Structural analysis of human Cdc20 supports multisite degron recognition by APC/C. *Proc Natl Acad Sci U S A* **109:** 18419-18424

26. Diaz-Martinez LA, Tian W, Li B, Warrington R, Jia L, Brautigam CA, Luo X, Yu H (2015) The Cdc20-binding Phe box of the spindle checkpoint protein BubR1 maintains the mitotic checkpoint complex during mitosis. *J Biol Chem* **290:** 2431-2443

27. Di Fiore B, Davey NE, Hagting A, Izawa D, Mansfeld J, Gibson TJ, Pines J (2015) The ABBA motif binds APC/C activators and is shared by APC/C substrates and regulators. *Dev Cell* **32:** 358-372

28. Davey NE, Morgan DO (2016) Building a Regulatory Network with Short Linear Sequence Motifs: Lessons from the Degrons of the Anaphase-Promoting Complex. *Mol Cell* **64:** 12-23

29. Hiraoka Y, Toda T, Yanagida M (1984) The NDA3 gene of fission yeast encodes beta-tubulin: a cold-sensitive nda3 mutation reversibly blocks spindle formation and chromosome movement in mitosis. *Cell* **39:** 349-358

30. Mulvihill DP, Petersen J, Ohkura H, Glover DM, Hagan IM (1999) Plo1 kinase recruitment to the spindle pole body and its role in cell division in Schizosaccharomyces pombe. *Mol Biol Cell* **10:** 2771-2785

31. Hardwick KG, Johnston RC, Smith DL, Murray AW (2000) MAD3 encodes a novel component of the spindle checkpoint which interacts with Bub3p, Cdc20p, and Mad2p. *J Cell Biol* **148:** 871-882

32. Larsen NA, Al-Bassam J, Wei RR, Harrison SC (2007) Structural analysis of Bub3 interactions in the mitotic spindle checkpoint. *Proc Natl Acad Sci U S A* **104:** 1201-1206

33. Wang X, Babu JR, Harden JM, Jablonski SA, Gazi MH, Lingle WL, de Groen PC, Yen TJ, van Deursen JM (2001) The mitotic checkpoint protein hBUB3 and the mRNA export factor hRAE1 interact with GLE2p-binding sequence (GLEBS)-containing proteins. *J Biol Chem* **276:** 26559-26567

34. Millband DN, Hardwick KG (2002) Fission yeast Mad3p is required for Mad2p to inhibit the anaphase-promoting complex and localizes to kinetochores in a Bub1p-, Bub3p-, and Mph1p-dependent manner. *Mol Cell Biol* **22:** 2728-2742

35. Taylor SS, Ha E, McKeon F (1998) The human homologue of Bub3 is required for kinetochore localization of Bub1 and a Mad3/Bub1-related protein kinase. *J Cell Biol* **142:** 1-11

36. Vanoosthuyse V, Valsdottir R, Javerzat JP, Hardwick KG (2004) Kinetochore targeting of fission yeast Mad and Bub proteins is essential for spindle checkpoint function but not for all chromosome segregation roles of Bub1p. *Mol Cell Biol* **24:** 9786-9801

37. Overlack K, Primorac I, Vleugel M, Krenn V, Maffini S, Hoffmann I, Kops GJ, Musacchio A (2015) A molecular basis for the differential roles of Bub1 and BubR1 in the spindle assembly checkpoint. *Elife* **4:** e05269

38. Hwang LH, Lau LF, Smith DL, Mistrot CA, Hardwick KG, Hwang ES, Amon A, Murray AW (1998) Budding yeast Cdc20: a target of the spindle checkpoint. *Science* **279:** 1041-1044

39. Kim SH, Lin DP, Matsumoto S, Kitazono A, Matsumoto T (1998) Fission yeast Slp1: an effector of the Mad2-dependent spindle checkpoint. *Science* **279:** 1045-1047

40. Nilsson J, Yekezare M, Minshull J, Pines J (2008) The APC/C maintains the spindle assembly checkpoint by targeting Cdc20 for destruction. *Nat Cell Biol* **10:** 1411-1420

41. Kimata Y, Baxter JE, Fry AM, Yamano H (2008) A role for the Fizzy/Cdc20 family of proteins in activation of the APC/C distinct from substrate recruitment. *Mol Cell* **32:** 576-583

42. Schwab M, Neutzner M, Mocker D, Seufert W (2001) Yeast Hct1 recognizes the mitotic cyclin Clb2 and other substrates of the ubiquitin ligase APC. *EMBO J* **20:** 5165-5175

43. Zhang S, Chang L, Alfieri C, Zhang Z, Yang J, Maslen S, Skehel M, Barford D (2016) Molecular mechanism of APC/C activation by mitotic phosphorylation. *Nature* **533:** 260-264

44. Izawa D, Pines J (2012) Mad2 and the APC/C compete for the same site on Cdc20 to ensure proper chromosome segregation. *J Cell Biol* **199:** 27-37

45. Heinrich S *et al* (2013) Determinants of robustness in spindle assembly checkpoint signalling. *Nat Cell Biol* **15:** 1328-1339

46. Petrova B, Dehler S, Kruitwagen T, Heriche JK, Miura K, Haering CH (2013) Quantitative analysis of chromosome condensation in fission yeast. *Mol Cell Biol* **33:** 984-998

47. Yamada HY, Matsumoto S, Matsumoto T (2000) High dosage expression of a zinc finger protein, Grt1, suppresses a mutant of fission yeast slp1(+), a homolog of CDC20/p55CDC/Fizzy. *J Cell Sci* **113 (Pt 22):** 3989-3999

48. Simonetta M, Manzoni R, Mosca R, Mapelli M, Massimiliano L, Vink M, Novak B, Musacchio A, Ciliberto A (2009) The influence of catalysis on mad2 activation dynamics. *PLoS Biol* **7:** e10

49. Lara-Gonzalez P, Westhorpe FG, Taylor SS (2012) The spindle assembly checkpoint. *Curr Biol* **22:** R966-980

50. Musacchio A, Ciliberto A (2012) The spindle-assembly checkpoint and the beauty of self-destruction. *Nat Struct Mol Biol* **19:** 1059-1061

51. Foster SA, Morgan DO (2012) The APC/C subunit Mnd2/Apc15 promotes Cdc20 autoubiquitination and spindle assembly checkpoint inactivation. *Mol Cell* **47:** 921-932

52. Mansfeld J, Collin P, Collins MO, Choudhary JS, Pines J (2011) APC15 drives the turnover of MCC-CDC20 to make the spindle assembly checkpoint responsive to kinetochore attachment. *Nat Cell Biol* **13:** 1234-1243

53. Uzunova K *et al* (2012) APC15 mediates CDC20 autoubiquitylation by APC/C(MCC) and disassembly of the mitotic checkpoint complex. *Nat Struct Mol Biol* **19:** 1116-1123

54. Reddy SK, Rape M, Margansky WA, Kirschner MW (2007) Ubiquitination by the anaphase-promoting complex drives spindle checkpoint inactivation. *Nature* **446:** 921-925

55. Stegmeier F *et al* (2007) Anaphase initiation is regulated by antagonistic ubiquitination and deubiquitination activities. *Nature* **446:** 876-881

56. Ma HT, Poon RY (2011) Orderly inactivation of the key checkpoint protein mitotic arrest deficient 2 (MAD2) during mitotic progression. *J Biol Chem* **286:** 13052-13059

57. Bahler J, Wu JQ, Longtine MS, Shah NG, McKenzie A, 3rd, Steever AB, Wach A, Philippsen P, Pringle JR (1998) Heterologous modules for efficient and versatile PCR-based gene targeting in Schizosaccharomyces pombe. *Yeast* **14:** 943-951

58. Matsuyama A, Shirai A, Yashiroda Y, Kamata A, Horinouchi S, Yoshida M (2004) pDUAL, a multipurpose, multicopy vector capable of chromosomal integration in fission yeast. *Yeast* **21:** 1289-1305

59. Russell P, Nurse P (1986) cdc25+ functions as an inducer in the mitotic control of fission yeast. *Cell* **45:** 145-153

60. Heinrich S, Windecker H, Hustedt N, Hauf S (2012) Mph1 kinetochore localization is crucial and upstream in the hierarchy of spindle assembly checkpoint protein recruitment to kinetochores. *J Cell Sci* **125:** 4720-4727

61. Yokobayashi S, Watanabe Y (2005) The kinetochore protein Moa1 enables cohesion-mediated monopolar attachment at meiosis I. *Cell* **123:** 803-817

62. Bernard P, Hardwick K, Javerzat JP (1998) Fission yeast bub1 is a mitotic centromere protein essential for the spindle checkpoint and the preservation of correct ploidy through mitosis. *J Cell Biol* **143:** 1775-1787

63. Windecker H, Langegger M, Heinrich S, Hauf S (2009) Bub1 and Bub3 promote the conversion from monopolar to bipolar chromosome attachment independently of shugoshin.

EMBO Rep **10:** 1022-1028

64. Nakamura Y, Arai A, Takebe Y, Masuda M (2011) A chemical compound for controlled expression of nmt1-driven gene in the fission yeast Schizosaccharomyces pombe. *Anal Biochem* **412:** 159-164

65. Mora-Santos MD, Hervas-Aguilar A, Sewart K, Lancaster TC, Meadows JC, Millar JB (2016) Bub3-Bub1 Binding to Spc7/KNL1 Toggles the Spindle Checkpoint Switch by Licensing the Interaction of Bub1 with Mad1-Mad2. *Curr Biol* **26:** 2642-2650

66. Koch A, Rode HB, Richters A, Rauh D, Hauf S (2012) A chemical genetic approach for covalent inhibition of analogue-sensitive aurora kinase. *ACS Chem Biol* **7:** 723-731

67. Duranteau M, Montagne JJ, Rahmani Z (2016) A novel mutation in the N-terminal domain of Drosophila BubR1 affects the spindle assembly checkpoint function of BubR1. *Biol Open*, 10.1242/bio.021196

Figure Legends

Figure 1 The Mad3 C-terminus binds to Slp1^{Cdc20} and is required for checkpoint activity

(A) Domain structure of *H. sapiens* BubR1 and *S. pombe* Mad3 and alignment of yeast Mad3 C-terminal sequences containing Slp1^{Cdc20}-binding motifs. See text for details. **(B)** Cells expressing *plo1+-mCherry*, the conditional tubulin mutant *nda3-KM311* and the indicated mutations or truncations in *mad3* were analyzed by live-cell imaging at the restrictive temperature of 16°C. The time that each cell spent in prometaphase was determined by localization of Plo1 to SPBs (circle). Cells that had not yet exited mitosis when filming stopped are indicated by triangles, cells that died during the experiment by filled circles. **(C)** Anti-GFP immunoprecipitates from mitotic cells of the indicated Mad3-GFP strains were analyzed by immunoblotting using anti-GFP, anti-Slp1 and anti-Mad2 antibodies. **(D)** Schematic of the likely assembly of the 'core MCC' with a second Slp1^{Cdc20} molecule bound via the different motifs in the Mad3 C-terminus. **(E)** Anti-GFP immunoprecipitates from mitotic sfGFP-Slp1 cells with the additional genetic modifications indicated on top were analyzed by immunoblotting using anti-GFP, anti-Slp1, anti-Mad3 and anti-Mad2 antibodies. The tagged sfGFP-Slp1^{Cdc20} was expressed from the endogenous promoter at the endogenous locus, untagged Slp1^{Cdc20} (Slp1 or Slp1-mr63) was expressed from the endogenous regulatory sequences at the exogenous *leu1* locus. **(F)** Checkpoint function of the indicated strains was analyzed as in (B). Wild type Slp1^{Cdc20} was expressed under the endogenous regulatory sequences from the exogenous *leu1* locus and Slp1^{Cdc20}-mr63 was expressed at the endogenous locus either from the endogenous promoter (*Pslp1*) or from the *rad21* promoter, which reduces the amount of Slp1^{Cdc20} (*Prad21*) (wt, wild type). **(G)** Anti-GFP immunoprecipitates from mitotic cells of the indicated strains were analyzed by immunoblotting using anti-Slp1, anti-Mad3 and anti-Mad2 antibodies.

Figure 2 The Mad3 C-terminus is less important for checkpoint activity at lower Slp1^{Cdc20} levels

(A) Checkpoint function of the indicated strains was analyzed as in Figure 1B. Slp1^{Cdc20} was expressed at the endogenous locus from either its endogenous promoter (*Pslp1*) or from the *rad21* promoter (*Prad21*), which lowers levels (see Supplementary Figure S2A). **(B)** Checkpoint function of the indicated strains was analyzed as in Figure 1B. Mad2 and Mad3 were overexpressed to about 200% and 120% of wild type levels, respectively. Slp1^{Cdc20} or Slp1^{Cdc20}-mr63 were expressed from the *rad21* promoter at the endogenous locus. **(C)** Checkpoint function

of the indicated strains was analyzed as in Figure 1B and mitotic arrest was assumed when cells spent more than 5 h in mitosis. Slp1^{Cdc20} was expressed from the regulatable *nmt41* promoter at the endogenous locus and expression level was controlled with increasing concentrations of YAM2. Shown is the mean with SEM. **(D)** Representative example of one experiment summarized in (C). Checkpoint function of the indicated strains was analyzed as in Figure 1B. **(E)** Schematic indicating that the Mad3 C-terminus becomes dispensable at low Slp1^{Cdc20} levels because all Slp1^{Cdc20} can be sequestered in the 'core MCC'.

Figure 3 The Mad3 C-terminus and Apc15 are required for MCC disassembly

(A) Anti-GFP immunoprecipitates of asynchronously growing cells of the indicated strains were analyzed by immunoblotting using anti-GFP, anti-Slp1 and anti-Mad2 antibodies. **(B)** Cells of the indicated genotypes were synchronized at the G2/M transition, released into mitosis and analyzed for cell cycle stage using Plo1-mCherry and DNA staining. Example pictures are shown at the bottom, quantitative analysis on top. Cells with Plo1 on SPBs were considered to be in mitosis, cells with two close nuclei were considered to be in anaphase (n > 150 cells per time point; scale bar 10 µm). Cells for the experiment in (C) were harvested at the last time point. **(C)** Anti-GFP immunoprecipitates from interphase cells of the indicated strains were analyzed by immunoblotting using anti-GFP, anti-Slp1 and anti-Mad2 antibodies. **(D)** Schematic for MCC persistence in different strains.

Figure 4 The Mad3 C-terminus and Apc15 are required for MCC binding to the APC/C

(A) Checkpoint function of the indicated strains was analyzed as in Figure 1B. **(B)** Anti-GFP immunoprecipitates of mitotic cells from the indicated strains were analyzed by immunoblotting using anti-Slp1, anti-Mad3 and anti-Mad2 antibodies. sfGFP-Slp1^{Cdc20} was expressed from the endogenous promoter at the endogenous locus, Slp1^{Cdc20}-mr63 was expressed from the endogenous regulatory sequences at the exogenous *leu1* locus. **(C)** Anti-GFP immunoprecipitates from mitotic Mad3-GFP cells, with the additional genetic modifications indicated on top, were analyzed for binding of myc-tagged Lid1/Apc4. Immunoblots were performed with anti-GFP, anti-myc, anti-Slp1, anti-Mad2 and anti-tubulin (loading control) antibodies (*cross-reaction band). **(D)** Anti-GFP immunoprecipitates from mitotic Cut9/Apc6-GFP cells, with the additional genetic modifications indicated on top, were analyzed for binding of the MCC. Immunoblots were performed with anti-GFP, anti-Slp1, anti-Mad3 and anti-Mad2 antibodies. **(E)** Checkpoint function of the indicated strains was analyzed as in Figure 1B. Slp1^{Cdc20} was expressed at the endogenous locus from either the endogenous promoter (*Pslp1*) or from the *rad21* promoter (*Prad21*). **(F)** Anti-GFP immunoprecipitates, as well as input and

supernatant after precipitation, from mitotic cells of the indicated Mad3-GFP strains were analyzed by immunoblotting using anti-GFP, anti-Slp1, anti-Mad2 and anti-Cdc2 (loading control) antibodies. Slp1^{Cdc20} was expressed at the endogenous locus from either the endogenous promoter (*Pslp1*) or from the *rad21* promoter (Prad21). In the strain with 2x *Prad21*, Slp1^{Cdc20} was expressed at the endogenous locus and at the exogenous *leu1* locus, both controlled by the *rad21* promoter.

Figure 5 Model for the molecular changes in *mad3-ΔCterm* and *apc15Δ* cells

In both *mad3-ΔCterm* and *apc15Δ* cells, the MCC does not associate with the APC/C, and MCC disassembly is impaired. We hypothesize that reduction of Slp1^{Cdc20} rescues the checkpoint defect in *apc15Δ* cells more efficiently, because sequestration within the MCC is more efficient.

Figure 1

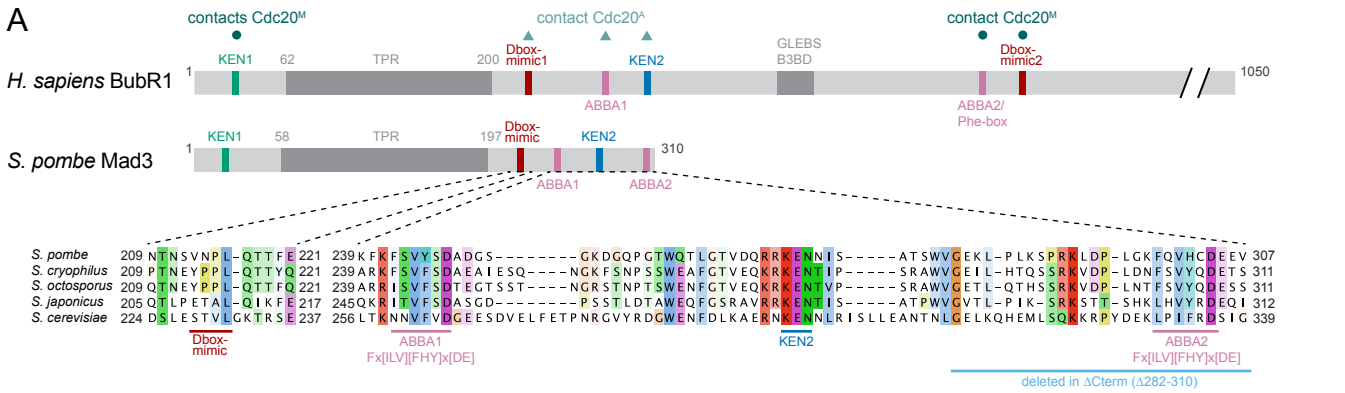
A
contacts Cdc20M
contact Cdc20A
contact Cdc20M
H. sapiens BubR1
KEN1
TPR
Dbox-mimic1
KEN2
GLEBS
B3BD
Dbox-mimic2
ABBA1
ABBA2/ Phe-box
S. pombe Mad3
Dbox-mimic
ABBA1
ABBA2
S. pombe
S. cryophilus
S. octosporus
S. japonicus
S. cerevisiae
Dbox-mimic
ABBA1 Fx[ILV][FHY]x[DE]
KEN2
ABBA2 Fx[ILV][FHY]x[DE]
deleted in ΔCterm (Δ282-310)

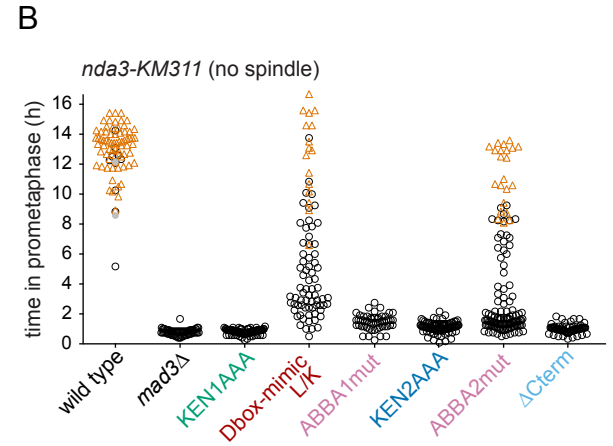
B
nda3-KM311 (no spindle)
time in prometaphase (h)
wild type
mad3Δ
KEN1AAA
Dbox-mimic L/K
ABBA1mut
KEN2AAA
ABBA2mut
ΔCterm

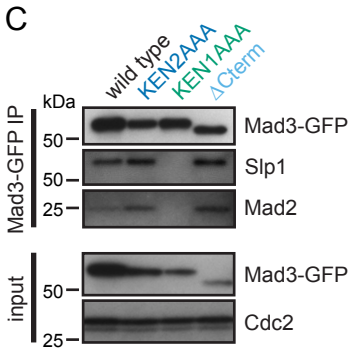
C
wild type
KEN2AAA
KEN1AAA
ΔCterm
kDa
Mad3-GFP IP
Mad3-GFP
Slp1
Mad2
input
Mad3-GFP
Cdc2

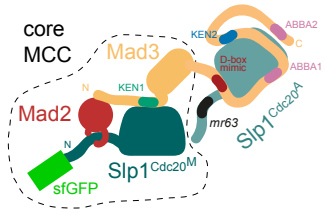
D
core MCC
Mad3
Mad2
Slp1Cdc20M
Slp1Cdc20A
mr63
sfGFP
KEN1
KEN2
ABBA1
ABBA2
D-box mimic

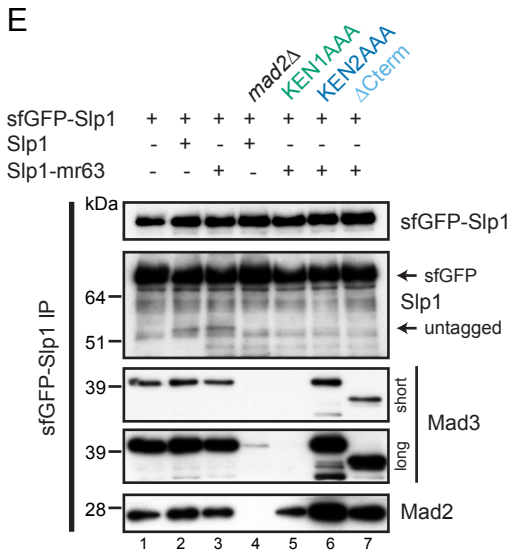
E
mad2Δ
KEN1AAA
KEN2AAA
ΔCterm
sfGFP-Slp1
Slp1
Slp1-mr63
kDa
sfGFP-Slp1 IP
sfGFP-Slp1
sfGFP Slp1 untagged
Mad3
short
long
Mad2
1 2 3 4 5 6 7

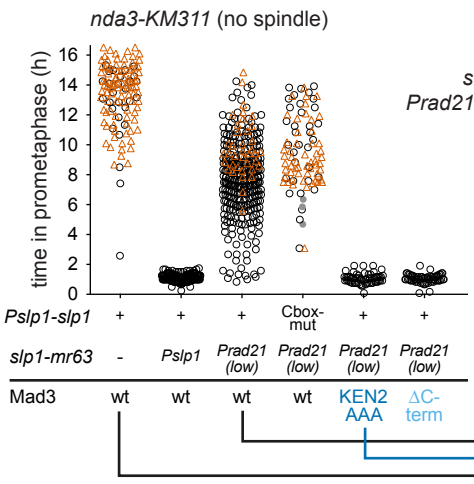
F
nda3-KM311 (no spindle)
time in prometaphase (h)
Pslp1-slp1
slp1-mr63
Cbox-mut
Pslp1
Prad21 (low)
Mad3
wt
KEN2 AAA
ΔC-term

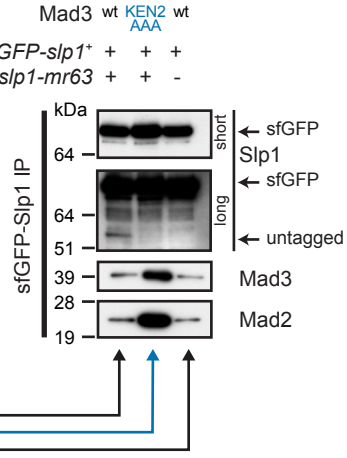
G
Mad3
wt
KEN2 AAA
sfGFP-slp1+
Prad21-slp1-mr63
kDa
sfGFP-Slp1 IP
short
long
sfGFP Slp1
sfGFP untagged
Mad3
Mad2

Figure 2

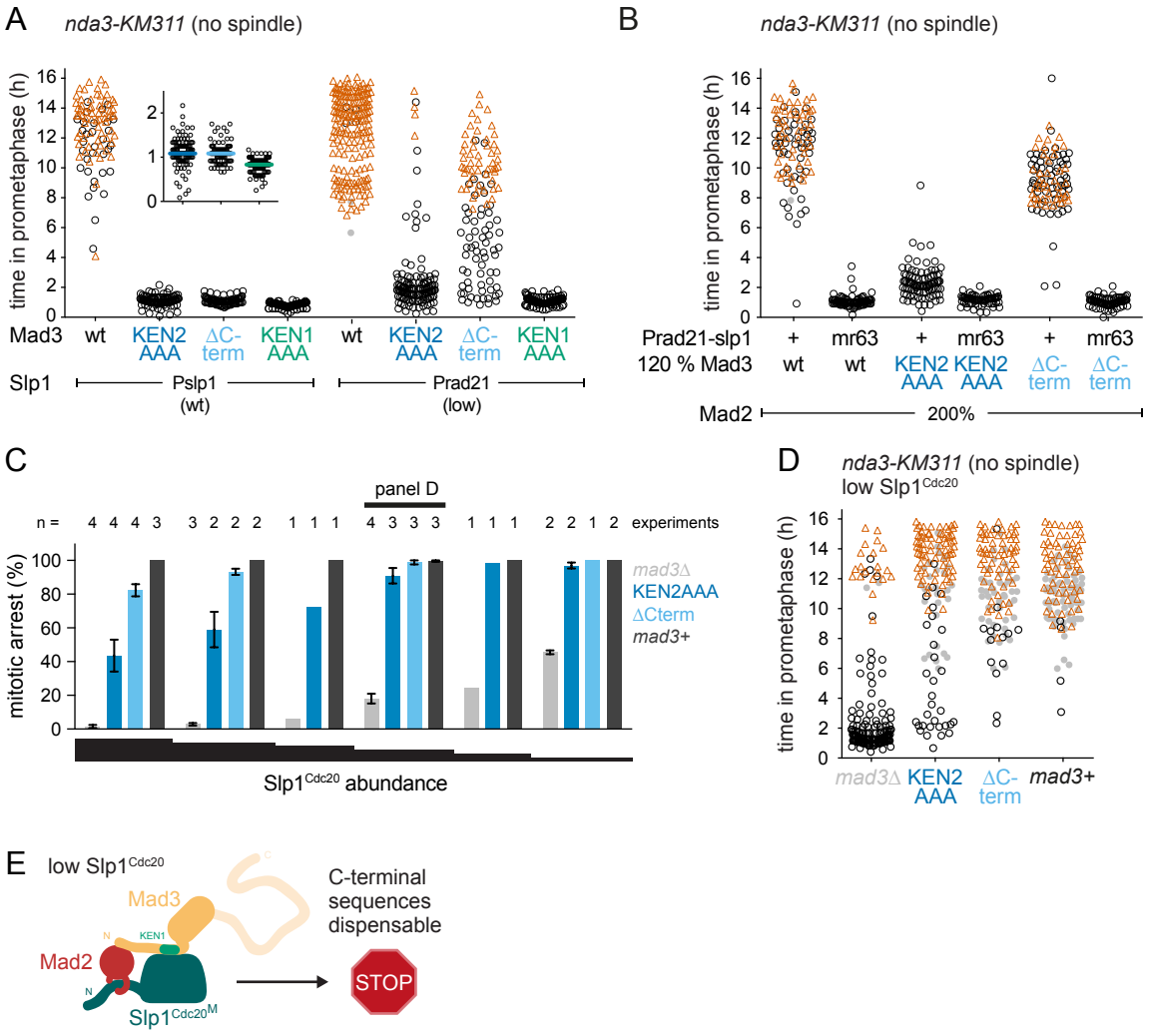
A
nda3-KM311 (no spindle)
time in prometaphase (h)
Mad3
wt
KEN2 AAA
ΔC-term
KEN1 AAA
Slp1
Pslp1 (wt)
Prad21 (low)
B
nda3-KM311 (no spindle)
time in prometaphase (h)
Prad21-slp1
120 % Mad3
mr63
Mad2
200%
C
panel D
n =
experiments
mitotic arrest (%)
mad3Δ
KEN2AAA
ΔCterm
mad3+
Slp1Cdc20 abundance
D
nda3-KM311 (no spindle)
low Slp1Cdc20
time in prometaphase (h)
E
low Slp1Cdc20
Mad3
KEN1
Mad2
Slp1Cdc20M
C-terminal sequences dispensable
STOP

Figure 3

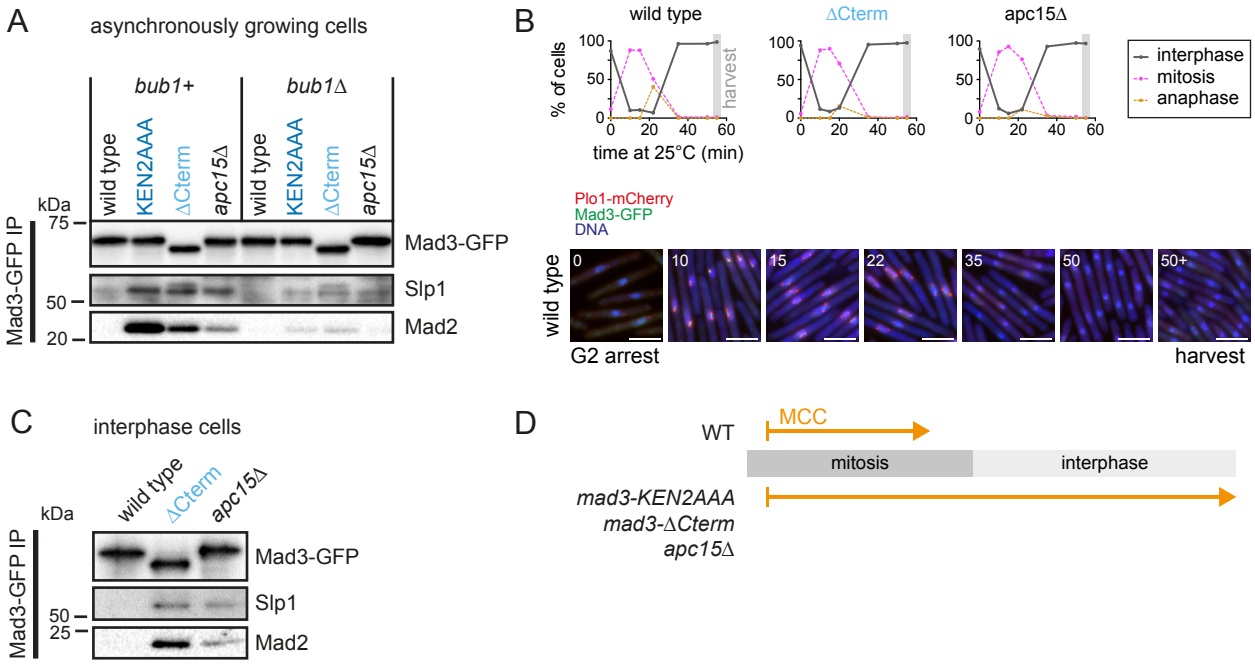
A
asynchronously growing cells
bub1+
bub1Δ
wild type
KEN2AAA
ΔCterm
apc15Δ
kDa
75
50
20
Mad3-GFP IP
Mad3-GFP
Slp1
Mad2
B
wild type
ΔCterm
apc15Δ
% of cells
time at 25°C (min)
harvest
interphase
mitosis
anaphase
Plo1-mCherry
Mad3-GFP
DNA
0
10
15
22
35
50
50+
G2 arrest
harvest
C
interphase cells
wild type
ΔCterm
apc15Δ
kDa
50
25
Mad3-GFP IP
Mad3-GFP
Slp1
Mad2
D
WT
MCC
mitosis
interphase
mad3-KEN2AAA
mad3-ΔCterm
apc15Δ

Figure 4

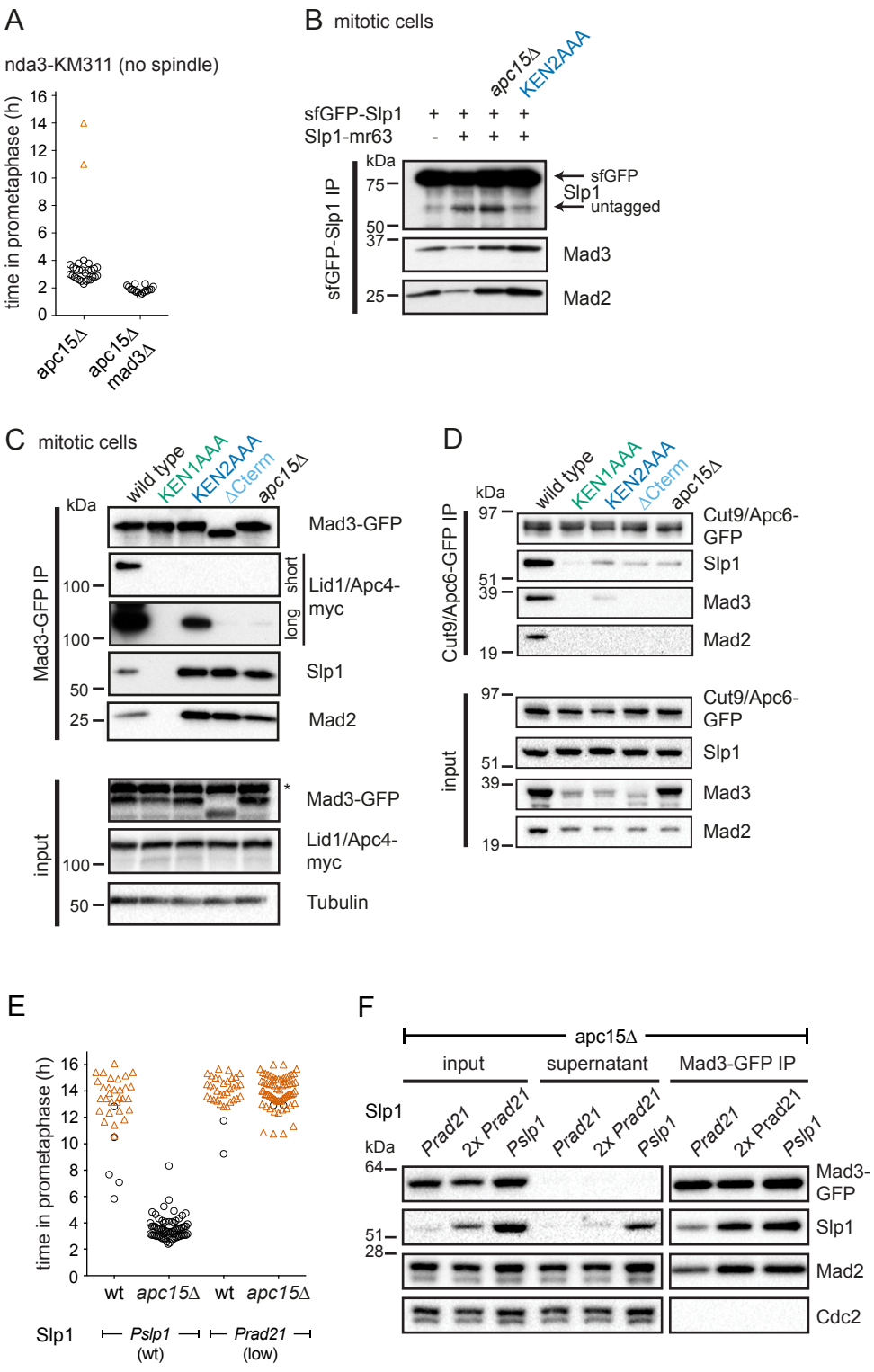
A
nda3-KM311 (no spindle)
time in prometaphase (h)
apc15Δ
apc15Δ mad3Δ
B mitotic cells
apc15Δ
KEN2AAA
sfGFP-Slp1
Slp1-mr63
kDa
sfGFP-Slp1 IP
sfGFP
Slp1
untagged
Mad3
Mad2
C mitotic cells
wild type
KEN1AAA
KEN2AAA
ΔCterm
apc15Δ
Mad3-GFP IP
Mad3-GFP
Lid1/Apc4-myc
short
long
Slp1
Mad2
input
Tubulin
D
Cut9/Apc6-GFP IP
Cut9/Apc6-GFP
Slp1
Mad3
Mad2
E
time in prometaphase (h)
wt
apc15Δ
Slp1
Pslp1 (wt)
Prad21 (low)
F
apc15Δ
input
supernatant
Mad3-GFP IP
Prad21
2x Prad21
Pslp1
Mad3-GFP
Cdc2

Figure 5

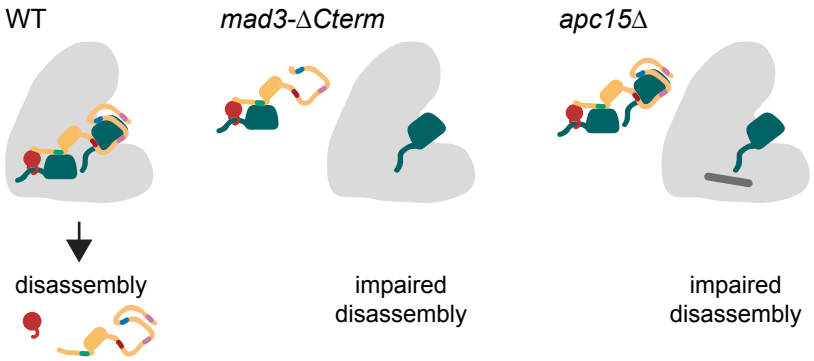
WT
mad3-ΔCterm
apc15Δ
disassembly
impaired
disassembly
impaired
disassembly

Figure S1 Bub1 is required for the interaction between Mad3 and Bub3

(A) Alignment of the Mad3 C-terminus and BubR1 middle region containing the GLEBS motif. **(B)** It has recently been proposed that *D. melanogaster* contains a KAN sequence instead of the 2nd KEN [67]. We rather think that the motif analogous to KEN2 in *Drosophila* is QEN, which shows higher conservation among different *Drosophila* species (see alignment in B). The proposed KAN motif is boxed. **(C)** Mass spectrometry of Mad3-GFP and Bub3-GFP immunoprecipitates from cells that were delayed in mitosis by the spindle assembly checkpoint due to the *nda3-KM311* mutation. The table shows the number of identified peptides (pep.) and the amino acid sequence coverage (seq.cov.) for each protein, which are semi-quantitative measures for the abundance of the protein in the immunoprecipitate. Mad2, Bub1 and Bub3 co-purified efficiently with Mad3, Bub1 and some Mad3 co-purified with Bub3. **(D)** Anti-GFP immunoprecipitates from asynchronously growing Mad3-GFP cells, with additional genetic modifications as indicated, were analyzed by immunoblotting using anti-Mad3 and anti-myc antibodies (#likely degradation product of Mad3; *cross-reaction bands; wt, wild type). **(E)** Anti-GFP immunoprecipitates from mitotic cells of the indicated Mad3-GFP strains were analyzed by immunoprecipitation using anti-Mad3 and anti-myc antibodies. Tubulin was detected in the input samples as a loading control. **(F)** Immunoblot of cell extracts from the indicated strains using anti-Mad3, anti-GFP and anti-Cdc2 (loading control) antibodies. A dilution step was loaded for each strain to compare intensities (*cross-reaction band overlapping with the Mad3-GFP band). **(G)** Checkpoint function of the indicated strains was analyzed as in Figure 1B. Data for wild type and *mad3Δ* are the same as in Figure 1B. **(H)** Checkpoint function of the indicated strains was analyzed as in Figure 1B. $Slp1^{Cdc20}$ and $Slp1^{Cdc20}$-mr63 were expressed at the endogenous locus from either the endogenous promoter (*Pslp1*) or from the *rad21* promoter (*Prad21*). Data for *Pslp1*/wt are the same as in Figure 1F. **(I)** Checkpoint function of the indicated strains was analyzed as in Figure 1B.

Figure S2 Levels of $Slp1^{Cdc20}$ expressed from different promoters and phenotype of *Padh1-slp1⁺* cells

(A,B) Immunoblotting of cell extracts from cells expressing $Slp1^{Cdc20}$ from different promoters. Some strains additionally contained the *mad3-ΔCterm* mutation or *apc15* deletion. Cells also expressed the tubulin *nda3-KM311* mutant. Samples were taken directly before (0 hrs) and 10 hrs after shifting the cultures to the restrictive temperature. A sample containing only sfGFP-tagged Slp1 was loaded as a control. In 2x *Prad21* strains, $Slp1^{Cdc20}$ was expressed at the endogenous locus as well as at the exogenous *leu1* locus, both copies controlled by the *rad21* promoter. In (B), cells expressed *slp1⁺* from the regulatable *nmt41* promoter and some samples were treated

with YAM2 to suppress expression. **(C)** Checkpoint function of the indicated strains was analyzed as in Figure 1B. $Slp1^{Cdc20}$ was expressed at the endogenous locus from the endogenous promoter (*Pslp1*) or from the *adh* promoter (*Padh1*).

Figure S1

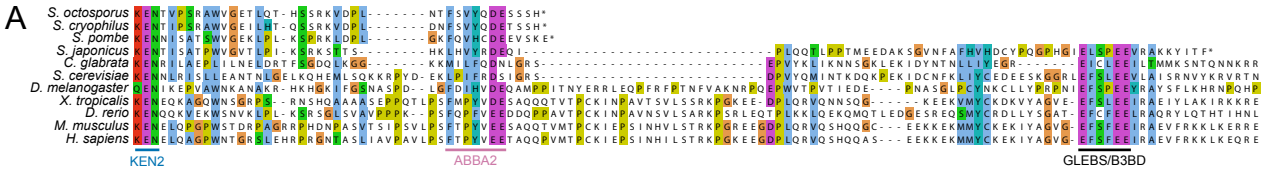

C

	Mad3-GFP IP *nda3-KM311* arrest pep.	Mad3-GFP IP *nda3-KM311* arrest seq.cov.	Bub3-GFP IP *nda3-KM311* arrest pep.	Bub3-GFP IP *nda3-KM311* arrest seq.cov.
Mad1	2	7 %	0	0 %
Mad2	15	61 %	2	8 %
Mad3	30	69 %	3	10 %
Bub1	62	65 %	50	46 %
Bub3	17	56 %	10	29 %

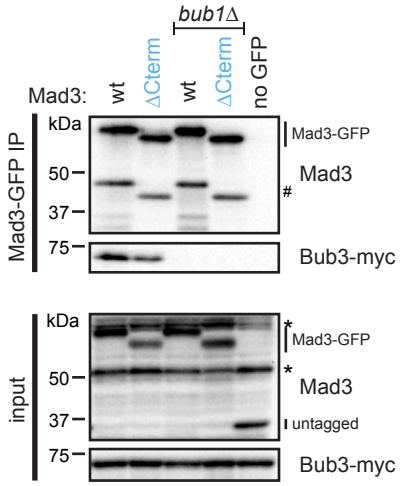

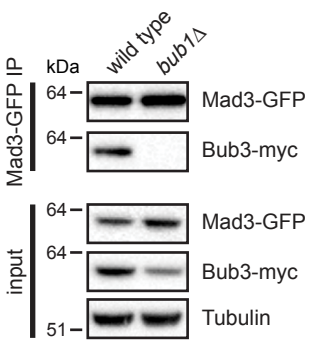

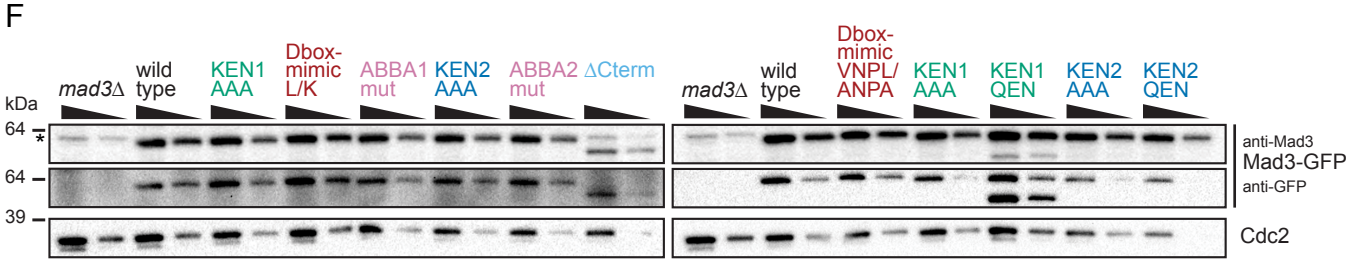

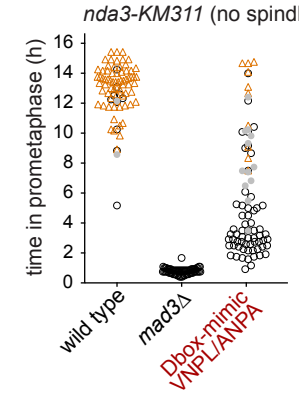

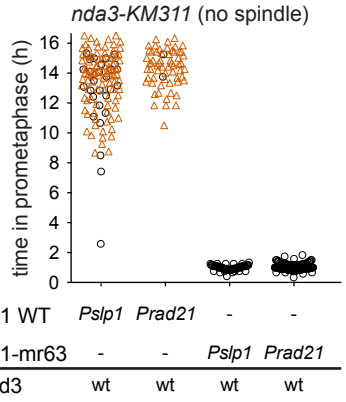

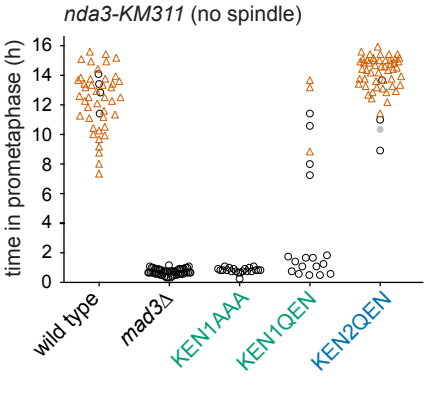

Figure S2

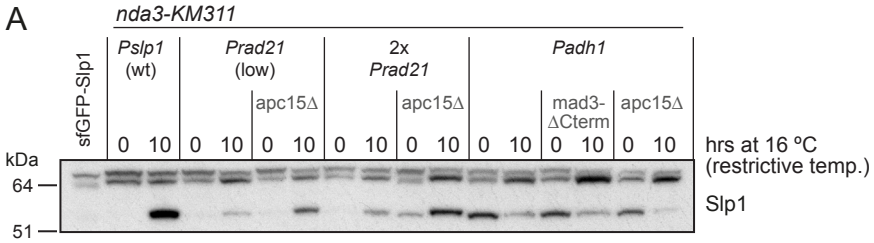
A
nda3-KM311
sfGFP-Slp1
Pslp1 (wt)
Prad21 (low)
apc15Δ
2x Prad21
apc15Δ
Padh1
mad3-ΔCterm
apc15Δ
0 10 0 10 0 10 0 10 0 10 0 10 0 10 0 10
kDa
64
51
hrs at 16 ºC (restrictive temp.)
Slp1

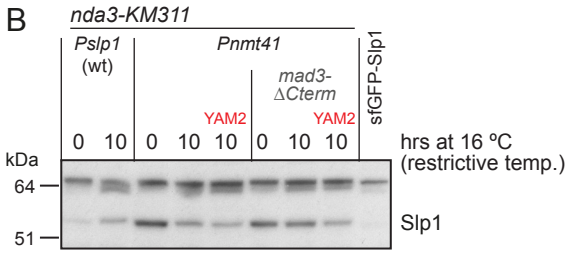
B
nda3-KM311
Pslp1 (wt)
Pnmt41
mad3-ΔCterm
sfGFP-Slp1
YAM2
YAM2
0 10 0 10 10 0 10 10
kDa
64
51
hrs at 16 ºC (restrictive temp.)
Slp1

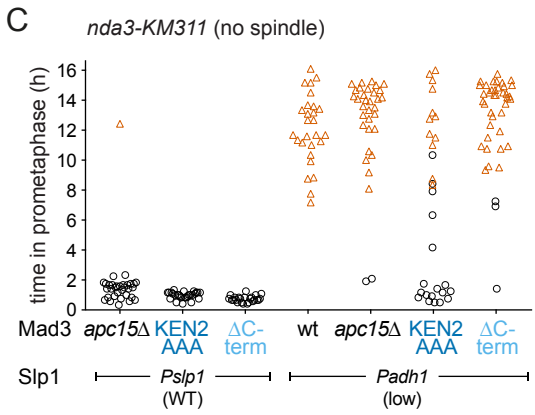
C
nda3-KM311 (no spindle)
time in prometaphase (h)
0
2
4
6
8
10
12
14
16
Mad3 apc15Δ KEN2 AAA ΔC-term wt apc15Δ KEN2 AAA ΔC-term
Slp1 Pslp1 (WT) Padh1 (low)

Supplementary Table S1

Figure 1B

SL759	h-	*leu1 mad3+-GFP<<kanR plo1+-mCherry<<natR nda3-KM311*
SL756	h-	*leu1 ade6-M210 mad3Δ::ura4+ plo1+-mCherry<<natR nda3-KM311*
SP259	h+	*ade6-M216 mad3-KEN(20)AAA-GFP<<kanR plo1+-mCherry<<natR nda3-KM311*
SU599, SU599'	h-	*leu1 mad3-Dbox(L/K)-GFP<<kanR plo1+-mCherry<<natR nda3-KM311*
SU581	h+	*leu1 ade6-M216 mad3-ABBA1mut-GFP<<kanR plo1+-mCherry<<natR nda3-KM311*
SP710	h+	*leu1 mad3-KEN271AAA-GFP<<kanR nda3-KM311 plo1+-mCherry<<natR*
SU582, SU582'	h+	*leu1 ade6-M216 mad3-ABBA2mut-GFP<<kanR plo1+-mCherry<<natR nda3-KM311*
SU074	h+	*leu1 mad3-ΔCterm(282-310)+-GFP-hphNT1 plo1+-mCherry<<natR nda3-KM311*
SU075	h-	*leu1 mad3-ΔCterm(282-310)+-GFP-hphNT1 plo1+-mCherry<<natR nda3-KM311*

Figure 1C

SP694	h+	*leu1 mad3+-GFP<<kanR plo1+-mCherry<<natR cdc25-22 lid1+-13xmyc<<natR*
SU048	h+	*mad3-KEN271AAA-GFP<<kanR plo1+-mCherry<<natR lid1+-13xmyc<<natR cdc25-22*
SU050	h+	*mad3-KEN20AAA-GFP<<kanR plo1+-mCherry<<natR lid1+-13xmyc<<natR cdc25-22*
SU052	h+	*leu1 mad3ΔCterm(282-310)+-GFP plo1+-mCherry<<natR lid1+-13xmyc<<natR cdc25-22*

Figure 1E

SU526	h-	*slp1::Pslp1-sfGFPopt-slp1-S(GGGGS)3-RIPGLIN-slp1 plo1+-mCherry<<natR cdc25-22*
SU519	h+	*pDUAL-Pslp1(long2)-slp1-Tslp1<<leu1+ slp1::Pslp1-sfGFPopt-slp1-S(GGGGS)3-RIPGLIN-slp1 plo1+-mCherry<<natR cdc25-22*
SU380	h-	*ade6-M210 pDUAL-Pslp1(long2)-slp1-mr63-Tslp1<<leu1+ slp1::Pslp1-sfGFPopt-slp1-S(GGGGS)3-RIPGLIN-slp1 plo1+-mCherry<<natR cdc25-22*
SU538	h+	*pDUAL-Pslp1(long2)-slp1-Tslp1<<leu1+ slp1::Pslp1-sfGFPopt-slp1-S(GGGGS)3-RIPGLIN-slp1 mad2::hygR plo1+-mCherry<<natR cdc25-22*
SU393	h-	*pDUAL-Pslp1(long2)-slp1-mr63-Tslp1<<leu1+ mad3-KEN20AAA-Tadh1-hphNT1 slp1::Pslp1-sfGFPopt-slp1-S(GGGGS)3-RIPGLIN-slp1 plo1+-mCherry<<natR cdc25-22*
SU392	h-	*pDUAL-Pslp1(long2)-slp1-mr63-Tslp1<<leu1+ mad3-KEN271AAA-Tadh1-hphNT1 slp1::Pslp1-sfGFPopt-slp1-S(GGGGS)3-RIPGLIN-slp1 plo1+-mCherry<<natR cdc25-22*
SU531	h+	*pDUAL-Pslp1(long2)-slp1-mr63-Tslp1<<leu1+ slp1::Pslp1-sfGFPopt-slp1-S(GGGGS)3-RIPGLIN-slp1 mad3-ΔCterm(282-310)-Tadh1-hphNT1 plo1+-mCherry<<natR cdc25-22*

Figure 1F

SK827	h-	*ade6-M216 plo1+-mCherry<<natR nda3-KM311*
SK828	h+	*leu1 ade6-M216 plo1+-mCherry<<natR nda3-KM311*
ST508, ST508', ST5	h?	*pDual-Pslp1(long2)-slp1<<leu1+ ade6-M216 or 210 plo1+-mCherry<<natR nda3-KM311 slp1-mr63*
SU389, SU389', SU	h+	*pDUAL-Pslp1(long2)-slp1-Tslp1<<leu1+ kanR<<Prad21-slp1-mr63 plo1+-mCherry<<natR nda3-KM311*
SU390	h-	*pDUAL-Pslp1(long2)-slp1-Tslp1<<leu1+ kanR<<Prad21-slp1-mr63 plo1+-mCherry<<natR nda3-KM311*
SU514, SU514'	h-	*pDUAL-Pslp1(long2)-slp1-Cboxmut-Tslp1<<leu1+ kanR<<Prad21-slp1-mr63 plo1+-mCherry<<natR nda3-KM311*
SU397	h+	*pDUAL-Pslp1(long2)-slp1-Tslp1<<leu1+ mad3-KEN271AAA-GFP<<kanR kanR<<Prad21-slp1-mr63 plo1+-mCherry<<natR nda3-KM311*
SU398	h-	*pDUAL-Pslp1(long2)-slp1-Tslp1<<leu1+ mad3-KEN271AAA-GFP<<kanR kanR<<Prad21-slp1-mr63 plo1+-mCherry<<natR nda3-KM311*
SU502, SU502'	h+	*pDUAL-Pslp1(long2)-slp1-Tslp1<<leu1+ kanR<<Prad21-slp1-mr63 mad3-ΔCterm(282-310)+-GFP-hphNT1 plo1+-mCherry<<natR nda3-KM311*

Figure 1G

SU528''	h-	*pDUAL-Pslp1(long2)-sfGFP-opt_S((GGGGS)3)RIPGLIN-slp1-Tslp1<<leu1+ kanR<<Prad21-slp1mr63 plo1+-mCherry<<natR cdc25-22*
SU530'	h-	*pDUAL-Pslp1(long2)-sfGFP-opt_S((GGGGS)3)RIPGLIN-slp1-Tslp1<<leu1+ kanR<<Prad21-slp1mr63 mad3-KEN271AAA-Tadh1-hphNT1 plo1+-mCherry<<natR cdc25-22*
SU526	h-	*slp1::Pslp1-sfGFPopt-slp1-S(GGGGS)3-RIPGLIN-slp1 plo1+-mCherry<<natR cdc25-22*

Figure 2A

SL760	h+	*leu1 mad3+-GFP<<kanR plo1+-mCherry<<natR nda3-KM311*
SP710	h+	*leu1 mad3-KEN271AAA-GFP<<kanR nda3-KM311 plo1+-mCherry<<natR*
SU074	h+	*leu1 mad3-ΔCterm(282-310)+-GFP-hphNT1 plo1+-mCherry<<natR nda3-KM311*
SU075	h-	*leu1 mad3-ΔCterm(282-310)+-GFP-hphNT1 plo1+-mCherry<<natR nda3-KM311*
SP259	h+	*ade6-M216 mad3-KEN(20)AAA-GFP<<kanR plo1+-mCherry<<natR nda3-KM311*
SU331	h+	*leu1 mad3+-GFP<<kanR kanR<<Prad21-slp1+ plo1+-mCherry<<natR nda3-KM311*
SU332	h-	*leu1 mad3+-GFP<<kanR kanR<<Prad21-slp1+ plo1+-mCherry<<natR nda3-KM311*
SU327	h-	*leu1 mad3-KEN271AAA-GFP<<kanR kanR<<Prad21-slp1+ plo1+-mCherry<<natR nda3-KM311*
SU561	h+	*kanR-Prad21-slp1+ mad3-ΔCterm(282-310)+-GFP-hphNT1 plo1+-mCherry<<natR nda3-KM311*
SU562	h-	*leu1 kanR-Prad21-slp1+ mad3-ΔCterm(282-310)+-GFP-hphNT1 plo1+-mCherry<<natR nda3-KM311*
SU324	h-	*ade6-M216 leu1 mad3-KEN(20)AAA-GFP<<kanR kanR<<Prad21-slp1+ plo1+-mCherry<<natR nda3-KM311*
SU325	h+	*ade6 mad3-KEN(20)AAA-GFP<<kanR kanR<<Prad21-slp1+ plo1+-mCherry<<natR nda3-KM311*

Figure 2B

SU535	h+	*kanR-Prad21-slp1 hphNT1<<Pmad2(259bp)-mad2+-GFP<<kanR hphNT1<<Pmad3(150bp)-mad3-GFP<<kanR plo1+-mCherry<<natR nda3-KM311*
SU536	h-	*leu1 kanR-Prad21-slp1 hphNT1<<Pmad2(259bp)-mad2+-GFP<<kanR hphNT1<<Pmad3(150bp)-mad3-GFP<<kanR plo1+-mCherry<<natR nda3-KM311*
SU533	h+	*leu1 kanR<<Prad21-slp1mr63 hphNT1<<Pmad2(259bp)-mad2+-GFP<<kanR hphNT1<<Pmad3(150bp)-mad3-GFP<<kanR plo1+-mCherry<<natR nda3-KM311*
SU534	h-	*leu1 kanR<<Prad21-slp1mr63 hphNT1<<Pmad2(259bp)-mad2+-GFP<<kanR hphNT1<<Pmad3(150bp)-mad3-GFP<<kanR plo1+-mCherry<<natR nda3-KM311*
SU555	h+	*leu1 kanR-Prad21-slp1 hphNT1<<Pmad2(259bp)-mad2+-GFP<<kanR hphNT1<<Pmad3(150bp)-mad3-KEN271AAA-GFP<<kanR plo1+-mCherry<<natR nda3-KM311*
SU556	h-	*leu1 kanR-Prad21-slp1 hphNT1<<Pmad2(259bp)-mad2+-GFP<<kanR hphNT1<<Pmad3(150bp)-mad3-KEN271AAA-GFP<<kanR plo1+-mCherry<<natR nda3-KM311*
SU554, SU554'	h-	*leu1 kanR<<Prad21-slp1-mr63 hphNT1<<Pmad2(259bp)-mad2+-GFP<<kanR hphNT1<<Pmad3(150bp)-mad3-KEN271AAA-GFP<<kanR plo1+-mCherry<<natR nda3-KM311*
SU557	h+	*kanR-Prad21-slp1 hphNT1<<Pmad2(259bp)-mad2+-GFP<<kanR hphNT1<<Pmad3(150bp)-mad3ΔCterm(282-310)+-GFP plo1+-mCherry<<natR nda3-KM311*
SU558	h-	*leu1 kanR-Prad21-slp1 hphNT1<<Pmad2(259bp)-mad2+-GFP<<kanR hphNT1<<Pmad3(150bp)-mad3ΔCterm(282-310)+-GFP plo1+-mCherry<<natR nda3-KM311*
SU559, SU559'	h+	*leu1 kanR<<Prad21-slp1-mr63 hphNT1<<Pmad2(259bp)-mad2+-GFP<<kanR hphNT1<<Pmad3(150bp)-mad3ΔCterm(282-310)+-GFP plo1+-mCherry<<natR nda3-KM311*

Figure 2C,D

SU545, SU545'	h-	*leu1 ade6-M210 hygroR<<Pnmt41-slp1 mad3Δ::ura4+ plo1+-mCherry<<natR nda3-KM311*
SU546	h-	*leu1 hygroR<<Pnmt41-slp1 mad3-KEN271AAA-GFP<<kanR plo1+-mCherry<<natR nda3?*
SU560, SU560'	h-	*leu1 hygroR<<Pnmt41-slp1 mad3-ΔCterm(282-310)+-GFP-hphNT1 plo1+-mCherry<<natR nda3-KM311*
SU544, SU544'	h-	*leu1 hygroR<<Pnmt41-slp1 plo1+-mCherry<<natR nda3-KM311*

Figure 3A

SU722	h+	*leu1 ura4D18? plo1+-mCherry<<natR mad3+-GFP<<kanR bub3+-13xMyc<<hphMX6*
SP710	h+	*leu1 mad3-KEN271AAA-GFP<<kanR nda3-KM311 plo1+-mCherry<<natR*
SU752'	h-	*bub3+-13xMyc<<hphMX6 mad3ΔCterm(282-310)+-GFP plo1+-mCherry<<natR*
SP841	h+	*leu1 apc15Δ::kanR mad3+-GFP<<kanR plo1+-mCherry<<natR nda3-KM311*
SU724	h+	*leu1 ura4D18? ade6-M216 bub1::ura4+ plo1+-mCherry<<natR mad3+-GFP<<kanR bub3+-13xMyc<<hphMX6*
SU771	h-	*leu1 ade6-M216 ura4? mad3-KEN271AAA-GFP<<kanR plo1+-mCherry<<natR bub1::ura4+*
SU754	h-	*ura4D18? ade6-M216 bub1::ura4+ bub3+-13xMyc<<hphMX6 mad3ΔCterm(282-310)+-GFP plo1+-mCherry<<natR*
SU773	h-	*leu1 ade6-M216 ura4? apc15Δ::kanR mad3+-GFP<<kanR plo1+-mCherry<<natR bub1::ura4+*

Figure 3B,C

SP694	h+	*leu1 mad3+-GFP<<kanR plo1+-mCherry<<natR lid1+-13xmyc<<natR cdc25-22*

SU052	h+	*leu1 mad3ΔCterm(282-310)+-GFP plo1+-mCherry<<natR lid1+-13xmyc<<natR cdc25-22*
SU746	h+	*leu1 apc15Δ::kanR mad3+-GFP<<kanR lid1+-13xmyc<<natR plo1+-mCherry<<natR cdc25-22*

Figure 4A

SP840	h-	*leu1 apc15Δ::kanR mad3+-GFP<<kanR plo1+-mCherry<<natR nda3-KM311*
SP831	h?	*leu1 ade6-M210 apc15Δ::kanR mad3Δ::ura4+ plo1+-mCherry<<natR nda3-KM311*

Figure 4B

SU526	h-	*slp1::Pslp1-sfGFPopt-slp1-S(GGGGS)3-RIPGLIN-slp1 plo1+-mCherry<<natR cdc25-22*
SU381	h-	*pDUAL-Pslp1(long2)-slp1-mr63-Tslp1<<leu1+ slp1::Pslp1-sfGFPopt-slp1-S(GGGGS)3-RIPGLIN-slp1 plo1+-mCherry<<natR cdc25-22*
SU768	h-	*ade6-M210 pDUAL-Pslp1(long2)-slp1-mr63-Tslp1<<leu1+ slp1::Pslp1-sfGFPopt-slp1-S(GGGGS)3-RIPGLIN-slp1 apc15Δ::kanR plo1+-mCherry<<natR cdc25-22*
SU392	h-	*pDUAL-Pslp1(long2)-slp1-mr63-Tslp1<<leu1+ mad3-KEN271AAA-Tadh1-hphNT1 slp1::Pslp1-sfGFPopt-slp1-S(GGGGS)3-RIPGLIN-slp1 plo1+-mCherry<<natR cdc25-22*

Figure 4C

SP694	h+	*leu1 mad3+-GFP<<kanR plo1+-mCherry<<natR cdc25-22 lid1+-13xmyc<<natR*
SU050	h+	*mad3-KEN20AAA-GFP<<kanR plo1+-mCherry<<natR lid1+-13xmyc<<natR cdc25-22*
SU048	h+	*mad3-KEN271AAA-GFP<<kanR plo1+-mCherry<<natR lid1+-13xmyc<<natR cdc25-22*
SU052	h+	*leu1 mad3ΔCterm(282-310)+-GFP plo1+-mCherry<<natR lid1+-13xmyc<<natR cdc25-22*
SU746	h+	*leu1 apc15Δ::kanR mad3+-GFP<<kanR lid1+-13xmyc<<natR plo1+-mCherry<<natR cdc25-22*

Figure 4D

SU774	h+	*leu1 cut9-GFP<<kanR plo1+-mCherry<<natR cdc25-22*
SU914	h+	*leu1 cut9-GFP<<kanR mad3-KEN20AAA-Tadh1-hphNT1 plo1+-mCherry<<natR cdc25-22*
SU916	h+	*leu1 cut9-GFP<<kanR mad3-KEN271AAA-Tadh1-hphNT1 plo1+-mCherry<<natR cdc25-22*
SU918	h+	*leu1 cut9-GFP<<kanR mad3-ΔCterm(282-310)-Tadh1-hphNT1 plo1+-mCherry<<natR cdc25-22*
SU920	h+	*leu1 apc15Δ::kanR cut9-GFP<<kanR plo1+-mCherry<<natR cdc25-22*

Figure 4E

SK827	h-	*ade6-M216 plo1+-mCherry<<natR nda3-KM311*
SP800	h+	*apc15Δ::kanR plo1+-mCherry<<natR nda3-KM311*
SP840	h-	*leu1 apc15Δ::kanR mad3+-GFP<<kanR plo1+-mCherry<<natR nda3-KM311*
SP457	h+	*ade6-M216? kanR-Prad21-slp1+ plo1+-mCherry<<natR nda3-KM311*
SP793	h+	*apc15Δ::kanR kanR-Prad21-slp1+ plo1+-mCherry<<natR nda3-KM311*
SP794	h-	*leu1 apc15Δ::kanR kanR-Prad21-slp1+ plo1+-mCherry<<natR nda3-KM311*

Figure 4F

SU910	h+	*leu1 apc15Δ::kanR kanR<<Prad21-slp1+ mad3+-GFP<<kanR lid1+-13xmyc<<natR plo1+-mCherry<<natR cdc25-22*
SU912	h-	*apc15Δ::kanR kanR<<Prad21-slp1+ leu1+<<Prad21-slp1+ mad3+-GFP<<kanR lid1+-13xmyc<<natR plo1+-mCherry<<natR cdc25-22*
SU746	h+	*leu1 apc15Δ::kanR mad3+-GFP<<kanR lid1+-13xmyc<<natR plo1+-mCherry<<natR cdc25-22*

Figure S1C

SK675	h-	*lys1 hph<<ark1-as3 (L166A, S229A) plo1+- mCherry<<natR mad3+-GFP<<kanR nda3- KM311*
SK678	h+	*lys1 hph<<ark1-as3 (L166A, S229A) plo1+- mCherry<<natR bub3+-S(GGGGS)3-triplemye- GFP<<kanR nda3-KM311*

Figure S1D

SU722	h+	*leu1 ura4D18? plo1+-mCherry<<natR mad3+-GFP<<kanR bub3+-13xMyc<<hphMX6*
SU752'	h-	*bub3+-13xMyc<<hphMX6 mad3ΔCterm(282-310)+-GFP plo1+-mCherry<<natR*
SU724	h+	*leu1 ura4D18? ade6-M216 bub1::ura4+ plo1+-mCherry<<natR mad3+-GFP<<kanR bub3+-13xMyc<<hphMX6*
SU754	h-	*ura4D18? ade6-M216 bub1::ura4+ bub3+-13xMyc<<hphMX6 mad3ΔCterm(282-310)+-GFP plo1+-mCherry<<natR*
SU043	h-	*leu1 bub3+-13xMyc<<hphMX6*

Figure S1E

SU926	h+	*leu1 bub3+-13xMyc<<hphMX6 mad3+-GFP<<kanR plo1+-mCherry<<natR cdc25-22*
SU928	h+	*leu1 ade6-M216 bub1::ura4+ bub3+-13xMyc<<hphMX6 mad3+-GFP<<kanR plo1+-mCherry<<natR cdc25-22*

Figure S1F

SL756	h-	*leu1 ade6-M210 mad3Δ::ura4+ plo1+-mCherry<<natR nda3-KM311*
SL759	h-	*leu1 mad3+-GFP<<kanR plo1+-mCherry<<natR nda3-KM311*
SP259	h+	*ade6-M216 mad3-KEN(20)AAA-GFP<<kanR plo1+-mCherry<<natR nda3-KM311*
SU599	h-	*leu1 mad3-Dbox(L/K)-GFP<<kanR plo1+-mCherry<<natR nda3-KM311*
SU581	h+	*leu1 ade6-M216 mad3-ABBA1mut-GFP<<kanR plo1+-mCherry<<natR nda3-KM311*
SP710	h+	*leu1 mad3-KEN271AAA-GFP<<kanR nda3-KM311 plo1+-mCherry<<natR*
SU582	h+	*leu1 ade6-M216 mad3-ABBA2mut-GFP<<kanR plo1+-mCherry<<natR nda3-KM311*
SU074	h+	*leu1 mad3-ΔCterm(282-310)+-GFP-hphNT1 plo1+-mCherry<<natR nda3-KM311*
SU703	h-	*leu1 mad3-Dbox(VNPL/ANPA)-GFP<<kanR plo1+-mCherry<<natR nda3-KM311*
SU714	h-	*leu1 ade6-M216 mad3-KEN20QEN+-GFP<<hphR plo1+-mCherry<<natR nda3-KM311*
SU570	h+	*leu1 ade6-M216 mad3-KEN271QEN-GFP<<kanR plo1+-mCherry<<natR nda3-KM311*

Figure S1G

SL759	h-	*leu1 mad3+-GFP<<kanR plo1+-mCherry<<natR nda3-KM311*
SL756	h-	*leu1 ade6-M210 mad3Δ::ura4+ plo1+-mCherry<<natR nda3-KM311*
SU703, SU703'	h-	*leu1 mad3-Dbox(VNPL/ANPA)-GFP<<kanR plo1+-mCherry<<natR nda3-KM311*

Figure S1H

SK827	h-	*ade6-M216 plo1+-mCherry<<natR nda3-KM311*
SK828	h+	*leu1 ade6-M216 plo1+-mCherry<<natR nda3-KM311*
SP457	h+	*ade6-M216? kanR-Prad21-slp1+ plo1+-mCherry<<natR nda3-KM311*
SM842	h+	*leu1-32 plo1+-mCherry<<natR nda3-KM311 slp1-mr63*
SU391, SU391', SU	h-	*leu1 kanR<<Prad21-slp1-mr63 plo1+-mCherry<<natR nda3-KM311*

Figure S1I

SL760	h+	*leu1 mad3+-GFP<<kanR plo1+-mCherry<<natR nda3-KM311*
SL756	h-	*leu1 ade6-M210 mad3Δ::ura4+ plo1+-mCherry<<natR nda3-KM311*
SP259	h+	*ade6-M216 mad3-KEN(20)AAA-GFP<<kanR plo1+-mCherry<<natR nda3-KM311*
SU714	h-	*leu1 ade6-M216 mad3-KEN20QEN+-GFP<<hphR plo1+-mCherry<<natR nda3-KM311*
SU570	h+	*leu1 ade6-M216 mad3-KEN271QEN-GFP<<kanR plo1+-mCherry<<natR nda3-KM311*

Figure S2A

SU526	h-	*slp1::Pslp1-sfGFPopt-slp1-S(GGGGS)3-RIPGLIN-slp1 plo1+-mCherry<<natR cdc25-22*
SK828	h+	*leu1 ade6-M216 plo1+-mCherry<<natR nda3-KM311*
SP457	h+	*ade6-M216? kanR-Prad21-slp1+ plo1+-mCherry<<natR nda3-KM311*
SP793	h+	*apc15Δ::kanR kanR-Prad21-slp1+ plo1+-mCherry<<natR nda3-KM311*
ST930	h-	*kanR<<Prad21-slp1+ leu1+<<Prad21-slp1+ plo1+-mCherry<<natR nda3-KM311*
ST928'	h-	*apc15Δ::kanR kanR<<Prad21-slp1+ leu1+<<Prad21-slp1+ plo1+-mCherry<<natR nda3-KM311*
SU789	h-	*leu1 natNT2<<Padh1(s)-Slp1 plo1+-mCherry<<natR nda3-KM311*
SU908	h-	*leu1 natNT2<<Padh1(s)-slp1 mad3-ΔCterm(282-310)-Tadh1-hphNT1 plo1+-mCherry<<natR nda3-KM311*
SU791	h-	*leu1 natNT2<<Padh1(s)-Slp1 apc15Δ::kanR plo1+-mCherry<<natR nda3-KM311*

Figure S2B

SM544	h+	*leu1 mad2+-GFP<<kanR mad3+-GFP<<kanR plo1+-mCherry<<natR nda3-KM311*
SU544	h-	*leu1 hygroR<<Pnmt41-slp1 plo1+-mCherry<<natR nda3-KM311*
SU560	h-	*leu1 hygroR<<Pnmt41-slp1 mad3-ΔCterm(282-310)+-GFP-hphNT1 plo1+-mCherry<<natR nda3-KM311*
SU526	h-	*slp1::Pslp1-sfGFPopt-slp1-S(GGGGS)3-RIPGLIN-slp1 plo1+-mCherry<<natR cdc25-22*

Figure S2C

SP800	h+	*apc15Δ::kanR plo1+-mCherry<<natR nda3-KM311*
SP710	h+	*leu1 mad3-KEN271AAA-GFP<<kanR nda3-KM311 plo1+-mCherry<<natR*
SU074	h+	*leu1 mad3-ΔCterm(282-310)+-GFP-hphNT1 plo1+-mCherry<<natR nda3-KM311*
SU789	h-	*leu1 natNT2<<Padh1(s)-Slp1 plo1+-mCherry<<natR nda3-KM311*
SU791	h-	*leu1 natNT2<<Padh1(s)-Slp1 apc15Δ::kanR plo1+-mCherry<<natR nda3-KM311*
SU907	h-	*leu1 natNT2<<Padh1(s)-slp1 mad3-KEN271AAA-Tadh1<<hphNT1 plo1+-mCherry<<natR nda3-KM311*
SU908	h-	*leu1 natNT2<<Padh1(s)-slp1 mad3-ΔCterm(282-310)-Tadh1-hphNT1 plo1+-mCherry<<natR nda3-KM311*

3 Discussion

3.1 The Mad1 C-terminus is actively involved in the spindle assembly checkpoint and links the Bub1-Bub3 complex with downstream checkpoint signaling (results part 2.1)

3.1.1 Analyzing the interaction between Mad1 and Bub1

Extensive work on the spindle assembly checkpoint and its molecular basis made the checkpoint appear to be resting on two important pillars: (i) the recruitment of the Bub1-Bub3 complex to kinetochores, which is Mps1-dependent, and (ii) dimerization of Mad1-bound and free Mad2 at kinetochores. This promotes Mad2 binding to Cdc20 and finally formation of the MCC to mediate APC/C inhibition. However, it is only partially understood how these two pillars are connected to create the checkpoint signal. Early work in *S. cerevisiae* suggested the presence of a Mad1-Bub1-Bub3 complex during mitosis and showed that formation of this complex depends not only on the other checkpoint proteins Mad2 and Mps1, but also on a conserved RLK motif in the C-terminus of Mad1 (Brady and Hardwick, 2000). Another budding yeast study indicated, that the central region of Bub1 is necessary for the interaction between Mad1 and Bub1 (Warren et al., 2002). Later it was shown that this central region encompasses the conserved motif 1 (cm1), which is important for kinetochore localization of Mad1 and checkpoint activity in human cells (Klebig et al., 2009). Although this suggested a role for Bub1 in Mad1 kinetochore-recruitment, a direct interaction between these two proteins was not observed in human cells (Kim et al., 2012; Kruse et al., 2014; Overlack et al., 2015). But despite all this work, the Mad1 kinetochore receptor remained elusive and it was still unclear if the interaction between Mad1 and Bub1 is direct, how Mad1 would be incorporated into the Bub1-Bub3 complex and if this interaction mechanism is conserved across species, making it an evolutionary conserved feature of checkpoint signaling.

In our study, we wanted to address whether the link between Mad1 and Bub1 is conserved across species. We were showed in fission yeast that mutation of Bub1-cm1 abolished checkpoint activity and greatly reduced kinetochore recruitment of Mad1 and Mad2 without influencing kinetochore localization of Bub1. This was in

accordance with the effect observed in human cells (Klebig et al., 2009). Similar to the mutation of Bub1-cm1, mutation of the conserved Mad1 RLK motif also abolished checkpoint activity and kinetochore localization of Mad1 and Mad2 without affecting Bub1 recruitment. Despite this striking similarity between the two mutants, we were unable to detect an interaction between Mad1 and Bub1 in co-immunoprecipitation experiments. One reason for this apparent lack of interaction could be that only a small fraction of the two proteins binds to each other. Indeed, newer experiments using a differently tagged Bub1 were able to detect co-immunoprecipitation of Bub1 with Mad1 (data not shown and part 2.2, Figure S3B). Furthermore, a study performed in budding yeast showed an Mps1-dependent interaction between Mad1 and Bub1 and corroborated the previous finding that the central region of Bub1 containing the cm1 is responsible for this interaction (London and Biggins, 2014). Additionally, fusion of the middle region of *S.c.* Bub1 to kinetochores was sufficient to co-recruit Mad1 (London and Biggins, 2014). Recent results from work performed with *C. elegans* also showed an interaction between Mad1 and Bub1 that is important for checkpoint activity (Moyle et al., 2014). This stands in contrast to a previous fission yeast study, which showed that artificial kinetochore recruitment of Bub1 through tethering of Mps1 to kinetochores does not automatically co-recruit Mad1 (Ito et al., 2012). Taken all these findings together, it is still unclear whether mediating Bub1-Mad1 interaction is the most important and conserved function of the Bub1-cm1 and Mad1-RLK motifs, or whether they contribute to checkpoint function in another way.

3.1.2 The conserved RLK motif in the Mad1 C-terminus has an additional function in the checkpoint

Mutation of the conserved RLK motif in Mad1 abolished kinetochore localization of Mad1 and Mad2 as well as overall checkpoint activity in our study in *S. pombe*. Interestingly, artificial tethering of the RLK/AAA mutant to the kinetochore co-recruited Mad2 but did not restore checkpoint activity. This is in agreement with a similar finding in human cells (Ballister et al., 2014). Kinetochore-tethered Mad1 was also not sufficient to restore checkpoint activity in *bub1Δ* cells or cells that contained a Bub1-cm1 mutant. This clearly indicated that both Bub1, most likely through its conserved motif 1, and Mad1-RLK have an additional function in the SAC that goes

beyond kinetochore recruitment of Mad1. Mad2 was co-recruited to kinetochore-tethered wild type Mad1 and Mad1-RLK/AAA to a similar extent and Mad2 dimerization at kinetochores did not seem to be influenced. This indicates that a step downstream of Mad2 dimerization is defective in this Mad1 mutant. The defective step(s) could be C-Mad2 binding to Cdc20 or BubR1/Mad3 binding to the Mad2-Cdc20 complex. It would be possible to test this by immunoprecipitation of Mad2. I found a complete loss of either Mad2-Cdc20 or MCC in cells containing Mad1-RLK/AAA (data not shown), which would indicate a defect in Mad2-Cdc20 binding. However, in this experiment the Mad1 mutant was not kinetochore-tethered, so that it remains unclear whether the observed effects are due to loss of Mad1 from kinetochores or result from the specific defect of Mad1-RLK/AAA cells. In any case, size exclusion and anion exchange chromatography would be able to further dissect whether conversion from O-Mad2 to C-Mad2 is defective, or whether C-Mad2 cannot bind Cdc20. Size exclusion chromatography of a cell extract can separate free Mad2 and a subsequent anion exchange chromatography of the isolated fraction can further distinguish O-Mad2 and C-Mad2 (Luo et al., 2004; Mapelli et al., 2007). Furthermore, artificial tethering of C-Mad2 to Cdc20 followed by analysis of MCC formation could provide information whether Mad1 and/or Bub1 are required only for Mad2-Cdc20 binding or whether they are additionally needed for incorporation of Mad3 into the MCC. These further analyses will contribute to fully revealing the functions of the RLK motif of Mad1 and Bub1-cm1, possibly in conjunction with each other, during checkpoint signaling.

3.1.3 The Mad1 C-terminal domain has an additional, unknown function beyond Mad2 dimerization

Since the RLK motif was required for Mad1 kinetochore recruitment as well as for some additional step in SAC signaling, we searched the Mad1 C-terminal region for separation-of-function mutants that retain kinetochore localization but impair checkpoint activity (part 2.1, Fig. S4A and Fig. 3). We were able to identify two mutants in the C-terminal domain (CTD) of Mad1 that showed the desired phenotype. One mutant contained three point mutations (EDD/QNN) in the last alpha-helix of the CTD, the other was a complete deletion of this alpha-helix (*Δhelix*). Like kinetochore-tethered Mad1-RLK/AAA, both mutants retained co-localization of Mad2 and did not

influence Mad2 dimerization. This again indicates a role of the Mad1 C-terminus further downstream. MCC formation was greatly reduced, but not completely abolished in Mad1-EDD/QNN (data not shown). As previously suggested for Mad1-RLK, the Mad1-CTD could also be involved in mediating Mad2-Cdc20 binding and/or subsequent incorporation of Mad3 into the MCC, which could be investigated by analyzing the pools of O- and C-Mad2 by chromatography and by testing the binding of Mad3 to artificially tethered Mad2-Cdc20. Work performed in human cells also showed an importance of the Mad1 C-terminus in checkpoint signaling beyond Mad2 recruitment (Ballister et al., 2014; Kruse et al., 2014), indicating that the function of the Mad1 C-terminus in SAC signaling is conserved across eukaryotes.

One idea how the Mad1 C-terminus could potentially influence downstream checkpoint signaling events is based on the structure of the Mad1-Mad2 heterotetramer (Sironi et al., 2002). This suggests that the two alpha-helices downstream of the Mad2 binding site can fold back onto each other (part 2.1, Fig. 4), which would place the Mad1-CTD close to the Mad2 binding site and thereby Mad2. Since so far no structure is available that covers all parts of Mad1 from the Mad2 binding site up to its C-terminus, it remains to be seen if this model holds true *in vivo* or if the Mad1 structure is maybe more dynamic.

In any case, more experiments are necessary to identify the full role of Mad1 in SAC signaling. Unbiased approaches like yeast two-hybrid screens to detect protein-protein interactions or immunoprecipitations followed by mass spectrometry (IP-MS) could help to reveal potential interaction partners with the Mad1 C-terminus. Preliminary results of IP-MS experiments showed that Mad1-RLK/AAA and Mad1Δhelix co-immunoprecipitated less Nup211, a component of the nuclear pore complex, compared to wild type Mad1. Otherwise, no difference was detected between the mutants and the wild type protein (data not shown). It is unclear if problems to localize to the nuclear rim in interphase could have an effect on the function of Mad1 at kinetochores in mitosis. In addition to the search for interaction partners, chemical cross-linking followed by mass spectrometry (CX-MS) could be utilized to further investigate the folding of Mad1 in its native state. While conventional methods to determine the structure of a molecule like X-ray crystallography, NMR spectroscopy or electron microscopy need concentrated homogeneous samples of the protein complex – often from recombinant expression, CX-MS could be performed on complexes purified from a cell extract.

While previous models for the spindle assembly checkpoint mainly saw Mad1 as a passive platform for presenting Mad2 at kinetochores, it became apparent with our and other recent findings that Mad1 is in fact an active player in checkpoint signaling. Nevertheless, we still do not fully understand how the checkpoint signal is propagated, but Bub1 as well as the Mad1 C-terminus seem to be connected and both play an important role.

3.2 Bub3-Bub1 binding to Spc7/KNL1 licenses the interaction of Bub1 with Mad1-Mad2 at kinetochores and thereby initiates checkpoint signaling (results part 2.2)

3.2.1 Phosphorylation of MELT motifs in Spc7 influences checkpoint activity, potentially by mediating Bub1 turnover at kinetochores

Upon detection of unattached kinetochores, kinetochore localization of Bub3-Bub1 is important for Mad1-Mad2 recruitment to facilitate checkpoint signaling (London and Biggins, 2014; Moyle et al., 2014). It was shown that Mph1 (Mps1) phosphorylates multiple conserved MELT motifs in the Spc7 (Spc105/KNL1) protein to recruit Bub1, Bub3, and Mad3 (BubR1) to kinetochores (London et al., 2012; Shepperd et al., 2012; Yamagishi et al., 2012), but the exact number of MELT repeats varies greatly between species (Vleugel et al., 2012; Tromer et al., 2015). Experiments performed in human cells revealed that a majority of MELT repeats can be mutated before an effect on SAC activity is observed (Vleugel et al., 2013; Zhang et al., 2014; Vleugel et al., 2015b). Spc105/KNL1 in Drosophilids contain repeats that differ from the MELT motif consensus observed in yeast, *C. elegans* and human orthologs (Schittenhelm et al., 2009). Deletion of the region of *D. melanogaster* Spc105 containing the repeats had no influence on Spc105 functionality (Schittenhelm et al., 2009). While this led to the assumption that the repeats are functionally unimportant in *D. melanogaster*, a later analysis showed that the truncation used to investigate the role of the motifs still contained two MELT-like motifs (Krenn et al., 2014), which complicates the interpretation of the results.

Since the N-terminus of fission yeast Spc7 contains 12 MELT motifs that can be phosphorylated by the Mph1 kinase *in vitro* (Shepperd et al., 2012; Yamagishi et al., 2012), we wanted to examine the role of MELT motifs in controlling Bub1 recruitment and checkpoint signaling and thereby address if this feature of the checkpoint is conserved across eukaryotes. *S. pombe* cells with some or all of the threonine and serine residues in the MELT motifs mutated to non-phosphorylatable alanine showed a gradual dependency of Bub1 kinetochore recruitment on the number of phosphorylatable MELT sites. Interestingly, the ability to arrest in mitosis did not follow the same gradual pattern. Instead, cells with at least five functional MELT motifs still showed an active checkpoint while cells with three or less functional MELT

motifs only mounted a partial checkpoint response. These results together indicate that Spc7 contains multiple functional binding sites for Bub1, but activity of only a subset of them is sufficient to promote checkpoint signaling, which is in agreement with similar results from human cells (Vleugel et al., 2013; Zhang et al., 2014; Vleugel et al., 2015b). The fact that not all MELT motifs are required for mounting a checkpoint response both in fission yeast and mammalian cells potentially explains why the exact number of MELT repeats is not strongly conserved. One can furthermore speculate that the MELT repeats are constantly phosphorylated and dephosphorylated during an active SAC and that this might be the molecular mechanism giving rise to turnover of Bub1 at kinetochores. Still unanswered are the questions why MELT repeats evolve rapidly, which factors drive this evolution and how changes in the number of MELT motifs force other cellular components that are functionally connected to KNL1 to adapt to the new situation (Tromer et al., 2015).

3.2.2 Bub3 has opposed functions in the nucleoplasm and at the kinetochore

In contrast to mammalian cells and budding yeast, Bub3 is not essential for checkpoint signaling in fission yeast (Tange and Niwa, 2008; Vanoosthuyse et al., 2009; Windecker et al., 2009). It was proposed that, at least in *S. pombe*, Bub3 has an inhibitory function on Bub1 (Yamagishi et al., 2012), and Bub1 might be released upon association with the kinetochore. We wanted to further investigate this theory to reveal the function of Bub3 during checkpoint activation in fission yeast. In budding yeast, an interaction between Bub1 and Mad1 could be detected, suggesting that kinetochore-localized Bub3-Bub1 subsequently recruits Mad1-Mad2 to kinetochores (Brady and Hardwick, 2000; London and Biggins, 2014). Contrary to this finding, we were initially unable to detect a Bub1-Mad1 interaction in fission yeast. However, newer experiments showed an interaction between a small fraction of Bub1 and Mad1. We hypothesized that release of the Bub3-mediated Bub1 inhibition could be required for Bub1-Mad1 interaction. We saw that mutation of MELT motifs, which prevents Bub3-Bub1 kinetochore recruitment (Primorac et al., 2013; Vleugel et al., 2015b), inhibits Bub1-Mad1 complex formation. Interestingly, deletion of Bub3 in combination with MELT motif mutation rescued Bub1-Mad1 binding. This result indicates that Bub3-mediated inhibition of Bub1 indeed needs to be released to allow

Bub1-Mad1 interaction. The Bub1-release and subsequent Mad1-interaction can happen both in the nucleoplasm (Bub3 deletion) or at the kinetochore (Bub3-Bub1 binding to MELT). This attributes Bub3 a dual role during checkpoint signaling: in the nucleoplasm, it inhibits Bub1 from binding to Mad1-Mad2 but once Bub3-Bub1 is recruited to kinetochores, Bub3 turns into a facilitator of the spindle assembly checkpoint by controlling the interaction of Bub1 with Mad1-Mad2. Preventing the Bub1-Mad1 interaction in the nucleoplasm inhibits premature checkpoint activation. One could speculate that the Bub3-Bub1 complex undergoes a conformational change upon binding to phosphorylated MELT motifs of Spc7, which in turn permits the binding to Mad1-Mad2. Reconstitution and structural studies will be needed to test this hypothesis. Deletion of Bub3 in *S. pombe* abolishes kinetochore localization of Bub1, Mad1, Mad2 and Mad3 without affecting checkpoint activity (Tange and Niwa, 2008; Vanoosthuyse et al., 2009; Windecker et al., 2009). Interestingly, I saw that although artificial kinetochore-recruitment of Mad1 or deletion of Bub3 each by themselves are checkpoint proficient, a combination of both abolished checkpoint activity (data not shown). This finding further corroborates that Bub1 and Mad1 need to be at the same location, both in the nucleoplasm or both at the kinetochore, and likely in a complex with each other to facilitate checkpoint signaling.

3.3 Cdc20 can be inhibited in several different ways to ensure mitotic checkpoint activity (results part 2.3)

3.3.1 Different motifs in the Mad3 C-terminus bind to Cdc20 to mediate SAC activity

It was shown in mammalian cells and yeast that both BubR1 and Mad3 contain a number of conserved motifs that all mediate binding to Cdc20. Recent structures of the human MCC-APC/C complex also revealed with which of the two Cdc20 molecules in the complex each of the motifs interacts (Alfieri et al., 2016; Yamaguchi et al., 2016). Despite these high resolution views of the MCC and MCC-APC/C interaction, the functional analysis of the different Mad3 motifs *in vivo* is currently lacking behind. Therefore, I wanted to dissect the role of these motifs in fission yeast, where Mad3 has over evolutionary timescales been trimmed down to a minimal Cdc20-inhibitory fragment (Malureanu et al., 2009; Vleugel et al., 2012). While both *S. pombe* Mad3 and mammalian BubR1 contain two KEN boxes, differences were seen in the number and/or location of putative ABBA motifs and the D-box. While position of the first ABBA motif and D-box between the TPR region and the second KEN box seems to be conserved, *S. pombe* Mad3 lacks a second D-box. Furthermore, human BubR1 contains the second ABBA motif C-terminal of the GLEBS motif, while Mad3 might contain the second ABBA motif at its very C-terminus and is lacking a functional GLEBS (Figure 1-2). Since the MCC-APC/C structure is derived from human proteins, it was unclear if the fission yeast MCC is also able to bind two Cdc20 molecules, and if so, if Mad3 establishes exactly the same interactions with them as seen in the human complex. Live cell imaging analyses revealed that all Cdc20-binding motifs (KEN1, KEN2, ABBA1, ABBA2, D-box) are important for the activity of the spindle assembly checkpoint, albeit to similar extents. Immunoprecipitation experiments showed that the fission yeast MCC, like human MCC, can associate with at least two Cdc20 molecules. While mutation of KEN1 abolished MCC formation entirely, mutation of KEN2 or deletion of the Mad3 C-terminus containing ABBA2 (ΔCterm) retained core MCC formation but inhibited binding of additional Cdc20. To further address the importance of the two KEN motifs in the checkpoint, I mutated them to QEN, which is the motif found at the KEN2 site in Drosophila species. While changing *S. pombe* KEN2 to QEN had no effect on

checkpoint activity, mutating KEN1 to QEN decreased the stability of Mad3 and abolished the checkpoint entirely. This supports the different functionality of KEN1 and KEN2 (Yamaguchi et al., 2016).

Overall, the results showed that, although all motifs mediate binding to Cdc20, they are nevertheless non-redundant in their function. It was shown for human BubR1 that KEN1, ABBA2 and D-box 2 contact the core MCC Cdc20 while D-box 1, ABBA1 and KEN2 interact with APC/C-associated Cdc20. Since the position of these motifs within Mad3 differs from their location within BubR1, it remains to be seen how each of them mediates interaction between $Cdc20^{MCC}$ and $Cdc20^{APC/C}$ in *S. pombe*. My results obtained so far indicate a crucial interaction of KEN1 with $Cdc20^{MCC}$ and KEN2 and ABBA2 with $Cdc20^{APC/C}$. Chemical cross-linking followed by mass spectrometry could be a helpful tool to investigate the exact inter-molecular interactions between Mad3 and Cdc20. Another approach to elucidate the interactions between the Mad3 motifs and the different Cdc20 molecules would be the *in vitro* reconstitution of a core MCC with each of the motifs mutated separately and subsequent addition of free Cdc20 to analyze binding to this molecule. To further address the function of each of the two Cdc20 molecules especially during checkpoint silencing, separation-of-function mutants could be created and expressed together. While one molecule contains a mutation in the ABBA receptor region and thereby can only become $Cdc20^{MCC}$, the other molecule contains a mutation of the Mad2-binding site, which confines it to being $Cdc20^{APC/C}$. Downstream analysis of for example ubiquitination of each of the molecules or their ability to activate the APC/C can dissect their different roles.

3.3.2 A Mad2-binding deficient Cdc20 molecule can be inhibited from activating the APC/C

It was shown that mutation of the Mad2-binding site in Cdc20 leads to a checkpoint defect in several species (Hwang et al., 1998; Kim et al., 1998; Nilsson et al., 2008). We reasoned that Cdc20 that is unable to bind to Mad2 should still be subject to checkpoint control through the Mad3 C-terminus, as long as core MCC can be formed. Live cell imaging assays revealed that mutation of this region leads to a non-functional checkpoint when present as the only version of Cdc20 or when equal levels of wild type and mutant Cdc20 were expressed. However, upon reduction of

mutant Cdc20 expression, the checkpoint could be partially restored as long as wild type Cdc20 was present. The checkpoint rescue was further enhanced upon mutation of the Mad2-binding proficient Cdc20 copy in its C-box motif, which is essential for Cdc20 to activate the APC/C and thereby made APC/C activation in my assay entirely dependent on the Mad2-binding deficient Cdc20 mutant. I furthermore showed in immunoprecipitation experiments that Mad2-binding deficient Cdc20 can be inhibited by the mitotic checkpoint through the Mad3 C-terminus as long as core MCC formation is initiated by Mad2-binding-competent Cdc20. This shows that the ability of Cdc20 to bind to Mad2 is only required for formation of the core MCC but neither for binding of the MCC to additional Cdc20 nor for APC/C activation.

3.3.3 The 'core MCC' inhibition mode is sufficient at high checkpoint protein to Cdc20 ratio

Although each of the Mad3-KEN boxes is required for the checkpoint, mutation of KEN1 tends to abolish checkpoint activity more than mutation of KEN2 (Lara-Gonzalez et al., 2011; Diaz-Martinez et al., 2015). This indicates a more crucial role of KEN1. Indeed, Mad3-KEN1 is needed for interaction of both $Cdc20^{MCC}$ and $Cdc20^{APC/C}$ with the MCC, whereas Mad3-KEN2 is only needed for interaction of $Cdc20^{APC/C}$. Because $Cdc20^{MCC}$ can be tightly captured in the core MCC, we reasoned that core MCC formation alone could theoretically be sufficient for checkpoint activity, as long as the amount of Cdc20 is low enough. Indeed, lowering the Cdc20 abundance by expressing the gene from the promoter of *rad21* (cohesin) or *adh1* or from the regulatable *nmt1* promoter partially or fully rescued checkpoint activity in the Mad3-KEN2 mutant and ΔCterm, but not in the KEN1 mutant. Mutation of the Mad2-binding site in Cdc20 abolished the mitotic delay, indicating that it was dependent on core MCC formation. This shows that core MCC formation is sufficient to promote a checkpoint arrest at low Cdc20 levels.

Immunoprecipitation experiments revealed, that even in wild type cells with an active checkpoint, both Cdc20 and the APC/C are not completely sequestered by the MCC, but also present as unbound forms. This raises the question how the cells nevertheless manage to arrest in mitosis without premature activation of the free APC/C by the free Cdc20. The apparently free Cdc20 could potentially be bound to Mad2, which keeps it inhibited from interacting with and/or activating the APC/C.

Another possibility is that the free Cdc20 is indeed completely unbound but in a conformational state that is unable to bind the APC/C. Sequential immunoprecipitations could be helpful to address the presence of different subcomplexes like Mad2-Cdc20 or Mad2-Cdc20-APC/C.

3.3.4 Mad3 C-terminus and Apc15 are required for MCC-APC/C interaction and MCC disassembly

We noticed that mutation of KEN2 or deletion of the Mad3 C-terminus increased the amount of MCC and also led to presence of MCC even in interphase, where it is usually absent in *S. pombe* due to disassembly during checkpoint silencing. In human cells and budding yeast, it was shown that the APC/C subunit Apc15 plays a crucial role in MCC disassembly (Mansfeld et al., 2011; Foster and Morgan, 2012; Uzunova et al., 2012) and consistently, I was able to detect interphasic MCC also in fission yeast cells lacking Apc15. This shows that also in *S. pombe*, Apc15 is required for MCC disassembly. But in contrast to human cells and budding yeast, where *APC15* deletion caused a prolonged mitotic arrest and impaired checkpoint silencing, deletion of *apc15* in fission yeast cells resulted in a failure to activate the checkpoint. This shows that while Apc15 is involved in MCC disassembly in human cells and both budding and fission yeast, it seems to play an additional role during checkpoint activation in fission yeast. While mutation of KEN2 and deletion of the Mad3 C-terminus lost association of additional Cdc20 with the core MCC, deletion of *apc15* retained this interaction and assembled a full MCC. I furthermore showed that Mad3-KEN2 mutation, Mad3-ΔCterm or deletion of *apc15* all resulted in reduced or abolished binding of the MCC to the APC/C and Cdc20 was still associated with the APC/C. Those findings together could explain the checkpoint defect of *apc15* deletion. Although the full MCC is formed, it cannot associate with the APC/C and therefore cannot inhibit free Cdc20 from binding and activating the APC/C. Just like the Mad3 C-terminus, Apc15 also becomes dispensable for the checkpoint at lower Cdc20 levels, indicating a complete sequestration of the available Cdc20 within the MCC, so that the APC/C remains Cdc20-free. We therefore envision that inhibition of the APC/C by the MCC encompasses (i) sequestration of one Cdc20 in the core MCC, (ii) inhibition of a second Cdc20 molecule through the Mad3 C-terminus, and (iii) competition between the MCC and other free Cdc20 for APC/C binding. Only (iii)

is defective in *apc15Δ* cells, whereas (ii) and (iii) are defective in *mad3Δ-Cterm* cells. All, (i), (ii) and (iii) are defective in the *mad3-KEN1* mutant – explaining the different extents of checkpoint impairment.

The structural analysis of MCC-APC/C revealed a role of Apc15 in stabilization of the MCC in a position on the APC/C that allows Cdc20 ubiquitination (Alfieri et al., 2016; Yamaguchi et al., 2016), which ultimately leads to MCC disassembly. How the failure of MCC-APC/C association in *apc15Δ* fission yeast cells can be explained on a structural level remains unclear. Strikingly, fission yeast also differs from many other eukaryotes in its lack of Bub3 in the MCC. The reasons for those differences are still unclear but one hypothesis could be that Apc15 in fission yeast took over the role of Bub3 in targeting the MCC to the APC/C. One possibility to address this question is to artificially fuse Bub3 or the GLEBS motif that binds Bub3 to the C-terminus of *S. pombe* Mad3 to mimic the interaction between BubR1 and Bub3 in other organisms that contain Bub3 in the MCC. Investigating MCC-APC/C interaction with this fusion construct in an *apc15Δ* background could provide an answer.

Although comparisons of the spindle assembly checkpoint signaling cascade in various organisms from yeast to humans generally show a striking degree of conservation, detailed investigations of the molecular mechanisms underlying the signaling also revealed differences between the organisms. This underlines that the checkpoint is an evolutionary conserved mechanism that likely has adapted to new cellular situations as the organisms diverged from each other. It would be interesting to understand in which way these changes are adaptive to the physiology and ecology of this organism. Despite a wealth of information about the function of the checkpoint, as well as about its various components and their interaction with each other, we still need more work to entirely grasp this highly complicated signaling network.

4 References

Alfieri, C., Chang, L., Zhang, Z., Yang, J., Maslen, S., Skehel, M., and Barford, D. (2016). Molecular basis of APC/C regulation by the spindle assembly checkpoint. Nature *536*, 431-436.

Andreassen, P.R., and Margolis, R.L. (1994). Microtubule dependency of p34cdc2 inactivation and mitotic exit in mammalian cells. J Cell Biol *127*, 789-802.

Aravamudhan, P., Goldfarb, A.A., and Joglekar, A.P. (2015). The kinetochore encodes a mechanical switch to disrupt spindle assembly checkpoint signalling. Nat Cell Biol *17*, 868-879.

Aravind, L., and Koonin, E.V. (1998). The HORMA domain: a common structural denominator in mitotic checkpoints, chromosome synapsis and DNA repair. Trends in biochemical sciences *23*, 284-286.

Bailer, S.M., Siniossoglou, S., Podtelejnikov, A., Hellwig, A., Mann, M., and Hurt, E. (1998). Nup116p and nup100p are interchangeable through a conserved motif which constitutes a docking site for the mRNA transport factor gle2p. EMBO J *17*, 1107-1119.

Balachandran, R.S., Heighington, C.S., Starostina, N.G., Anderson, J.W., Owen, D.L., Vasudevan, S., and Kipreos, E.T. (2016). The ubiquitin ligase $CRL2^{ZYG11}$ targets cyclin B1 for degradation in a conserved pathway that facilitates mitotic slippage. The Journal of Cell Biology.

Ballister, E.R., Riegman, M., and Lampson, M.A. (2014). Recruitment of Mad1 to metaphase kinetochores is sufficient to reactivate the mitotic checkpoint. J Cell Biol *204*, 901-908.

Bar-Even, A., Paulsson, J., Maheshri, N., Carmi, M., O'Shea, E., Pilpel, Y., and Barkai, N. (2006). Noise in protein expression scales with natural protein abundance. Nature genetics *38*, 636-643.

Barisic, M., and Geley, S. (2011). Spindly switch controls anaphase: spindly and RZZ functions in chromosome attachment and mitotic checkpoint control. Cell cycle (Georgetown, Tex.) *10*, 449-456.

Barnhart, E.L., Dorer, R.K., Murray, A.W., and Schuyler, S.C. (2011). Reduced Mad2 expression keeps relaxed kinetochores from arresting budding yeast in mitosis. Mol Biol Cell *22*, 2448-2457.

Biggins, S., and Murray, A.W. (2001). The budding yeast protein kinase Ipl1/Aurora allows the absence of tension to activate the spindle checkpoint. Genes Dev *15*, 3118-3129.

Bock, L.J., Pagliuca, C., Kobayashi, N., Grove, R.A., Oku, Y., Shrestha, K., Alfieri, C., Golfieri, C., Oldani, A., Dal Maschio, M*., et al.* (2012). Cnn1 inhibits the interactions between the KMN complexes of the yeast kinetochore. Nat Cell Biol *14*, 614-624.

Bolanos-Garcia, V.M., Kiyomitsu, T., D'Arcy, S., Chirgadze, D.Y., Grossmann, J.G., Matak-Vinkovic, D., Venkitaraman, A.R., Yanagida, M., Robinson, C.V., and Blundell, T.L. (2009). The crystal structure of the N-terminal region of BUB1 provides insight into the mechanism of BUB1 recruitment to kinetochores. Structure *17*, 105-116.

Bolanos-Garcia, V.M., Lischetti, T., Matak-Vinkovic, D., Cota, E., Simpson, P.J., Chirgadze, D.Y., Spring, D.R., Robinson, C.V., Nilsson, J., and Blundell, T.L. (2011). Structure of a Blinkin-BUBR1 complex reveals an interaction crucial for kinetochore-mitotic checkpoint regulation via an unanticipated binding Site. Structure *19*, 1691-1700.

Brady, D.M., and Hardwick, K.G. (2000). Complex formation between Mad1p, Bub1p and Bub3p is crucial for spindle checkpoint function. Current biology : CB *10*, 675-678.

Brandeis, M. (2016). Slip slidin' away of mitosis with $CRL2^{Zyg11}$. The Journal of Cell Biology.

Brito, D.A., and Rieder, C.L. (2006). Mitotic checkpoint slippage in humans occurs via cyclin B destruction in the presence of an active checkpoint. Current biology : CB *16*, 1194-1200.

Brown, N.G., VanderLinden, R., Watson, E.R., Qiao, R., Grace, C.R., Yamaguchi, M., Weissmann, F., Frye, J.J., Dube, P., Ei Cho, S.*, et al.* (2015). RING E3 mechanism for ubiquitin ligation to a disordered substrate visualized for human anaphase-promoting complex. Proc Natl Acad Sci U S A *112*, 5272-5279.

Burgess, D.R., and Chang, F. (2005). Site selection for the cleavage furrow at cytokinesis. Trends in Cell Biology *15*, 156-162.

Burton, J.L., and Solomon, M.J. (2007). Mad3p, a pseudosubstrate inhibitor of APCCdc20 in the spindle assembly checkpoint. Genes Dev *21*, 655-667.

Burton, J.L., Xiong, Y., and Solomon, M.J. (2011). Mechanisms of pseudosubstrate inhibition of the anaphase promoting complex by Acm1. EMBO J *30*, 1818-1829.

Camasses, A., Bogdanova, A., Shevchenko, A., and Zachariae, W. (2003). The CCT chaperonin promotes activation of the anaphase-promoting complex through the generation of functional Cdc20. Mol Cell *12*, 87-100.

Campbell, L., and Hardwick, K.G. (2003). Analysis of Bub3 spindle checkpoint function in Xenopus egg extracts. J Cell Sci *116*, 617-628.

Carmena, M., Wheelock, M., Funabiki, H., and Earnshaw, W.C. (2012). The Chromosomal Passenger Complex (CPC): From Easy Rider to the Godfather of Mitosis. Nature reviews. Molecular cell biology *13*, 789-803.

Carroll, C.W., Milks, K.J., and Straight, A.F. (2010). Dual recognition of CENP-A nucleosomes is required for centromere assembly. J Cell Biol *189*, 1143-1155.

Chan, K.S., Koh, C.G., and Li, H.Y. (2012). Mitosis-targeted anti-cancer therapies: where they stand. Cell Death Dis *3*, e411.

Chang, L., Zhang, Z., Yang, J., McLaughlin, S.H., and Barford, D. (2014). Molecular architecture and mechanism of the anaphase-promoting complex. Nature *513*, 388-393.

Chang, L., Zhang, Z., Yang, J., McLaughlin, S.H., and Barford, D. (2015). Atomic structure of the APC/C and its mechanism of protein ubiquitination. Nature *522*, 450-454.

Chao, W.C., Kulkarni, K., Zhang, Z., Kong, E.H., and Barford, D. (2012). Structure of the mitotic checkpoint complex. Nature *484*, 208-213.

Cheeseman, I.M., Chappie, J.S., Wilson-Kubalek, E.M., and Desai, A. (2006). The conserved KMN network constitutes the core microtubule-binding site of the kinetochore. Cell *127*, 983-997.

Chen, R.H. (2002). BubR1 is essential for kinetochore localization of other spindle checkpoint proteins and its phosphorylation requires Mad1. J Cell Biol *158*, 487-496.

Chen, R.H., Brady, D.M., Smith, D., Murray, A.W., and Hardwick, K.G. (1999). The spindle checkpoint of budding yeast depends on a tight complex between the Mad1 and Mad2 proteins. Mol Biol Cell *10*, 2607-2618.

Chen, R.H., Shevchenko, A., Mann, M., and Murray, A.W. (1998). Spindle checkpoint protein Xmad1 recruits Xmad2 to unattached kinetochores. J Cell Biol *143*, 283-295.

Chung, E., and Chen, R.H. (2002). Spindle checkpoint requires Mad1-bound and Mad1-free Mad2. Mol Biol Cell *13*, 1501-1511.

Cimini, D., Wan, X., Hirel, C.B., and Salmon, E.D. (2006). Aurora kinase promotes turnover of kinetochore microtubules to reduce chromosome segregation errors. Current biology : CB *16*, 1711-1718.

Collin, P., Nashchekina, O., Walker, R., and Pines, J. (2013). The spindle assembly checkpoint works like a rheostat rather than a toggle switch. Nat Cell Biol *15*, 1378-1385.

Coudreuse, D., and Nurse, P. (2010). Driving the cell cycle with a minimal CDK control network. Nature *468*, 1074-1079.

Courtheoux, T., Gay, G., Reyes, C., Goldstone, S., Gachet, Y., and Tournier, S. (2007). Dynein participates in chromosome segregation in fission yeast. Biology of the Cell *99*, 627-637.

D'Arcy, S., Davies, O.R., Blundell, T.L., and Bolanos-Garcia, V.M. (2010). Defining the molecular basis of BubR1 kinetochore interactions and APC/C-CDC20 inhibition. J Biol Chem *285*, 14764-14776.

da Fonseca, P.C., Kong, E.H., Zhang, Z., Schreiber, A., Williams, M.A., Morris, E.P., and Barford, D. (2011). Structures of APC/C(Cdh1) with substrates identify Cdh1 and Apc10 as the D-box co-receptor. Nature *470*, 274-278.

Dai, W., Wang, Q., Liu, T., Swamy, M., Fang, Y., Xie, S., Mahmood, R., Yang, Y.M., Xu, M., and Rao, C.V. (2004). Slippage of mitotic arrest and enhanced tumor development in mice with BubR1 haploinsufficiency. Cancer Res *64*, 440-445.

Davenport, J., Harris, L.D., and Goorha, R. (2006). Spindle checkpoint function requires Mad2-dependent Cdc20 binding to the Mad3 homology domain of BubR1. Exp Cell Res *312*, 1831-1842.

De Antoni, A., Pearson, C.G., Cimini, D., Canman, J.C., Sala, V., Nezi, L., Mapelli, M., Sironi, L., Faretta, M., Salmon, E.D.*, et al.* (2005a). The Mad1/Mad2 complex as a template for Mad2 activation in the spindle assembly checkpoint. Current biology : CB *15*, 214-225.

De Antoni, A., Sala, V., and Musacchio, A. (2005b). Explaining the oligomerization properties of the spindle assembly checkpoint protein Mad2. Philos Trans R Soc Lond B Biol Sci *360*, 637-647, discussion 447-638.

De Souza, C.P., and Osmani, S.A. (2007). Mitosis, not just open or closed. Eukaryotic cell *6*, 1521-1527.

DeLuca, J., and Musacchio, A. (2012). Structural organization of the kinetochore-microtubule interface. Curr Opin Cell Biol *24*, 48-56.

DeLuca, J.G., Gall, W.E., Ciferri, C., Cimini, D., Musacchio, A., and Salmon, E.D. (2006). Kinetochore microtubule dynamics and attachment stability are regulated by Hec1. Cell *127*, 969-982.

Di Fiore, B., Davey, N.E., Hagting, A., Izawa, D., Mansfeld, J., Gibson, T.J., and Pines, J. (2015). The ABBA motif binds APC/C activators and is shared by APC/C substrates and regulators. Developmental cell *32*, 358-372.

Diaz-Martinez, L.A., Tian, W., Li, B., Warrington, R., Jia, L., Brautigam, C.A., Luo, X., and Yu, H. (2015). The Cdc20-binding Phe box of the spindle checkpoint protein BubR1 maintains the mitotic checkpoint complex during mitosis. J Biol Chem *290*, 2431-2443.

Dick, A.E., and Gerlich, D.W. (2013). Kinetic framework of spindle assembly checkpoint signalling. Nat Cell Biol *15*, 1370-1377.

Ding, R., West, R.R., Morphew, D.M., Oakley, B.R., and McIntosh, J.R. (1997). The spindle pole body of Schizosaccharomyces pombe enters and leaves the nuclear envelope as the cell cycle proceeds. Mol Biol Cell *8*, 1461-1479.

Elowe, S., Dulla, K., Uldschmid, A., Li, X., Dou, Z., and Nigg, E.A. (2010). Uncoupling of the spindle-checkpoint and chromosome-congression functions of BubR1. J Cell Sci *123*, 84-94.

Essex, A., Dammermann, A., Lewellyn, L., Oegema, K., and Desai, A. (2009). Systematic analysis in Caenorhabditis elegans reveals that the spindle checkpoint is composed of two largely independent branches. Mol Biol Cell *20*, 1252-1267.

Etemad, B., and Kops, G.J.P.L. (2016). Attachment issues: kinetochore transformations and spindle checkpoint silencing. Current Opinion in Cell Biology *39*, 101-108.

Eytan, E., Wang, K., Miniowitz-Shemtov, S., Sitry-Shevah, D., Kaisari, S., Yen, T.J., Liu, S.T., and Hershko, A. (2014). Disassembly of mitotic checkpoint complexes by the joint action of the AAA-ATPase TRIP13 and p31(comet). Proc Natl Acad Sci U S A *111*, 12019-12024.

Fang, G. (2002). Checkpoint protein BubR1 acts synergistically with Mad2 to inhibit anaphase-promoting complex. Mol Biol Cell *13*, 755-766.

Fang, G., Yu, H., and Kirschner, M.W. (1998a). The checkpoint protein MAD2 and the mitotic regulator CDC20 form a ternary complex with the anaphase-promoting complex to control anaphase initiation. Genes Dev *12*, 1871-1883.

Fang, G., Yu, H., and Kirschner, M.W. (1998b). Direct binding of CDC20 protein family members activates the anaphase-promoting complex in mitosis and G1. Mol Cell *2*, 163-171.

Fava, L.L., Kaulich, M., Nigg, E.A., and Santamaria, A. (2011). Probing the in vivo function of Mad1:C-Mad2 in the spindle assembly checkpoint. EMBO J *30*, 3322-3336.

Foley, E.A., and Kapoor, T.M. (2013). Microtubule attachment and spindle assembly checkpoint signalling at the kinetochore. Nature reviews. Molecular cell biology *14*, 25-37.

Forsburg, S.L. (2003). Overview of Schizosaccharomyces pombe. Curr Protoc Mol Biol *Chapter 13*, Unit 13 14.

Forsburg, S.L., and Rhind, N. (2006). Basic methods for fission yeast. Yeast *23*, 173-183.

Foster, S.A., and Morgan, D.O. (2012). The APC/C subunit Mnd2/Apc15 promotes Cdc20 autoubiquitination and spindle assembly checkpoint inactivation. Mol Cell *47*, 921-932.

Fowler, K.R., Sasaki, M., Milman, N., Keeney, S., and Smith, G.R. (2014). Evolutionarily diverse determinants of meiotic DNA break and recombination landscapes across the genome. Genome Res *24*, 1650-1664.

Fraschini, R., Beretta, A., Sironi, L., Musacchio, A., Lucchini, G., and Piatti, S. (2001). Bub3 interaction with Mad2, Mad3 and Cdc20 is mediated by WD40 repeats and does not require intact kinetochores. EMBO J *20*, 6648-6659.

Gascoigne, K.E., and Taylor, S.S. (2008). Cancer cells display profound intra- and interline variation following prolonged exposure to antimitotic drugs. Cancer Cell *14*, 111-122.

Gascoigne, K.E., and Taylor, S.S. (2009). How do anti-mitotic drugs kill cancer cells? Journal of Cell Science *122*, 2579-2585.

Gassmann, R., Holland, A.J., Varma, D., Wan, X., Civril, F., Cleveland, D.W., Oegema, K., Salmon, E.D., and Desai, A. (2010). Removal of Spindly from microtubule-attached kinetochores controls spindle checkpoint silencing in human cells. Genes Dev *24*, 957-971.

Ghaemmaghami, S., Huh, W.K., Bower, K., Howson, R.W., Belle, A., Dephoure, N., O'Shea, E.K., and Weissman, J.S. (2003). Global analysis of protein expression in yeast. Nature *425*, 737-741.

Gillett, E.S., Espelin, C.W., and Sorger, P.K. (2004). Spindle checkpoint proteins and chromosome-microtubule attachment in budding yeast. J Cell Biol *164*, 535-546.

Glotzer, M., Murray, A.W., and Kirschner, M.W. (1991). Cyclin is degraded by the ubiquitin pathway. Nature *349*, 132-138.

Godek, K.M., Kabeche, L., and Compton, D.A. (2015). Regulation of kinetochore-microtubule attachments through homeostatic control during mitosis. Nature reviews. Molecular cell biology *16*, 57-64.

Gregan, J., Polakova, S., Zhang, L., Tolić-Nørrelykke, I.M., and Cimini, D. (2011). Merotelic kinetochore attachment: causes and effects. Trends in Cell Biology *21*, 374-381.

Guse, A., Carroll, C.W., Moree, B., Fuller, C.J., and Straight, A.F. (2011). In vitro centromere and kinetochore assembly on defined chromatin templates. Nature *477*, 354-358.

Hall, M.N., and Linder, P. (1993). The Early days of yeast genetics (Plainview, N.Y.: Cold Spring Harbor Laboratory Press).

Han, J.S., Holland, A.J., Fachinetti, D., Kulukian, A., Cetin, B., and Cleveland, D.W. (2013). Catalytic assembly of the mitotic checkpoint inhibitor BubR1-Cdc20 by a Mad2-induced functional switch in Cdc20. Mol Cell *51*, 92-104.

Hardwick, K.G., Johnston, R.C., Smith, D.L., and Murray, A.W. (2000). MAD3 encodes a novel component of the spindle checkpoint which interacts with Bub3p, Cdc20p, and Mad2p. J Cell Biol *148*, 871-882.

Hardwick, K.G., Li, R., Mistrot, C., Chen, R.H., Dann, P., Rudner, A., and Murray, A.W. (1999). Lesions in many different spindle components activate the spindle checkpoint in the budding yeast Saccharomyces cerevisiae. Genetics *152*, 509-518.

Hartwell, L.H., and Weinert, T.A. (1989). Checkpoints: controls that ensure the order of cell cycle events. Science *246*, 629-634.

Hauf, S., Cole, R.W., LaTerra, S., Zimmer, C., Schnapp, G., Walter, R., Heckel, A., van Meel, J., Rieder, C.L., and Peters, J.M. (2003). The small molecule Hesperadin reveals a role for Aurora B in correcting kinetochore-microtubule attachment and in maintaining the spindle assembly checkpoint. J Cell Biol *161*, 281-294.

He, X., Patterson, T.E., and Sazer, S. (1997). The Schizosaccharomyces pombe spindle checkpoint protein mad2p blocks anaphase and genetically interacts with the anaphase-promoting complex. Proc Natl Acad Sci U S A *94*, 7965-7970.

He, X., Rines, D.R., Espelin, C.W., and Sorger, P.K. (2001). Molecular analysis of kinetochore-microtubule attachment in budding yeast. Cell *106*, 195-206.

Heckman, D.S., Geiser, D.M., Eidell, B.R., Stauffer, R.L., Kardos, N.L., and Hedges, S.B. (2001). Molecular Evidence for the Early Colonization of Land by Fungi and Plants. Science *293*, 1129-1133.

Hein, J.B., and Nilsson, J. (2014). Stable MCC binding to the APC/C is required for a functional spindle assembly checkpoint. EMBO Rep *15*, 264-272.

Heinrich, S., Geissen, E.M., Kamenz, J., Trautmann, S., Widmer, C., Drewe, P., Knop, M., Radde, N., Hasenauer, J., and Hauf, S. (2013). Determinants of robustness in spindle assembly checkpoint signalling. Nat Cell Biol *15*, 1328-1339.

Heinrich, S., Sewart, K., Windecker, H., Langegger, M., Schmidt, N., Hustedt, N., and Hauf, S. (2014). Mad1 contribution to spindle assembly checkpoint signalling goes beyond presenting Mad2 at kinetochores. EMBO Rep *15*, 291-298.

Heinrich, S., Windecker, H., Hustedt, N., and Hauf, S. (2012). Mph1 kinetochore localization is crucial and upstream in the hierarchy of spindle assembly checkpoint protein recruitment to kinetochores. J Cell Sci *125*, 4720-4727.

Herzog, F., Primorac, I., Dube, P., Lenart, P., Sander, B., Mechtler, K., Stark, H., and Peters, J.M. (2009). Structure of the anaphase-promoting complex/cyclosome interacting with a mitotic checkpoint complex. Science *323*, 1477-1481.

Hewitt, L., Tighe, A., Santaguida, S., White, A.M., Jones, C.D., Musacchio, A., Green, S., and Taylor, S.S. (2010). Sustained Mps1 activity is required in mitosis to recruit O-Mad2 to the Mad1-C-Mad2 core complex. J Cell Biol *190*, 25-34.

Hiruma, Y., Sacristan, C., Pachis, S.T., Adamopoulos, A., Kuijt, T., Ubbink, M., von Castelmur, E., Perrakis, A., and Kops, G.J. (2015). CELL DIVISION CYCLE. Competition between MPS1 and microtubules at kinetochores regulates spindle checkpoint signaling. Science *348*, 1264-1267.

Hoffman, C.S., Wood, V., and Fantes, P.A. (2015). An Ancient Yeast for Young Geneticists: A Primer on the Schizosaccharomyces pombe Model System. Genetics *201*, 403-423.

Hori, T., Amano, M., Suzuki, A., Backer, C.B., Welburn, J.P., Dong, Y., McEwen, B.F., Shang, W.H., Suzuki, E., Okawa, K.*, et al.* (2008). CCAN makes multiple contacts with centromeric DNA to provide distinct pathways to the outer kinetochore. Cell *135*, 1039-1052.

Howell, B.J., Hoffman, D.B., Fang, G., Murray, A.W., and Salmon, E.D. (2000). Visualization of Mad2 dynamics at kinetochores, along spindle fibers, and at spindle poles in living cells. J Cell Biol *150*, 1233-1250.

Howell, B.J., McEwen, B.F., Canman, J.C., Hoffman, D.B., Farrar, E.M., Rieder, C.L., and Salmon, E.D. (2001). Cytoplasmic dynein/dynactin drives kinetochore protein transport to the spindle poles and has a role in mitotic spindle checkpoint inactivation. J Cell Biol *155*, 1159-1172.

Howell, B.J., Moree, B., Farrar, E.M., Stewart, S., Fang, G., and Salmon, E.D. (2004). Spindle checkpoint protein dynamics at kinetochores in living cells. Current biology : CB *14*, 953-964.

Hoyt, M.A., Totis, L., and Roberts, B.T. (1991). S. cerevisiae genes required for cell cycle arrest in response to loss of microtubule function. Cell *66*, 507-517.

Hunt, T., Luca, F.C., and Ruderman, J.V. (1992). The requirements for protein synthesis and degradation, and the control of destruction of cyclins A and B in the meiotic and mitotic cell cycles of the clam embryo. J Cell Biol *116*, 707-724.

Hwang, L.H., Lau, L.F., Smith, D.L., Mistrot, C.A., Hardwick, K.G., Hwang, E.S., Amon, A., and Murray, A.W. (1998). Budding yeast Cdc20: a target of the spindle checkpoint. Science *279*, 1041-1044.

Ito, D., Saito, Y., and Matsumoto, T. (2012). Centromere-tethered Mps1 pombe homolog (Mph1) kinase is a sufficient marker for recruitment of the spindle checkpoint protein Bub1, but not Mad1. Proc Natl Acad Sci U S A *109*, 209-214.

Izawa, D., and Pines, J. (2012). Mad2 and the APC/C compete for the same site on Cdc20 to ensure proper chromosome segregation. The Journal of Cell Biology *199*, 27-37.

Izawa, D., and Pines, J. (2015). The mitotic checkpoint complex binds a second CDC20 to inhibit active APC/C. Nature *517*, 631-634.

Jelluma, N., Dansen, T.B., Sliedrecht, T., Kwiatkowski, N.P., and Kops, G.J. (2010). Release of Mps1 from kinetochores is crucial for timely anaphase onset. J Cell Biol *191*, 281-290.

Ji, Z., Gao, H., and Yu, H. (2015). CELL DIVISION CYCLE. Kinetochore attachment sensed by competitive Mps1 and microtubule binding to Ndc80C. Science *348*, 1260-1264.

Ji, Z., and Yu, H. (2014). A Protective Chaperone for the Kinetochore Adaptor Bub3. Developmental cell *28*, 223-224.

Jia, L., Kim, S., and Yu, H. (2013). Tracking spindle checkpoint signals from kinetochores to APC/C. Trends in biochemical sciences *38*, 302-311.

Jia, L., Li, B., Warrington, R.T., Hao, X., Wang, S., and Yu, H. (2011). Defining pathways of spindle checkpoint silencing: functional redundancy between Cdc20 ubiquitination and p31(comet). Molecular Biology of the Cell *22*, 4227-4235.

Jia, L., Li, B., and Yu, H. (2016). The Bub1-Plk1 kinase complex promotes spindle checkpoint signalling through Cdc20 phosphorylation. Nat Commun *7*, 10818.

Jiang, H., He, X., Wang, S., Jia, J., Wan, Y., Wang, Y., Zeng, R., Yates, J., 3rd, Zhu, X., and Zheng, Y. (2014). A microtubule-associated zinc finger protein, BuGZ, regulates mitotic chromosome alignment by ensuring Bub3 stability and kinetochore targeting. Developmental cell *28*, 268-281.

Kadura, S., He, X., Vanoosthuyse, V., Hardwick, K.G., and Sazer, S. (2005). The A78V mutation in the Mad3-like domain of Schizosaccharomyces pombe Bub1p perturbs nuclear accumulation and kinetochore targeting of Bub1p, Bub3p, and Mad3p and spindle assembly checkpoint function. Mol Biol Cell *16*, 385-395.

Kalitsis, P., Earle, E., Fowler, K.J., and Choo, K.H. (2000). Bub3 gene disruption in mice reveals essential mitotic spindle checkpoint function during early embryogenesis. Genes Dev *14*, 2277-2282.

Kang, J., Yang, M., Li, B., Qi, W., Zhang, C., Shokat, K.M., Tomchick, D.R., Machius, M., and Yu, H. (2008). Structure and substrate recruitment of the human spindle checkpoint kinase Bub1. Mol Cell *32*, 394-405.

Karess, R. (2005). Rod-Zw10-Zwilch: a key player in the spindle checkpoint. Trends in Cell Biology *15*, 386-392.

Kastenmayer, J.P., Lee, M.S., Hong, A.L., Spencer, F.A., and Basrai, M.A. (2005). The C-terminal half of Saccharomyces cerevisiae Mad1p mediates spindle checkpoint function, chromosome transmission fidelity and CEN association. Genetics *170*, 509-517.

Kato, H., Jiang, J., Zhou, B.R., Rozendaal, M., Feng, H., Ghirlando, R., Xiao, T.S., Straight, A.F., and Bai, Y. (2013). A conserved mechanism for centromeric nucleosome recognition by centromere protein CENP-C. Science *340*, 1110-1113.

Kerscher, O., Crotti, L.B., and Basrai, M.A. (2003). Recognizing chromosomes in trouble: association of the spindle checkpoint protein Bub3p with altered kinetochores and a unique defective centromere. Mol Cell Biol *23*, 6406-6418.

Kim, S., Sun, H., Tomchick, D.R., Yu, H., and Luo, X. (2012). Structure of human Mad1 C-terminal domain reveals its involvement in kinetochore targeting. Proc Natl Acad Sci U S A *109*, 6549-6554.

Kim, S., and Yu, H. (2015). Multiple assembly mechanisms anchor the KMN spindle checkpoint platform at human mitotic kinetochores. J Cell Biol *208*, 181-196.

Kim, S.H., Lin, D.P., Matsumoto, S., Kitazono, A., and Matsumoto, T. (1998). Fission yeast Slp1: an effector of the Mad2-dependent spindle checkpoint. Science *279*, 1045-1047.

King, E.M., van der Sar, S.J., and Hardwick, K.G. (2007). Mad3 KEN boxes mediate both Cdc20 and Mad3 turnover, and are critical for the spindle checkpoint. PLoS One *2*, e342.

King, R.W., Glotzer, M., and Kirschner, M.W. (1996). Mutagenic analysis of the destruction signal of mitotic cyclins and structural characterization of ubiquitinated intermediates. Mol Biol Cell *7*, 1343-1357.

Kiyomitsu, T., Murakami, H., and Yanagida, M. (2011). Protein interaction domain mapping of human kinetochore protein Blinkin reveals a consensus motif for binding of spindle assembly checkpoint proteins Bub1 and BubR1. Mol Cell Biol *31*, 998-1011.

Kiyomitsu, T., Obuse, C., and Yanagida, M. (2007). Human Blinkin/AF15q14 is required for chromosome alignment and the mitotic checkpoint through direct interaction with Bub1 and BubR1. Developmental cell *13*, 663-676.

Klebig, C., Korinth, D., and Meraldi, P. (2009). Bub1 regulates chromosome segregation in a kinetochore-independent manner. J Cell Biol *185*, 841-858.

Kong, X., Murphy, K., Raj, T., He, C., White, P.S., and Matise, T.C. (2004). A combined linkage-physical map of the human genome. Am J Hum Genet *75*, 1143-1148.

Kops, G.J., Kim, Y., Weaver, B.A., Mao, Y., McLeod, I., Yates, J.R., 3rd, Tagaya, M., and Cleveland, D.W. (2005a). ZW10 links mitotic checkpoint signaling to the structural kinetochore. J Cell Biol *169*, 49-60.

Kops, G.J., Saurin, A.T., and Meraldi, P. (2010). Finding the middle ground: how kinetochores power chromosome congression. Cellular and molecular life sciences : CMLS *67*, 2145-2161.

Kops, G.J., Weaver, B.A., and Cleveland, D.W. (2005b). On the road to cancer: aneuploidy and the mitotic checkpoint. Nature reviews. Cancer *5*, 773-785.

Krenn, V., Overlack, K., Primorac, I., van Gerwen, S., and Musacchio, A. (2014). KI motifs of human Knl1 enhance assembly of comprehensive spindle checkpoint complexes around MELT repeats. Current biology : CB *24*, 29-39.

Krenn, V., Wehenkel, A., Li, X., Santaguida, S., and Musacchio, A. (2012). Structural analysis reveals features of the spindle checkpoint kinase Bub1-kinetochore subunit Knl1 interaction. J Cell Biol *196*, 451-467.

Kruse, T., Larsen, M.S., Sedgwick, G.G., Sigurdsson, J.O., Streicher, W., Olsen, J.V., and Nilsson, J. (2014). A direct role of Mad1 in the spindle assembly checkpoint beyond Mad2 kinetochore recruitment. EMBO Rep *15*, 282-290.

Kruse, T., Zhang, G., Larsen, M.S., Lischetti, T., Streicher, W., Kragh Nielsen, T., Bjorn, S.P., and Nilsson, J. (2013). Direct binding between BubR1 and B56-PP2A phosphatase complexes regulate mitotic progression. J Cell Sci *126*, 1086-1092.

Kuijt, T.E.F., Omerzu, M., Saurin, A.T., and Kops, G. (2014). Conditional targeting of MAD1 to kinetochores is sufficient to reactivate the spindle assembly checkpoint in metaphase. Chromosoma *123*, 471-480.

Kulukian, A., Han, J.S., and Cleveland, D.W. (2009). Unattached kinetochores catalyze production of an anaphase inhibitor that requires a Mad2 template to prime Cdc20 for BubR1 binding. Developmental cell *16*, 105-117.

Lampson, M.A., Renduchitala, K., Khodjakov, A., and Kapoor, T.M. (2004). Correcting improper chromosome-spindle attachments during cell division. Nat Cell Biol *6*, 232-237.

Lara-Gonzalez, P., Scott, M.I., Diez, M., Sen, O., and Taylor, S.S. (2011). BubR1 blocks substrate recruitment to the APC/C in a KEN-box-dependent manner. J Cell Sci *124*, 4332-4345.

Lara-Gonzalez, P., Westhorpe, F.G., and Taylor, S.S. (2012). The spindle assembly checkpoint. Current biology : CB *22*, R966-980.

Larsen, N.A., Al-Bassam, J., Wei, R.R., and Harrison, S.C. (2007). Structural analysis of Bub3 interactions in the mitotic spindle checkpoint. Proc Natl Acad Sci U S A *104*, 1201-1206.

Lau, D.T., and Murray, A.W. (2012). Mad2 and Mad3 cooperate to arrest budding yeast in mitosis. Current biology : CB *22*, 180-190.

Lee, J., Kim, J.A., Margolis, R.L., and Fotedar, R. (2010). Substrate degradation by the anaphase promoting complex occurs during mitotic slippage. Cell cycle (Georgetown, Tex.) *9*, 1792-1801.

Lee, K.K., Gruenbaum, Y., Spann, P., Liu, J., and Wilson, K.L. (2000). C. elegans nuclear envelope proteins emerin, MAN1, lamin, and nucleoporins reveal unique timing of nuclear envelope breakdown during mitosis. Mol Biol Cell *11*, 3089-3099.

Lee, S.H., Sterling, H., Burlingame, A., and McCormick, F. (2008). Tpr directly binds to Mad1 and Mad2 and is important for the Mad1-Mad2-mediated mitotic spindle checkpoint. Genes Dev *22*, 2926-2931.

Li, D., Morley, G., Whitaker, M., and Huang, J.Y. (2010). Recruitment of Cdc20 to the kinetochore requires BubR1 but not Mad2 in Drosophila melanogaster. Mol Cell Biol *30*, 3384-3395.

Li, R., and Murray, A.W. (1991). Feedback control of mitosis in budding yeast. Cell *66*, 519-531.

Li, X., and Nicklas, R.B. (1995). Mitotic forces control a cell-cycle checkpoint. Nature *373*, 630-632.

Lischetti, T., and Nilsson, J. (2015). Regulation of mitotic progression by the spindle assembly checkpoint. Mol Cell Oncol *2*, e970484.

Lischetti, T., Zhang, G., Sedgwick, G.G., Bolanos-Garcia, V.M., and Nilsson, J. (2014). The internal Cdc20 binding site in BubR1 facilitates both spindle assembly checkpoint signalling and silencing. Nat Commun *5*, 5563.

Logarinho, E., Resende, T., Torres, C., and Bousbaa, H. (2008). The human spindle assembly checkpoint protein Bub3 is required for the establishment of efficient kinetochore-microtubule attachments. Mol Biol Cell *19*, 1798-1813.

London, N., and Biggins, S. (2014). Mad1 kinetochore recruitment by Mps1-mediated phosphorylation of Bub1 signals the spindle checkpoint. Genes Dev *28*, 140-152.

London, N., Ceto, S., Ranish, J.A., and Biggins, S. (2012). Phosphoregulation of Spc105 by Mps1 and PP1 regulates Bub1 localization to kinetochores. Current biology : CB *22*, 900-906.

Lopes, C.S., Sampaio, P., Williams, B., Goldberg, M., and Sunkel, C.E. (2005). The Drosophila Bub3 protein is required for the mitotic checkpoint and for normal accumulation of cyclins during G2 and early stages of mitosis. J Cell Sci *118*, 187-198.

Luo, X., Tang, Z., Rizo, J., and Yu, H. (2002). The Mad2 spindle checkpoint protein undergoes similar major conformational changes upon binding to either Mad1 or Cdc20. Mol Cell *9*, 59-71.

Luo, X., Tang, Z., Xia, G., Wassmann, K., Matsumoto, T., Rizo, J., and Yu, H. (2004). The Mad2 spindle checkpoint protein has two distinct natively folded states. Nat Struct Mol Biol *11*, 338-345.

Ma, H.T., and Poon, R.Y. (2011). Orderly inactivation of the key checkpoint protein mitotic arrest deficient 2 (MAD2) during mitotic progression. J Biol Chem *286*, 13052-13059.

Maciejowski, J., George, K.A., Terret, M.E., Zhang, C., Shokat, K.M., and Jallepalli, P.V. (2010). Mps1 directs the assembly of Cdc20 inhibitory complexes during interphase and mitosis to control M phase timing and spindle checkpoint signaling. J Cell Biol *190*, 89-100.

Maldonado, M., and Kapoor, T.M. (2011). Constitutive Mad1 targeting to kinetochores uncouples checkpoint signalling from chromosome biorientation. Nat Cell Biol *13*, 475-482.

Malureanu, L.A., Jeganathan, K.B., Hamada, M., Wasilewski, L., Davenport, J., and van Deursen, J.M. (2009). BubR1 N terminus acts as a soluble inhibitor of cyclin B degradation by APC/C(Cdc20) in interphase. Developmental cell *16*, 118-131.

Malvezzi, F., Litos, G., Schleiffer, A., Heuck, A., Mechtler, K., Clausen, T., and Westermann, S. (2013). A structural basis for kinetochore recruitment of the Ndc80 complex via two distinct centromere receptors. EMBO J *32*, 409-423.

Mansfeld, J., Collin, P., Collins, M.O., Choudhary, J.S., and Pines, J. (2011). APC15 drives the turnover of MCC-CDC20 to make the spindle assembly checkpoint responsive to kinetochore attachment. Nat Cell Biol *13*, 1234-1243.

Mapelli, M., Filipp, F.V., Rancati, G., Massimiliano, L., Nezi, L., Stier, G., Hagan, R.S., Confalonieri, S., Piatti, S., Sattler, M.*, et al.* (2006). Determinants of conformational dimerization of Mad2 and its inhibition by p31comet. EMBO J *25*, 1273-1284.

Mapelli, M., Massimiliano, L., Santaguida, S., and Musacchio, A. (2007). The Mad2 conformational dimer: structure and implications for the spindle assembly checkpoint. Cell *131*, 730-743.

Mapelli, M., and Musacchio, A. (2007). MAD contortions: conformational dimerization boosts spindle checkpoint signaling. Curr Opin Struct Biol *17*, 716-725.

Mariani, L., Chiroli, E., Nezi, L., Muller, H., Piatti, S., Musacchio, A., and Ciliberto, A. (2012). Role of the Mad2 dimerization interface in the spindle assembly checkpoint independent of kinetochores. Current biology : CB *22*, 1900-1908.

Martin-Lluesma, S., Stucke, V.M., and Nigg, E.A. (2002). Role of Hec1 in spindle checkpoint signaling and kinetochore recruitment of Mad1/Mad2. Science *297*, 2267-2270.

Maure, J.F., Kitamura, E., and Tanaka, T.U. (2007). Mps1 kinase promotes sister-kinetochore bi-orientation by a tension-dependent mechanism. Current biology : CB *17*, 2175-2182.

McIntosh, J.R., Grishchuk, E.L., Morphew, M.K., Efremov, A.K., Zhudenkov, K., Volkov, V.A., Cheeseman, I.M., Desai, A., Mastronarde, D.N., and Ataullakhanov, F.I. (2008). Fibrils connect microtubule tips with kinetochores: a mechanism to couple tubulin dynamics to chromosome motion. Cell *135*, 322-333.

Meadows, J.C., Shepperd, L.A., Vanoosthuyse, V., Lancaster, T.C., Sochaj, A.M., Buttrick, G.J., Hardwick, K.G., and Millar, J.B. (2011). Spindle checkpoint silencing requires association of PP1 to both Spc7 and kinesin-8 motors. Developmental cell *20*, 739-750.

Michel, L.S., Liberal, V., Chatterjee, A., Kirchwegger, R., Pasche, B., Gerald, W., Dobles, M., Sorger, P.K., Murty, V.V., and Benezra, R. (2001). MAD2 haplo-insufficiency causes premature anaphase and chromosome instability in mammalian cells. Nature *409*, 355-359.

Millband, D.N., and Hardwick, K.G. (2002). Fission yeast Mad3p is required for Mad2p to inhibit the anaphase-promoting complex and localizes to kinetochores in a Bub1p-, Bub3p-, and Mph1p-dependent manner. Mol Cell Biol *22*, 2728-2742.

Miniowitz-Shemtov, S., Teichner, A., Sitry-Shevah, D., and Hershko, A. (2010). ATP is required for the release of the anaphase-promoting complex/cyclosome from inhibition by the mitotic checkpoint. Proc Natl Acad Sci U S A *107*, 5351-5356.

Mitchison, J.M. (1990). The fission yeast, Schizosaccharomyces pombe. Bioessays *12*, 189-191.

Morgan, D.O. (1995). Principles of CDK regulation. Nature *374*, 131-134.

Morgan, D.O. (1997). Cyclin-dependent kinases: engines, clocks, and microprocessors. Annu Rev Cell Dev Biol *13*, 261-291.

Morgan, D.O. (2007). The Cell Cycle: Principles of Control (OUP/New Science Press).

Moyle, M.W., Kim, T., Hattersley, N., Espeut, J., Cheerambathur, D.K., Oegema, K., and Desai, A. (2014). A Bub1-Mad1 interaction targets the Mad1-Mad2 complex to unattached kinetochores to initiate the spindle checkpoint. J Cell Biol *204*, 647-657.

Musacchio, A. (2015a). Closing the Mad2 cycle. eLife *4*, e08283.

Musacchio, A. (2015b). The Molecular Biology of Spindle Assembly Checkpoint Signaling Dynamics. Current biology : CB *25*, R1002-1018.

Musacchio, A., and Salmon, E.D. (2007). The spindle-assembly checkpoint in space and time. Nature reviews. Molecular cell biology *8*, 379-393.

Nasmyth, K. (2005). How do so few control so many? Cell *120*, 739-746.

Newman, J.R.S., Ghaemmaghami, S., Ihmels, J., Breslow, D.K., Noble, M., DeRisi, J.L., and Weissman, J.S. (2006). Single-cell proteomic analysis of S. cerevisiae reveals the architecture of biological noise. Nature *441*, 840-846.

Nezi, L., Rancati, G., De Antoni, A., Pasqualato, S., Piatti, S., and Musacchio, A. (2006). Accumulation of Mad2-Cdc20 complex during spindle checkpoint activation requires binding of open and closed conformers of Mad2 in Saccharomyces cerevisiae. J Cell Biol *174*, 39-51.

Nilsson, J., Yekezare, M., Minshull, J., and Pines, J. (2008). The APC/C maintains the spindle assembly checkpoint by targeting Cdc20 for destruction. Nat Cell Biol *10*, 1411-1420.

Nishino, T., Rago, F., Hori, T., Tomii, K., Cheeseman, I.M., and Fukagawa, T. (2013). CENP-T provides a structural platform for outer kinetochore assembly. EMBO J *32*, 424-436.

Nurse, P., Thuriaux, P., and Nasmyth, K. (1976). Genetic control of the cell division cycle in the fission yeast Schizosaccharomyces pombe. Molecular & general genetics : MGG *146*, 167-178.

Oliveira, R.A., and Nasmyth, K. (2010). Getting through anaphase: splitting the sisters and beyond. Biochemical Society transactions *38*, 1639-1644.

Olson, M.V., Dutchik, J.E., Graham, M.Y., Brodeur, G.M., Helms, C., Frank, M., MacCollin, M., Scheinman, R., and Frank, T. (1986). Random-clone strategy for genomic restriction mapping in yeast. Proc Natl Acad Sci U S A *83*, 7826-7830.

Orth, J.D., Tang, Y., Shi, J., Loy, C.T., Amendt, C., Wilm, C., Zenke, F.T., and Mitchison, T.J. (2008). Quantitative live imaging of cancer and normal cells treated with Kinesin-5 inhibitors indicates significant differences in phenotypic responses and cell fate. Molecular cancer therapeutics *7*, 3480-3489.

Overlack, K., Primorac, I., Vleugel, M., Krenn, V., Maffini, S., Hoffmann, I., Kops, G.J., and Musacchio, A. (2015). A molecular basis for the differential roles of Bub1 and BubR1 in the spindle assembly checkpoint. Elife *4*, e05269.

Pan, J., and Chen, R.H. (2004). Spindle checkpoint regulates Cdc20p stability in Saccharomyces cerevisiae. Genes Dev *18*, 1439-1451.

Paweletz, N. (2001). Walther Flemming: pioneer of mitosis research. Nature reviews. Molecular cell biology *2*, 72-75.

Pereira, G., and Schiebel, E. (1997). Centrosome-microtubule nucleation. J Cell Sci *110 (Pt 3)*, 295-300.

Pesenti, M.E., Weir, J.R., and Musacchio, A. (2016). Progress in the structural and functional characterization of kinetochores. Current Opinion in Structural Biology *37*, 152-163.

Peters, J.M. (2006). The anaphase promoting complex/cyclosome: a machine designed to destroy. Nature reviews. Molecular cell biology *7*, 644-656.

Petrovic, A., Pasqualato, S., Dube, P., Krenn, V., Santaguida, S., Cittaro, D., Monzani, S., Massimiliano, L., Keller, J., Tarricone, A.*, et al.* (2010). The MIS12 complex is a protein interaction hub for outer kinetochore assembly. J Cell Biol *190*, 835-852.

Pfleger, C.M., Lee, E., and Kirschner, M.W. (2001). Substrate recognition by the Cdc20 and Cdh1 components of the anaphase-promoting complex. Genes & Development *15*, 2396-2407.

Pines, J. (2011). Cubism and the cell cycle: the many faces of the APC/C. Nature reviews. Molecular cell biology *12*, 427-438.

Pines, J., and Rieder, C.L. (2001). Re-staging mitosis: a contemporary view of mitotic progression. Nat Cell Biol *3*, E3-6.

Pinsky, B.A., Nelson, C.R., and Biggins, S. (2009). Protein phosphatase 1 regulates exit from the spindle checkpoint in budding yeast. Current biology : CB *19*, 1182-1187.

Poddar, A., Stukenberg, P.T., and Burke, D.J. (2005). Two complexes of spindle checkpoint proteins containing Cdc20 and Mad2 assemble during mitosis independently of the kinetochore in Saccharomyces cerevisiae. Eukaryotic cell *4*, 867-878.

Powers, A.F., Franck, A.D., Gestaut, D.R., Cooper, J., Gracyzk, B., Wei, R.R., Wordeman, L., Davis, T.N., and Asbury, C.L. (2009). The Ndc80 kinetochore complex forms load-bearing attachments to dynamic microtubule tips via biased diffusion. Cell *136*, 865-875.

Primorac, I., and Musacchio, A. (2013). Panta rhei: the APC/C at steady state. J Cell Biol *201*, 177-189.

Primorac, I., Weir, J.R., Chiroli, E., Gross, F., Hoffmann, I., van Gerwen, S., Ciliberto, A., and Musacchio, A. (2013). Bub3 reads phosphorylated MELT repeats to promote spindle assembly checkpoint signaling. Elife *2*, e01030.

Przewloka, M.R., Venkei, Z., Bolanos-Garcia, V.M., Debski, J., Dadlez, M., and Glover, D.M. (2011). CENP-C is a structural platform for kinetochore assembly. Current biology : CB *21*, 399-405.

Reddy, S.K., Rape, M., Margansky, W.A., and Kirschner, M.W. (2007). Ubiquitination by the anaphase-promoting complex drives spindle checkpoint inactivation. Nature *446*, 921-925.

Rieder, C.L., Cole, R.W., Khodjakov, A., and Sluder, G. (1995). The checkpoint delaying anaphase in response to chromosome monoorientation is mediated by an inhibitory signal produced by unattached kinetochores. J Cell Biol *130*, 941-948.

Rieder, C.L., and Maiato, H. (2004). Stuck in division or passing through: what happens when cells cannot satisfy the spindle assembly checkpoint. Developmental cell *7*, 637-651.

Rieder, C.L., Schultz, A., Cole, R., and Sluder, G. (1994). Anaphase onset in vertebrate somatic cells is controlled by a checkpoint that monitors sister kinetochore attachment to the spindle. J Cell Biol *127*, 1301-1310.

Rosenberg, J.S., Cross, F.R., and Funabiki, H. (2011). KNL1/Spc105 recruits PP1 to silence the spindle assembly checkpoint. Current biology : CB *21*, 942-947.

Rossio, V., Galati, E., Ferrari, M., Pellicioli, A., Sutani, T., Shirahige, K., Lucchini, G., and Piatti, S. (2010). The RSC chromatin-remodeling complex influences mitotic exit and adaptation to the spindle assembly checkpoint by controlling the Cdc14 phosphatase. The Journal of Cell Biology *191*, 981-997.

Rowald, K., Mantovan, M., Passos, J., Buccitelli, C., Mardin, B.R., Korbel, J.O., Jechlinger, M., and Sotillo, R. (2016). Negative Selection and Chromosome Instability Induced by Mad2 Overexpression Delay Breast Cancer but Facilitate Oncogene-Independent Outgrowth. Cell Rep *15*, 2679-2691.

Ruchaud, S., Carmena, M., and Earnshaw, W.C. (2007). Chromosomal passengers: conducting cell division. Nature reviews. Molecular cell biology *8*, 798-812.

Russell, P., and Nurse, P. (1986). Schizosaccharomyces pombe and Saccharomyces cerevisiae: a look at yeasts divided. Cell *45*, 781-782.

Sacristan, C., and Kops, G.J. (2015). Joined at the hip: kinetochores, microtubules, and spindle assembly checkpoint signaling. Trends in Cell Biology *25*, 21-28.

Santaguida, S., Tighe, A., D'Alise, A.M., Taylor, S.S., and Musacchio, A. (2010). Dissecting the role of MPS1 in chromosome biorientation and the spindle checkpoint through the small molecule inhibitor reversine. J Cell Biol *190*, 73-87.

Saurin, A.T., van der Waal, M.S., Medema, R.H., Lens, S.M., and Kops, G.J. (2011). Aurora B potentiates Mps1 activation to ensure rapid checkpoint establishment at the onset of mitosis. Nat Commun *2*, 316.

Schittenhelm, R.B., Chaleckis, R., and Lehner, C.F. (2009). Intrakinetochore localization and essential functional domains of Drosophila Spc105. EMBO J *28*, 2374-2386.

Schleiffer, A., Maier, M., Litos, G., Lampert, F., Hornung, P., Mechtler, K., and Westermann, S. (2012). CENP-T proteins are conserved centromere receptors of the Ndc80 complex. Nat Cell Biol *14*, 604-613.

Schwab, M., Neutzner, M., Mocker, D., and Seufert, W. (2001). Yeast Hct1 recognizes the mitotic cyclin Clb2 and other substrates of the ubiquitin ligase APC. Embo j *20*, 5165-5175.

Schweizer, N., Ferras, C., Kern, D.M., Logarinho, E., Cheeseman, I.M., and Maiato, H. (2013). Spindle assembly checkpoint robustness requires Tpr-mediated regulation of Mad1/Mad2 proteostasis. J Cell Biol *203*, 883-893.

Scott, R.J., Lusk, C.P., Dilworth, D.J., Aitchison, J.D., and Wozniak, R.W. (2005). Interactions between Mad1p and the nuclear transport machinery in the yeast Saccharomyces cerevisiae. Mol Biol Cell *16*, 4362-4374.

Screpanti, E., De Antoni, A., Alushin, G.M., Petrovic, A., Melis, T., Nogales, E., and Musacchio, A. (2011). Direct binding of Cenp-C to the Mis12 complex joins the inner and outer kinetochore. Current biology : CB *21*, 391-398.

Sczaniecka, M., Feoktistova, A., May, K.M., Chen, J.S., Blyth, J., Gould, K.L., and Hardwick, K.G. (2008). The spindle checkpoint functions of Mad3 and Mad2 depend on a Mad3 KEN box-mediated interaction with Cdc20-anaphase-promoting complex (APC/C). J Biol Chem *283*, 23039-23047.

Seeley, T.W., Wang, L., and Zhen, J.Y. (1999). Phosphorylation of human MAD1 by the BUB1 kinase in vitro. Biochemical and biophysical research communications *257*, 589-595.

Shah, J.V., Botvinick, E., Bonday, Z., Furnari, F., Berns, M., and Cleveland, D.W. (2004). Dynamics of centromere and kinetochore proteins; implications for checkpoint signaling and silencing. Current biology : CB *14*, 942-952.

Shepperd, L.A., Meadows, J.C., Sochaj, A.M., Lancaster, T.C., Zou, J., Buttrick, G.J., Rappsilber, J., Hardwick, K.G., and Millar, J.B. (2012). Phosphodependent recruitment of Bub1 and Bub3 to Spc7/KNL1 by Mph1 kinase maintains the spindle checkpoint. Current biology : CB *22*, 891-899.

Silio, V., McAinsh, A.D., and Millar, J.B. (2015). KNL1-Bubs and RZZ Provide Two Separable Pathways for Checkpoint Activation at Human Kinetochores. Developmental cell *35*, 600-613.

Simonetta, M., Manzoni, R., Mosca, R., Mapelli, M., Massimiliano, L., Vink, M., Novak, B., Musacchio, A., and Ciliberto, A. (2009). The influence of catalysis on mad2 activation dynamics. PLoS Biol *7*, e10.

Sironi, L., Mapelli, M., Knapp, S., De Antoni, A., Jeang, K.T., and Musacchio, A. (2002). Crystal structure of the tetrameric Mad1-Mad2 core complex: implications of a 'safety belt' binding mechanism for the spindle checkpoint. EMBO J *21*, 2496-2506.

Sironi, L., Melixetian, M., Faretta, M., Prosperini, E., Helin, K., and Musacchio, A. (2001). Mad2 binding to Mad1 and Cdc20, rather than oligomerization, is required for the spindle checkpoint. EMBO J *20*, 6371-6382.

Sivaram, M.V., Wadzinski, T.L., Redick, S.D., Manna, T., and Doxsey, S.J. (2009). Dynein light intermediate chain 1 is required for progress through the spindle assembly checkpoint. Embo j *28*, 902-914.

Sotillo, R., Hernando, E., Díaz-Rodríguez, E., Teruya-Feldstein, J., Cordón-Cardo, C., Lowe, S.W., and Benezra, R. (2007). Mad2 Overexpression Promotes Aneuploidy and Tumorigenesis in Mice. Cancer Cell *11*, 9-23.

Sudakin, V., Chan, G.K., and Yen, T.J. (2001). Checkpoint inhibition of the APC/C in HeLa cells is mediated by a complex of BUBR1, BUB3, CDC20, and MAD2. J Cell Biol *154*, 925-936.

Suijkerbuijk, S.J., van Dam, T.J., Karagoz, G.E., von Castelmur, E., Hubner, N.C., Duarte, A.M., Vleugel, M., Perrakis, A., Rudiger, S.G., Snel, B.*, et al.* (2012a). The vertebrate mitotic checkpoint protein BUBR1 is an unusual pseudokinase. Developmental cell *22*, 1321-1329.

Suijkerbuijk, S.J., Vleugel, M., Teixeira, A., and Kops, G.J. (2012b). Integration of kinase and phosphatase activities by BUBR1 ensures formation of stable kinetochore-microtubule attachments. Developmental cell *23*, 745-755.

Sullivan, M., and Morgan, D.O. (2007). Finishing mitosis, one step at a time. Nature reviews. Molecular cell biology *8*, 894-903.

Tan, C.H., Gasic, I., Huber-Reggi, S.P., Dudka, D., Barisic, M., Maiato, H., and Meraldi, P. (2015). The equatorial position of the metaphase plate ensures symmetric cell divisions. eLife *4*, e05124.

Tang, Z., Shu, H., Oncel, D., Chen, S., and Yu, H. (2004). Phosphorylation of Cdc20 by Bub1 provides a catalytic mechanism for APC/C inhibition by the spindle checkpoint. Mol Cell *16*, 387-397.

Tange, Y., and Niwa, O. (2008). Schizosaccharomyces pombe Bub3 is dispensable for mitotic arrest following perturbed spindle formation. Genetics *179*, 785-792.

Taylor, S.S., Ha, E., and McKeon, F. (1998). The human homologue of Bub3 is required for kinetochore localization of Bub1 and a Mad3/Bub1-related protein kinase. J Cell Biol *142*, 1-11.

Teichner, A., Eytan, E., Sitry-Shevah, D., Miniowitz-Shemtov, S., Dumin, E., Gromis, J., and Hershko, A. (2011). p31comet Promotes disassembly of the mitotic checkpoint complex in an ATP-dependent process. Proc Natl Acad Sci U S A *108*, 3187-3192.

Tipton, A.R., Ji, W., Sturt-Gillespie, B., Bekier, M.E., 2nd, Wang, K., Taylor, W.R., and Liu, S.T. (2013). Monopolar spindle 1 (MPS1) kinase promotes production of closed MAD2 (C-MAD2) conformer and assembly of the mitotic checkpoint complex. J Biol Chem *288*, 35149-35158.

Tipton, A.R., Wang, K., Link, L., Bellizzi, J.J., Huang, H., Yen, T., and Liu, S.T. (2011). BUBR1 and closed MAD2 (C-MAD2) interact directly to assemble a functional mitotic checkpoint complex. J Biol Chem *286*, 21173-21179.

Toledo, C.M., Herman, J.A., Olsen, J.B., Ding, Y., Corrin, P., Girard, E.J., Olson, J.M., Emili, A., DeLuca, J.G., and Paddison, P.J. (2014). BuGZ is required for Bub3 stability, Bub1 kinetochore function, and chromosome alignment. Developmental cell *28*, 282-294.

Tromer, E., Snel, B., and Kops, G.J. (2015). Widespread Recurrent Patterns of Rapid Repeat Evolution in the Kinetochore Scaffold KNL1. Genome biology and evolution *7*, 2383-2393.

Uchida, K., and Hirota, T. (2016). Spindle Assembly Checkpoint: Its Control and Aberration. In DNA Replication, Recombination, and Repair: Molecular Mechanisms and Pathology, F. Hanaoka, and K. Sugasawa, eds. (Tokyo: Springer Japan), pp. 429-447.

Uzunova, K., Dye, B.T., Schutz, H., Ladurner, R., Petzold, G., Toyoda, Y., Jarvis, M.A., Brown, N.G., Poser, I., Novatchkova, M.*, et al.* (2012). APC15 mediates CDC20 autoubiquitylation by APC/C(MCC) and disassembly of the mitotic checkpoint complex. Nat Struct Mol Biol *19*, 1116-1123.

van der Horst, A., and Lens, S.M. (2014). Cell division: control of the chromosomal passenger complex in time and space. Chromosoma *123*, 25-42.

Vanoosthuyse, V., and Hardwick, K.G. (2009). A novel protein phosphatase 1-dependent spindle checkpoint silencing mechanism. Current biology : CB *19*, 1176-1181.

Vanoosthuyse, V., Meadows, J.C., van der Sar, S.J., Millar, J.B., and Hardwick, K.G. (2009). Bub3p facilitates spindle checkpoint silencing in fission yeast. Mol Biol Cell *20*, 5096-5105.

Vanoosthuyse, V., Valsdottir, R., Javerzat, J.P., and Hardwick, K.G. (2004). Kinetochore targeting of fission yeast Mad and Bub proteins is essential for spindle checkpoint function but not for all chromosome segregation roles of Bub1p. Mol Cell Biol *24*, 9786-9801.

Varma, D., Wan, X., Cheerambathur, D., Gassmann, R., Suzuki, A., Lawrimore, J., Desai, A., and Salmon, E.D. (2013). Spindle assembly checkpoint proteins are positioned close to core microtubule attachment sites at kinetochores. J Cell Biol *202*, 735-746.

Vernieri, C., Chiroli, E., Francia, V., Gross, F., and Ciliberto, A. (2013). Adaptation to the spindle checkpoint is regulated by the interplay between Cdc28/Clbs and PP2ACdc55. J Cell Biol *202*, 765-778.

Vidwans, S.J., and Su, T.T. (2001). Cycling through development in Drosophila and other metazoa. Nat Cell Biol *3*, E35-E39.

Vigneron, S., Prieto, S., Bernis, C., Labbe, J.C., Castro, A., and Lorca, T. (2004). Kinetochore localization of spindle checkpoint proteins: who controls whom? Mol Biol Cell *15*, 4584-4596.

Vink, M., Simonetta, M., Transidico, P., Ferrari, K., Mapelli, M., De Antoni, A., Massimiliano, L., Ciliberto, A., Faretta, M., Salmon, E.D.*, et al.* (2006). In vitro FRAP identifies the minimal requirements for Mad2 kinetochore dynamics. Current biology : CB *16*, 755-766.

Vleugel, M., Hoek, T.A., Tromer, E., Sliedrecht, T., Groenewold, V., Omerzu, M., and Kops, G.J. (2015a). Dissecting the roles of human BUB1 in the spindle assembly checkpoint. J Cell Sci *128*, 2975-2982.

Vleugel, M., Hoogendoorn, E., Snel, B., and Kops, G.J. (2012). Evolution and function of the mitotic checkpoint. Developmental cell *23*, 239-250.

Vleugel, M., Omerzu, M., Groenewold, V., Hadders, M.A., Lens, S.M., and Kops, G.J. (2015b). Sequential multisite phospho-regulation of KNL1-BUB3 interfaces at mitotic kinetochores. Mol Cell *57*, 824-835.

Vleugel, M., Tromer, E., Omerzu, M., Groenewold, V., Nijenhuis, W., Snel, B., and Kops, G.J. (2013). Arrayed BUB recruitment modules in the kinetochore scaffold KNL1 promote accurate chromosome segregation. J Cell Biol *203*, 943-955.

Vodermaier, H.C., Gieffers, C., Maurer-Stroh, S., Eisenhaber, F., and Peters, J.M. (2003). TPR subunits of the anaphase-promoting complex mediate binding to the activator protein CDH1. Current biology : CB *13*, 1459-1468.

Wan, X., O'Quinn, R.P., Pierce, H.L., Joglekar, A.P., Gall, W.E., DeLuca, J.G., Carroll, C.W., Liu, S.T., Yen, T.J., McEwen, B.F.*, et al.* (2009). Protein Architecture of the Human Kinetochore Microtubule Attachment Site. Cell *137*, 672-684.

Wang, K., Sturt-Gillespie, B., Hittle, J.C., Macdonald, D., Chan, G.K., Yen, T.J., and Liu, S.T. (2014). Thyroid hormone receptor interacting protein 13 (TRIP13) AAA-ATPase is a novel mitotic checkpoint-silencing protein. J Biol Chem *289*, 23928-23937.

Wang, X., Babu, J.R., Harden, J.M., Jablonski, S.A., Gazi, M.H., Lingle, W.L., de Groen, P.C., Yen, T.J., and van Deursen, J.M.A. (2001). The Mitotic Checkpoint Protein hBUB3 and the mRNA Export Factor hRAE1 Interact with GLE2p-binding Sequence (GLEBS)-containing Proteins. Journal of Biological Chemistry *276*, 26559-26567.

Warren, C.D., Brady, D.M., Johnston, R.C., Hanna, J.S., Hardwick, K.G., and Spencer, F.A. (2002). Distinct chromosome segregation roles for spindle checkpoint proteins. Mol Biol Cell *13*, 3029-3041.

Weir, J.R., Faesen, A.C., Klare, K., Petrovic, A., Basilico, F., Fischböck, J., Pentakota, S., Keller, J., Pesenti, M.E., Pan, D.*, et al.* (2016). Insights from biochemical reconstitution into the architecture of human kinetochores. Nature *537*, 249-253.

Weiss, E., and Winey, M. (1996). The Saccharomyces cerevisiae spindle pole body duplication gene MPS1 is part of a mitotic checkpoint. J Cell Biol *132*, 111-123.

Westhorpe, F.G., and Straight, A.F. (2013). Functions of the centromere and kinetochore in chromosome segregation. Curr Opin Cell Biol *25*, 334-340.

Westhorpe, F.G., Tighe, A., Lara-Gonzalez, P., and Taylor, S.S. (2011). p31comet-mediated extraction of Mad2 from the MCC promotes efficient mitotic exit. J Cell Sci *124*, 3905-3916.

Windecker, H., Langegger, M., Heinrich, S., and Hauf, S. (2009). Bub1 and Bub3 promote the conversion from monopolar to bipolar chromosome attachment independently of shugoshin. EMBO Rep *10*, 1022-1028.

Wolfe, K.H., and Shields, D.C. (1997). Molecular evidence for an ancient duplication of the entire yeast genome. Nature *387*, 708-713.

Wood, V., Gwilliam, R., Rajandream, M.A., Lyne, M., Lyne, R., Stewart, A., Sgouros, J., Peat, N., Hayles, J., Baker, S.*, et al.* (2002). The genome sequence of Schizosaccharomyces pombe. Nature *415*, 871-880.

Xia, G., Luo, X., Habu, T., Rizo, J., Matsumoto, T., and Yu, H. (2004). Conformation-specific binding of p31(comet) antagonizes the function of Mad2 in the spindle checkpoint. EMBO J *23*, 3133-3143.

Xu, P., Raetz, E.A., Kitagawa, M., Virshup, D.M., and Lee, S.H. (2013). BUBR1 recruits PP2A via the B56 family of targeting subunits to promote chromosome congression. Biol Open *2*, 479-486.

Yamagishi, Y., Yang, C.H., Tanno, Y., and Watanabe, Y. (2012). MPS1/Mph1 phosphorylates the kinetochore protein KNL1/Spc7 to recruit SAC components. Nat Cell Biol *14*, 746-752.

Yamaguchi, M., VanderLinden, R., Weissmann, F., Qiao, R., Dube, P., Brown, N.G., Haselbach, D., Zhang, W., Sidhu, S.S., Peters, J.M.*, et al.* (2016). Cryo-EM of Mitotic Checkpoint Complex-Bound APC/C Reveals Reciprocal and Conformational Regulation of Ubiquitin Ligation. Mol Cell *63*, 593-607.

Yamaguchi, S., Decottignies, A., and Nurse, P. (2003). Function of Cdc2p-dependent Bub1p phosphorylation and Bub1p kinase activity in the mitotic and meiotic spindle checkpoint. EMBO J *22*, 1075-1087.

Yang, M., Li, B., Liu, C.J., Tomchick, D.R., Machius, M., Rizo, J., Yu, H., and Luo, X. (2008). Insights into mad2 regulation in the spindle checkpoint revealed by the crystal structure of the symmetric mad2 dimer. PLoS Biol *6*, e50.

Yang, M., Li, B., Tomchick, D.R., Machius, M., Rizo, J., Yu, H., and Luo, X. (2007). p31comet blocks Mad2 activation through structural mimicry. Cell *131*, 744-755.

Ye, Q., Rosenberg, S.C., Moeller, A., Speir, J.A., Su, T.Y., and Corbett, K.D. (2015). TRIP13 is a protein-remodeling AAA+ ATPase that catalyzes MAD2 conformation switching. Elife *4*.

Yu, H. (2006). Structural activation of Mad2 in the mitotic spindle checkpoint: the two-state Mad2 model versus the Mad2 template model. J Cell Biol *173*, 153-157.

Zhang, G., Lischetti, T., and Nilsson, J. (2014). A minimal number of MELT repeats supports all the functions of KNL1 in chromosome segregation. J Cell Sci *127*, 871-884.

Zhang, S., Chang, L., Alfieri, C., Zhang, Z., Yang, J., Maslen, S., Skehel, M., and Barford, D. (2016). Molecular mechanism of APC/C activation by mitotic phosphorylation. Nature *533*, 260-264.

Zhang, Y., and Lees, E. (2001). Identification of an Overlapping Binding Domain on Cdc20 for Mad2 and Anaphase-Promoting Complex: Model for Spindle Checkpoint Regulation. Mol Cell Biol *21*, 5190-5199.

LIST OF PUBLICATIONS

Accepted manuscripts:

1. Heinrich S, **Sewart K**, Windecker H, Langegger M, Schmidt N, Hauf S
Mad1 promotes checkpoint function independently of recruiting Mad1:Mad2 to kinetochores.
EMBO Reports, 2014 Mar;15(3):291-8

2. Mora-Santos MD, Hervas-Aguilar A, **Sewart K**, Lancaster TC, Meadows JC, Millar JB
Bub3-Bub1 Binding to Spc7/KNL1 Toggles the Spindle Checkpoint Switch by Licensing the Interaction of Bub1 with Mad1-Mad2.
Curr Biol. 2016 Oct 10;26(19):2642-2650

Manuscript in preparation:

1. **Sewart K**, Hauf S
Different modes of Cdc20 inhibition by the mitotic checkpoint.
EMBO Reports, to be submitted